

**Development of  
class IIa histone deacetylase inhibitors**

Inaugural dissertation

for the attainment of the title of doctor  
in the Faculty of Mathematics and Natural Sciences  
at the Heinrich Heine University Düsseldorf

presented by

**Yodita Asfaha**  
from Kassel

Düsseldorf, September 2020

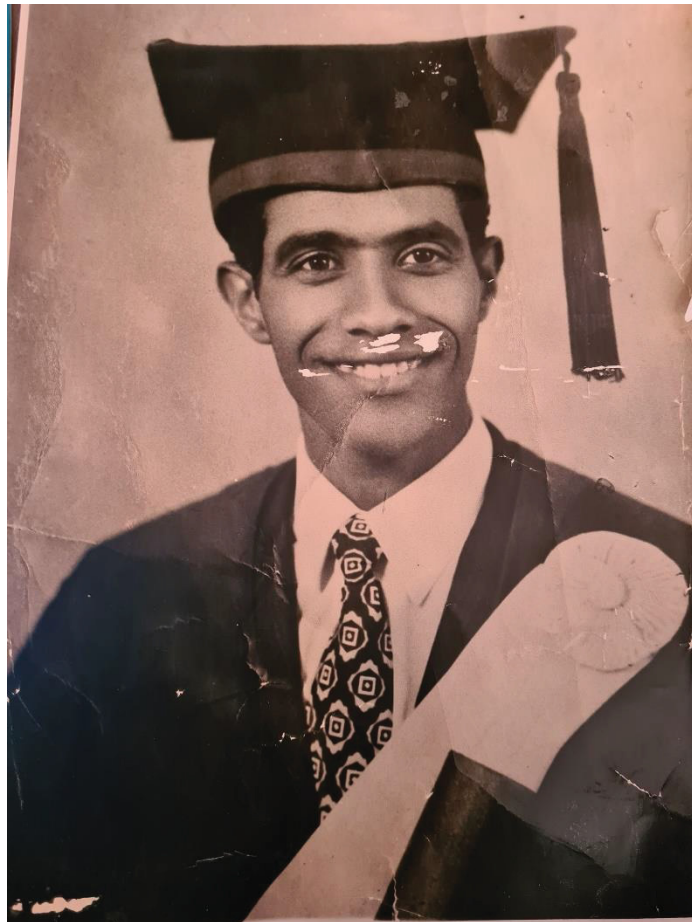
from the Institute of Pharmaceutical and Medicinal Chemistry  
at the Heinrich Heine University Düsseldorf

Published by permission of the  
Faculty of Mathematics and Natural Sciences  
at Heinrich Heine University Düsseldorf

Supervisor: Prof. Dr. Thomas Kurz  
Co-supervisor: Prof. Dr. Matthias U. Kassack

Date of the oral examination: 14.08.2020

*In loving memory of my uncle Tecleyohannes Asghedom*



## **Affidavit**

I declare under oath that I have produced my thesis independently and without any undue assistance by third parties under consideration of the “Principles for the Safeguarding of Good Scientific Practice” at Heinrich Heine University Düsseldorf. The presented dissertation has not been submitted to another faculty. So far, I have not attempted to earn a doctoral degree (neither successfully nor unsuccessfully).

Düsseldorf, September 2020

The presented dissertation was conducted under the supervision of Prof. Dr. Thomas Kurz from September 2016 to June 2020 at the Institute for Pharmaceutical and Medicinal Chemistry, Heinrich Heine University Düsseldorf.

## Acknowledgments

Firstly, I would like to thank my supervisor Prof. Thomas Kurz without whom this research would not have been possible. Thank you, Thomas, for your enthusiasm, ideas, encouragement and for giving me the amazing opportunity to work in your research group.

Secondly, I would like to acknowledge Prof. Matthias U. Kassack for co-directing my thesis and the successful cooperation, as well as his valuable contributions to this project.

I would like to thank his research group, especially Christian Schrenk, Alexander Jan Skerhut and Nadine Horstick-Muche, for the biological evaluation of my “little” compound library. Thank you very much.

I would like to thank the graduate school 2158 (GRK2158), especially Martina Holz, for cultivating a nurturing environment and promoting intercultural exchange, as well as for supporting my personal and professional development.

I would like to acknowledge the financial support from the Deutsche Forschungsgemeinschaft (DFG, grant numbers: KU 1577/2-1 and 270650915/GRK2158), which undoubtedly contributed to the completion of this work.

Furthermore, I would like to highlight the amazing team of proof-readers: Thomas, Marc, Matthias, Leandro, Christian and Alex. Despite the time pressure, you took the time to read through my thesis carefully. Thank you so much.

I would like to thank Ms. Maria Beuer, Mr. Mohanad Aian, Dr. Schaper, Mr. Peter Behm, Dr. Tommes and Ms. Gabriele Zerta from the departments of NMR spectroscopy, mass spectroscopy and elementary analysis for the analytical analyses of my compounds.

During my time in the Kurz group, I have been privileged to work with so many kind and brilliant people. Beate, Marc, Leandro, Viktoria, Tanja, Petra, Alex, Vitalij, Mona and Olli: Thank you all so much for your support and the amazing team dynamics. Special thanks to Beate, Marc and Leandro: You have helped me grow through our fruitful discussions and your endless support. I cannot thank you enough.

Special thanks to my project students, Stella Pauls, Thomas Marsh, Stefan Klinken and Fabian Fischer, who consistently put a lot of effort and dedication into their lab work.

Big thanks to Prof. Dr. Stark and his research group, especially Dr. Aleksandra Zivkovic, Mili, Stephen, David, Markus (2x) and Lars, for sharing their equipment with our group.

During my PhD-time in Düsseldorf, I have lived together with open-hearted, funny and crazy roommates. Big thanks to Lea and Lennard for the amazing time.

Furthermore, I want to extend my thanks to the “Marburg crew”. Special thanks to Kirsten, Martin, Max, Francesca, Emre and Matthias. We had an unforgettable time in Marburg. I am so grateful that I got to meet you guys.

Special thanks and love to my amazing friends who have loved and supported me through all these years. I must highlight my ladies: Rahwa and Olga. I am so grateful to have you in my life. When I am with you, there is laughter, happiness and joy all around. Keep it up, ladies! I am so proud of you.

Much love and thanks go out to the Eritrean community in Kassel, especially to all the ladies I grew up with (the Dr. Yohannes Ladies: Astier and Sarah & the Yemane Ladies: Luwam and Selam). You are the definition of black girl magic. Keep it up! I am so proud of all of you.

Special thanks and love go out to Yvette, who is a strong and inspiring woman for all black women all around the world. I am so proud of you.

And finally, to my family: Thank you Adey and Baba for all your unconditional love, encouragement and believing in me. The love you have for us, your children, is endless. I am blessed to have you as my parents. I admire your strength and compassion. You gave your children everything and we are so proud of you. You are the true Eritrean heroes of my life. I love you so much.

Thank you, my siblings: Eden, Naza, Adiam, Yohannes and Samson. I love you so much and I am so grateful to be your sister. I feel very lucky to have you all in my life.

I would also like to thank my relatives all over the world; from Canada to America, Europe and Eritrea. Thank you so much. I love you all.

This work is dedicated to my loving uncle: Tecleyohannes Asghedom. You sacrificed your life for the independence of our beloved country, Eritrea. To me, you are more than just an independence activist. You were a strong, loving and dedicated man with so much potential, dreams and visions. I was raised with your graduation picture hanging in our living room. Every time I look at this picture, I feel a strong connection to you. You are alive in me and in all of us. You have been, and still are, the force of motivation in my life. I love you so much. You are not forgotten and never will be. Your dreams and visions are still alive.

Life is precious, and I want to thank all of you for all the love you give me. I am so grateful and blessed to have you in my life.

## Table of Contents

Abbreviations and Acronyms .....	II
Introduction.....	1
Histone deacetylases .....	1
Natural products in Medicinal Chemistry.....	5
Natural Compounds as Histone deacetylase inhibitors (HDACi).....	5
Natural Compound scaffolds in clinically used HDAC inhibitors .....	7
Strategies for the development of isozyme-selective and/or complex-specific HDAC inhibitors.....	9
Combination therapy with HDACi for the treatment of cancer .....	10
Recent advances in class IIa histone deacetylases research.....	13
Objective .....	30
References.....	32
Novel alkoxyamide-based histone deacetylase inhibitors reverse cisplatin resistance in chemoresistant cancer cells .....	38
Synthesis of thiazolyl-based hydroxamic acids as histone deacetylase inhibitors .....	72
Are thioether-based hydroxamic acids HDAC8 or class IIa HDAC selective inhibitors? .....	91
Alkoxyamide-based TFMO-derivatives: Potent and Selective Class IIa Histone Deacetylase Inhibitors .....	142
The Second Generation of Potent and Selective Class IIa Histone Deacetylase Inhibitors ...	180
Summary and Outlook .....	217

## Abbreviations and Acronyms

Å	Angstrom
A2780	human ovarian cancer cell line
Ac	Acetyl
ACN	Acetonitrile
°C	Celsius
calcd.	Calculated
Cal27	human oral adenosquamous carcinoma cell line
CDDP	Cisplatin
CisR	Cisplatin-resistant
conc.	Concentrated
CTCL	Cutaneous T-cell lymphoma
CU	Connecting unit
DIPEA	<i>N,N</i> -Diisopropylethylamine
DMF	<i>N,N</i> -Dimethylformamide
DMSO	Dimethyl sulfoxide
DNA	Deoxyribonucleic acid
e.g.	<i>exempli gratia</i> (Latin: for example)
eq.	Equivalents
ESI	Electrospray ionization
Et	Ethyl
<i>et al.</i>	<i>et alii</i> (Latin: and others)
FDA	Food and Drug Administration
g	Gram(s)
h	Hour(s)
HAT	Histone acetyltransferase
HATU	1-[Bis(dimethylamino)methylene]-1 <i>H</i> -1,2,3-triazolo[4,5- <i>b</i> ]pyridinium 3-oxide hexafluorophosphate
HDAC	Histone deacetylase

## Abbreviations and Acronyms

---

HDACi	Histone deacetylase inhibitor(s)
HPLC	High performance liquid chromatography
HRMS	High resolution mass spectrometry
Hz	Hertz
IC <sub>50</sub>	Half maximal inhibitory concentration
<i>in situ</i>	Latin: in position
<i>in vacuo</i>	Latin: in a vacuum
<i>J</i>	Coupling constant (Hz)
M	Molar
Me	Methyl
mg	Milligram
min	Minute(s)
mL	Milliliter(s)
MM	Multiple myeloma
mmol	Millimole(s)
mp.	Melting point
MTT	3-(4,5-Dimethylthiazol-2-yl)-2,5-diphenyltetrazolium bromide
<i>m/z</i>	Mass to charge ratio
NBS	<i>N</i> -bromosuccinimide
Nm	Nanometers
NMR	Nuclear magnetic resonance
PDB	Protein Data Bank
Ph	Phenyl
ppm	Parts per million
PTCL	Peripheral T-cell lymphoma
RNA	Ribonucleic acid
rt	Room temperature
SI	Selectivity index
TFA	Trifluoroacetic acid
TFAA	Trifluoroacetic anhydride
TFMO	Trifluoromethyloxadiazole

## Abbreviations and Acronyms

---

THF	Tetrahydrofuran
THP-1	Human monocytic cell line
UV	Ultraviolet
ZBG	Zinc binding group

### Introduction

Cancer is the second leading cause of mortality worldwide, accounting for an estimated 9.6 million deaths in 2018.<sup>[1]</sup> The most common cancer types in men are lung, prostate, colorectal, stomach and liver cancer, whereas breast, colorectal, lung, cervical and thyroid cancer are frequently diagnosed in women.<sup>[2]</sup> The “Hallmarks of Cancer”-concept was coined by Hanahan et al.<sup>[3]</sup> in 2000 and describes qualities that distinguish normal cells from cancer cells which allow them to undergo uncontrolled proliferation and metastatic dissemination. In particular, sustaining proliferative signaling, evading growth suppressors, resisting cell death, enabling replicative immortality, inducing angiogenesis, activating invasion and metastasis, avoiding immune destruction, cancer-promoting inflammation, genome instability and mutation, and deregulating cellular energetics were identified as the most prominent hallmarks.<sup>[3–5]</sup> Epigenetic changes can often contribute to tumor degeneration.<sup>[6]</sup> The term “Epigenetic” refers to changes of gene expression without altering the underlying DNA sequence.<sup>[7]</sup> Major reversible epigenetic changes are: DNA methylation, histone protein modification, and post-transcriptional gene regulation by non-coding RNAs.<sup>[8]</sup>

### Histone deacetylases

Histone acetylation has been one of most extensively studied epigenetic modification.<sup>[9]</sup> Acetylation and deacetylation of  $\epsilon$ -amino group at lysine residues are modulated by histone acetyltransferases (HATs) and histone deacetylases (HDACs).<sup>[10]</sup> Histone hypoacetylation leads to a stronger interaction between the histones and the DNA, which maintains chromatin in its condensed state, resulting in a down regulation of gene transcription.<sup>[11–15]</sup> Hence, histone acetylation causes a relaxation of chromatin and an increased accessibility of the transcriptional machinery (Figure 1). HDACs can also act on numerous non-histone proteins such as signaling molecules, transcription factors, chaperones and inflammatory mediators.<sup>[16,17]</sup> Therefore, alterations of the acetylome has consequences for protein-DNA interactions, protein-protein interactions and protein stability.<sup>[18]</sup> In humans, 18 HDACs have been identified which are segregated into four classes according to their yeast homologues: class I (HDACs 1, 2, 3, and 8), class II (IIa: HDACs 4,5,7,9 and IIb: HDACs 6, 10), class III (sirtuin family: sirt1-sirt7) and class IV (HDAC11).<sup>[19]</sup> Classes I, II and IV share a conserved catalytic

domain with a zinc ion as an active cofactor, whereas class III enzymes are  $\text{NAD}^+$ -dependent and known as sirtuins.<sup>[20]</sup> The class III series of enzymes are beyond the scope of this work and are, therefore, not further discussed.

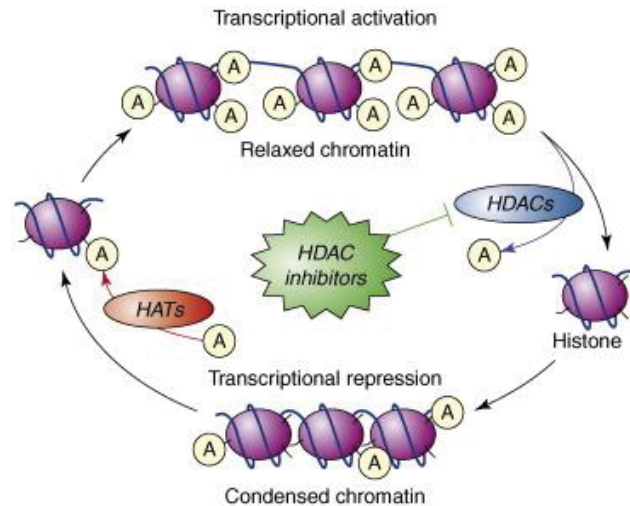


Figure 1: Effects of HATs and HDACs on chromatin remodeling. Inhibition of HDACs by HDAC inhibitors results in a relaxation of chromatin and an increased accessibility of the transcriptional machinery.<sup>[21]</sup>

The active site of the  $\text{Zn}^{2+}$ -dependent HDAC family is highly conserved. At the bottom of the active site is a catalytically active  $\text{Zn}^{2+}$ -ion located, which is chelated by one His residue and two Asp residues, as well as a water molecule.<sup>[22]</sup> Surrounding this center are two His-Asp charge-relay systems, and adjacent to these is a Tyr residue, with an inward-facing hydroxyl group. Numerous hydrolytic mechanisms have been proposed for HDAC deacetylation. However, all share three common features: 1) activation of the substrate and water 2) proton shuttling 3) liberation of lysine and acetate (Figure 2).<sup>[22–25]</sup> The  $\text{Zn}^{2+}$ -ion in the active site increases the nucleophilicity of the water molecule and stabilizes the transition state upon the formation of the tetrahedral intermediate during hydrolysis. The His-Asp charge-relay systems enables proton shuttling during the various stages of the mechanism, as well as potentially providing polarization of the water molecule via H-bonding prior to hydrolysis. The Tyr residue activates the acetyl lysine carbonyl of the respective substrate and provides a hydrogen bonding stabilization of the tetrahedral intermediate after the attack by water at the C=O bond.<sup>[23–26]</sup>

## Introduction

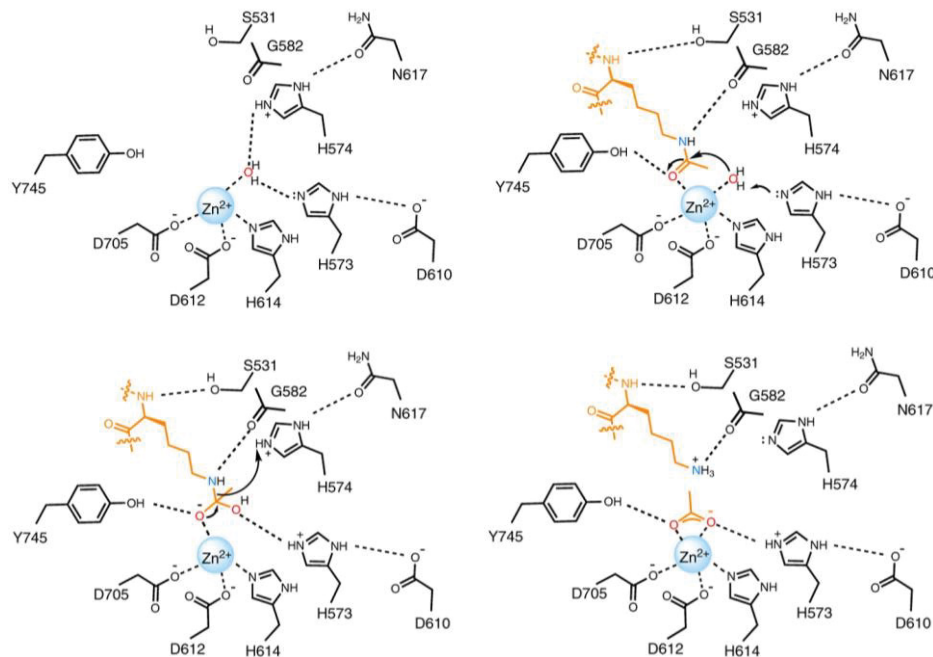


Figure 2: Proposed mechanism for the hydrolysis of acetylated lysine residues by HDACs.<sup>[22]</sup>

According to recent studies, of the dissonance between the abundance of HATs and HDACs are linked to the development and progression of a variety of cancers. It has been demonstrated that the expression levels of HDACs is increased in some hematological cancers as well as in solid tumors, and is associated with a poor prognosis in some cancer cell lines.<sup>[27–33]</sup> Table 1 summarizes observed modifications detected in HDAC protein and alterations of gene expression levels in cancer cell lines.

## Introduction

Table 1: Modifications in histone deacetylase proteins and gene expression pattern in cancer cell lines. HDAC in italics marks the corresponding gene.

Class	Members	Type of Variation	Cancer involved
I	HDAC1	Overexpression	Gastrointestinal carcinoma <sup>[34]</sup> Prostate carcinoma <sup>[34]</sup> Breast carcinoma <sup>[34]</sup> Colon adenocarcinoma <sup>[35]</sup> Chronic lymphocytic <sup>[36]</sup>
		<i>HDAC1</i> overexpression	Ovarian cancer <sup>[18]</sup> Gastric cancer <sup>[18]</sup> Hodgkin's lymphoma <sup>[18]</sup> Prostate cancer <sup>[18]</sup>
		<i>HDAC1</i> downregulation	Colorectal cancer <sup>[18]</sup>
	HDAC2	Overexpression	Uterine cancer <sup>[34]</sup> Gastric cancer <sup>[34]</sup> Cervical cancer <sup>[34]</sup>
		<i>HDAC2</i> overexpression	Ovarian cancer <sup>[18]</sup> Hodgkin's lymphoma <sup>[18]</sup>
		Truncating <i>HDAC2</i> mutation	Colon cancer <sup>[18]</sup> Gastric cancer <sup>[18]</sup> Endometrial cancer <sup>[18]</sup>
	HDAC3	Overexpression	Colon cancer <sup>[34]</sup> Hodgkin's lymphoma <sup>[18]</sup> Chronic lymphocytic leukemia <sup>[36]</sup>
		<i>HDAC3</i> overexpression	Ovarian cancer <sup>[18]</sup> Lung cancer <sup>[18]</sup>
	IIa	HDAC4	HDAC4 mutations
<i>HDAC4</i> overexpression			Prostate cancer <sup>[18]</sup> Breast cancer <sup>[18]</sup>
<i>HDAC4</i> downregulation			Colon cancer <sup>[37]</sup> Lung cancer <sup>[37]</sup>
HDAC5		<i>HDAC5</i> downregulation	Colorectal cancer <sup>[18]</sup>
HDAC7		Overexpression	Chronic lymphocytic leukemia <sup>[36]</sup>
		<i>HDAC7</i> overexpression	Colorectal cancer <sup>[18]</sup> Pancreatic cancer <sup>[18]</sup>
HDAC9	Overexpression	Chronic lymphocytic leukemia <sup>[36]</sup>	
IIb	HDAC6	Overexpression	Acute lymphoblastic leukemia <sup>[38]</sup> Acute myeloid leukemia <sup>[38]</sup> Breast cancer <sup>[38]</sup> Chronic lymphocytic leukemia <sup>[38]</sup> Cutaneous T-cell lymphoma <sup>[38]</sup> Hepatocellular carcinoma <sup>[38]</sup> Ovarian cancer <sup>[38]</sup> Urothelial cancer <sup>[38]</sup> Oral squamous cell carcinoma <sup>[38]</sup>
	HDAC10	Overexpression	Chronic lymphocytic leukemia <sup>[36]</sup>

## Natural products in Medicinal Chemistry

Plants and terrestrial microorganisms are traditionally a source for the discovery of new drug candidates.<sup>[39–42]</sup> Many natural products (secondary metabolites) and their semisynthetic derivatives of terrestrial and marine origins have been reported to exhibit significant anticancer properties (Figure 3).<sup>[43–49]</sup> It was demonstrated that natural products can address multiple signaling pathways leading to apoptotic, autophagic and non-canonical types of cell death.<sup>[50,51]</sup> Moreover, compounds from natural origin have been shown to modulate several epigenetic modifications known to regulate underlying molecular mechanisms (proliferation, cell death) involved in tumorigenesis.<sup>[48]</sup> Nowadays, approximately 60% of the approved drugs are based on natural products due to their unique structural diversity and the defined orientations of functionalities enabling selective interactions with biological targets.<sup>[52,53]</sup>

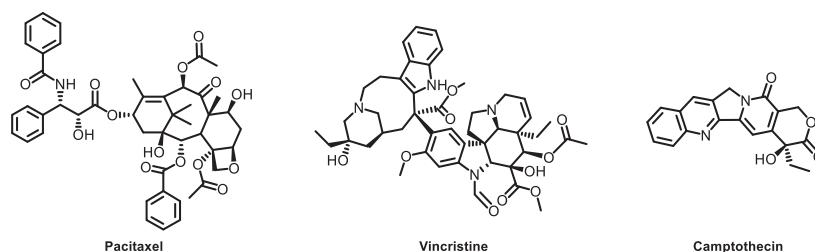


Figure 3: Selected natural products with anticancer properties.<sup>[54–57]</sup>

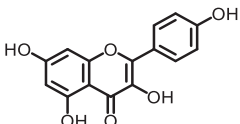
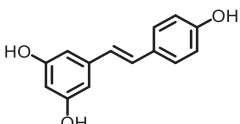
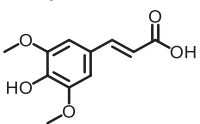
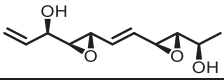
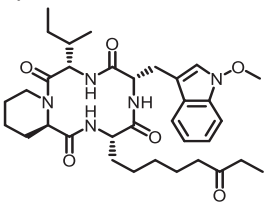
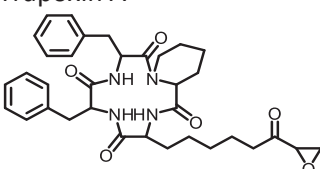
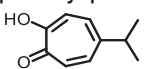
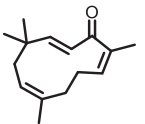
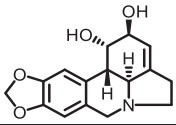
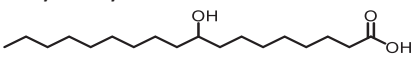
## Natural Compounds as Histone deacetylase inhibitors (HDACi)

HDAC inhibitors (HDACi) belong to a large family of biological active compounds which are categorized into hydroxamic acids, benzamides, cyclic peptides, short-chain fatty acids and thiols.<sup>[10]</sup>

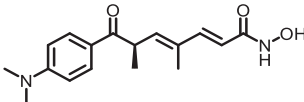
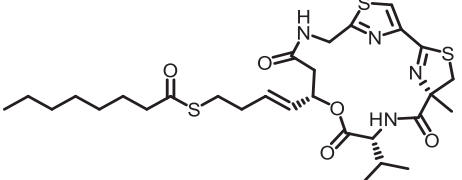
So far, naturally occurring HDACi were extracted from fungus, marine organism and several plants. In 1977, the natural compound *n*-butyric acid was identified as the first significant HDACi by Riggs et al., causing a hyperacetylation of histones in HeLa cells.<sup>[58]</sup> Later in 1980, McKnight et al. examined the effect of propionic acid on histone acetylation in chick oviduct, which displayed less activity than *n*-butyric acid.<sup>[59]</sup> Both short chain fatty acids revealed an activity in the millimolar range. Longer chained fatty acids like valproic acid (VPA) have also been reported to exhibit significant HDAC inhibitory activities by binding to the active site of HDACs, causing differentiation of human leukemia cells characterized e.g. by reduced proliferation and morphological alterations.<sup>[60]</sup> Since the 1960s, valproic acid is clinically approved for the treatment of epilepsy.<sup>[61]</sup> Table 2 summarizes information of selected natural HDACi reported in literature which are currently not employed in clinics.

## Introduction

Table 2: Examples of the natural compounds with HDAC inhibitory activity.

Chemical category	Compound name & Structure	HDAC Specificity	Origin
Phenolics	<b>Kaempferol</b> 	Class I, II, IV	Aloe vera <sup>[62]</sup>
	<b>Resveratrol</b> 	Class I, II, IV	Vitis vinifera <sup>[63]</sup>
	<b>Sinapinic acid</b> 	Pan-HDAC	Hydnophytum formicarum Jack <sup>[64]</sup>
Polyketides	<b>Depudecin</b> 	HDAC1	Alternaria brassicicola <sup>[65]</sup>
Tetrapeptide	<b>Apicidin</b> 	Class I	Fusarium spp. <sup>[66]</sup>
	<b>Trapoxin A</b> 	Class I	Helicoma ambiens RF-1023 <sup>[67]</sup>
Terpenoids	<b><math>\beta</math>-Thujaplicin</b> 	HDAC2	Cupressaceae spp. <sup>[68]</sup>
	<b>Zerumbone</b> 	Pan-HDAC	Zingiber zerumbet <sup>[69]</sup>
Alkaloid	<b>Lycorine</b> 	Pan-HDAC	Amaryllidaceae <sup>[70]</sup>
Fatty acid	<b>9-Hydroxystearic acid</b> 	Class I	Lipid peroxidation product <sup>[71]</sup>

## Introduction

Hydroxamic acid	<p>Trichostatin A</p> 	Class I & II	<i>S. hygroscopicus</i> <sup>[18]</sup>
Desipeptide	<p>Largazole</p> 	Class I	<i>Symploca</i> spp. <sup>[72]</sup>

### Natural Compound scaffolds in clinically used HDAC inhibitors

The four FDA-approved HDACi are based on the lead compound trichostatin A (TSA, Table 2) originally isolated from *Streptomyces hygroscopicus*, in 1976. TSA induces cell differentiation and arrests the cell cycle for both normal and cancer cells, resulting from acetylated histones.<sup>[73]</sup> With TSA as lead structure four hydroxamate based HDACi, vorinostat (SAHA), belinostat (PXD101) and panobinostat (LBH589) were developed and present the first FDA approved HDACi for the treatment of specific types of blood cancer. The most recent approved HDACi is chidamide. So far, this *ortho*-amino anilide is only approved in China (Figure 4).<sup>[74–79]</sup> In 1994, the cyclic peptide HDACi romidepsin (FK228) was isolated from *Chromobacterium violaceum*.<sup>[80]</sup> The disulphide prodrug is reductively activated inside a cell liberating a mercapto group as ZBG. Its HDAC inhibitory capacity results in cell cycle arrest in G1 and G2/M stages.

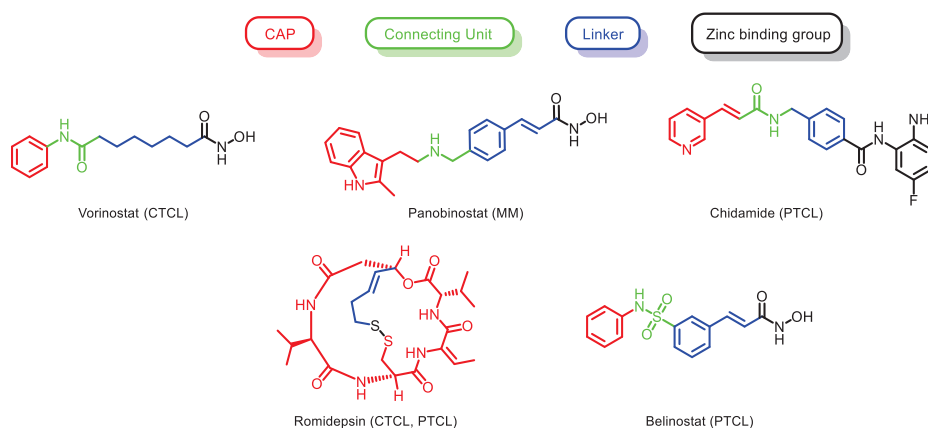


Figure 4: General pharmacophore model of HDACi. and chemical structures of approved HDAC inhibitors and their indications. CTCL: cutaneous T-cell lymphoma, MM: multiple myeloma, PTCL: peripheral T-cell lymphoma. <sup>[74–79]</sup>

The effect of the inhibition of HDACs in cancer cells is illustrated in Figure 5. HDACi exhibit their anticancer activity by e.g. cell cycle arrest, induction of apoptosis and autophagy in

cancer cells. It was demonstrated that the anticancer effect of HDACi depends on multiple factors such as cancer type, stage and the applied dosage.<sup>[81,82]</sup>

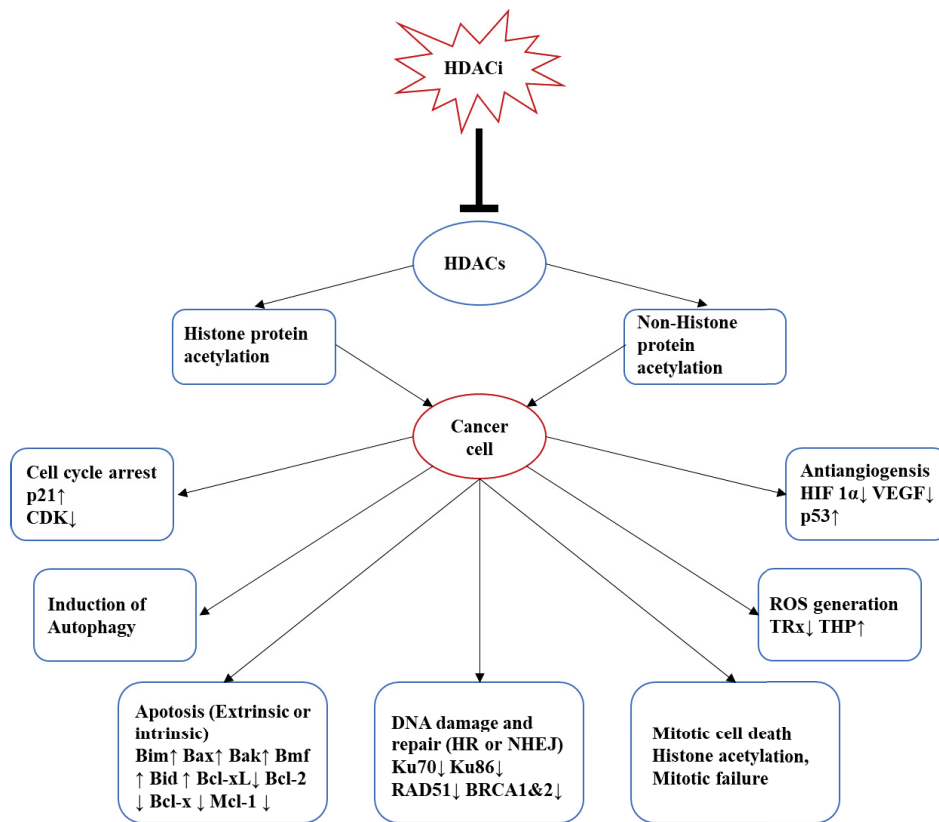


Figure 5: The effect of HDACi in cancer cells. Arrows (↑ and ↓) mark the in- and decrease of the respective protein.

Adverse effects of the currently approved HDACi are e.g. diarrhea, neutropenia, thrombocytopenia and cardiac toxicity.<sup>[83]</sup> In addition, hydroxamate-based HDACi exert potential mutagenetic effects caused by a Losson rearrangement. This reaction transforms the activated hydroxamate (e.g. via Acetyl-CoA) into its corresponding isocyanate which can form adducts with DNA.<sup>[84]</sup> The currently used pharmacophore model for HDAC inhibitors (HDACi) features the following three elements: a zinc binding group (ZBG), a linker, that mimics the acetyl-lysine motif and interacts with the substrate binding tunnel as well as a cap, also known as surface recognition domain. Nevertheless, this model is not fully applicable for inhibitors that target HDAC class-specific cavities, such as the side pocket (HDAC6 / HDAC8), the foot pocket (HDAC1-3) and the lower pocket (HDAC class IIa). Therefore, Melesina *et al.* proposed an extended HDACi pharmacophore model exhibiting six elements: ZBG, linker, S-cap (cap targeting the surface), SP-cap (cap targeting the side pocket), FP-group (foot pocket) and the LP-group (lower pocket).<sup>[85]</sup> These new pharmacophore models are relevant for the design of novel and selective HDAC inhibitors (Figure 6).

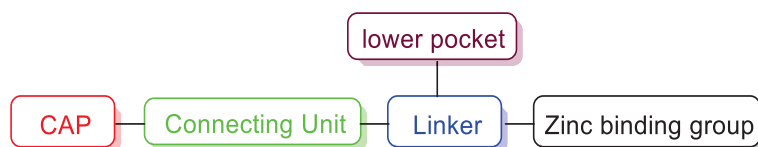


Figure 6: Pharmacophore model for class IIa selective HDAC inhibitors.<sup>[85]</sup>

Resistances to the currently approved HDACi are often observed and it was demonstrated that these inhibitors have limited therapeutic efficacy against solid tumors as single therapeutic agents.<sup>[86–88]</sup> However, the combination of HDACi with common chemotherapeutic drugs e.g. cisplatin, has displayed promising anticancer effects in both preclinical and clinical studies.<sup>[89]</sup> The employment of HDACi as chemosensitizers to increase the efficiency of other anticancer drugs has been shown to have a great potential for the treatment of a broad range of cancer types.<sup>[89,90]</sup>

In regard to the distinct tissue distribution and cellular localization of individual HDACs as well as their various implication in different cancer types, isozyme-selective HDACi may provide a wider therapeutic window and hence, less severe side effects. However, the therapeutic advantages of isozyme selective HDACs is not yet clinically confirmed and are still matter of current research.

### **Strategies for the development of isozyme-selective and/or complex-specific HDAC inhibitors**

The design of isozyme-selective HDAC inhibitors has proven to be challenging due to the high similarities in the structure of HDAC active sites.<sup>[91,92]</sup> A further challenge is that several HDACs are recruited to various large multi-subunit complexes such as CoREST complex (co-repressor of repressor element-1 silencing transcription factor)<sup>[93]</sup> and NuRD complex (nucleosome remodelling and deacetylase).<sup>[94,95]</sup> Moreover, multiple complexes may incorporate the same HDAC isozyme, yet have distinctive biological functions.<sup>[96]</sup> There are several strategies to develop isozyme-selective and/or complex-specific inhibitors.

Promising strategies to achieve selectivity among the HDAC isozymes are targeting the so-called selectivity pockets within the active site and/or the employment of selectivity directing ZBG.<sup>[97,98]</sup> Another approach to gain selectivity is to exploit the differences in the surface and around the rim of the active site of HDACs e.g. by modifications in the CAP region of the respective HDACi.<sup>[96]</sup> In addition, dual – or multitarget HDAC inhibitors have been emerged as a promising alternative to combination therapies. For instance, proteasome inhibitors

demonstrate synergistic activities with HDACi due to the simultaneous blockage of the ubiquitin degradation and aggresomal pathways.<sup>[99]</sup> RTS-V5, a dual HDAC-proteasome inhibitor, displays an inhibition against both HDAC6 and the chymotrypsin-like proteasome in the submicromolar range. It was shown that RTS-V5 induces e.g. apoptosis and autophagy in the acute lymphoblastic leukemia SEM cell line.<sup>[99]</sup>

Furthermore, addressing allosteric sites<sup>[100]</sup> or functional domains<sup>[101]</sup> of HDACs provide attractive strategies since these sites tend to be more diverse in the structure and sequence than the catalytic domain of HDACs. The design of a coupled inhibitor which targets both the allosteric and active sites on HDACs presents also a promising approach to achieve isozyme specificity. Such coupled inhibitors have been successfully employed in the inhibition of individual protein kinases.<sup>[102]</sup>

Another promising strategy is to block the formation of the respective HDAC complex through the disruption of protein-protein interfaces via protein-protein inhibitor (PPI).<sup>[96]</sup> Moreover, HDAC complexes that incorporate two distinct enzymatic activities provide the opportunity to develop dual inhibitors. The so called “dual warhead” inhibitors consist of two pharmacophores, connected via a short linker, address simultaneously both active sites within the same complex. 4SC-202 is a dual warhead LSD1-HDAC inhibitor that targets simultaneously HDAC and histone demethylase activities of the CoREST complex. It is currently investigated in clinical trials.<sup>[103]</sup>

To sum up, isozyme-selective and complex-specific inhibitors may be advantageous due to the more directed targeting compared to pan-HDACi and therefore may induce less severe side effects.

### **Combination therapy with HDACi for the treatment of cancer**

The application of platin-based anticancer agents represent a long-term success story in medicinal inorganic chemistry. For almost 40 years, platinum complexes persist among the most widely used chemotherapeutic drugs.<sup>[104]</sup>

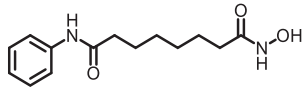
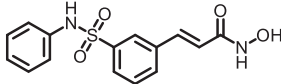
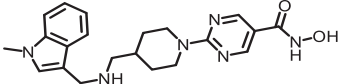
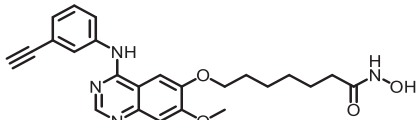
Cis-diamminedichloroplatinum(II) (cisplatin, CDDP) was first approved in 1976 and is currently employed as first-line therapy for the treatment of a variety of solid tumors, including head and neck, ovarian, bladder, testicular, cervical, lung and esophageal cancers.<sup>[105–107]</sup> CDDPs anticancer activity has been associated with the cross linkage of purine bases of the DNA, interfering with DNA repair mechanisms and the generation of DNA strand lesions. As a result,

the cell undergoes proliferative arrest and the induction of apoptosis.<sup>[108]</sup> Despite the initial therapeutic success, chemoresistance and numerous severe side effects such as decreased immunity to infections, gastrointestinal disorders and allergic reactions were reported.<sup>[108]</sup> CDDP-resistance is generally a result of a wide panel of genetic or epigenetic changes. Galluzzi *et al.* have classified these molecular mechanisms based on functional and hierarchical criteria. These modifications can (a) influence molecular mechanism that precede the actual binding of cisplatin to its targets (pre-target resistance) (b) enhance the capacity of the cells to repair the damage provoked by CDDP (on-target resistance) (c) diminish the lethal signaling pathways triggered by such molecular lesion (post-target resistance) (d) affect molecular circuitries that have not yet been directly linked with CDDP-elicited signals (off-target resistance).<sup>[109]</sup>

To overcome cisplatin resistance, great efforts have been made to develop and evaluate other platinum-containing drugs. So far, six platin-based anticancer agents are on the market.<sup>[104]</sup> Furthermore, combination therapies of cisplatin with other anticancer agents comprise a promising strategy to increase the efficacy of cisplatin and to overcoming resistances. The combination of HDACi with platinum-based chemotherapeutics has demonstrated encouraging results in both preclinical and clinical studies. For instance, in a phase I clinical study, the combination of belinostat with carboplatin showed no evidence of a drug-drug interactions.<sup>[110]</sup> A summary of HDACi as combination therapy with platinum-based chemotherapeutics in ongoing clinical trials is shown in Table 3.<sup>[89]</sup>

## Introduction

Table 3: Selected HDACi in combination with platinum-based chemotherapeutics, CP: clinical phase, NSCLC: Non-small cell lung cancerinoma.<sup>[89]</sup>

HDACi	Combination	Cancer type	CP
 Vorinostat (SAHA)	Carboplatin & paclitaxel	Advanced solid malignances	I
	Carboplatin, paclitaxel, placebo	NSCLC	II
	Carboplatin or paclitaxel	Advanced solid malignances	I
 Belinostat (PDX101)	Carboplatin and/or paclitaxel	Solid tumors	I
 Quisinostat (JNJ-26481585)	Paclitaxel	Ovarian	II
 CUDC-101	Cisplatin	Head and neck	I

In previous studies, the Kurz and Kassack groups identified a variety of HDACi exhibiting antiproliferative effects and HDAC inhibitory activity in the human ovarian cancer cell line A2780, the human squamous carcinoma cell line Cal27, and their cisplatin resistant sublines A2780CisR and Cal27CisR (Figure 7).<sup>[111–114]</sup> In addition, the most potent HDACi were evaluated in an HDAC isozyme-profiling. It was demonstrated that HDAC1/6 inhibitors reveal remarkable chemosensitizing properties.

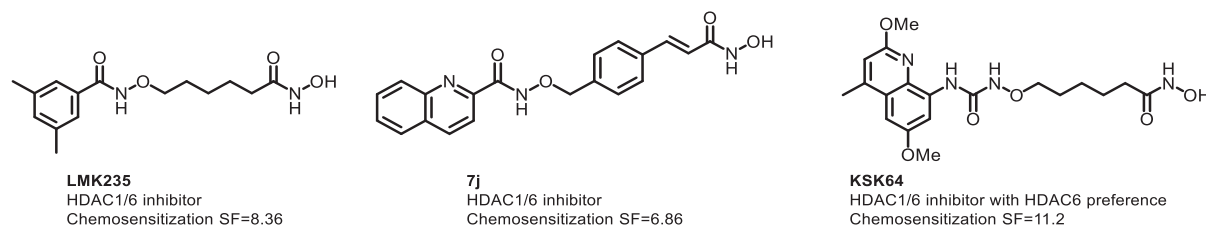


Figure 7: Selected HDACi from Kurz group displaying anti-proliferative and HDAC inhibition in A2780 and Cal27 as well as significantly enhanced cisplatin-induced cytotoxicity in a combination treatment mediated by increased apoptosis induction and caspase-3/7 activation.<sup>[111–114]</sup>

## **Recent advances in class IIa histone deacetylases research**

Published in: Bioorganic and Medicinal Chemistry

Impact Factor: 2.802 (2018-2019)

DOI: 10.1016/j.bmc.2019.115087

Contribution:

- Paragraph 1: Introduction
- Paragraph 4: Class IIa HDAC inhibitors



## Recent advances in class IIa histone deacetylases research

Yodita Asfaha<sup>1</sup>, Christian Schrenk<sup>1</sup>, Leandro A. Alves Avelar, Alexandra Hamacher, Marc Pflieger, Matthias U. Kassack<sup>\*,2</sup>, Thomas Kurz<sup>\*,2</sup>

Institut für Pharmazeutische und Medizinische Chemie, Heinrich-Heine-Universität Düsseldorf, Universitätsstr. 1, 40225 Düsseldorf, Germany



### ARTICLE INFO

#### Keywords:

Histone deacetylases  
Synthesis of HDACi  
Anticancer activity  
Neurodegenerative diseases  
Immune disorders

### ABSTRACT

Epigenetic control plays an important role in gene regulation through chemical modifications of DNA and post-translational modifications of histones. An essential post-translational modification is the histone acetylation/deacetylation-process which is regulated by histone acetyltransferases (HATs) and histone deacetylases (HDACs). The mammalian zinc dependent HDAC family is subdivided into three classes: class I (HDACs 1-3, 8), class II (IIa: HDACs 4, 5, 7, 9; IIb: HDACs 6, 10) and class IV (HDAC 11). In this review, recent studies on the biological role and regulation of class IIa HDACs as well as their contribution in neurodegenerative diseases, immune disorders and cancer will be presented. Furthermore, the development, synthesis, and future perspectives of selective class IIa inhibitors will be highlighted.

### 1. Introduction

Acetylation of the  $\epsilon$ -amino group of lysine residues is a fundamental post-translational modification of histones and cytosolic proteins. Lysine acetylation of histones catalyzed by histone acetyltransferases (HATs) leads to the relaxation of chromatin and consequently an increase in gene transcription. In contrast, histone deacetylases (HDACs) catalyze the opposite process thereby causing a condensation of chromatin.<sup>1</sup> HDACs are classically divided into four classes (Class I-IV) according to their yeast homologues. The classes I (HDAC1, 2, 3 and 8), II and IV (HDAC11) are zinc-dependent hydrolases whilst class III comprises NAD<sup>+</sup>-dependent hydrolases. Class II HDACs are further subdivided into class IIa (HDAC4, 5, 7, and 9) (Fig. 1) and class IIb (HDAC6 and HDAC10).<sup>2</sup> Class IIa HDACs have distinctive features separating them from other HDACs. Interestingly, nature is a vast source of HDAC inhibitors (HDACi) as shown by the approval of the depsipeptide romidepsin. Trichostatin A, a naturally occurring hydroxamate HDACi served as a lead compound for the development of the first approved HDACi vorinostat. Further, a large number of dietary compounds has been identified as HDACi.<sup>3</sup> This review summarizes current knowledge about the structure and mechanisms governing the activity of these

enzymes, and their involvement in pathological processes. Furthermore, potential targets for chemical intervention and the rational design of selective inhibitors for class IIa HDACs will be discussed.

#### 1.1. Structural features of class IIa HDACs

Class IIa HDACs are large enzymes (120–135 kDa) in comparison to the other zinc-dependent HDACs with the exception of HDAC6.<sup>4,5</sup>

Some recognition sequences are essential for their cellular distribution due to the presence of a nuclear localization signal (NLS). Another region of the enzyme bears a specific domain known to interact with different members of the MEF2 (myocyte enhancer factor-2) family. These interactions can influence different types of physiological processes ranging from development of myocytes and thymocytes to neuronal activity.<sup>5</sup> In various positions of the *N*-terminus of class IIa HDACs, specific serine residues are targeted by signal-dependent phosphorylation, a process which alters not only the interaction of the enzyme with other proteins, but also has a critical effect on their cellular localization.<sup>6</sup>

Similar to the *N*-terminus, the structure of the C-terminus is also involved in the cellular localization due to the presence of a NES

**Abbreviations:** cd, Catalytic domain; CD, cluster of differentiation; Cl<sub>int</sub>, intrinsic clearance; dr, diastereomer ratio; EDCl, 1-ethyl-3-(3-dimethylaminopropyl)-carbodiimide; EER, effective efflux ratio; GM-CSF, granulocyte colony stimulating factor; HDACi, histone deacetylase inhibitor; HIF-1- $\alpha$ , hypoxia induced factor 1- $\alpha$ ; MCF7, Michigan cancer foundation 7; M-CSF, macrophage colony-stimulating factor; MDCK, Madin-Darby Canine Kidney; N-CoR/SMRT, corepressor/silencing mediator for retinoid and thyroid; NES, nuclear export signal; NLS, nuclear localization signal; PPI, protein-protein interaction inhibitor; TF, transcription factor

\* Corresponding authors.

E-mail addresses: [matthias.kassack@uni-duesseldorf.de](mailto:matthias.kassack@uni-duesseldorf.de) (M.U. Kassack), [thomas.kurz@uni-duesseldorf.de](mailto:thomas.kurz@uni-duesseldorf.de) (T. Kurz).

<sup>1</sup> YA and CS share first authorship.

<sup>2</sup> MUK and TK share senior authorship.

<https://doi.org/10.1016/j.bmc.2019.115087>

Received 29 March 2019; Received in revised form 25 June 2019; Accepted 3 September 2019

Available online 06 September 2019

0968-0896/ © 2019 Elsevier Ltd. All rights reserved.

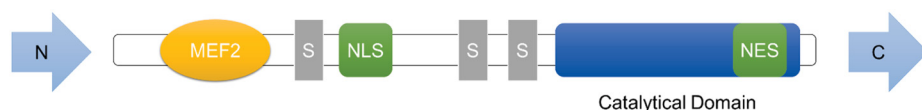


**Fig. 1.** Schematic view of class IIa structural domains. The catalytic domain is localized at the C-terminus (C), while the N-terminus (N) harbors a recognition sequence for the interaction with different types of proteins (e.g. gene expression repressors, transcription factors, etc.). MEF2, myocyte enhancer factor-2; S, serine residue (phosphorylation); NLS, nuclear localization signal; NES, nuclear export signal.

(nuclear export signal). The catalytic site of class IIa HDACs has limited deacetylase activity, despite of 57% sequence identity in the catalytic site compared to class I HDACs whereas the overall sequence identity is only around 29% (HDAC4 versus HDAC1).<sup>7</sup>

HDACs catalyze the hydrolysis of the N-acetyl amide group by activation of the carbonyl function with the zinc cation in the catalytic domain. This catalytic hydrolysis of the acetyl group is mediated by an aspartic acid (D)-histidine (H) dyad and a tyrosine (Y) residue which is also essential for the carbonyl activation.<sup>8</sup> However, in the catalytic center of class IIa HDACs, the Y residue is replaced by an H residue while the D-H dyads remain unchanged. This divergence (H976) dramatically decreases the deacetylase activity of class IIa HDACs compared to the other classes of zinc dependent HDACs.<sup>7</sup> Besides altering the enzymatic activity of class IIa HDAC enzymes, the H976 (HDAC4) residue renders the amino acid to assume two different conformations. In one of these conformations, the imidazole ring faces the lysine binding site (inward) similarly to the tyrosine residue present in the crystal structure of the gain of function mutant (H976Y), while in the other conformation, the imidazole faces the opposite direction (outward) resulting in the formation of a sub-pocket.<sup>9</sup>

## 2. Regulation of class IIa HDAC activity

### 2.1. Regulation of subcellular localization

Nucleo-cytoplasmic transport is an important mechanism how protein activity can be controlled. The functional and spatial division of eukaryotic cells is represented by the nuclear envelope that separates the cytoplasm from the nucleus.<sup>10</sup> Transport between these two compartments takes place through nuclear pores and is regulated by specific signals of the transport cargo and transport receptors.<sup>10</sup> Class I HDACs lack a NES and are therefore mainly restricted to the nucleus to fulfill their function as histone modifiers.<sup>11</sup> HDAC6 and HDAC10 as members of class IIb HDACs are predominantly localized in the cytoplasm due to a NES.<sup>12</sup> Recent studies have shown that HDAC10 acts as a polyamine deacetylase whereas HDAC11 was identified as a fatty acid deacetylase.<sup>13,14</sup> The highly dynamic localization within the cell is a hallmark of class IIa HDACs. They exhibit a NLS and a NES allowing them to shuttle between nucleus and cytoplasm (Fig. 2).

There are several kinases that are able to alter the balance between nuclear import and nuclear export of class IIa HDACs. Phosphorylation of HDAC 4, 5, 7, and 9 occurs at least at 3 conserved serine residues (HDAC4: Ser246, 467, 632; HDAC5: Ser259, 497, 661; HDAC7: Ser155, 178, 181, 321, 344, 446; 479, HDAC9: Ser220, 451, 611). Phosphorylation of these sites promotes the binding of 14-3-3 protein.<sup>15,16</sup> This can be associated with cytoplasmic localization of the HDAC enzyme either by masking the NLS, which blocks the interaction with importin  $\alpha$ , or unmasking the NES thereby promoting the interaction with chromosomal-region maintenance 1 (CRM1). This allows a quick and reversible adaptation of the cells to new environmental influences depending on the cellular demands.<sup>17</sup> The best studied kinase families known targeting class IIa HDACs are: Ca<sup>2+</sup>/calmodulin-dependent kinase families (CaMK), protein kinase D (PKD), microtubule affinity regulating kinase (MARK) and salt-inducible kinase (SIK1). The first kinases that have been reported to phosphorylate HDAC class IIa enzymes are CaMK I and CaMK IV.<sup>18–20</sup> McKinsey et al. demonstrated

that HDAC4 and HDAC5 respond to CaMK I signaling by translocation from the nucleus to the cytoplasm. They further pointed out that nuclear exclusion as a result of CaMK I signaling was not observed with HDAC1 and HDAC3. HDAC4 and HDAC5 have six consensus CaMK sites (Ser259, Ser279, Ser498, Ser661, Ser713, Ser736 in HDAC5). Only mutation of Ser259 and Ser498 to alanine led to a considerable reduction of CaMK I-mediated nuclear export of HDAC5. Mutation of both residues (Ser259/498 A) completely blocked the CaMK I-mediated nuclear export of HDAC5.<sup>18</sup> CaMK I also induced the nuclear export of HDAC7. The responsible amino acids are Ser178, Ser344 and Ser479.<sup>19</sup> CaMK IV is able to phosphorylate HDAC4, which also leads to cytoplasmic localization.<sup>20</sup> CaMK II was found to selectively induce phosphorylation of HDAC4 by binding to a unique docking site (R601) that is not present in other HDAC enzymes. This leads to the cytosolic accumulation of the protein.<sup>21</sup> Interestingly, a later study from the same working group showed that the subcellular localization of HDAC5 is also affected by CaMK II, although the unique docking site present in HDAC4 is missing. HDAC4 and HDAC5 can form homo- and heterooligomers by a conserved coiled-coil domain which is located near the amino-terminal end. Through direct binding with HDAC4, HDAC5 can be exported out of the nucleus, either by phosphorylation of HDAC4 or transphosphorylation of HDAC4 that is bound to CaMK II.<sup>22</sup> Further studies identified PKD as a kinase that directly phosphorylates the 14-3-3 binding sites of class IIa HDACs and leads to their cytoplasmic accumulation. The interaction of PKD and class IIa HDACs has been linked to B-cell receptor signaling,<sup>23</sup> T-cell apoptosis,<sup>24</sup> cardiac hypertrophy,<sup>25</sup> and mitogenic signaling.<sup>16</sup> Another kinase family that is associated with class IIa HDACs is the microtubule affinity regulating kinase (MARK). MARK 2 is expressed in the human heart, skeletal muscle and brain, where it causes microtubule disruption by phosphorylation of microtubule associated proteins.<sup>26</sup> It was initially identified as a class IIa HDAC kinase in a cDNA library expression screen.<sup>6</sup> This study further provided evidence that phosphorylation of class IIa HDACs may occur both *in vitro* and *in vivo*.<sup>6</sup> One of the upstream kinases of MARK is LKB1. It is involved in several stress responses, for example upon high osmolarity<sup>27</sup> and DNA damage.<sup>28</sup> It seems reasonable to suppose that class IIa HDACs are also involved in these stress responses. In fact, HDAC4 has also been implicated to play a role in the DNA damage response.<sup>29</sup> The fact that multiple kinase families phosphorylate class IIa HDACs, even multiple kinase isoforms within one family, suggests that these enzymes play a pivotal role in a variety of biological processes. The selectivity of some of these kinases towards specific members of class IIa HDACs or towards specific 14-3-3 sites further demonstrates the complexity. Multisite phosphorylation by one or more kinases might represent a mechanism to fine tune the regulation of distinct target genes in a highly orchestrated response to a specific signal. Since phosphorylation is a reversible posttranslational modification, it is thus not surprising that phosphatases can counteract the influence of these kinases on class IIa HDACs. Further studies have shown that PP1 $\beta$ , MYPT1 and PP2A indeed dephosphorylate members of class IIa HDACs and lead to their nuclear localization.<sup>30–32</sup> The nucleo-cytoplasmic transport is mainly dependent on phosphorylation and plays a major role in regulating the activity of class IIa HDACs. However, other posttranslational modifications of class IIa HDACs such as ubiquitination, sumoylation, acetylation and proteolytic cleavage also contribute to the regulation of class IIa HDAC activity and are reviewed

by DiGiorgio & Brancolini and Mathias et al.<sup>17,33</sup>

## 2.2. Catalytic activity

A unique property of HDAC class IIa enzymes is their highly reduced catalytic activity on acetyl-lysine compared to HDAC enzymes of class I and Iib.<sup>7</sup> This is due to a tyrosine to histidine substitution (Y976H) within the catalytic domain of class IIa HDACs. The tyrosine acts as transition state stabilizer of the catalytic reaction. Consequently, the H976Y mutant of HDAC4 results in a gain of function phenotype with a catalytic activity similar to class I HDAC enzymes.<sup>7</sup> So far no natural substrate of class IIa HDACs is known which raises the question about the importance of the catalytic activity for their biological function. A general notion is that they rather act as acetyl lysine recognition domains ("acetyl lysine readers") and exert their function within large multiprotein-complexes.<sup>34</sup> Within these complexes (e.g. HDAC3 and N-Cor/SMRT) they can make use of the deacetylase activity of other HDAC enzymes to modulate epigenetic changes.<sup>35</sup> The fact that the catalytic domain of class IIa HDACs is not necessarily required is also corroborated by a splice variant of HDAC9 (MTR – myocyte enhancer factor-2 interacting transcription repressor). This splice variant, lacking the catalytic domain, still maintains full transcriptional repressive function.<sup>36</sup>

## 3. Class IIa HDAC enzymes in human diseases

Class IIa HDACs are not only contributing to cancer, (auto)immune- and neurological disorders but also play a role in diabetes and muscle degenerative diseases.<sup>37,38</sup> HDAC5 is of particular importance in diabetes. It regulates GLUT4 expression which is critically involved in the resistance to insulin.<sup>37</sup> Neurogenic muscle atrophy is the result of dead or dysfunctional motor neurons and muscle fibers or alterations in neuromuscular junctions. HDAC4 and HDAC5 are involved in the execution of the muscle atrophy program by regulation of the transcription factor myogenin.<sup>39</sup> As briefly described in these few citations, class IIa HDACs play an important role in diabetes and muscle degenerative diseases. However, the focus of this review and in particular of this chapter is the involvement of class IIa HDACs in neurological disorders, immune disorders and cancer.

### 3.1. Neurological disorders

HDAC class IIa enzymes have been well studied in the physiological and pathological context of neuronal development and function. HDAC4 is highly expressed in neurons, predominantly localized in the cytoplasm and is involved in synaptic plasticity and memory formation.<sup>40–41</sup> Several reports have shown that chromosomal microdeletions and point mutations of the HDAC4 gene play an important role in brachydactyly mental retardation syndrome (BDMR).<sup>42–44</sup> BDMR patients suffer from developmental delays, intellectual disabilities, behavioral abnormalities, craniofacial and skeletal abnormalities.<sup>42</sup> One clinical study revealed that the expression level of HDAC4 mRNA inversely correlated with the phenotype of BDMR syndrome. Low expression led to more severe symptoms.<sup>43</sup> Another clinical study from Villavicencio-Lorini et al. pointed out that haploinsufficiency of HDAC4 also contributes to the BDMR syndrome phenotype.<sup>44</sup> Another neurological disorder that is related to HDAC4 is Huntington's disease.<sup>45</sup> It is caused by an increased number of CAG repeats within the exon 1 of the Huntingtin (HTT) gene compared to the wild type situation. The resulting prolonged polyglutamine (polyQ) stretch in HTT has the tendency to self-aggregate, leading to misfolded proteins and ultimately to neuronal dysfunction and cell death. Mielcarek et al. have shown in R6/2 mice that HDAC4 co-localizes with huntingtin in the cytoplasm.<sup>45</sup> HDAC4 was able to interact with mutant huntingtin (mutant exon 1) in a polyQ-dependent manner. A reduction of HDAC4 protein reduced the HTT aggregation process. This led to the rescue of neuronal synaptic

function and an increased survival in the Huntington's disease mouse models.<sup>45</sup> HDAC5 is involved in the axon regeneration by tubulin deacetylation upon axon injury. Interaction with protein kinase C leads to activation of HDAC5 which results in tubulin deacetylation of the peripheral neurons.<sup>46</sup> Furthermore, the calcium- and protein kinase C dependent nuclear export of HDAC5 leads to an increase in histone acetylation, reinstating the transcription of pro-regenerative genes.<sup>47</sup> HDAC7 has been reported to protect cerebellar granule neurons (CGNs) from apoptosis. This neuroprotective function is independent of the deacetylase activity and involves inhibition of c-jun expression.<sup>48</sup> HDAC9 has been linked to schizophrenia. In a small proportion of schizophrenia patients, HDAC9 is hemizygotously deleted.<sup>49</sup> Lang et al. also found out that HDAC9 is widely expressed in areas of the mouse brain which are associated with schizophrenia. Of note, HDAC9 was expressed exclusively in post-mitotic and mature neurons which indicates an important role in the function of neurons in the mature brain.<sup>50</sup>

### 3.2. Immunological role

The engagement of HDACs in the immune system has been intensively studied over the past decade. A prominent example is HDAC7. It is highly expressed during the development of CD4+ CD8+ thymocytes. Within the nucleus, it represses transcription of the orphan nuclear receptor Nur77. Nur77 has pro-apoptotic functions and is involved in negative T cell selection.<sup>51</sup> Upon T cell activation, HDAC7 becomes phosphorylated via protein kinase D1 and is transported into the cytoplasm. This results in a derepression of Nur77 and an induction of apoptosis.<sup>52</sup> In another study, conditional knockout mice showed a reduced survival or positive selection of CD4+ lymphocytes upon deletion of HDAC7 in double positive thymocytes. This was accompanied by the nuclear export of HDAC7.<sup>53</sup> Consequently, a nuclear export deficient mutant of HDAC7 lacking the phosphorylation sites (HDAC7-ΔP; S155A; S358A; S486A) blocked negative thymic selection, but was still able to go through positive selection. This led to the escape of autoreactive T cells to the periphery and correlated with the development of lethal multi-organ autoimmunity.<sup>54</sup> More recently, the same laboratory conducted a study on the effects of HDAC7 on natural killer T (NKT) cells. Again using the HDAC7-ΔP mutant, they showed that NKT development is impaired and conversion to naïve-like T cells is initiated. Moreover, they could establish a connection between these events and tissue specific autoimmunity.<sup>55</sup> Azagra et al. demonstrated that HDAC7 is required for B lymphocyte identity and development. By using a conditional knockout mouse model, this study showed that deletion of HDAC7 represses early B cell development and leads to lymphopenia in peripheral organs.<sup>56</sup>

With one of the first selective class IIa HDACi (TMP195) in hand, Lobera and colleagues could establish a link towards monocyte differentiation. They used phytohemagglutinin (PHA) stimulated PBMC cells and purified T cells (CD3+), B cells (CD19+) and monocytes (CD14+). These cells were then separately treated with TMP195. T cells and B cells were considerably less sensitive than monocytes (17 and 36 genes regulated vs. 587 genes). Genes affected by class IIa HDAC inhibition included chemokines and genes associated with immune response.<sup>57</sup> Further investigations led to the discovery that TMP195 treatment induced an anti-tumor macrophage phenotype. It induced the recruitment of phagocytic macrophages, thereby changing the tumor microenvironment of a mouse model of breast cancer.<sup>58</sup> This study provided a first hint that inhibiting class IIa HDACs can be used to modulate the immune system to create an anti-tumor response.

### 3.3. Cancer

There is emerging evidence that HDAC class IIa is also involved in cancer. Kao and colleagues reported that reduced expression of HDAC4 via RNAi leads to a decrease in cell viability in HeLa cells.<sup>29</sup> They

further demonstrated that HDAC4 and the tumor suppressor p53 co-localized upon DNA damage. By immunoprecipitation experiments, they could show a direct interaction between HDAC4 and p53.<sup>29</sup> However, there are also studies reporting the opposite effect of HDAC4. In urothelial cancer cells, HDAC4 expression rather impedes proliferation, and HDAC4 inhibition did not reduce cell growth.<sup>59</sup> Another study from Geng et al. showed that irradiation (IR) leads to the translocation of cytoplasmic HDAC4 into the nucleus in human non-small cell lung cancer cell lines H23 and H460. Treatment with the pan-HDACi panobinostat counteracted IR induced nuclear localization of HDAC4. Moreover, the administration of panobinostat prior to irradiation (IR) increased the duration of  $\gamma$ -H2AX foci.<sup>60</sup> It is intriguing to speculate whether inhibition of HDAC4 leads to cytoplasmic localization, thereby interfering with the DNA damage response. These studies are now possible due to availability of highly selective class IIa HDAC inhibitors and need to be performed to shed light on the possible involvement of HDAC4 in the described effects of panobinostat. Another possible explanation for nuclear export of HDAC4 by panobinostat could be the inhibition of nuclear interaction partners like HDAC3. One study demonstrated a NLS-independent nuclear import of HDAC4. A mutant comprising aa1-208 was directed to the nucleus due to its interaction with the transcription factor MEF2.<sup>61</sup> Studies from Stronach et al. showed that there is a connection between the resistance of platinum-based DNA damaging drugs and the expression of HDAC4.<sup>62</sup> They analyzed 16 paired tumor biopsies of ovarian cancer, that were taken prior and after the development of platinum resistance. 44% showed a significant increase in HDAC4 expression in the platinum-resistant biopsies. They also shed some light on the molecular mechanism by linking the acetylation status of STAT1 to the protein level of HDAC4. STAT1 is activated by phosphorylation at Y701 and is transported into the nucleus when platinum-resistant cells were treated with cisplatin. Silencing of HDAC4 increased acetylation of STAT1, counteracting its platinum-induced activation and restored sensitivity towards cisplatin in ovarian cancer cells.<sup>62</sup> Another study by Cadot and colleagues investigated cell cycle progression upon knockdown and knockout of HDAC4 in tumor and normal cells. The knockdown in HeLa cells led to mitotic arrest subsequently leading to apoptosis. Chromosome segregation defects were only present in p53 deficient cells.<sup>63</sup> There are also p53-independent mechanisms how class IIa HDACs can contribute to cancer cell growth by upregulation of the cyclin-dependent kinase inhibitor p21<sup>WAF1/CIP1</sup>. siRNA mediated silencing of HDAC4 led to an increase in p21<sup>WAF1/CIP1</sup> expression in a variety of cancer cell lines. Repression of p21<sup>WAF1/CIP1</sup> by HDAC4 was dependent on the interaction with the transcription factor Sp1, which was then recruited to the Sp1/Sp3 binding site of the p21<sup>WAF1/CIP1</sup> promoter.<sup>64</sup> Because HDAC4 is enzymatically "silent", additional binding partners might contribute to suppress p21<sup>WAF1/CIP1</sup> expression. One possibility might be the recruitment of transcriptional corepressor complexes like HDAC3-NCoR/SMRT with catalytic activity.<sup>35</sup> In this case, another study indeed demonstrated that HDAC4 associates with the HDAC3-NCoR/SMRT complex to repress p21<sup>WAF1/CIP1</sup> expression in colon cancer cells.<sup>65</sup> In 2004, two different working groups have simultaneously identified a caspase cleavage site (Asp289) within the amino acid sequence of HDAC4.<sup>66,67</sup> Upon caspase cleavage of HDAC4, the amino-terminal part of HDAC4 accumulates in the nucleus, eventually triggering cytochrome c release and caspase-9 dependent apoptosis.<sup>66</sup> The amino-terminal part of HDAC4 lacking the MEF2 binding site (HDAC4/1-165) indicated that repression of MEF2 was necessary for the proapoptotic function. The interaction of HDAC4 with MEF2 has also been shown to induce cell transformation and tumorigenesis.<sup>68</sup> By mutational studies the authors proved that nuclear localization as well as an intact MEF2 binding site are crucial for the transforming activity of HDAC4. A more recent publication links nuclear HDAC4 to p53-dependent senescence in fibroblasts favoring cell transformation.<sup>69</sup> HDAC7 like HDAC4 has an oncogenic potential.<sup>68</sup> High HDAC7 expression in lung cancer correlates with poor patient survival. In lung cancer cells, HDAC7 promoted

tumorigenesis by deacetylation of STAT3 resulting in an inhibition of STAT3 activation.<sup>70</sup> Similar to HDAC4, HDAC7 has a caspase cleavage site (D375) that is a target for caspase-8. Although proteolytic cleavage of HDAC7 was also accompanied by altered subcellular localization of the two resulting fragments and repression of MEF2, a proapoptotic effect in cancer cells like HDAC4 has not been described until now.<sup>71</sup> HDAC5 has been linked to cancer-related processes like angiogenesis. Recent evidence suggests that overexpression of HDAC5 is involved in the proliferation, invasion and survival of lung cancer cells.<sup>72</sup> Other studies observed the opposite effect in osteogenic sarcoma cells, neuroblastoma and breast carcinoma cells where HDAC5 overexpression led to growth suppression and spontaneous apoptosis that was associated with the activation of tumor necrosis factor death receptor pathway.<sup>73</sup> Another study showed that estrogen receptor positive tamoxifen-resistant MCF7-TamC3 breast cancer cells exhibit an increased expression of HDAC2 and HDAC5 compared to parental MCF7 tamoxifen-sensitive cells. In this case an increased expression of HDAC5 was associated with downregulation of the tumor suppressor miR-125a-5p and the upregulation of the anti-apoptotic protein survivin. Of note, in tamoxifen-treated ER<sup>+</sup> breast cancer patients, low expression of miR-125a-5p correlates with poor overall survival.<sup>74</sup> Since the expression of class IIa HDACs is rather tissue-specific, it is likely that the cellular response to HDAC5 overexpression (or knockdown) varies depending on the cellular origin. To a lesser extent, HDAC7 and HDAC9 have been described in cancer-related processes. As with HDAC5, HDAC7 has been linked to angiogenesis. Silencing of HDAC7 in endothelial cells led to upregulation of the platelet-derived growth factor-B (PDGF-B) and platelet-derived growth factor-receptor beta (PDGFR-beta), which changed migration properties and therefore affected angiogenesis.<sup>75</sup> High levels of cytoplasmic HDAC7 expression were shown in pancreatic tumors.<sup>76</sup> Poor prognosis in childhood acute lymphoblastic leukemia (ALL) has also been linked to high levels of HDAC7 and HDAC9 expression.<sup>77</sup> HDAC7 affects cancer cell proliferation in various tumor cell lines by upregulation of the proto-oncogene c-Myc and downregulation of the cell cycle regulators p21 and p27. Knockdown of HDAC7 led to cell cycle arrest and cellular senescence.<sup>78</sup> B-cell malignancies on the other hand show low expression of HDAC7. Overexpression of HDAC7 in these cells leads to downregulation of c-Myc and promotes apoptosis.<sup>79</sup> Overexpression of HDAC9 mRNA and protein level has been implicated as a negative prognostic marker in breast cancer, lymphoma and osteosarcoma.<sup>77,80-82</sup> In breast cancer cells, high levels of HDAC9 led to a decrease in apoptosis and increased proliferation. This was associated with deregulation of CDKN1A, BAX and TNFRSF10A genes. In these tumors, the efficacy of HDACi to reduce cell proliferation and CDKN1A expression was impaired. In a genetically engineered mouse model that constitutively expressed a HDAC9 transgene during B-cell development, Gil and colleagues showed that these mice developed splenic marginal zone lymphoma and lymphoproliferative disease. Further analysis suggested that, by altering pathways involved in growth and survival mainly by modulation of BCL6 and p53 activity, HDAC9 might contribute to lymphomagenesis.<sup>83</sup> Four HDACi have been approved for cancer therapy by the food & drug administration (FDA). However, these HDACi have common side effects that are linked to their inhibitory activity against multiple HDAC enzymes across several classes. Therefore, the focus of current research is to identify novel compounds selective for single HDAC enzymes or classes to reduce side effects and maintain the anti-tumor activity of pan HDACi. This further demonstrates the need for studies to develop new selective class IIa HDACi.

#### 4. Class IIa HDAC inhibitors

In the 1990s, Jung et al. introduced a pharmacophore model of HDAC inhibitors (HDACi), which has been facilitating their rational design.<sup>84-86</sup> The currently used and widely accepted pharmacophore model features the following three elements: a zinc binding group

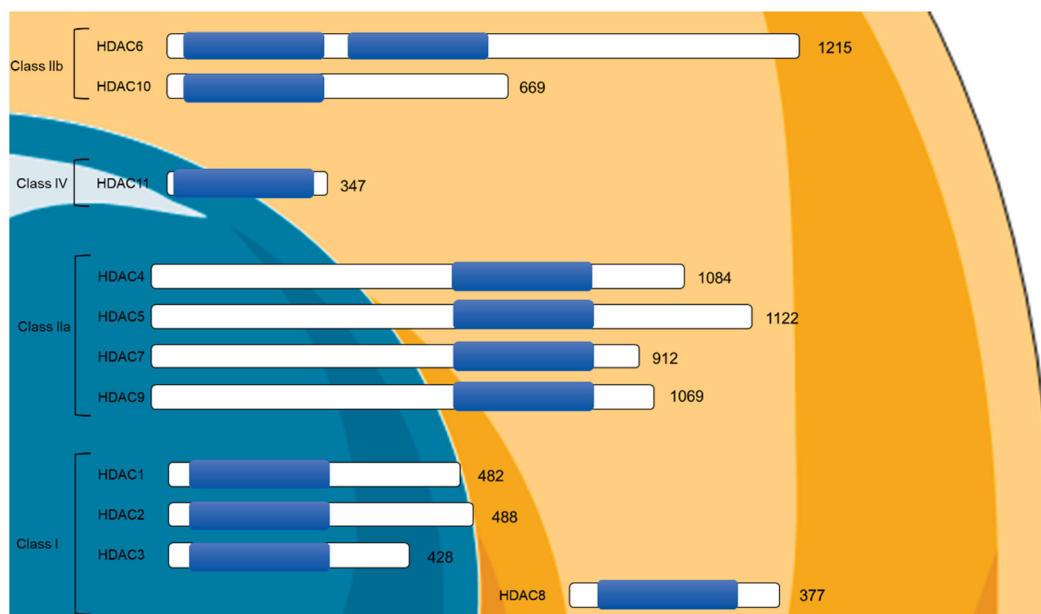


Fig. 2. Cellular localization of zinc dependent-HDACs. Light blue background indicates the nucleus whereas yellow background reflects the cytosol. The depicted dark blue bars represent the catalytic domain within the amino acid sequence (white bars). Numbers indicate the length of the amino acid sequence.

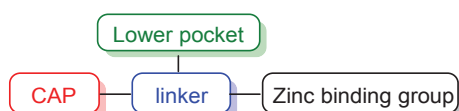


Fig. 3. Pharmacophore model for class IIa HDACi.<sup>87</sup>

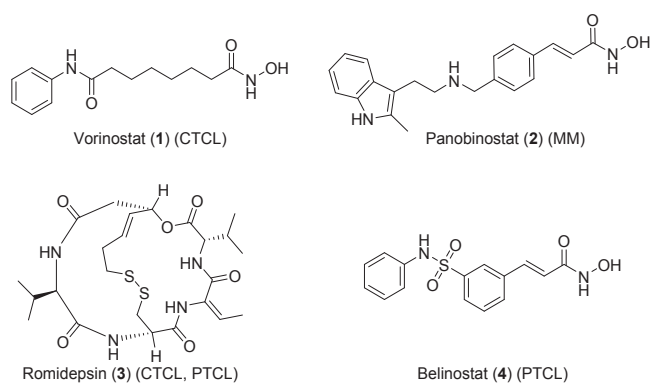


Fig. 4. Chemical structures of FDA approved HDAC inhibitors 1–4 and their indications. CTCL: cutaneous T-cell lymphoma, MM: multiple myeloma, PTCL: peripheral T-cell lymphoma.<sup>99–102</sup>

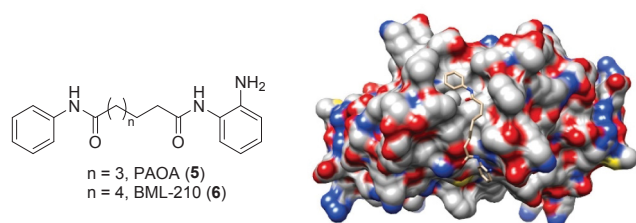


Fig. 5. Chemical structures of PAOA (5) and BML-210 (6) (left). A surface representation of the binding mode of BML-210 (6) in the hydrophobic pocket of MEF2A (PDB:3MU6) (right)<sup>113</sup>

(ZBG), a linker, that mimics the acetyl-lysine and interacts with the substrate binding tunnel and a cap, also known as surface recognition domain.

However, this model is not fully applicable for inhibitors that addresses cavities besides the main pocket, such as the side pocket, the foot pocket and the lower pocket. Therefore, Melesine et al. proposed an extended HDACi pharmacophore model exhibiting six elements: ZBG, linker, S-cap (cap targeting the surface), SP-cap (cap targeting the side pocket), FP-group (foot pocket) and the LP-group (lower pocket).<sup>87</sup> In Fig. 3 the pharmacophore model for class IIa HDACi is illustrated. This new pharmacophore model is relevant for the design of novel and selective inhibitors. HDAC inhibitors can be unspecific for a certain isozyme (pan-inhibitors) or selective for a specific HDAC subtype (isozyme-selective).

Important inhibitor classes are hydroxamic acids, cyclic peptides and depsipeptides, thiols, carboxylic acids, *o*-amino anilides and TFMO-containing inhibitors.<sup>88–90</sup> Due to their strong chelation ability the hydroxamic acid group is the most frequently used ZBG. Trichostatin A (TSA) was the first natural hydroxamate that has been shown to inhibit HDACs.<sup>91</sup> TSA was isolated from the culture broth of *Streptomyces hygroscopicus* as an antifungal agent against *Trichophyton* species.<sup>92,93</sup> With TSA as lead structure, vorinostat (SAHA) (1), a pan inhibitor, was developed and represents the first FDA approved HDACi.<sup>91,94,95</sup>

In 2012, our groups published the synthesis and biological evaluation of vorinostat analogues with a novel connecting unit linker region.<sup>96</sup> The frontrunner of this study (termed 19i or LMK235) exhibited superior effects over vorinostat against chemoresistant cancer cells. In our initial publication, 19i (LMK235) was described as a class IIa (HDAC4, HDAC5) selective HDACi. Since further studies on 19i (LMK235) have rather suggested vorinostat-like HDAC inhibition properties, the HDAC inhibitory profiles of 19i (LMK235) were re-assessed using current state *in vitro* assays including reference compounds not available in 2012. The new results revealed a class I and class IIb selective profile for 19i (LMK235).<sup>59,97</sup>

The cyclic peptide HDACi are structurally complex and include the natural product romidepsin (FK228) (3).<sup>98</sup> This disulphide prodrug is reductively activated *in vivo* and exhibits a thiole group as ZBG. The above-mentioned compounds as well as panobinostat (LBH589) (2) and belinostat (PXD101) (4) are approved by the FDA for the treatment of

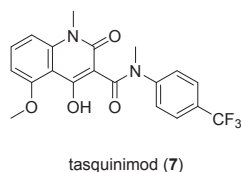


Fig. 6. Chemical structure of tasquinimod (7).

specific types of blood cancer (Fig. 4).<sup>99–101</sup>

However, drawbacks of the currently approved HDACi are e.g. ineffectiveness in solid tumours and cardiac toxicity. To overcome these side effects and increase their potency, there are two strategies: (i) Target preference: designing and developing HDACi with high potency and selectivity (ii) Selective delivery: release of drug at target of interest.<sup>103</sup>

In this review we will focus on the design of class IIa specific HDACi. Nevertheless, it is still not clear whether the inhibition of a specific HDAC isoform will have a clinical benefit.<sup>104</sup> Currently, there are two promising approaches for the design of specific HDACi for class IIa:<sup>105</sup>

- Targeting the *N*-terminal region and the interaction with client proteins
- Targeting the catalytic site

Despite the lower deacetylation activity of all class IIa HDACs compared to other zinc dependent HDACs, targeting the catalytic domain could have an impact on the interaction with other proteins. Targeting the protein–protein interaction (PPI) directly is more challenging due the large and flat size of the PPI interface compared to targeting the well-defined pockets.<sup>106</sup> As described above, class IIa's regulatory *N*-terminus interacts with client proteins such as the transcription factor MEF2A–D. MEF2 plays a key role in the development of the adaptive response in many tissues and organs. Class IIa HDACs do not interact directly with DNA but need to bind to the sequence-specific MEF2 for genomic targeting.<sup>61,107</sup> Moreover, many biological functions of class IIa are referred to MEF2 transcriptional repression.<sup>15,108,109</sup> It was shown that a single knock-out of class IIa HDACs in mice results in a phenotypic change due to MEF2 over activation in bone (HDAC4), heart (HDAC5/9) and cardiovascular system (HDAC7).<sup>6,25,110</sup> Crystallographic analysis and *in vitro* biochemical studies revealed that the amphipathic helix, conserved in the *N*-terminus of class IIa HDAC, interacts with the highly conserved hydrophobic channel on the MADS-is/MEF2 domain of MEF2.<sup>111,112</sup> Jayatilaka et al. identified and characterized small molecules that inhibit the interaction between MEF2 and class IIa HDACs by binding directly to the MADS-box domain of MEF2 and thereby block the recruitment of class IIa HDACs.<sup>113</sup> By performing virtual screening of the ZINC-database and using the crystal structure of the HDAC9:MEF2, BML-210 (6) and PAOA-like compounds (5) were determined as potential PPIs. In Fig. 5, the structural characterization of the binding mode of BML-210 (6) to MEF2A is shown. The aliphatic chain binds between helix H2 of the two MEF2 monomers and the phenyl group interacts with the hydrophobic pocket formed by Leu66, Leu67 and Thr70 from each monomer. The 2-aminophenyl group is involved in several hydrophilic interactions with Asn73, Gln56, Asp51 and Asp63 (prime sign indicates residues from the other monomer)

These PPI inhibitors were originally discovered as class I HDAC inhibitors leading to acetylation of histone but not tubulin.<sup>114,115</sup> Moreover, it was reported that in several leukaemia cell lines BML-210 (6) induces growth inhibition and apoptosis.<sup>116</sup> Further studies are necessary to clarify whether the anti-tumor effect of BML-210 (6) and its analogues is due to the interaction with MEF2 or other pathways. Furthermore, these PPIs can be used as leads to improve their selectivity and to develop epigenetic therapies against diseases in which the dysregulation of MEF2 and class IIa HDACs play a key role.

In 2013, Issacs et al. identified tasquinimod (7) as a negative allosteric modulator of HDAC4 ( $K_d = 10–30$  nM) that interacts with the carboxamide moiety at the zinc binding domain of HDAC 4 (Fig. 6).<sup>117</sup> Tasquinimod (7) is used as an anti-angiogenic drug for the treatment of advanced castration-resistant prostate cancers (CRPC).<sup>118,119</sup> It was reported that tasquinimod (7) stabilizes the inactive form of HDAC4 (open conformation) and thereby causing a conformational change in the binding pocket. As a result, the HDAC4/*N*-CoR/HDAC3 complex formation, the colocalization of *N*-CoR/HDAC3, the deacetylation of histones and HDAC4 client transcription factors (e.g. HIF-1 $\alpha$ ) are inhibited. These client TFs are bound to promoters/enhancers where epigenetic reprogramming takes place for cancer cell survival and angiogenic response.<sup>120</sup> In this way, tasquinimod (7) blocks the angiogenic switch.<sup>118</sup>

In 2008, P. Jones et al. reported, a series of 2-trifluoroacetylthiophenes as potent and selective class II histone deacetylase inhibitors.<sup>121</sup> A screening of a compound library against wt and a gain-of-function (GOF, H976Y) mutant of HDAC4 revealed ethyl-5-(trifluoroacetyl)thiophene-2-carboxylate as a potent class II inhibitor. Based on this compound, a series of 5-(trifluoroacetyl)thiophene-2-carboxamides was developed that showed 10-fold selectivity for HDAC4 and HDAC6 over class I HDACs. These inhibitors consist of three structural elements:

- trifluoroacetyl group that binds to the zinc ion in a bidentate manner (hydrate)
- 2,5-disubstituted thiophene scaffold as a linker
- amide group attached to cap-group that interacts with the surrounding residues.

Compound 8 was identified as a modest inhibitor of HDAC4 (GOF/WT  $IC_{50} = 370/320$  nM). The inhibition profile of compounds 8 is given in Table 1.<sup>121</sup>

Table 1  
 $IC_{50}$  values of compound 8 against selected HDAC enzymes of class I, IIa and IIb.<sup>121</sup>

Enzyme	Cpd. 8 $IC_{50}$ [nM]
HDAC4 WT	320
HDAC4 GOF <sup>a</sup>	370
HDAC1	5550
HDAC3	44% inh at 5 $\mu$ M
HDAC6	310

<sup>a</sup> Gain of function mutant H976Y.

The X-ray crystal structure of HDAC4WT with inhibitor 8 verified that this compound binds in its hydrated form in the catalytic center (Fig. 7). These oxygen-zinc bonds are in the range of 2.04–2.4 Å. Moreover, a water molecule mediates a hydrogen bonding between the inhibitor and Gly945 of the active site. This water molecule might be

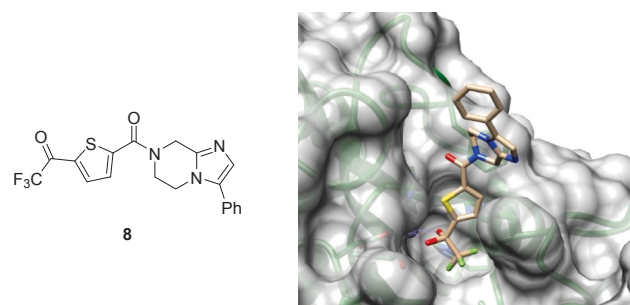


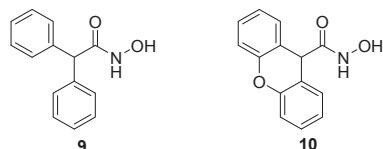
Fig. 7. Chemical structure of compound 8 (left). X-ray crystal structure of 8 bound to HDAC4 WT catalytic domain (PDB: 2VQJ) (right).<sup>121</sup>

important to stabilize the transition state during the deacetylation.<sup>121</sup>

The first potent class IIa HDACi, a series of diphenylmethyle hydroxamic acids, were reported in 2009 by the Besterman group.<sup>122</sup> *N*-hydroxy-2,2-diphenylacetamide (**9**) and *N*-hydroxy-9H-xanthene-9-carboxamide (**10**) displayed activities in the sub-micromolar range (Table 2). The rigidified oxygen analogue **10** of compound **9** showed comparable HDAC 4 and 5 inhibitory activities, but marginally higher selectivity for HDAC7. Both inhibitors **9** and **10** were synthesized by the conversion of commercially available carboxylic acids to hydroxamic acids by coupling the appropriate acid with hydroxylamine.

**Table 2**

IC<sub>50</sub> values of compound **9** and **10** against HDAC4, 5 and 7.<sup>122</sup>



Enzyme	Cpd. <b>9</b> IC <sub>50</sub> [μM]	Cpd. <b>10</b> IC <sub>50</sub> [μM]
HDAC4	0.75	0.25
HDAC5	0.14	0.11
HDAC7	0.39	0.05

In our performed docking studies (PDB:6FYZ)<sup>123</sup>, we could demonstrate that the xanthene derivative **10** provided the required 3D-geometry to fit into the catalytic site of class IIa HDACs (Fig. 8).

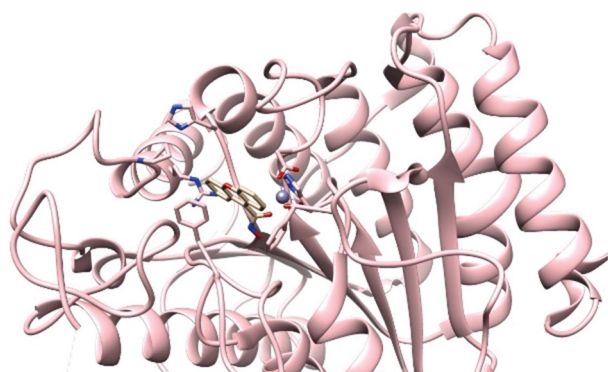
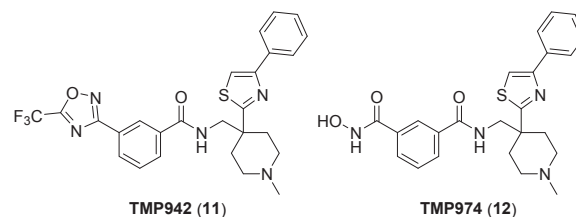


**Fig. 8.** The docking poses of the xanthene derivative **10** in the binding site of HDAC4. (PDB:6FYZ)<sup>123</sup>

In 2013, *Lobera et al.* described eleven selective class IIa HDAC inhibitors with a trifluoromethyloxadiazolyl group (TFMO) as a novel ZBG.<sup>124</sup> The IC<sub>50</sub> values of these eleven TFMO derivatives in comparison to their hydroxamate analogues revealed that the TFMO moiety is preferred by class IIa HDACs (150-10000-fold), HDAC8, **10** and **11** were indifferent, whereas HDAC6 preferred hydroxamic acids (10-fold) (Table 3).

**Table 3**

Calculated K<sub>i</sub> values for TMP942 (**11**) and TMP974 (**12**).<sup>124</sup>



Enzyme	K <sub>m</sub> [μM]	TMP942 ( <b>11</b> ) K <sub>i</sub> [μM]	TMP974 ( <b>12</b> ) K <sub>i</sub> [μM]
HDAC4	55.8	0.075	23.8
HDAC5	67.1	0.182	24.3
HDAC7	63.5	0.039	3.94
HDAC9	6.7	0.008	5.98
HDAC1	15.2	> 23	11.9
HDAC2	11.6	> 19	> 19
HDAC3	37.5	> 43	> 43
HDAC6	14.1	2.81	0.189
HDAC8	6.35	7.66	1.33
HDAC10	5.6	> 10	> 10
HDAC11	11.7	> 19	> 19

A crystallographic analysis confirmed that the TFMO group acts as a non-chelating ZBG which interacts by one of the fluorine atoms and its oxygen with the active Zn<sup>2+</sup> atom in the catalytic center (Fig. 9). It is suggested that a class IIa selectivity is the result of the bulkiness but modest zinc binding ability of the TFMO-group as well as the U-shaped conformation of these inhibitors. Due to the weak electrostatic interaction of the ZBG with the metal ion, it is assumed that the TFMO series has fewer pan-inhibitor associated off-targets effects. Compared to the structurally related trifluoromethylketone series by *Bottomley et al.*, the TFMO series are chemically more stable due to the rigid ring-structure.<sup>9</sup>

TMP269 (**13**) was synthesized according to Scheme 1–3 in a convergent synthesis.<sup>124</sup> In the first step, the Hantzsch thiazole synthesis was performed to obtain **16**. Under basic conditions, compound **16** was reacted with 1,2-bis-(2-bromoethoxy)ethane. Subsequently, the terminal nitrile **17** was reduced to its corresponding amine **18**.

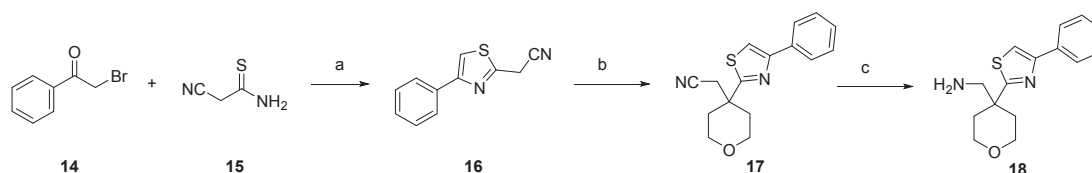
The TFMO moiety was obtained by converting the benzonitrile **19** to an amidoxime **20** which was cyclized with trifluoroacetic anhydride (Scheme 2).

In the final step, the acid **21** was coupled with amine **18** to obtain TMP269 (**13**) (Scheme 3).

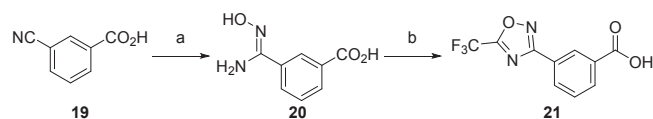
In cell-based assays, it was reported that the class IIa selective inhibitors did not induce cell death and apoptosis in contrast to the class I and pan inhibitors. Gene expression profiling of PHA-activated human peripheral blood mononuclear cells (PBMC) revealed that TMP195 had barely an impact on gene expression (regulates 76 genes), whereas SAHA regulates the expression of 4556 genes.<sup>125</sup> These differences raise the question whether class IIa HDACs are classical epigenetic enzymes altering the condensation state of chromatin and gene expression. However, the effect of TMP195 on monocytes was remarkable (regulation of 587 genes). The inhibitor induces monocyte responses to mitogen (PHA), M-CSF and GM-CSF, which is a proof that the function of



Fig. 9. Chemical structure of TMP269 (13) (left). Binding mode of TMP269 (13) in HDAC7. (PDB:3ZNR) (right)<sup>124</sup>



Scheme 1. Synthesis of amine 18. Reagents and conditions: a) EtOH, 80 °C, 4 h, 75%; b) (i) NaH, THF, 0 °C, 30 min, (ii) 1,2-bis-(2-bromoethoxy)ethane, THF, rt, 1 h, 85% c) LiAlH<sub>4</sub>, THF, 0 °C – rt, 1 h, 37%.



Scheme 2. Synthesis of the TFMO moiety. Reagents and conditions: a) 8-hydroxyquinoline, NH<sub>2</sub>OH·HCl, Na<sub>2</sub>CO<sub>3</sub>, EtOH / H<sub>2</sub>O (5:2), reflux, 4 h, 82%; b) (i) TFAA, pyridine, 0 °C – 50 °C, 3 h, 28%.

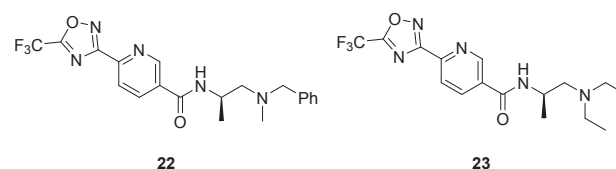


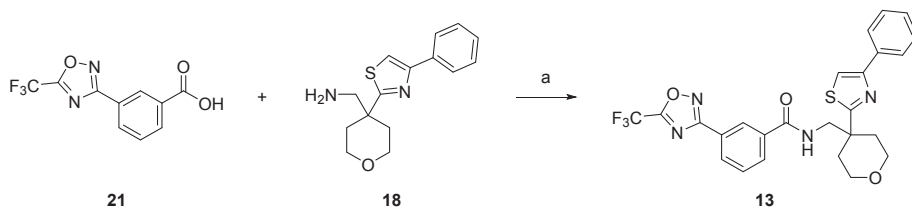
Fig. 10. Chemical structures of 22 and 23.<sup>126</sup>

the catalytic or reader domain of class IIa HDAC are not evolutionary remnant. The TFMO-series indicated that class IIa HDACs are potential targets for immunological diseases and provide an important tool for identifying natural substrates of class IIa HDACs.<sup>124</sup>

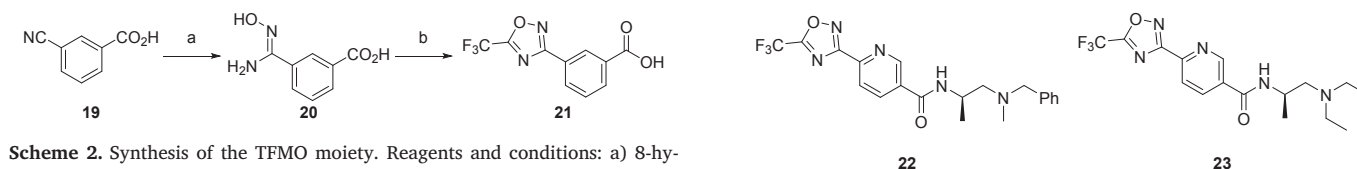
Simultaneously, Novartis described 46 novel TFMO derivatives as selective HDAC4 inhibitors for their potential clinical use in the treatment of Huntington's disease, muscle atrophy, and diabetes/metabolic syndrome. Those inhibitors exhibit a TFMO ZBG that is attached to a heterocycle (e.g. pyridine, pyrimidine).<sup>126,127</sup> The cap-region is connected in para position to the ZBG via an amine or amide moiety to the heterocycle. In Fig. 10, the structures of 22 and 23 are illustrated.

The TFMO derivatives were synthesized in high yields using a different procedure described in Scheme 4. The *para*-substituted pyridine carbonitrile 24 was converted into the amidoxime 25 under basic conditions after which a cyclisation was realized by the addition of TFAA.

The HDAC enzyme inhibition data for 22 and 23 are shown in Table 4. They show 300–500-fold selectivity for HDAC4 over HDAC1 and 6.



Scheme 3. Synthesis of TMP269 (13). Reagents and conditions: a) EDCI, DCM, rt, 8 h, 62%.

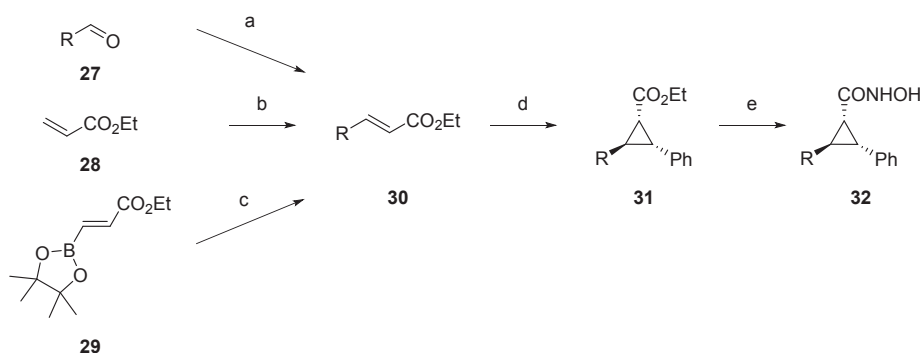


Scheme 4. Synthesis of *para*-substituted TFMO-compounds 26. Reagents and conditions: a) NH<sub>2</sub>OH, NEt<sub>3</sub>, EtOH, 80 °C, 1 h, 63%; b) TFAA, THF, 5 °C, 15 min, 77%.

Table 4  
HDAC enzyme inhibition data for 22 and 23.<sup>126</sup>

Cpd	22 IC <sub>50</sub> [μM]	23 IC <sub>50</sub> [μM]
HDAC4	0.018	0.028
HDAC1	> 10	> 10
HDAC6	> 10	> 10

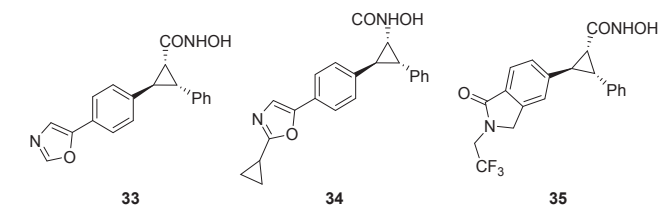
The biological role of HDAC4 in Huntington disease (HD) was also investigated by Bürli et al.<sup>128</sup> The potential therapeutic benefit by class IIa HDAC inhibition was mainly confirmed by genetic suppression studies of class IIa HDACs. Bürli et al. identified, by crystallography analysis and structure-based design, trisubstituted diarylcyclopropane-hydroxamic acids as potent and selective class IIa HDAC inhibitors. Due to the geometry of the cyclopropane scaffold, selectivity was achieved by addressing the lower pocket. However, the synthesis of these cyclopropane scaffolds is demanding (Scheme 5).  $\alpha,\beta$ -Unsaturated esters **30** were used as starting materials and were obtained either by Heck, Wittig or Suzuki reactions. In the following step, the cyclization was performed by conversion of the ester **30** with the corresponding sulfur ylide. The addition of 12-crown-4 improved the diastereoselectivity of this reaction. Bürli et al. were the first ones that described this cyclization condition to obtain 1,2,3-trisubstituted cyclopropanes **31**. In the final step, the cap group was introduced by Heck, Suzuki or Stille coupling. Finally, the esters **31** were converted into the hydroxamic acids **32** (Scheme 5).<sup>128</sup>



**Scheme 5.** Synthesis of trisubstituted cyclopropanes. Reagents and conditions: a)  $(\text{EtO})_2\text{P}(\text{O})\text{CH}_2\text{CO}_2\text{Et}$ , NaH, THF, 0 °C to rt, 1 h, 44–99%; b) RCl or RBr, Pd  $(\text{OAc})_2$ , P(o-tol)<sub>3</sub>, NEt<sub>3</sub>, MeCN, 80 °C, 3–18 h, 17–93%; c) RBr, Pd(PPh<sub>3</sub>)<sub>4</sub>, K<sub>2</sub>CO<sub>3</sub>, dioxane, 100 °C, 17 h, 68%; d) X (OTf or Br salt), LiHMDS, 12-crown-4, –20 °C, 2 h, 16–100% (dr > 98:2 to 5:4), e) NH<sub>2</sub>OH, KOH, MeOH-THF (1:1), rt, 1 h, 5–86%.

*Para*-substitution of the phenylene linker with heteroaryl capping groups, e.g. pyridazine and pyrimidine resulted in an improvement of

**Table 5**  
Cellular HDAC inhibition ( $\text{IC}_{50}$ ) and *in vitro* ADME data for compounds **33–35**.<sup>128</sup>



Cpd.	cell-based activity [ $\mu\text{M}$ ]		microsomal stability		MDCK-MDR1		AlogP TPSA ( $\text{\AA}^2$ ) <sup>e</sup> M <sub>w</sub>
	Lys-TFA	Lys-Ac	MLM <sup>a</sup>	HLM <sup>b</sup>	EER <sup>c</sup>	P <sub>appA→B</sub> <sup>d</sup>	
<b>33</b>	0.22	> 50	89	< 36	2.4	442	2.2 76 320
<b>34</b>	0.28	> 50	< 65	40	4.1	130	2.7 70 390
<b>35</b>	0.30	> 50	531	< 36	3.4	460	3.2 76 360

<sup>a</sup>MLM = mouse liver microsomes <sup>b</sup>HLM = human liver microsomes <sup>c</sup>EER = effective efflux ratio <sup>d</sup>P<sub>app</sub> = apparent permeability <sup>e</sup>TPSA = topological polar surface area.

enzyme inhibition and *ex-vivo* potency. Further optimization of ADME properties for CNS permeability was supported by the prediction of physicochemical properties and resulted in the oxazole derivatives **33** and **34** with a reasonable microsomal stability and limited P-gp mediated efflux (Table 5). Interestingly, compound **35** is well distributed in muscle but not in brain tissue.<sup>128</sup>

In enzyme assays Bürli et al. demonstrated the excellent HDAC class IIa selectivity. Compound **33** had a more pronounced activity against class IIa HDACs with a 2000 fold and 20 fold higher selectivity over HDAC2 and HDAC8, respectively (Table 6).<sup>128</sup>

In co-crystallisation studies the expected binding mode of the 5-fluoropyridimidine **36** with HDAC4(cd) (WT) was confirmed (Fig. 11). The protein adopted a closed-loop conformation. The hydroxamic moiety interacts via its carbonyl (2.00 Å) and hydroxy oxygen (2.36 Å) with the zinc ion. The phenyl group of the ligand occupies the lower pocket and features an edge-to-face  $\pi$ -stacking interaction with Arg681, and Phe812. The cocrystal structure of oxazole **33** with HDAC4(cd) (L278A) is similar to the **36** - HDAC4(cd) (WT) cocrystal structure.

However, one drawback of the trisubstituted cyclopropane hydroxamic acids is the high intrinsic clearance, probably due to *o*-glucuronidation of the ZBG. In the 2nd generation of these inhibitors, a derivatization of the ZBGs alpha hydrogen was performed in order to limit this *o*-glucuronidation by the introduction of steric or electronic effects. Indeed, a methyl and fluoro substitution showed an improved pharmacokinetic profile and higher HDAC4 inhibition.<sup>129</sup> The compounds were synthesized according to Scheme 6. After cyclopropanation of the methyl cinnamate derivative **37**, a fluorination of the racemate **38** under basic conditions with *N*-fluorobenzenesulfonimide (NFSI) was performed to obtain the tetrasubstituted cyclopropanes **39** and **40**. The enantiomerically pure compound **39** was isolated by chiral supercritical fluid chromatography (SFC). After introduction of the heterocyclic cap-group via Suzuki coupling, the ester was finally transformed into the desired hydroxamic acid **41**.

Compound **41** showed a high oral bioavailability with good brain and muscle distribution (Table 7). The distomer was 40-fold less potent in HDAC4 enzyme and cell assays.<sup>129</sup>

**Table 6**  
HDAC enzyme inhibition data for lead molecule **33**.<sup>128</sup>

Enzyme	Cpd. <b>33</b> $\text{IC}_{50}$ [ $\mu\text{M}$ ]
HDAC4	0.02
HDAC5	0.004
HDAC7	0.03
HDAC9	0.04
HDAC1	32
HDAC2	43
HDAC3	12
HDAC8	0.36

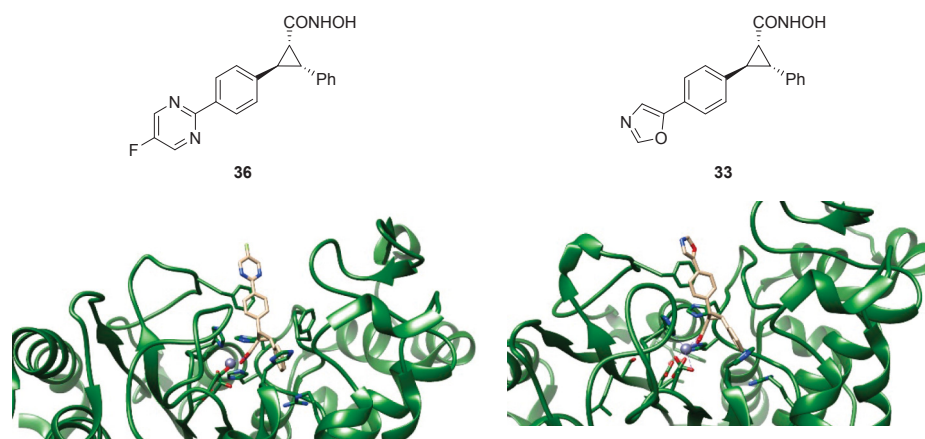
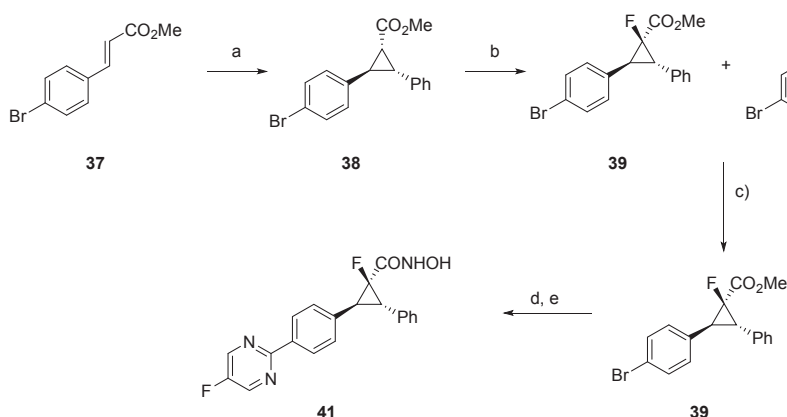


**Fig. 11.** (A) Chemical structure of **36**. (B) X-ray structure of 5-fluoropyridimidine **36** with HDAC4(cd) (WT) (PDB:5A2S) (C) Chemical structure of compound **33** (D) X-ray structure of oxazole **33** with HDAC4(cd) (L278A). (PDB:4C8Y).<sup>128</sup>



**Scheme 6.** Synthesis of tetrasubstituted cyclopropanes. Reagents and conditions: a) 1-benzyltetrahydro-1H-thiophen-1-ium (OTf or Br salt), LiHMDS, 12-crown-4, DCM,  $-20\text{ }^{\circ}\text{C}$ , 1 h, b) LDA in THF,  $-78\text{ }^{\circ}\text{C}$ , 30 min then NFSI, 2 h; c) SFC chiral chromatography; d) (i) bis(pinacolato)diboron, KOAc, Pd(dppf) $\text{Cl}_2$ , dioxane,  $90\text{ }^{\circ}\text{C}$ , 4 h; (ii) 2-chloro-5-fluoropyrimidine, Pd(dppf) $\text{Cl}_2$ , CsF, dioxane,  $100\text{ }^{\circ}\text{C}$ , 17 h; e)  $\text{NH}_2\text{OH}$  50% aq, KOH, MeOH-THF (1:1), rt, 16 h.

**Table 7**  
Cellular HDAC inhibition and *in vitro* ADME data for Compound **41**.<sup>129</sup>

Cpd.	cell-based activity [ $\mu\text{M}$ ] Lys-TFA	microsomal stability $\text{Cl}_{\text{int}}$ [mL/min/kg]		MDCK $\text{P}_{\text{app}}$ A→B [nm/s]	EER
		MLM	HLM		
<b>41</b>	$0.12 \pm 0.03$	306	< 36	418	1.4

<sup>a</sup>MLM = mouse liver microsomes <sup>b</sup>HLM = human liver microsomes <sup>c</sup>EER = effective efflux ratio <sup>d</sup> $\text{P}_{\text{app}}$  = apparent permeability.

The  $\text{IC}_{50}$  value of each HDAC enzyme inhibited by compound **41** is shown in Table 8. Compound **41** displayed > 100-fold selectivity over HDAC 1, 2, and 3.

**Table 8**  
HDAC enzyme inhibition data for compound **41**.<sup>129</sup>

Enzyme	Cpd. <b>41</b> $\text{IC}_{50}$ [ $\mu\text{M}$ ]
HDAC4	$0.01 \pm 0.001$
HDAC5	$0.01 \pm 0.004$
HDAC7	$0.03 \pm 0.01$
HDAC9	$0.06 \pm 0.03$
HDAC1	$14 \pm 4$
HDAC2	> 50
HDAC3	$7.4 \pm 2.1$
HDAC8	$0.28 \pm 0.03$
HDAC6	$3.1 \pm 0.4$

To sum up, *Bürli et al.* and *Luckhurst et al.* designed and developed selective class IIa HDACi for further investigation of the biological roles of class IIa HDACs in preclinical Huntington disease models.<sup>128,129</sup>

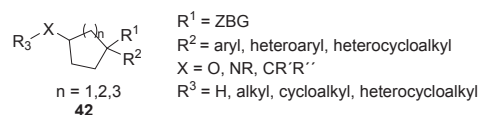


**Fig. 12.** General structure of the inhibitors **42** from CHDI-Foundation.

In 2016, the Cure Huntington's Disease Initiative (CHDI)-Foundation identified a novel class of HDAC class IIa inhibitors.<sup>130</sup> The general structure of the inhibitors is illustrated in Fig. 12.

Compound **43** was the most potent inhibitor in the *in vitro* HDAC4 enzyme assay. Compound **44** was the most active compound in cellular assays (Fig. 13).

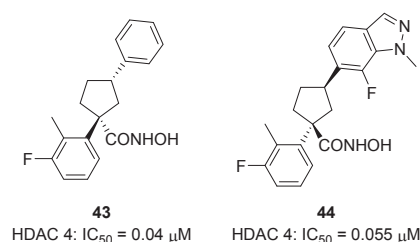
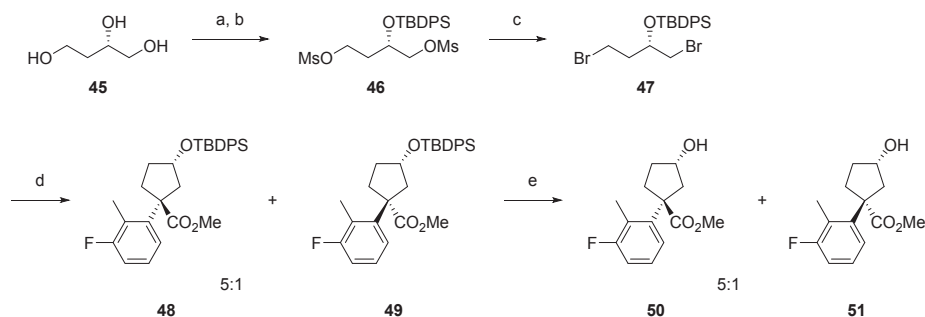
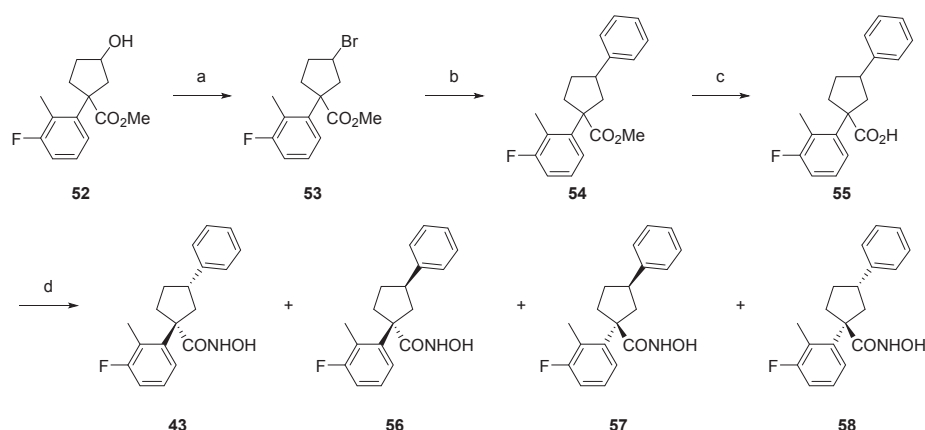


**Fig. 13.** Chemical structures of **43** and **44** with the corresponding HDAC4  $\text{IC}_{50}$  values.<sup>130</sup>



**Scheme 7.** Synthesis of the diastereomers **50** and **51**. Reagents and conditions: a) MsCl, pyridine,  $-10^{\circ}\text{C}$  –  $4^{\circ}\text{C}$ , 4 h; b) *tert* butyl-chlorodiphenylsilane, imidazole, DMF,  $4^{\circ}\text{C}$  – rt, 1 h; c) LiBr, DMF,  $105^{\circ}\text{C}$ , 1.5 h; d) methyl-2-(3-fluoro-2-methylphenyl)acetate, 18-crown-6, NaH, DMF, rt, 16 h e) TBAF, THF, rt, 3 h.



**Scheme 8.** Synthesis of hydroxamic acids **43**, **56–58**. Reagents and conditions: a)  $\text{Br}_2$ ,  $\text{PPh}_3$ , MeCN,  $0^{\circ}\text{C}$  – rt, 18 h b)  $\text{NiBr}_2\cdot\text{glyme}$ , Bphen, phenyl trifluoroborate potassium salt, LiHMDS,  $60^{\circ}\text{C}$ , 16 h c) 2 M KOH, MeOH,  $120^{\circ}\text{C}$ , 2 h; d) (i) oxalyl chloride, DCM, rt, 16 h, (ii)  $\text{NH}_2\text{OH}$  (50% aq), DCM, rt, 4 h.

The synthesis of compound **43** is illustrated in [Scheme 7](#) and [Scheme 8](#). In the first step the terminal hydroxy groups of (*S*)-butane-1,2,4-triol (**45**) were mesylated and the secondary hydroxy group was protected as a silyl ether. After bromination, cyclisation was performed with methyl-2-(3-fluoro-2-methylphenyl) acetate under basic conditions to yield the corresponding compounds **48** and **49**. Afterwards deprotection was performed to receive **50** and **51**.

The secondary hydroxyl group was then transfunctionalized into its bromo derivative **53** ([Scheme 8](#)). Subsequently, the phenyl group was

introduced by a Ni-catalysed coupling. After ester hydrolysis, the hydroxamic acid **43**, **56–58** was generated via an acid chloride. Finally, the desired compound **43** was purified by chiral HPLC chromatography.

Hsu *et al.* performed a structure-based virtual screening (National Cancer Institute database) to detect class IIa selective HDACi that do not carry a hydroxamic acid as ZBG.<sup>131</sup> As a result, six compounds were identified which were subjected for HDAC enzyme assays. The tested compounds showed a preference for class IIa over class I HDACs (30-fold selectivity) ([Table 9](#)).

Docking studies indicate that all inhibitors interact with the lower pocket residues F812, H842, F871 and L943 ([Fig. 14](#)). A3630007 (**59**) was the most promising class II HDACi among this series. Compound **59** contains a phosphonic acid moiety as ZBG. Both phosphonic acids are essential for forming hydrogen bonds with the residues D759, H802, G811 and G975. These data may increase the knowledge about structural requirements for class IIa inhibition and selectivity. However, compound A3630007 (**59**) owns rather weak potency, moderate selectivity and is unlikely to have good *in vivo* bioavailability due the phosphonic acid groups.

In 2018, Luckhurst *et al.* optimized the previous described

**Table 9**  
HDAC enzyme inhibition ( $\text{IC}_{50}$ ) data for compound A3630007 (**59**).<sup>131</sup>

Enzyme	A3630007 ( <b>59</b> ) $\text{IC}_{50}$ [ $\mu\text{M}$ ]
HDAC4	4.16
HDAC5	1.27
HDAC7	16.16
HDAC9	7.84
HDAC6	> 40
HeLa nuclear HDACs	> 40

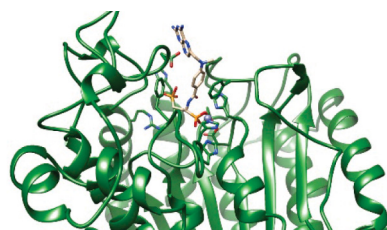
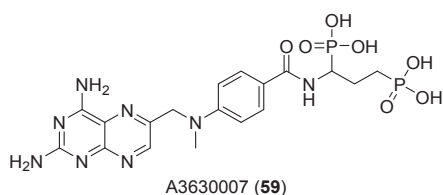
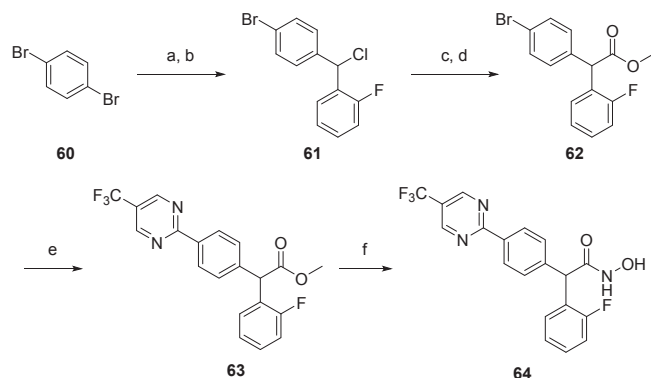


**Fig. 14.** Chemical structure of A3630007 (**59**) (left). Docking pose of A3630007 (**59**) in HDAC4 (PDB:6FYZ) (right).<sup>123</sup>



**Scheme 9.** Synthesis of CHDI-390576 (**64**). Reagents and conditions: a) Mg, Et<sub>2</sub>O, 2-fluorobenzaldehyde, 55%; b) SOCl<sub>2</sub>, DCM, rt, 94%; c) TMSCN, TiCl<sub>4</sub>, DCM, rt, 99%; d) MeOH, conc. H<sub>2</sub>SO<sub>4</sub>, reflux, 63%; e) (i) bis(pinacolato)diboron, CsF, Pd(PPh<sub>3</sub>)<sub>4</sub>, DME, MeOH, 1 h, 100 °C; ii) 2-chloro-5-trifluoromethylpyrimidine, K<sub>2</sub>CO<sub>3</sub>, Pd(PPh<sub>3</sub>)<sub>4</sub>, dioxane, water, 100 °C, 16 h, 60% f) NH<sub>2</sub>OH 50% aq, 15% w/v NaOH, MeOH, 82%.

**Table 10**  
HDAC enzyme inhibition data for compound **64**.<sup>123</sup>

Enzyme	Cpd. <b>64</b> IC <sub>50</sub> [μM]
HDAC4	0.054
HDAC5	0.060
HDAC7	0.031
HDAC9	0.050
HDAC1	39.7
HDAC2	> 50
HDAC3	25.8
HDAC8	9.1
HDAC6	6.2

benzhydryl hydroxamic acids regarding CNS properties and class IIa selectivity.<sup>123</sup> A series of potent, cell permeable and CNS-permeable class IIa selective HDAC inhibitors were identified. It was also confirmed that inhibitors with the 2-fluorophenyl lower pocket moiety were more potent in cell assays than the unsubstituted phenyl ring, although with similar HDAC4 inhibition. Optimization in the cap-region led to compounds with heteroaromatic cap-groups directly attached to the phenylene linker. One of the lead structures is compound **64** (CHDI-390576) showing reasonable PK-properties. CHDI-390576 (**64**) was synthesized according to [Scheme 9](#). The starting material, 1,4-dibromobenzene (**60**), was functionalized as Grignard reagent and

converted with 2-fluorobenzaldehyde to the benzhydryl alcohol. Subsequently, a chlorination followed to obtain **61**. The chloride **61** was substituted with a nitrile and converted into the methyl ester **62** by methanolysis under acidic conditions. The cap-group was introduced by Suzuki coupling with bromopyrimidine. In the final step, the methyl ester **63** was converted into the hydroxamic acid **64** with aqueous hydroxylamine under basic conditions.

The isoform profiling of compound **60** demonstrated a > 500-fold selectivity over class I HDACs and ~150-fold selectivity over HDAC 8, and class IIb HDAC 6 ([Table 10](#)). Moreover, **60** showed reasonable PK properties.<sup>123</sup>

In [Fig. 15](#) the cocrystal structure of 2-methyl pyrimidin-5-yl **64** with HDAC4(cd) (WT) is illustrated. The hydroxamic acid **64** interacts in a bidentate manner with the zinc-ion. The lower pocket is occupied by the 2-fluorophenyl moiety. Due to the fact, that aa 729–760 were not visible in the electron density maps, the interaction between the ligand **64** and Asp759 could not be studied.

## 5. Conclusion

HDAC enzymes have been proven to participate in a wide variety of pathological conditions, e.g. cancer and neurodegenerative diseases. Developing class IIa selective HDACi has been particularly challenging due to the high sequence homology among zinc-dependent HDACs. Nevertheless, the design of a variety of class IIa selective and active HDACi, addressing the catalytic domain, has been accomplished. Further investigations should focus on class IIa HDAC's catalytic domains and their relevance in biological and pathological processes. The diverse posttranslational modifications that members of class IIa HDACs participate in, demonstrate the complexity of their function. There is evidence that the catalytic domain of class IIa HDACs is involved in recruiting class I HDACs, in particular HDAC3. Addressing the catalytic domain of class IIa HDACs might therefore be an indirect way to influence the deacetylase function of other HDACs. In this respect, the design of selective PPI inhibitors that target e.g. HDAC3-HDAC4, MEF2-HDAC4, or p53-HDAC4 would be a valuable approach for solving many unanswered questions that revolve around the biological significance of this highly complex class of epigenetic regulators.

## Acknowledgements

We gratefully acknowledge financial support from the Deutsche Forschungsgemeinschaft DFG: 270650915/GRK 2158; grant number KA 1942/1-1 to MUK; grant number KU 1577/2-1 to TK.



**Fig. 15.** Chemical structure of **64**. (left) Cocrystal structure of **64** with HDAC4(cd) (WT). (PDB:6FYZ) (right).<sup>123</sup>

## References

- Ali I, Conrad RJ, Verdin E, Ott M. Lysine acetylation goes global: from epigenetics to metabolism and therapeutics. *Chem Rev.* 2018;118(3):1216–1252. <https://doi.org/10.1021/acs.chemrev.7b00181>.
- López JE, Sullivan ED, Fierke CA. Metal-dependent deacetylases: cancer and epigenetic regulators. *ACS Chem Biol.* 2016;11(3):706–716. <https://doi.org/10.1021/acschembio.5b01067>.
- Seidel C, Schnekenburger M, Dicato M, Diederich M. Histone deacetylase modulators provided by Mother Nature. *Genes Nutr.* 2012;7(3):357–367. <https://doi.org/10.1007/s12263-012-0283-9>.
- Zhang H, Shang Y-P, Chen H, Li J. Histone deacetylases function as novel potential therapeutic targets for cancer. *Hepatol Res.* 2017;47(2):149–159. <https://doi.org/10.1111/hepr.12757>.
- Verdin E, Dequiedt F, Kasler HG. Class II histone deacetylases: versatile regulators. *Trends Genet.* 2003;19(5):286–293. [https://doi.org/10.1016/S0168-9525\(03\)00073-8](https://doi.org/10.1016/S0168-9525(03)00073-8).
- Chang S, Bezprozvannaya S, Li S, Olson EN. An expression screen reveals modulators of class II histone deacetylase phosphorylation. *Proc Natl Acad Sci.* 2005;102(23):8120–8125. <https://doi.org/10.1073/pnas.0503275102>.
- Lahm A, Paolini C, Pallaro M, et al. Unraveling the hidden catalytic activity of vertebrate class IIa histone deacetylases. *Proc Natl Acad Sci.* 2007;104(44):17335–17340. <https://doi.org/10.1073/pnas.0706487104>.
- Gantt SML, Decroos C, Lee MS, et al. General base-general acid catalysis in human histone deacetylase 8. *Biochemistry.* 2016;55(5):820–832. <https://doi.org/10.1021/acs.biochem.5b01327>.
- Bottomley MJ, Lo Surdo P, Lo Di, Giovine PDI, et al. Structural and functional analysis of the human HDAC4 catalytic domain reveals a regulatory structural zinc-binding domain. *J Biol Chem.* 2008;283(39):26694–26704. <https://doi.org/10.1074/jbc.M803514200>.
- Görlich, Dirk, Mattaj IW. Nucleocytoplasmic Transport. *Science* (80-). 1996; 271(March): 1513–1519.
- Gräff J, Tsai L-H. The potential of HDAC inhibitors as cognitive enhancers. *Annu Rev Pharmacol Toxicol.* 2013;53(1):311–330. <https://doi.org/10.1146/annurev-pharmtox-011112-140216>.
- Verdel A, Curtet S, Brocard MP, et al. Active maintenance of mHDA2/mHDAC6 histone-deacetylase in the cytoplasm. *Curr Biol.* 2000;10(12):747–749 accessed 27.02.19.
- Hai Y, Shinsky SA, Porter NJ, Christianson DW. Histone deacetylase 10 structure and molecular function as a polyamine deacetylase. *Nat Commun.* 2017;8:1–9. <https://doi.org/10.1038/ncomms15368>.
- Novakova Z, Meleshin M, Mikesova J, Schutkowski M, Barinka C. Histone deacetylase 11 is a fatty-acid. *Deacylase.* 2018. <https://doi.org/10.1021/acschembio.7b00942>.
- Martin M, Kettmann R, Dequiedt F. Class IIa histone deacetylases: regulating the regulators. *Oncogene.* 2007. <https://doi.org/10.1038/sj.onc.1210613>.
- Sinnett-Smith J, Ni Y, Wang J, Ming M, Young SH, Rozengurt E. Protein kinase D1 mediates class IIa histone deacetylase phosphorylation and nuclear extrusion in intestinal epithelial cells: role in mitogenic signaling. *Am J Physiol Physiol.* 2014;306(10):C961–C971. <https://doi.org/10.1152/ajpcell.00048.2014>.
- Di Giorgio E, Brancolini C. Regulation of class IIa HDAC activities: it is not only matter of subcellular localization. *Epigenomics.* 2016;8(2):251–269. <https://doi.org/10.2217/epi.15.106>.
- McKinsey TA, Zhang C-L, Lu J, Olson EN. Signal-dependent nuclear export of a histone deacetylase regulates muscle differentiation. *Nature.* 2000;408(6808):106–111. <https://doi.org/10.1038/35040593>.
- Kao H-Y, Verdel A, Tsai C-C, Simon C, Juguilon H, Khochbin S. Mechanism for nucleocytoplasmic shuttling of histone deacetylase 7. *J Biol Chem.* 2001;276(50):47496–47507. <https://doi.org/10.1074/jbc.M107631200>.
- Davis FJ, Gupta M, Camoretti-Mercado B, Schwartz RJ, Gupta MP. Calcium/calmodulin-dependent protein kinase activates serum response factor transcription activity by its dissociation from histone deacetylase, HDAC4. *J Biol Chem.* 2003;278(22):20047–20058. <https://doi.org/10.1074/jbc.M20998200>.
- Backs J, Song K, Bezprozvannaya S, Chang S, Olson EN. CaM kinase II selectively signals to histone deacetylase 4 during cardiomyocyte hypertrophy. *J Clin Invest.* 2006;116(7):1853–1864. <https://doi.org/10.1172/JCI27438>.
- Backs J, Backs T, Bezprozvannaya S, McKinsey TA, Olson EN. Histone deacetylase 5 acquires calcium/calmodulin-dependent kinase II responsiveness by oligomerization with histone deacetylase 4. *Mol Cell Biol.* 2008;28(10):3437–3445. <https://doi.org/10.1128/MCB.01611-07>.
- Matthews SA, Liu P, Spitaler M, et al. Essential role for protein kinase D family kinases in the regulation of class II histone deacetylases in B lymphocytes. *Mol Cell Biol.* 2006;26(4):1569–1577. <https://doi.org/10.1128/MCB.26.4.1569-1577.2006>.
- Dequiedt F, Van Lint J, Lecomte E, et al. Phosphorylation of histone deacetylase 7 by protein kinase D mediates T cell receptor-induced Nur77 expression and apoptosis. *J Exp Med.* 2005;201(5):793–804. <https://doi.org/10.1084/jem.20042034>.
- Vega RB, Harrison BC, Meadows E, et al. Protein kinases C and D mediate agonist-dependent cardiac hypertrophy through nuclear export of histone deacetylase 5. *Mol Cell Biol.* 2004;24(19):8374–8385. <https://doi.org/10.1128/MCB.24.19.8374-8385.2004>.
- Drewes G, Ebneth A, Preuss U, Mandelkow EM, Mandelkow E. MARK, a novel family of protein kinases that phosphorylate microtubule-associated proteins and trigger microtubule disruption. *Cell.* 1997;89(2):297–308 accessed 27.12.19.
- Wang J-W, Imai Y, Lu B. Activation of PAR-1 kinase and stimulation of tau phosphorylation by diverse signals require the tumor suppressor protein LKB1. *J Neurosci.* 2007;27(3):574–581. <https://doi.org/10.1523/JNEUROSCI.5094-06.2007>.
- Zeng P-Y, Berger SL. LKB1 Is recruited to the p21/WAF1 promoter by p53 to mediate transcriptional activation. *Cancer Res.* 2006;66(22):10701–10708. <https://doi.org/10.1158/0008-5472.CAN-06-0999>.
- Kao GD, McKenna WG, Guenther MG, Muschel RJ, Lazar MA, Yen TJ. Histone deacetylase 4 interacts with 53BP1 to mediate the DNA damage response. *J Cell Biol.* 2003;160(7):1017–1027. <https://doi.org/10.1083/jcb.200209065>.
- Grozinger CM, Schreiber SL. Regulation of histone deacetylase 4 and 5 and transcriptional activity by 14–3–3-dependent cellular localization. *Proc Natl Acad Sci.* 2000;97(14):7835–7840. <https://doi.org/10.1073/pnas.140199597>.
- Parra M, Mahmoudi T, Verdin E. Myosin phosphatase dephosphorylates HDAC7, controls its nucleocytoplasmic shuttling, and inhibits apoptosis in thymocytes. *Genes Dev.* 2007;21(6):638–643. <https://doi.org/10.1101/gad.1513107>.
- Taniguchi M, Carreira MB, Smith LN, Zirlin BC, Neve RL, Cowan CW. Histone deacetylase 5 limits cocaine reward through cAMP-induced nuclear import. *Neuron.* 2012;73(1):108–120. <https://doi.org/10.1016/j.neuron.2011.10.032>.
- Mathias RA, Guise AJ, Cristea IM. Post-translational modifications regulate class IIa histone deacetylase (HDAC) function in health and disease. *Mol Cell Proteom.* 2015;14(3):456–470. <https://doi.org/10.1074/mcp.O114.046565>.
- Baas T. Closer to class IIa HDAC inhibitors. *Sci Exch.* 2013;6(13):301. <https://doi.org/10.1038/scibx.2013.301>.
- Fischle W, Dequiedt F, Hendzel MJ, et al. Enzymatic activity associated with class II HDACs is dependent on a multiprotein complex containing HDAC3 and SMRT/N-CoR. *Mol Cell.* 2002;9(1):45–57 accessed 5.05.19.
- Sparrow DB, Miska EA, Langley E, et al. MEF-2 function is modified by a novel corepressor, MITR. *EMBO J.* 1999;18(18):5085–5098. <https://doi.org/10.1093/emboj/18.18.5085>.
- McGee SL, van Denderen BJW, Howlett KF, et al. AMP-activated protein kinase regulates GLUT4 transcription by phosphorylating histone deacetylase 5. *Diabetes.* 2008;57(4):860–867. <https://doi.org/10.2337/db07-0843>.
- Moresi V, Marroncelli N, Pigna E, et al. Histone Deacetylase 4 is crucial for proper skeletal muscle development and disease. *Ital J Anat Embryol.* 2015;120(1):150. <https://doi.org/10.13128/ijae-17022>.
- Moresi V, Williams AH, Meadows E, et al. Myogenin and class II HDACs control neurogenic muscle atrophy by inducing E3 ubiquitin ligases. *Cell.* 2010;143(1):35–45. <https://doi.org/10.1016/j.cell.2010.09.004>.
- Darcy MJ, Calvin K, Cavnar K, Ouimet CC. Regional and subcellular distribution of HDAC4 in mouse brain. *J Comp Neurol.* 2010;518(5):722–740. <https://doi.org/10.1002/cne.22241>.
- Fitzsimons HL. The Class IIa histone deacetylase HDAC4 and neuronal function: nuclear nuisance and cytoplasmic stalwart? *Neurobiol Learn Mem.* 2015;123:149–158. <https://doi.org/10.1016/j.nlm.2015.06.006>.
- Williams SR, Aldred MA, Der Kaloustian VM, et al. Haploinsufficiency of HDAC4 causes brachydactyly mental retardation syndrome, with brachydactyly type E, developmental delays, and behavioral problems. *Am J Hum Genet.* 2010;87(2):219–228. <https://doi.org/10.1016/j.ajhg.2010.07.011>.
- Morris B, Etoubleau C, Bourthoumieu S, et al. Dose dependent expression of HDAC4 causes variable expressivity in a novel inherited case of brachydactyly mental retardation syndrome. *Am J Med Genet A.* 2012;158A(8):2015–2020. <https://doi.org/10.1002/ajmg.a.35463>.
- Villavicencio-Lorini P, Kloppock E, Trimborn M, Koll R, Mundlos S, Horn D. Phenotypic variant of Brachydactyly-mental retardation syndrome in a family with an inherited interstitial 2q37.3 microdeletion including HDAC4. *Eur J Hum Genet.* 2013;21(7):743–748. <https://doi.org/10.1038/ejhg.2012.240>.
- Mielcarek M, Landles C, Weiss A, et al. HDAC4 reduction: a novel therapeutic strategy to target cytoplasmic huntingtin and ameliorate neurodegeneration. Lindquist SL, ed. *PLoS Biol.* 2013;11(11) <https://doi.org/10.1371/journal.pbio.1001717> e1001717.
- Cho Y, Cavalli V, Van Lint J, et al. HDAC5 is a novel injury-regulated tubulin deacetylase controlling axon regeneration. *EMBO J.* 2012;31(14):3063–3078. <https://doi.org/10.1038/emboj.2012.160>.
- Cho Y, Sloutsky R, Naegle KM, Cavalli V. Injury-induced HDAC5 nuclear export is essential for axon regeneration. *Cell.* 2013;155(4):894–908. <https://doi.org/10.1016/j.cell.2013.10.004>.
- Ma C, D'Mello SR. Neuroprotection by histone deacetylase-7 (HDAC7) occurs by inhibition of c-jun expression through a deacetylase-independent mechanism. *J Biol Chem.* 2011;286(6):4819–4828. <https://doi.org/10.1074/jbc.M110.146860>.
- Lang B, Alrahbeni TMA, Clair DS, et al. HDAC9 is implicated in schizophrenia and expressed specifically in post-mitotic neurons but not in adult neural stem cells. *Am J Stem Cells.* 2012;1(1):31–41 accessed 26.03.19.
- Lang B, Alrahbeni TMA, Clair DS, et al. HDAC9 is implicated in schizophrenia and expressed specifically in post-mitotic neurons but not in adult neural stem cells. *Am J Stem Cells.* 2012;1(1):31–41 accessed 29.01.19.
- Dequiedt F, Kasler H, Fischle W, et al. HDAC7, a thymus-specific class II histone deacetylase, regulates Nur77 transcription and TCR-mediated apoptosis. *Immunity.*

- 2003;18(5):687–698 accessed 30.01.19.
52. Parra M, Kasler H, McKinsey TA, Olson EN, Verdin E. Protein kinase D1 phosphorylates HDAC7 and induces its nuclear export after T-cell receptor activation. *J Biol Chem.* 2005;280(14):13762–13770. <https://doi.org/10.1074/jbc.M413396200>.
  53. Kasler HG, Young BD, Mottet D, et al. Histone deacetylase 7 regulates cell survival and TCR signaling in CD4/CD8 double-positive thymocytes. *J Immunol.* 2011;186(8):4782–4793. <https://doi.org/10.4049/jimmunol.1001179>.
  54. Kasler HG, Lim HW, Mottet D, Collins AM, Lee IS, Verdin E. Nuclear export of histone deacetylase 7 during thymic selection is required for immune self-tolerance. *EMBO J.* 2012;31(23):4453–4465. <https://doi.org/10.1038/emboj.2012.295>.
  55. Kasler HG, Lee IS, Lim HW, Verdin E. Histone deacetylase 7 mediates tissue-specific autoimmunity via control of innate effector function in invariant Natural Killer T Cells. *Elife.* 2018;7:32109. <https://doi.org/10.7554/eLife>.
  56. Azagra A, Roman-Gonzalez L, Collazo O, et al. In vivo conditional deletion of HDAC7 reveals its requirement to establish proper B lymphocyte identity and development. *J Exp Med.* 2016;213(12):2591–2601. <https://doi.org/10.1084/jem.20150821>.
  57. Lobera M, Madauss KP, Pohlhaus DT, et al. Selective class IIa histone deacetylase inhibition via a nonchelating zinc-binding group. *Nat Chem Biol.* 2013;9(5):319–325. <https://doi.org/10.1038/nchembio.1223>.
  58. Guerriero JL, Sotayo A, Ponichtera HE, et al. Class IIa HDAC inhibition reduces breast tumours and metastases through anti-tumour macrophages. *Nature.* 2017;543(7645):428–432. <https://doi.org/10.1038/nature21409>.
  59. Kaletsch A, Pinkerle M, Hoffmann MJ, et al. Effects of novel HDAC inhibitors on urothelial carcinoma cells. *Clin Epigenetics.* 2018;10(1):100. <https://doi.org/10.1186/s13148-018-0531-y>.
  60. Geng L, Cuneo KC, Fu A, Tu T, Atadja PW, Hallahan DE. Histone deacetylase (HDAC) inhibitor LBH589 increases duration of gamma-H2AX foci and confines HDAC4 to the cytoplasm in irradiated non-small cell lung cancer. *Cancer Res.* 2006;66(23):11298–11304. <https://doi.org/10.1158/0008-5472.CAN-06-0049>.
  61. Wang AH, Yang X-JJ. Histone deacetylase 4 possesses intrinsic nuclear import and export signals. *Mol Cell Biol.* 2002;21(17):5992–6005. <https://doi.org/10.1128/mcb.21.17.5992-6005.2001>.
  62. Stronach EA, Alfraidi A, Rama N, et al. HDAC4-regulated STAT1 activation mediates platinum resistance in ovarian cancer. *Cancer Res.* 2011;71(13):4412–4422. <https://doi.org/10.1158/0008-5472.CAN-10-4111>.
  63. Cadot B, Brunetti M, Coppari S, et al. Loss of histone deacetylase 4 causes segregation defects during mitosis of p53-deficient human tumor cells. *Cancer Res.* 2009;69(15):6074–6082. <https://doi.org/10.1158/0008-5472.CAN-08-2796>.
  64. Mottet D, Pirotte S, Lamour V, et al. HDAC4 represses p21(WAF1/Cip1) expression in human cancer cells through a Sp1-dependent, p53-independent mechanism. *Oncogene.* 2009;28(2):243–256. <https://doi.org/10.1038/onc.2008.371>.
  65. Wilson AJ, Byun D-S, Nasser S, et al. HDAC4 promotes growth of colon cancer cells via repression of p21. *Cleveland JL, ed. Mol Biol Cell.* 2008;19(10):4062–4075. <https://doi.org/10.1091/mbc.e08-02-0139>.
  66. Paroni G, Mizzau M, Henderson C, Del Sal G, Schneider C, Brancolini C. Caspase-dependent regulation of histone deacetylase 4 nuclear-cytoplasmic shuttling promotes apoptosis. *Mol Biol Cell.* 2004;15(6):2804–2818. <https://doi.org/10.1091/mbc.e03-08-0624>.
  67. Liu F, Dowling M, Yang X-J, Kao GD. Caspase-mediated specific cleavage of human histone deacetylase 4. *J Biol Chem.* 2004;279(33):34537–34546. <https://doi.org/10.1074/jbc.M402475200>.
  68. Di Giorgio E, Clocchiatti A, Piccinin S, et al. MEF2 is a converging hub for histone deacetylase 4 and phosphatidylinositol 3-kinase/Akt-induced transformation. *Mol Cell Biol.* 2013;33(22):4473–4491. <https://doi.org/10.1128/MCB.01050-13>.
  69. Paluvai H, Di Giorgio E, Brancolini C. Unscheduled HDAC4 repressive activity in human fibroblasts triggers TP53-dependent senescence and favors cell transformation. *Mol Oncol.* 2018;12(12):2165–2181. <https://doi.org/10.1002/1878-0261.12392>.
  70. Lei Y, Liu L, Zhang S, et al. Hdac7 promotes lung tumorigenesis by inhibiting Stat3 activation. *Mol Cancer.* 2017;16(1):170. <https://doi.org/10.1186/s12943-017-0736-2>.
  71. Scott FL, Fuchs GJ, Boyd SE, et al. Caspase-8 cleaves histone deacetylase 7 and abolishes its transcription repressor function. *J Biol Chem.* 2008;283(28):19499–19510. <https://doi.org/10.1074/jbc.M800331200>.
  72. Zhong L, Sun S, Yao S, Han X, Gu M, Shi J. Histone deacetylase 5 promotes the proliferation and invasion of lung cancer cells. *Oncol Rep.* 2018;40(4):2224–2232. <https://doi.org/10.3892/or.2018.6591>.
  73. Huang Y, Tan M, Gosink M, Wang KKW, Sun Y. Histone deacetylase 5 is not a p53 target gene, but its overexpression inhibits tumor cell growth and induces apoptosis. *Cancer Res.* 2002;62(10):2913–2922.
  74. Huang W-T, Tsai Y-H, Chen S-H, et al. HDAC2 and HDAC5 Up-regulations modulate survivin and miR-125a-5p expressions and promote hormone therapy resistance in estrogen receptor positive breast cancer cells. *Front Pharmacol.* 2017;8:902. <https://doi.org/10.3389/fphar.2017.00902>.
  75. Mottet D, Bellahcène A, Pirotte S, et al. Histone deacetylase 7 silencing alters endothelial cell migration, a key step in angiogenesis. *Circ Res.* 2007;101(12):1237–1246. <https://doi.org/10.1161/CIRCRESAHA.107.149377>.
  76. Ouaissi M, Sieleznoff I, Silvestre R, et al. High histone deacetylase 7 (HDAC7) expression is significantly associated with adenocarcinomas of the pancreas. *Ann Surg Oncol.* 2008;15(8):2318–2328. <https://doi.org/10.1245/s10434-008-9940-z>.
  77. Moreno DA, Scrideli CA, Cortez MAA, et al. research paper: Differential expression of HDAC3, HDAC7 and HDAC9 is associated with prognosis and survival in childhood acute lymphoblastic leukaemia. *Br J Haematol.* 2010;150(6):665–673. <https://doi.org/10.1111/j.1365-2141.2010.08301.x>.
  78. Zhu C, Chen Q, Xie Z, et al. The role of histone deacetylase 7 (HDAC7) in cancer cell proliferation: regulation on c-Myc. *J Mol Med.* 2011;89(3):279–289. <https://doi.org/10.1007/s00109-010-0701-7>.
  79. Barneda-Zahonero B, Collazo O, Azagra A, et al. The transcriptional repressor HDAC7 promotes apoptosis and c-Myc downregulation in particular types of leukemia and lymphoma. *e1635 Cell Death Dis.* 2015;6(2) <https://doi.org/10.1038/cddis.2014.594>.
  80. Lapiere M, Linares A, Dalvai M, et al. Histone deacetylase 9 regulates breast cancer cell proliferation and the response to histone deacetylase inhibitors. *Oncotarget.* 2016;7(15):19693–19708. <https://doi.org/10.18632/oncotarget.7564>.
  81. Zhao Y-X, Wang Y-S, Cai Q-Q, Wang J-Q, Yao W-T. Up-regulation of HDAC9 promotes cell proliferation through suppressing p53 transcription in osteosarcoma. *Int J Clin Exp Med.* 2015;8(7):11818–11823.
  82. Clocchiatti A, Di Giorgio E, Ingrao S, Meyer-Almes F-J, Tripodo C, Brancolini C. Class IIa HDACs repressive activities on MEF2-dependent transcription are associated with poor prognosis of ER<sup>+</sup> breast tumors. *FASEB J.* 2013;27(3):942–954. <https://doi.org/10.1096/fj.12-209346>.
  83. Gil VS, Bhagat G, Howell L, et al. Deregulated expression of HDAC9 in B cells promotes development of lymphoproliferative disease and lymphoma in mice. *Dis Model Mech.* 2016;9(12):1483–1495. <https://doi.org/10.1242/dmm.023366>.
  84. Jung M, Hoffmann K, Brosch G, Loidl P. Analogues of trichostatin A and trapoxin B as histone deacetylase inhibitors. *Biorganic Med Chem Lett.* 1997. [https://doi.org/10.1016/S0960-894X\(97\)00284-9](https://doi.org/10.1016/S0960-894X(97)00284-9).
  85. Finnin MS, Donigian JR, Cohen A, et al. Structures of a histone deacetylase homologue bound to the TSA and SAHA inhibitors. *Nature.* 1999. <https://doi.org/10.1038/43710>.
  86. Jung M. Inhibitors of histone deacetylase as new anticancer agents. *Curr Med Chem.* 2012. <https://doi.org/10.2174/0929867013372058>.
  87. Melesina J, Praetorius L, Simoben CV, Robaa D, Sippl W. Design of selective histone deacetylase inhibitors: rethinking classical pharmacophore. *Future Med Chem.* 2018. <https://doi.org/10.4155/fmc-2018-0125>.
  88. Bolden JE, Peart MJ, Johnstone RW. Anticancer activities of histone deacetylase inhibitors. *Nat Rev Drug Discov.* 2006. <https://doi.org/10.1038/nrd2133>.
  89. Dokmanovic M, Marks PA. Prospects: histone deacetylase inhibitors. *J Cell Biochem.* 2005;96(2):293–304. <https://doi.org/10.1002/jcb.20532>.
  90. Miller TA, Witter DJ, Belvedere S. Histone deacetylase inhibitors. *J Med Chem.* 2003;46(24):5097–5116. <https://doi.org/10.1021/jm0303094>.
  91. Marks PA. Histone deacetylase inhibitor. *Mol Oncol Causes Cancer Targets Treat.* 2015;46(24):912–920. <https://doi.org/10.1017/CBO9781139046947.088>.
  92. Tsuji N, Kobayashi M. Trichostatin C, a glucopyranosyl hydroxamate. *J Antibiot (Tokyo).* 1978;31(10):939–944. <https://doi.org/10.7164/antibiotics.31.939>.
  93. Tsuji N, Kobayashi M, Nagashima K, Wakiska Y, Koizumi K. A new antifungal antibiotic, trichostatin. *J Antibiot (Tokyo).* 1976. <https://doi.org/10.7164/antibiotics.29.1>.
  94. Duvic M, Talpur R, Ni X, et al. Phase 2 trial of oral vorinostat (suberoylanilide hydroxamic acid, SAHA) for refractory cutaneous T-cell lymphoma (CTCL). *Blood.* 2007. <https://doi.org/10.1182/blood-2006-06-025999>.
  95. Minucci S, Pellicci PG. Histone deacetylase inhibitors and the promise of epigenetic (and more) treatments for cancer. *Nat Rev Cancer.* 2006. <https://doi.org/10.1038/nrc1779>.
  96. Marek L, Hamacher A, Hansen FK, et al. Histone deacetylase (HDAC) inhibitors with a novel connecting unit linker region reveal a selectivity profile for HDAC4 and HDAC5 with improved activity against chemoresistant cancer cells. *J Med Chem.* 2013. <https://doi.org/10.1021/jm301254q>.
  97. Choi SY, Kee HJ, Sun S, et al. Histone deacetylase inhibitor LMK235 attenuates vascular constriction and aortic remodelling in hypertension. *J Cell Mol Med.* 2019;23(4):2801–2812. <https://doi.org/10.1111/jcmm.14188>.
  98. Jose B, Oniki Y, Kato T, Nishino N, Sumida Y, Yoshida M. Novel histone deacetylase inhibitors: cyclic tetrapeptide with trifluoromethyl and pentafluoroethyl ketones. *Biorganic Med Chem Lett.* 2004. <https://doi.org/10.1016/j.bmcl.2004.08.016>.
  99. Richon VM, Emiliani S, Verdin E, et al. A class of hybrid polar inducers of transformed cell differentiation inhibits histone deacetylases. *Proc Natl Acad Sci.* 1998. <https://doi.org/10.1073/PNAS.95.6.3003>.
  100. Hose CD, Petersen KD, Shoemaker RH, et al. Gene expression-signature of belinostat in cell lines is specific for histone deacetylase inhibitor treatment, with a corresponding signature in xenografts. *Anticancer Drugs.* 2009;20(8):682–692. <https://doi.org/10.1097/cad.0b013e32832e14e1>.
  101. Atadja P. Development of the pan-DAC inhibitor panobinostat (LBH589): Successes and challenges. *Cancer Lett.* 2009. <https://doi.org/10.1016/j.canlet.2009.02.019>.
  102. Furumai R, Matsuyama A, Kobashi N, et al. FK228 (depsipeptide) as a natural prodrug that inhibits class I histone deacetylases. *Cancer Res.* 2002.
  103. Sawyers C. Targeted cancer therapy. *Nature.* 2004. <https://doi.org/10.1038/nature03095>.
  104. Gryder BE, Sodji QH, Oyeler AK. Targeted cancer therapy: Giving histone deacetylase inhibitors all they need to succeed. *Future Med Chem.* 2012. <https://doi.org/10.4155/fmc.12.3>.
  105. Di Giorgio E, Gagliostro E, Brancolini C. Selective class IIa HDAC inhibitors: Myth or

- reality. *Cell Mol Life Sci.* 2015. <https://doi.org/10.1007/s00018-014-1727-8>.
106. Milroy LG, Grossmann TN, Hennig S, Brunsveld L, Ottmann C. Modulators of protein-protein interactions. *Chem Rev.* 2014. <https://doi.org/10.1021/cr400698c>.
  107. Lu J, McKinsey TA, Zhang CL, Olson EN. Regulation of skeletal myogenesis by association of the MEF2 transcription factor with class II histone deacetylases. *Mol Cell.* 2000. [https://doi.org/10.1016/S1097-2765\(00\)00025-3](https://doi.org/10.1016/S1097-2765(00)00025-3).
  108. Clocchiatti A, Florean C, Brancolini C. Class IIa HDACs: From important roles in differentiation to possible implications in tumorigenesis. *J Cell Mol Med.* 2011;15(9):1833–1846. <https://doi.org/10.1111/j.1582-4934.2011.01321.x>.
  109. Zhang CL, McKinsey TA, Olson EN. Association of class II histone deacetylases with heterochromatin protein 1: potential role for histone methylation in control of muscle differentiation. *Mol Cell Biol.* 2002. <https://doi.org/10.1128/mcb.22.20.7302-7312.2002>.
  110. Chang S, McKinsey TA, Zhang CL, Richardson JA, Hill JA, Olson EN. Histone deacetylases 5 and 9 govern responsiveness of the heart to a subset of stress signals and play redundant roles in heart development. *Mol Cell Biol.* 2004. <https://doi.org/10.1128/MCB.24.19.8467-8476.2004>.
  111. Han A, He J, Wu Y, Liu JO, Chen L. Mechanism of recruitment of class II histone deacetylases by myocyte enhancer factor-2. *J Mol Biol.* 2005. <https://doi.org/10.1016/j.jmb.2004.10.033>.
  112. Han A, Pan F, Stroud JC, Youn HD, Liu JO, Chen L. Sequence-specific recruitment of transcriptional co-repressor Cabin1 by myocyte enhancer factor-2. *Nature.* 2003. <https://doi.org/10.1038/nature01555>.
  113. Jayathilaka N, Han A, Gaffney KJ, et al. Inhibition of the function of class IIa HDACs by blocking their interaction with MEF2. *Nucleic Acids Res.* 2012. <https://doi.org/10.1093/nar/gks189>.
  114. Wong JC, Hong R, Schreiber SL. Structural biasing elements for in-cell histone deacetylase paralog selectivity. *J Am Chem Soc.* 2003. <https://doi.org/10.1021/ja0341440>.
  115. Haggarty SJ, Koeller KM, Wong JC, Butcher RA, Schreiber SL. Multidimensional chemical genetic analysis of diversity-oriented synthesis-derived deacetylase inhibitors using cell-based assays. *Chem Biol.* 2003. [https://doi.org/10.1016/S1074-5521\(03\)00095-4](https://doi.org/10.1016/S1074-5521(03)00095-4).
  116. Savickiene J, Borutinskaite VV, Treigyte G, Magnusson KE, Navakauskiene R. The novel histone deacetylase inhibitor BML-210 exerts growth inhibitory, proapoptotic and differentiation stimulating effects on the human leukemia cell lines. *Eur J Pharmacol.* 2006. <https://doi.org/10.1016/j.ejphar.2006.08.010>.
  117. Isaacs JT, Antony L, Dalrymple SL, et al. Tasquinimod is an allosteric modulator of HDAC4 survival signaling within the compromised cancer microenvironment. *Cancer Res.* 2013. <https://doi.org/10.1158/0008-5472.CAN-12-2730>.
  118. Olsson A, Björk A, Vallon-Christersson J, Isaacs JT, Leanderson T. Tasquinimod (ABR-215050), a quinoline-3-carboxamide anti-angiogenic agent, modulates the expression of thrombospondin-1 in human prostate tumors. *Mol Cancer.* 2010. <https://doi.org/10.1186/1476-4598-9-107>.
  119. Dalrymple SL, Becker RE, Zhou H, Dewese TL, Isaacs JT. Tasquinimod prevents the angiogenic rebound induced by fractionated radiation resulting in an enhanced therapeutic response of prostate cancer xenografts. *Prostate.* 2012. <https://doi.org/10.1002/pros.21467>.
  120. Hanahan D, Folkman J. Patterns and emerging mechanisms of the angiogenic switch during tumorigenesis. *Cell.* 1996. [https://doi.org/10.1016/S0092-8674\(00\)80108-7](https://doi.org/10.1016/S0092-8674(00)80108-7).
  121. Jones P, Bottomley MJ, Carfi A, et al. 2-Trifluoroacetylthiophenes, a novel series of potent and selective class II histone deacetylase inhibitors. *Bioorganic Med Chem Lett.* 2008. <https://doi.org/10.1016/j.bmcl.2008.02.026>.
  122. Tessier P, Smil DV, Wahhab A, et al. Diphenylmethane hydroxamic acids as selective class IIa histone deacetylase inhibitors. *Bioorganic Med Chem Lett.* 2009. <https://doi.org/10.1016/j.bmcl.2009.08.010>.
  123. Luckhurst CA, Aziz O, Beaumont V, et al. Development and characterization of a CNS-penetrant benzhydryl hydroxamic acid class IIa histone deacetylase inhibitor. *Bioorganic Med Chem Lett.* 2019. <https://doi.org/10.1016/j.bmcl.2018.11.009>.
  124. Lobera M, Madauss KP, Pohlhaus DT, et al. Selective class IIa histone deacetylase inhibition via a nonchelating zinc-binding group. *Nat Chem Biol.* 2013. <https://doi.org/10.1038/nchembio.1223>.
  125. Kewitz S, Bernig T, Staeger MS. Histone deacetylase inhibition restores cisplatin sensitivity of Hodgkin's lymphoma cells. *Leuk Res.* 2012. <https://doi.org/10.1016/j.leukres.2012.02.021>.
  126. Hebach, C. Kallen, J. Nozulak, J. Tintelnot-Blomley, M. Widler L. WO 2013/080120 A1; 2013. doi: 10.1021/ml4002216.
  127. Abdel-Magid AF. Histone deacetylase 4 (HDAC4) inhibitors: a promising treatment for Huntington's disease. *ACS Med Chem Lett.* 2013;4(8):692–693. <https://doi.org/10.1021/ml4002216>.
  128. Bürli RW, Luckhurst CA, Aziz O, et al. Design, synthesis, and biological evaluation of potent and selective class IIa histone deacetylase (HDAC) inhibitors as a potential therapy for huntington's disease. *J Med Chem.* 2013. <https://doi.org/10.1021/jm4011884>.
  129. Luckhurst CA, Breccia P, Stott AJ, et al. Potent, selective, and CNS-penetrant tetrasubstituted cyclopropane class IIa histone deacetylase (HDAC) inhibitors. *ACS Med Chem Lett.* 2016. <https://doi.org/10.1021/acsmchemlett.5b00302>.
  130. Lausberg N, Josten H, Fieg G, et al. (12) Patent Application Publication (10) Pub. No.: US 2006/0222585 A1 Figure 1. 2006; 1(19). doi: 10.1037/t24245-000.
  131. Hsu K-C, Liu C-Y, Lin TE, et al. Novel class IIa-selective histone deacetylase inhibitors discovered using an in silico virtual screening approach. *Sci Rep.* 2017;7. <https://doi.org/10.1038/s41598-017-03417-1>.



Yodita Asfaha was born on March 12, 1990 in Kassel, Germany. She received her BSc and MSc in Chemistry from the Philipps-University Marburg. Currently, she is a PhD candidate of the Kurz research group at the Institute of Pharmaceutical and Medicinal Chemistry, Heinrich-Heine University of Düsseldorf. Her research interest is developing new class IIa Histone deacetylase inhibitors.



Christian Schrenk, born on 18.12.1986 in Mainz, is doctorate student at the Institute of Pharmaceutical and Medicinal Chemistry at the Heinrich-Heine University Düsseldorf. He studied biosciences at the University of Frankfurt (B.Sc. degree) and biology at the University of Mainz (M.Sc. degree). Since 2016, Christian Schrenk is working on epigenetics in cancer at the working group of Prof. Dr. Kassack. His research interests are: (1) chemoresistance in cancer, molecular mechanisms of chemoresistance, and exploration of combination treatments to overcome intrinsic and acquired drug resistance. (2) Role of histone deacetylases (HDACs) in cancer: use of novel and selective HDACi to overcome chemoresistance in various cancers. He is a member of a graduate school (GRK2158)

and his current project is supported from the Deutsche Forschungsgemeinschaft (DFG) (KA 1942/1-1).



Dr. Leandro Antonio Alves Avelar was born in Passos, Brazil on March 15<sup>th</sup>, 1988. He studied Pharmacy in the University of Londrina and received his MSc in Chemistry from the University of Sao Paulo. He obtained his PhD in Pharmacy at the Heinrich-Heine University Düsseldorf and currently works as a postdoctoral researcher at the group of Prof. Dr. Thomas Kurz in the same university. His research interests are design and synthesis of enzymatic inhibitors as potential anticancer and antiparasitic drugs.



Dr. Alexandra Hamacher, born on 29.06.1971 in Eschweiler, is senior scientist and lecturer at the Institute of Pharmaceutical and Medicinal Chemistry at the Heinrich-Heine University Düsseldorf. She studied pharmacy at the University of Bonn and obtained her PhD from the University of Bonn. After 2 years as guest researcher (postdoc) at CAESAR (Center of advanced European Studies and Research, MPG), she started her work as a postdoctoral scientist in the working group of Prof. Dr. Kassack. Her research interests are: (1) enhancement of cisplatin-induced cytotoxicity in HNSCC by combination treatment of cisplatin with small molecule inhibitors. (2) Epigenetic treatment of cisplatin-resistant HNSCC to overcome and prevent chemoresistance.



Marc Pflieger was born in Wittlich, Germany in 1991 and graduated with a BSc degree in Biochemistry from Ruhr-University Bochum in 2013. In 2014 he did an Erasmus exchange year at Cardiff University. After returning to Germany, he graduated with an MSc in Biochemistry from Ruhr-University Bochum. Marc moved back to the UK and graduated from the University of Bath in 2016 with an MRes in Sustainable Chemical Technologies. Since 2016 he is a PhD student under the supervision of Prof Kurz and focusses on the development of selective histone deacetylase inhibitors.



Thomas Kurz was born in Hannover, Germany on February 8<sup>th</sup> 1967. He received his Pharmacy degree from the University of Hamburg in 1995 and his approbation as Pharmacist in 1996. Thomas obtained his PhD in Pharmaceutical Chemistry in 1999 from the University of Hamburg followed by postdoctoral research on heterocyclic chemistry and crop protection at the University of Florida (Gainesville, FL) and Nippon Soda Co., Ltd. (Alachua, FL). In 2007 he obtained his Habilitation degree in Pharmaceutical Chemistry from the University of Hamburg and in the same year he was appointed Professor of Pharmaceutical and Medicinal Chemistry at the Heinrich Heine University, Duesseldorf. His research interests are the development

of metalloenzyme inhibitors and inhibitors of protein protein interactions for the treatment of infectious diseases and cancer.



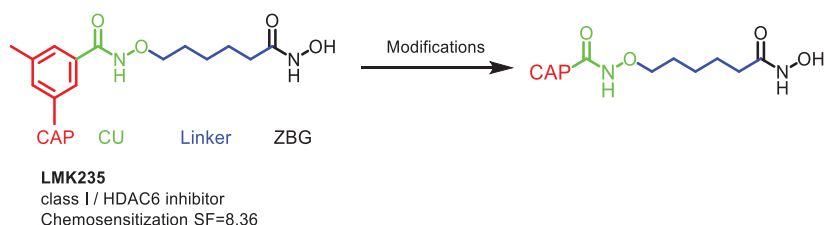
Professor Dr. Matthias U. Kassack, born on 05.06.1964 in Leverkusen, is Director of the Institute of Pharmaceutical and Medicinal Chemistry at the Heinrich-Heine University Düsseldorf. He studied pharmacy at the University of Regensburg and obtained his PhD from the University of Bonn. After 2 years of postdoctoral studies at the University of California San Francisco, he returned to the University of Bonn for his habilitation. Since 2006, Professor Kassack holds a position as full professor at the Heinrich-Heine University Düsseldorf. His research interests are: (1) chemoresistance in cancer, discovery of therapeutic targets, and development of combination treatments for overcoming chemoresistance. (2) Epigenetics in cancer chemoresistance: use of epigenetic drugs to overcome and prevent chemoresistance in various cancers. (3) Medicinal chemistry of histone deacetylase inhibitors: biological evaluation, phenotypic screening, high content fluorescence imaging. He has published more than 100 peer-reviewed publications.

more than 100 peer-reviewed publications.

## Objective

Histone deacetylases (HDACs) are metalloproteases that catalyze the removal of acetyl groups from lysine residues of both histone and nonhistone proteins. They are clinically validated targets for the treatment of cancer. The currently approved HDAC inhibitors (HDACi) have been successfully applied for the treatment of lymphoma and myeloma. However, the first-generation HDACi addresses multiple HDAC isozymes (pan-inhibitor) which might cause the observed adverse effects. Therefore, the design and development of isozyme-selective HDACi present a promising strategy in order to improve the risk-benefit profiles compared to pan-HDACi. Furthermore, selective HDACi provide important tool molecules to elucidate the biological role of individual HDACs in health and disease.

In the course of the first project, we focused on the structural optimization of LMK235. Due to the promising anticancer properties of LMK235, modifications of the cap group were performed to increase the antiproliferative and synergistic activity in cisplatin-sensitive and cisplatin-resistant cancer cells (Scheme 1).



Scheme 1: Modification of LMK235 in its cap region (highlighted in red).

The second research project aimed to design and develop class IIa selective HDAC inhibitors by addressing the lower pocket and the employment of selectivity directing zinc binding groups (e.g. the 5-(trifluoromethyl)-1,2,4-oxadiazole (TFMO) moiety).

The target structures are illustrated in Figure 8. For addressing the lower pocket, the following structural motifs were proposed:

- 4-Phenyl substituted thiazolyl-based hydroxamates **1** exhibiting various cap groups.
- $\alpha$ -Phenyl substituted derivatives demonstrating either a hydroxamic acid **2-4** or 2-(trifluoromethyl)-1,3,4-oxadiazole moiety **5-7** as ZBG.

## Objective

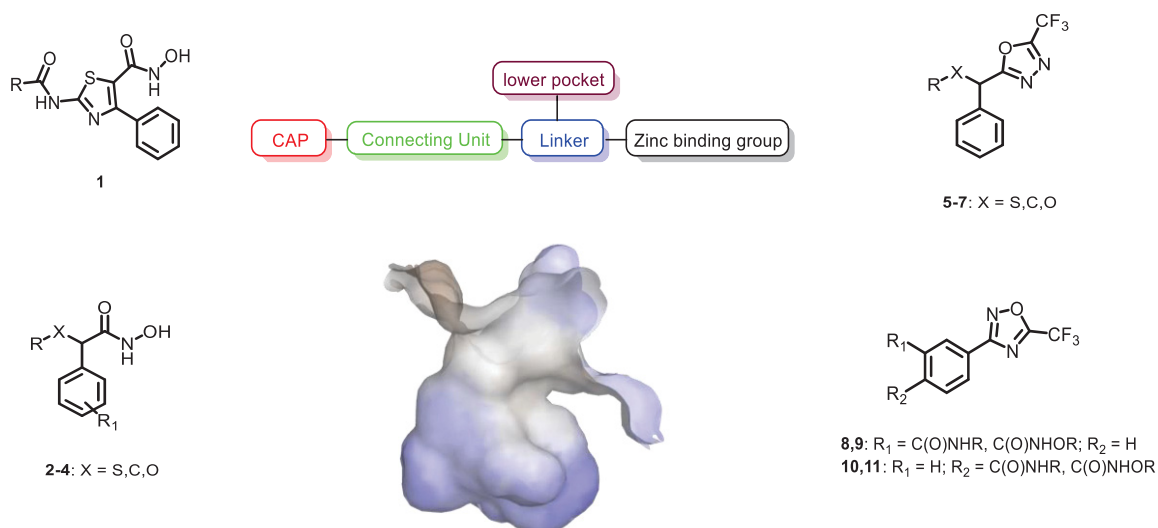


Figure 8: The target structures (left and right). Pharmacophore model of class IIa HDAC inhibitors and the binding pocket of HDAC4 (PDB:4CBT).<sup>[97]</sup>

Another approach to generate class IIa selective HDAC inhibitors was the evaluation of the TFMO moiety as a selectivity directing ZBG (Figure 9). In this respect, *meta*- and *para*-substituted TFMO-derivatives **8-11** were synthesized with a variable alkoxyamide/amide domain.

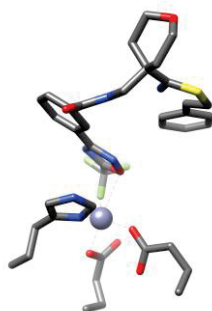


Figure 9: Stick representation of the active zinc interactions of TMP269 and HDAC7 (PDB: 3ZNR).<sup>[98]</sup>

All synthesized target structures were evaluated in an HDAC isozyme profiling and in respect to their antiproliferative and HDAC inhibitory activity in carcinoma cell lines (collaboration with the Kassack group, Heinrich Heine University, Düsseldorf).

---

## References

- [1] World Health Organization, *WHO Report on Cancer*, **2020**.
- [2] R. L. Siegel, K. D. Miller, A. Jemal, *CA. Cancer J. Clin.* **2018**, *68*, 7–30.
- [3] D. Hanahan, R. A. Weinberg, *Cell* **2011**, *144*, 646–674.
- [4] D. Hanahan, R. A. Weinberg, *Cell* **2000**, *100*, 57–70.
- [5] S. L. Floor, J. E. Dumont, C. Maenhaut, E. Raspe, *Trends Mol. Med.* **2012**, *18*, 509–515.
- [6] P. W. Laird, *Hum. Mol. Genet.* **2005**, *14*, R65–R76.
- [7] S. Sharma, T. K. Kelly, P. A. Jones, *Carcinogenesis* **2010**, *31*, 27–36.
- [8] S. Kumar, A. K. Pandey, in *Oxidative Stress Diagnostic Methods Appl. Med. Sci.*, Springer Singapore, Singapore, **2017**, pp. 113–125.
- [9] Z. Zhao, A. Shilatifard, *Genome Biol.* **2019**, *20*, 245.
- [10] C. Seidel, M. Schnekenburger, M. Dicato, M. Diederich, *Genes Nutr.* **2012**, *7*, 357–367.
- [11] M. Grunstein, *Nature* **1997**, *389*, 349–352.
- [12] M. K. Shanmugam, F. Arfuso, S. Arumugam, A. Chinnathambi, B. Jinsong, S. Warriar, L. Z. Wang, A. P. Kumar, K. S. Ahn, G. Sethi, et al., *Oncotarget* **2018**, *9*, 11414–11426.
- [13] M. K. Shanmugam, G. Sethi, in *Pharmacol. Ther.*, **2013**, pp. 627–657.
- [14] R. B. Selvi, A. Swaminathan, S. Chatterjee, M. K. Shanmugam, F. Li, G. B. Ramakrishnan, K. S. Siveen, A. Chinnathambi, M. E. Zayed, S. A. Alharbi, et al., *Oncotarget* **2015**, *6*, 43806–43818.
- [15] M. K. Shanmugam, G. Sethi, in *Subcell. Biochem.*, **2013**, pp. 627–657.
- [16] S. C. Kim, R. Sprung, Y. Chen, Y. Xu, H. Ball, J. Pei, T. Cheng, Y. Kho, H. Xiao, L. Xiao, et al., *Mol. Cell* **2006**, *23*, 607–618.
- [17] C. Choudhary, C. Kumar, F. Gnad, M. L. Nielsen, M. Rehman, T. C. Walther, J. V. Olsen, M. Mann, *Science (80- )*. **2009**, *325*, 834–840.
- [18] S. Bassett, M. Barnett, *Nutrients* **2014**, *6*, 4273–4301.
- [19] H. J. Kim, S. C. Bae, *Am. J. Transl. Res.* **2011**.
- [20] J. M. Villalba, F. J. Alcaín, *BioFactors* **2012**, *38*, 349–359.
- [21] D.-M. Chuang, Y. Leng, Z. Marinova, H.-J. Kim, C.-T. Chiu, *Trends Neurosci.* **2009**, *32*, 591–601.
- [22] Y. Hai, D. W. Christianson, *Nat. Chem. Biol.* **2016**, *12*, 741–747.

- 
- [23] M. S. Finnin, J. R. Donigian, A. Cohen, V. M. Richon, R. A. Rifkind, P. A. Marks, R. Breslow, N. P. Pavletich, *Nature* **1999**, *401*, 188–193.
- [24] C. Corminboeuf, P. Hu, M. E. Tuckerman, Y. Zhang, *J. Am. Chem. Soc.* **2006**, *128*, 4530–4531.
- [25] K. Vanommeslaeghe, F. De Proft, S. Loverix, D. Tourwé, P. Geerlings, *Bioorg. Med. Chem.* **2005**, *13*, 3987–3992.
- [26] Y. Hai, D. W. Christianson, *Nat. Chem. Biol.* **2016**, *12*, 741–747.
- [27] W. Weichert, A. Röske, V. Gekeler, T. Beckers, C. Stephan, K. Jung, F. R. Fritzsche, S. Niesporek, C. Denkert, M. Dietel, et al., *Br. J. Cancer* **2008**, *98*, 604–610.
- [28] W. Weichert, A. Roske, S. Niesporek, A. Noske, A.-C. Buckendahl, M. Dietel, V. Gekeler, M. Boehm, T. Beckers, C. Denkert, *Clin. Cancer Res.* **2008**, *14*, 1669–1677.
- [29] Y. Minamiya, T. Ono, H. Saito, N. Takahashi, M. Ito, M. Mitsui, S. Motoyama, J. Ogawa, *Lung Cancer* **2011**, *74*, 300–304.
- [30] H. Osada, Y. Tatematsu, H. Saito, Y. Yatabe, T. Mitsudomi, T. Takahashi, *Int. J. Cancer* **2004**, *112*, 26–32.
- [31] T. Rikimaru, A. Taketomi, Y. Yamashita, K. Shirabe, T. Hamatsu, M. Shimada, Y. Maehara, *Oncology* **2007**, *72*, 69–74.
- [32] W. Weichert, A. Röske, V. Gekeler, T. Beckers, M. P. Ebert, M. Pross, M. Dietel, C. Denkert, C. Röcken, *Lancet Oncol.* **2008**, *9*, 139–148.
- [33] C. A. Krusche, P. Wülfing, C. Kersting, A. Vloet, W. Böcker, L. Kiesel, H. M. Beier, J. Alfer, *Breast Cancer Res. Treat.* **2005**, *90*, 15–23.
- [34] S. Yoon, G. H. Eom, *Chonnam Med. J.* **2016**, *52*, 1.
- [35] A. A. Lane, B. A. Chabner, *J. Clin. Oncol.* **2009**, *27*, 5459–5468.
- [36] J. C. Wang, M. I. Kafeel, B. Avezbakiyev, C. Chen, Y. Sun, C. Rathnasabapathy, M. Kalavar, Z. He, J. Burton, S. Lichter, *Oncology* **2011**, *81*, 325–329.
- [37] M. LLeonart, F. Vidal, D. Gallardo, M. Diaz-Fuertes, F. Rojo, M. Cuatrecasas, L. López-Vicente, H. Kondoh, C. Blanco, A. Carnero, et al., *Oncol. Rep.* **2006**, *16*, 603–608.
- [38] C. Seidel, M. Schnekenburger, M. Dicato, M. Diederich, *Epigenomics* **2015**, *7*, 103–118.
- [39] B. B. Mishra, V. K. Tiwari, *Eur. J. Med. Chem.* **2011**, *46*, 4769–4807.
- [40] J. Rey-Ladino, A. G. Ross, A. W. Cripps, D. P. McManus, R. Quinn, *Vaccine* **2011**, *29*, 6464–6471.
- [41] B. Haefner, *Drug Discov. Today* **2003**, *8*, 536–544.

## References

---

- [42] M. S. Butler, *J. Nat. Prod.* **2004**, *67*, 2141–2153.
- [43] M. K. Shanmugam, J. H. Lee, E. Z. P. Chai, M. M. Kanchi, S. Kar, F. Arfuso, A. Dharmarajan, A. P. Kumar, P. S. Ramar, C. Y. Looi, et al., *Semin. Cancer Biol.* **2016**, *40–41*, 35–47.
- [44] M. Shanmugam, R. Kannaiyan, G. Sethi, *Nutr. Cancer* **2011**, *63*, 161–173.
- [45] A. Deorukhkar, S. Krishnan, G. Sethi, B. B. Aggarwal, *Expert Opin. Investig. Drugs* **2007**, *16*, 1753–1773.
- [46] C. Cerella, M.-H. Teiten, F. Radogna, M. Dicato, M. Diederich, *Biotechnol. Adv.* **2014**, *32*, 1111–1122.
- [47] F. Morceau, S. Chateauvieux, M. Orsini, A. Trécul, M. Dicato, M. Diederich, *Biotechnol. Adv.* **2015**, *33*, 785–797.
- [48] M. Schnekenburger, M. Dicato, M. Diederich, *Biotechnol. Adv.* **2014**, *32*, 1123–1132.
- [49] M. Schumacher, M. Kelkel, M. Dicato, M. Diederich, *Biotechnol. Adv.* **2011**, *29*, 531–547.
- [50] M. A. Holbert, R. Marmorstein, *Curr. Opin. Struct. Biol.* **2005**, *15*, 673–680.
- [51] G. P. Delcuve, D. H. Khan, J. R. Davie, *Clin. Epigenetics* **2012**, *4*, 1–13.
- [52] G. M. Cragg, D. J. Newman, *Pure Appl. Chem.* **2005**, *77*, 7–24.
- [53] I. Paterson, E. Anderson, *Science (80- )*. **2005**, *310*, 451–453.
- [54] P.-M. Yang, Y.-L. Liu, Y.-C. Lin, C.-T. Shun, M.-S. Wu, C.-C. Chen, *Cancer Res.* **2010**, *70*, 7699–7709.
- [55] V. J. Venditto, E. E. Simanek, *Mol. Pharm.* **2010**, *7*, 307–349.
- [56] M. M. Alam, M. Naeem, M. M. A. Khan, M. Uddin, in *Cathar. Roseus*, Springer International Publishing, Cham, **2017**, pp. 277–307.
- [57] A. Barbuti, Z.-S. Chen, *Cancers (Basel)*. **2015**, *7*, 2360–2371.
- [58] M. G. Riggs, R. G. Whittaker, J. R. Neumann, V. M. Ingram, *Nature* **1977**, *268*, 462–464.
- [59] G. Stanley McKnight, L. Hager, R. D. Palmiter, *Cell* **1980**, *22*, 469–477.
- [60] M. Gottlicher, *EMBO J.* **2001**, *20*, 6969–6978.
- [61] S. Chateauvieux, S. Eifes, F. Morceau, C. Grigorakaki, M. Schnekenburger, E. Henry, M. Dicato, M. Diederich, *Biochem. Pharmacol.* **2011**, *81*, 498–509.
- [62] A. Berger, S. Venturelli, M. Kallnischkies, A. Böcker, C. Busch, T. Weiland, S. Noor, C. Leischner, T. S. Weiss, U. M. Lauer, et al., *J. Nutr. Biochem.* **2013**, *24*, 977–985.
- [63] S. Venturelli, A. Berger, A. Böcker, C. Busch, T. Weiland, S. Noor, C. Leischner, S. Schleicher, M. Mayer, T. S. Weiss, et al., *PLoS One* **2013**, *8*, e73097.

## References

---

- [64] T. Senawong, S. Misuna, S. Khaopha, S. Nuchadomrong, P. Sawatsitang, C. Phaosiri, A. Surapaitoon, B. Sripana, *BMC Complement. Altern. Med.* **2013**, *13*, 232.
- [65] H.-W. Ryu, D.-H. Lee, D.-H. Shin, S. Hyun Kim, S. Kwon, *Planta Med.* **2015**, *81*, 222–227.
- [66] P. Jones, S. Altamura, P. K. Chakravarty, O. Cecchetti, R. De Francesco, P. Gallinari, R. Ingenito, P. T. Meinke, A. Petrocchi, M. Rowley, et al., *Bioorg. Med. Chem. Lett.* **2006**, *16*, 5948–5952.
- [67] H. Itazaki, K. Nagashima, K. Sugita, H. Yoshida, Y. Kawamura, Y. Yasuda, K. Matsumoto, K. Ishii, N. Uotani, H. Nakai, et al., *J. Antibiot. (Tokyo)*. **1990**, *43*, 1524–1532.
- [68] S. N. Ononye, M. D. VanHeyst, E. Z. Oblak, W. Zhou, M. Ammar, A. C. Anderson, D. L. Wright, *ACS Med. Chem. Lett.* **2013**, *4*, 757–761.
- [69] I. M. Chung, M. Y. Kim, W. H. Park, H. I. Moon, *Pharmazie* **2008**, *63*, 774–776.
- [70] L. Li, H.-J. Dai, M. Ye, S.-L. Wang, X.-J. Xiao, J. Zheng, H.-Y. Chen, Y. Luo, J. Liu, *Cancer Cell Int.* **2012**, *12*, 49.
- [71] C. Parolin, N. Calonghi, E. Presta, C. Boga, P. Caruana, M. Naldi, V. Andrisano, L. Masotti, G. Sartor, *Biochim. Biophys. Acta - Mol. Cell Biol. Lipids* **2012**, *1821*, 1334–1340.
- [72] A. K. Ghosh, S. Kulkarni, *Org. Lett.* **2008**, *10*, 3907–3909.
- [73] M. Yoshida, M. Kijima, M. Akita, T. Beppu, *J. Biol. Chem.* **1990**.
- [74] P. A. Marks, *Mol. Oncol. Causes Cancer Targets Treat.* **2015**, *46*, 912–920.
- [75] M. Duvic, R. Talpur, X. Ni, C. Zhang, P. Hazarika, C. Kelly, J. H. Chiao, J. F. Reilly, J. L. Ricker, V. M. Richon, et al., *Blood* **2007**, *109*, 31–39.
- [76] S. Minucci, P. G. Pelicci, *Nat. Rev. Cancer* **2006**, *6*, 38–51.
- [77] V. M. Richon, S. Emiliani, E. Verdin, Y. Webb, R. Breslow, R. A. Rifkind, P. A. Marks, *Proc. Natl. Acad. Sci.* **1998**, *95*, 3003–3007.
- [78] C. D. Hose, K. D. Petersen, R. H. Shoemaker, S. Kondapaka, P. Pezzoli, J. Monforte, A. Monks, M. Sehested, G. Vansant, *Anticancer. Drugs* **2009**, *20*, 682–692.
- [79] P. Atadja, *Cancer Lett.* **2009**, *280*, 233–241.
- [80] H. Ueda, H. Nakajima, Y. Hori, T. Goto, M. Okuhara, *Biosci. Biotechnol. Biochem.* **1994**, *58*, 1579–1583.
- [81] L. Bao, H. Diao, N. Dong, X. Su, B. Wang, Q. Mo, H. Yu, X. Wang, C. Chen, *Cell Biol. Toxicol.* **2016**, *32*, 469–482.
- [82] A. Kretsovali, C. Hadjimichael, N. Charmpilas, *Stem Cells Int.* **2012**, *2012*, 1–10.
- [83] B. E. Gryder, Q. H. Sodji, A. K. Oyelere, *Future Med. Chem.* **2012**, *4*, 505–524.

- 
- [84] S. Shen, A. P. Kozikowski, *ChemMedChem* **2016**, *11*, 15–21.
- [85] J. Melesina, L. Praetorius, C. V. Simoben, D. Robaa, W. Sippl, *Future Med. Chem.* **2018**, *10*, 1537–1540.
- [86] M. Mottamal, S. Zheng, T. Huang, G. Wang, *Molecules* **2015**, *20*, 3898–3941.
- [87] G. Powis, D. Mustacich, A. Coon, *Free Radic. Biol. Med.* **2000**, *29*, 312–322.
- [88] Y. Pommier, O. Sordet, S. Antony, R. L. Hayward, K. W. Kohn, *Oncogene* **2004**, *23*, 2934–2949.
- [89] A. Suraweera, K. J. O’Byrne, D. J. Richard, *Front. Oncol.* **2018**, *8*, 1–15.
- [90] H. P. Mohammad, O. Barbash, C. L. Creasy, *Nat. Med.* **2019**, *25*, 403–418.
- [91] N. Deschamps, C. A. Simões-Pires, P.-A. Carrupt, A. Nurisso, *Drug Discov. Today* **2015**, *20*, 736–742.
- [92] A. R. Maolanon, A. S. Madsen, C. A. Olsen, *Cell Chem. Biol.* **2016**, DOI 10.1016/j.chembiol.2016.06.011.
- [93] M. Yang, C. B. Gocke, X. Luo, D. Borek, D. R. Tomchick, M. Machius, Z. Otwinowski, H. Yu, *Mol. Cell* **2006**, *23*, 377–387.
- [94] S. S. M. Alqarni, A. Murthy, W. Zhang, M. R. Przewloka, A. P. G. Silva, A. A. Watson, S. Lejon, X. Y. Pei, A. H. Smits, S. L. Kloet, et al., *J. Biol. Chem.* **2014**, *289*, 21844–21855.
- [95] J. M. Cramer, J. N. Scarsdale, N. M. Walavalkar, W. A. Buchwald, G. D. Ginder, D. C. Williams, *J. Biol. Chem.* **2014**, *289*, 1294–1302.
- [96] C. J. Millard, P. J. Watson, L. Fairall, J. W. R. Schwabe, *Trends Pharmacol. Sci.* **2017**, DOI 10.1016/j.tips.2016.12.006.
- [97] R. W. Bürli, C. A. Luckhurst, O. Aziz, K. L. Matthews, D. Yates, K. A. Lyons, M. Beconi, G. McAllister, P. Breccia, A. J. Stott, et al., *J. Med. Chem.* **2013**, *56*, 9934–9954.
- [98] M. Lobera, K. P. Madauss, D. T. Pohlhaus, Q. G. Wright, M. Trocha, D. R. Schmidt, E. Baloglu, R. P. Trump, M. S. Head, G. A. Hofmann, et al., *Nat. Chem. Biol.* **2013**, *9*, 319–325.
- [99] S. Bhatia, V. Krieger, M. Groll, J. D. Osoko, N. Reißing, H. Ahlert, A. Borkhardt, T. Kurz, D. W. Christianson, J. Hauer, et al., *J. Med. Chem.* **2018**, DOI 10.1021/acs.jmedchem.8b01487.
- [100] D. Wootten, A. Christopoulos, P. M. Sexton, *Nat. Rev. Drug Discov.* **2013**, DOI 10.1038/nrd4052.
- [101] R. Ferreira De Freitas, R. J. Harding, I. Franzoni, M. Ravichandran, M. K. Mann, H.

- Ouyang, M. Lautens, V. Santhakumar, C. H. Arrowsmith, M. Schapira, *J. Med. Chem.* **2018**, DOI 10.1021/acs.jmedchem.8b00258.
- [102] Z. H. Foda, M. A. Seeliger, *Nat. Chem. Biol.* **2014**, DOI 10.1038/nchembio.1630.
- [103] H. Zhijun, W. Shusheng, M. Han, L. Jianping, Q. Li-sen, L. Dechun, *Tumor Biol.* **2016**, *37*, 10257–10267.
- [104] T. C. Johnstone, K. Suntharalingam, S. J. Lippard, *Chem. Rev.* **2016**, *116*, 3436–3486.
- [105] D. Lebwohl, R. Canetta, *Eur. J. Cancer* **1998**, *34*, 1522–1534.
- [106] M. Galanski, *Recent Pat. Anticancer. Drug Discov.* **2006**, *1*, 285–295.
- [107] A. W. Prestayko, J. C. D’Aoust, B. F. Issell, S. T. Crooke, *Cancer Treat. Rev.* **1979**, *6*, 17–39.
- [108] S. Dasari, P. Bernard Tchounwou, *Eur. J. Pharmacol.* **2014**, *740*, 364–378.
- [109] L. Galluzzi, I. Vitale, J. Michels, C. Brenner, G. Szabadkai, A. Harel-Bellan, M. Castedo, G. Kroemer, *Cell Death Dis.* **2014**, *5*, e1257–e1257.
- [110] U. Lassen, L. R. Molife, M. Sorensen, S. A. Engelholm, L. Vidal, R. Sinha, R. T. Penson, P. Buhl-Jensen, E. Crowley, J. Tjornelund, et al., *Br. J. Cancer* **2010**, *103*, 12–17.
- [111] K. Stenzel, A. Hamacher, F. K. Hansen, C. G. W. Gertzen, J. Senger, V. Marquardt, L. Marek, M. Marek, C. Romier, M. Remke, et al., *J. Med. Chem.* **2017**, *60*, 5334–5348.
- [112] M. Pflieger, A. Hamacher, T. Öz, N. Horstick-Muche, B. Boesen, C. Schrenk, M. U. Kassack, T. Kurz, *Bioorg. Med. Chem.* **2019**, *27*, 115036.
- [113] L. Marek, A. Hamacher, F. K. Hansen, K. Kuna, H. Gohlke, M. U. Kassack, T. Kurz, *J. Med. Chem.* **2013**, *56*, 427–436.
- [114] A. Kaletsch, M. Pinkerneil, M. J. Hoffmann, A. A. Jaguva Vasudevan, C. Wang, F. K. Hansen, C. Wiek, H. Hanenberg, C. Gertzen, H. Gohlke, et al., *Clin. Epigenetics* **2018**, *10*, 100.

## **Novel alkoxyamide-based histone deacetylase inhibitors reverse cisplatin resistance in chemoresistant cancer cells**

Published in: Bioorganic and Medicinal Chemistry

Impact Factor: 2.802 (2018-2019)

DOI: 10.1016/j.bmc.2019.115108

Contribution:

- Synthesis of the compounds **7-9, 10a-e, 11, 12a-c, 13a-h, 14**
- Manuscript and supporting information



## Novel alkoxyamide-based histone deacetylase inhibitors reverse cisplatin resistance in chemoresistant cancer cells

Yodita Asfaha, Christian Schrenk, Leandro A. Alves Avelar, Friedrich Lange, Chenyin Wang, Jan J. Bandolik, Alexandra Hamacher, Matthias U. Kassack<sup>\*,1</sup>, Thomas Kurz<sup>\*,1</sup>

Institut für Pharmazeutische und Medizinische Chemie, Heinrich-Heine-Universität Düsseldorf, Universitätsstr. 1, 40225 Düsseldorf, Germany

### ARTICLE INFO

#### Keywords:

Histone deacetylases  
Cisplatin resistance  
Chemosensitizing effects

### ABSTRACT

Although histone deacetylase inhibitors (HDACi) have shown promising antitumor effects in specific types of blood cancer, their effects on solid tumors are limited. Previously, we developed LMK235 (**5**), a class I and class IIb preferential HDACi with chemosensitizing effects on breast cancer, ovarian cancer and HNSCC. Based on its promising effects on solid tumor cells, we modified the cap group of **5** to improve its anticancer activity. The tri- and dimethoxy-phenyl substituted compounds **13a** and **13d** turned out to be the most potent HDAC inhibitors of this study. The isoform profiling revealed a dual HDAC2/HDAC6 inhibition profile, which was confirmed by the acetylation of  $\alpha$ -tubulin and histone H3 in Cal27 and Cal27CisR. In combination with cisplatin, both compounds enhanced the cisplatin-induced cytotoxicity via caspase-3/7 activation. The effect was more pronounced in the cisplatin resistant subline Cal27CisR. The pretreatment with **13d** resulted in a complete resensitisation of Cal27CisR with IC<sub>50</sub> values in the range of the parental cell line. Therefore, **13d** may serve as an epigenetic tool to analyze and modulate the cisplatin resistance of solid tumors.

### 1. Introduction

Epigenetic control plays an essential role in gene regulation through chemical modifications of DNA and post-translational modifications of histones.<sup>1</sup> An important post-translational modification is the reversible histone acetylation, which is regulated by histone acetyltransferases (HATs) and histone deacetylases (HDACs). The mammalian zinc dependent HDACs are subdivided into three classes: class I (HDACs 1–3, 8), class II (IIa: HDACs 4, 5, 7, 9; IIb: HDACs 6, 10) and class IV (HDAC 11).<sup>2</sup> Recent studies have shown that HDACs are overexpressed in a wide spectrum of cancer types.<sup>3–5</sup> Therefore, their inhibition provides a promising tool for developing novel anticancer drugs. The success of this approach is shown by the FDA approval of four HDAC inhibitors (HDACi) for the treatment of specific types of blood cancer (Fig. 1). The currently used and widely accepted pharmacophore model for HDACi features the following three elements: a zinc binding group (ZBG), a linker, that mimics the alkylic chain of the acetyl-lysine motif and interacts with the substrate binding tunnel and a cap, also known as surface recognition domain.<sup>6,7</sup> According to their structural features, HDACi can be classified into 4 main classes:

hydroxamates, cyclic peptides, carboxylic acids and *o*-amino amides.<sup>7,8</sup>

Most of the currently approved HDACi inhibit a broad isoform spectrum (pan-inhibitor) and can cause severe side effects such as diarrhea, fatigue or cardiac toxicity. It is still under debate if inhibition of specific HDAC isoforms will improve these drawbacks.<sup>13</sup>

In a previous study, we have varied the CAP and linker region of vorinostat resulting in compound LMK235 (**5**) (*N*-((6-(hydroxyamino)-6-oxohexyl)oxy)-3,5-dimethylbenzamide) with improved cytotoxic and synergistic effects against several human cancer cell lines compared to vorinostat.<sup>14</sup> Reassessment of the HDAC isoform profile with improved assays and reference compounds showed a class I/class IIb preference of LMK235 (**5**).<sup>15,16</sup> Due to the promising anticancer properties of **5**, we aimed to explore the effects of further chemical cap group modifications with regard to antiproliferative and synergistic activity in cisplatin-sensitive and cisplatin-resistant cancer cells. (Scheme 1).

Abbreviations: HATU, Hexafluorophosphate Azabenzotriazole Tetramethyl Uronium; MTT, 3-(4,5-Dimethylthiazole-2-yl)-2,5-diphenyltetrazoliumbromide

\* Corresponding authors.

E-mail addresses: [matthias.kassack@hhu.de](mailto:matthias.kassack@hhu.de) (M.U. Kassack), [thomas.kurz@hhu.de](mailto:thomas.kurz@hhu.de) (T. Kurz).

<sup>1</sup> MUK and TK share senior and corresponding authorship.

<https://doi.org/10.1016/j.bmc.2019.115108>

Received 29 March 2019; Received in revised form 3 September 2019; Accepted 11 September 2019

Available online 13 September 2019

0968-0896/ © 2019 Elsevier Ltd. All rights reserved.

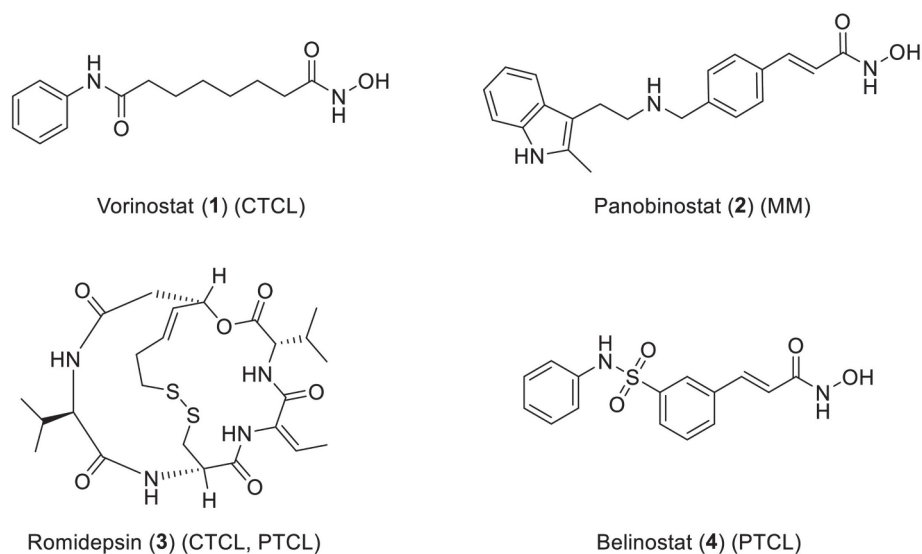
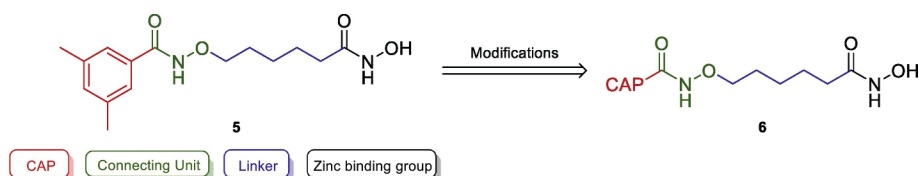


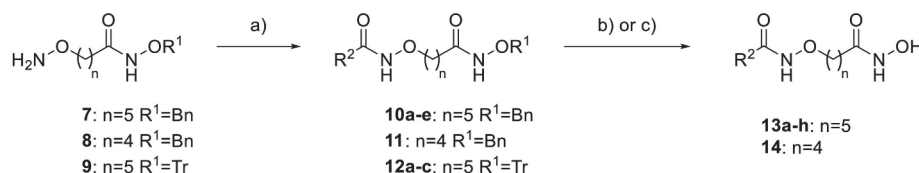
Fig. 1. Chemical structures of FDA approved HDAC inhibitors 1–4 and their indications. CTCL: cutaneous T-cell lymphoma, MM: multiple myeloma, PTCL: peripheral T-cell lymphoma.<sup>9–12</sup>



## 2. Results and discussion

### 2.1. Chemistry

The synthesis of the alkoxyamide-based HDACi 5 has been reported previously by Marek et al.<sup>14</sup> Here, we report the synthesis of nine novel analogs (**13a–h**, **14**) starting from the *O*-protected aminoxy-hydroxamates **7**, **8** and **9**. Initial attempts to introduce the alkoxyamide moiety using 1-ethyl-3-(3-dimethylaminopropyl)-carbodiimide (EDCI) mediated standard protocols were unsuccessful. However, HATU mediated acylation of **7**, **8** and **9** with the respective carboxylic acid provided the protected intermediates **10a–e**, **11**, **12a–c**. Finally, their deprotection was accomplished by hydrolysis and by a Lewis acid mediated procedure,<sup>17</sup> respectively (Scheme 2).



Scheme 2. Reagents and conditions: a) 1.00 eq R<sup>2</sup>COOH, 1.00 eq HATU, 2.00 eq DIPEA, DMF, rt., 16 h, 40–65% b) Pd/C, H<sub>2</sub>, (1 bar), MeOH, rt., 35–40% c) 10.0 eq TFA, 10.0 eq Et<sub>3</sub>SiH, DCM, 30–40%.

### 2.2. Biological evaluation

#### 2.2.1. Cellular HDAC inhibitory activity and antiproliferative effects

The novel derivatives of compound **5**, **13a–13h** and **14**, were first tested for their antiproliferative effects by MTT assay and for cellular HDAC inhibitory activity in the ovarian cancer cell line A2780 and the head-neck cancer cell line Cal27 (Table 1). Since the cellular HDAC assay only serves as an explorative assay and needs confirmation in enzymatic assays, it was performed only once. Thus, no errors are reported for the cellular HDAC assay. Results are presented in Table 1.

Compound **5**, vorinostat, and cisplatin served as controls. The compounds with the highest antiproliferative activity against the cell line A2780 and Cal27 were **13b** and **13d** with IC<sub>50</sub> values ranging from 0.72 to 1.55 μM. **13b** and **13d** were also the most active compounds in the cellular HDAC assay with similar IC<sub>50</sub> values compared to the MTT assay. Interestingly **13a** and **13f** showed moderate antiproliferative activity in contrast to **13b** and **13d**, and at the same time increased HDAC inhibitory activity with IC<sub>50</sub> values similar to **13b** but slightly higher than **13d**. 2 Methoxy groups (**13d**) attached to the cap group instead of 3 (**13a**) seem to play a minor role for the HDAC inhibitory activity of the compounds, while cytotoxicity is increased (over 15-fold in A2780, approx. 4-fold in Cal27). Of note, all tested compounds were slightly more potent in Cal27 cells (MTT assay). We could confirm the superior potency of compound **5** (LMK235) over vorinostat. The initial

evaluation revealed comparable cytotoxicity and cellular HDAC inhibition for **13d** and **5**. Interestingly, increasing the size of the phenyl substituents was tolerated (**13b**) whereas introduction of halogen, -CF<sub>3</sub>, the pyridyl heterocycle or a shorter linker (**14**) reduced activity.

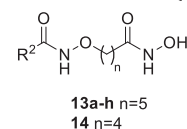


**Table 1**  
Antiproliferative effects and HDAC inhibitory activity of 13a-13h, 14, 5, vorinostat and cisplatin in A2780 and Cal27.

Compound	R <sup>2</sup>	A2780 (μM)		Cal27 (μM)	
		HDAC <sup>b</sup>	MTT	HDAC <sup>b</sup>	MTT
13a		1.18	13.8 ± 0.84	1.48	3.07 ± 0.15
13b		0.93	1.55 ± 0.12	1.30	1.0 ± 0.001
13c		3.79	13.7 ± 1.38	3.77	7.98 ± 1.10
13d		0.83	0.89 ± 0.006	0.45	0.72 ± 0.09
13e		11.0	30.5 ± 4.16	10.56	15.8 ± 0.57
13f		1.65	10.2 ± 0.22	1.80	3.63 ± 0.16
13g		7.20	64.0 ± 6.68	9.40	45.0 ± 11.3
13h		14.5	68.4 ± 6.50	12.7	28.1 ± 1.67
14		4.24	9.34 ± 0.14	3.36	8.67 ± 0.40
5		0.17	0.97 ± 0.01	0.55	0.76 ± 0.04
vorinostat		0.91	2.04 ± 0.20	0.59	1.50 ± 0.10
cisplatin <sup>a</sup>		n.d.	1.88 ± 0.06	n.d.	2.27 ± 0.20

n.d. = not determined.

<sup>a</sup> Data taken from<sup>18</sup>.

<sup>b</sup> Cellular HDAC assay was only performed once with 3 replicates due to its explorative character. Values are the mean ± SEM of three independent experiments conducted in triplicate.

### 2.2.2. Inhibitory activity on HDAC2, HDAC4, HDAC6 and HDAC8

For further evaluation, compounds were tested against human recombinant HDAC2, HDAC4, HDAC6 and HDAC8. Compound 5, vorinostat, and CHDI-00390576-0000-004 served as reference compounds (Table 2). Cellular HDAC assay revealed compounds 13a, 13b, 13d and 13f as the most promising inhibitors. The two compounds with methoxy substituents attached to the cap group showed the strongest inhibition of HDAC2 and HDAC6. 13a and 13d displayed K<sub>i</sub> values of

0.03 μM to 0.09 μM for HDAC2 and HDAC6, with low inhibition of HDAC4 (K<sub>i</sub>: 93.1 μM and 49.2 μM) and moderate inhibition of HDAC8 (K<sub>i</sub>: 6.40 μM and 5.69 μM).

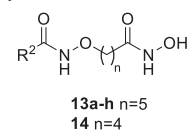


**Table 2**

Inhibitory activity of 13a – 13h, 14, vorinostat and CHDI-00390576-0000-004 on recombinant human HDAC2, HDAC4, HDAC6 and HDAC8.

Compound	R <sup>2</sup>	K <sub>i</sub> (μM)			
		HDAC2	HDAC4	HDAC6	HDAC8
13a		0.09	93.1	0.06	6.40
13b		1.57	> 100	2.15	28.1
13c		0.58	> 100	0.10	14.7
13d		0.06	49.2	0.03	5.69
13e		0.55	83.7	0.56	4.90
13f		0.21	31.8	0.12	4.44
13g		1.33	> 100	0.33	10.0
13h		1.36	> 100	0.35	18.9
14		0.37	> 100	0.42	22.3
5		0.08	> 100	0.05	4.81
vorinostat		0.09	28.4	0.02	5.33
CHDI-00390576-0000-004		n.d.	0.17	n.d.	n.d.

Data shown are the mean of pooled data from at least three experiments each carried out in triplicates. The standard deviations are < 10% of the mean. nd = not determined.

### 2.2.3. Acetylation of $\alpha$ -tubulin and histone H3

In order to prove HDAC inhibition at a cellular level, acetylation of  $\alpha$ -tubulin and histone-H3 was tested by western blot analysis in Cal27 and Cal27CisR (Fig. 2). Incubation with vorinostat, compound 5, 13a, or 13d induced accumulation of acetyl  $\alpha$ -tubulin compared to control indicating that all four compounds inhibit HDAC6. Further, the four compounds increased acetylation of histone-H3 proving cellular inhibition of class I HDACs.

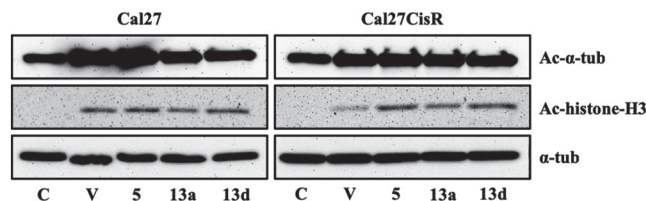


**Fig. 2.** Compound-induced  $\alpha$ -tubulin and histone H3 acetylation in Cal27 and Cal27CisR. Representative immunoblot analysis of  $\alpha$ -tubulin ( $\alpha$ -tub), acetylated  $\alpha$ -tubulin (Ac- $\alpha$ -tub), and acetylated histone H3 (Ac-histone-H3) in Cal27 and Cal27CisR after 24 h incubation with vehicle (C) or 3  $\mu$ M vorinostat (V), 1.5  $\mu$ M 5, 5  $\mu$ M 13a, or 1.5  $\mu$ M 13d, respectively.

### 2.2.4. Enhancement of cisplatin-induced cytotoxicity

Next, the effect of the most active compounds 13a and 13d on cisplatin-induced cytotoxicity was tested in comparison to compound 5 at Cal27 and the cisplatin-resistant subline Cal27CisR. Cal27CisR is about 10-fold resistant compared to Cal27 and was established by intermittent treatment of Cal27 with cisplatin over several weeks.<sup>19</sup> Results are displayed in Table 3. Overall, both new HDACi 13a and 13d induce an increase in cisplatin potency with 13d being more potent than 13a. Interestingly, 13d gave a higher shift factor than compound 5, thus indicating a higher potency to reverse cisplatin resistance than compound 5. Fig. 3 displays these results: 13d is able to shift the cisplatin concentration-effect curve of Cal27CisR back to the one of Cal27. Furthermore, the effect of increased cisplatin potency by HDACi was higher in the cisplatin-resistant cell line Cal27CisR than it was in

**Table 3**

IC<sub>50</sub> values of cisplatin in the absence and presence of 0.4  $\mu$ M/0.8  $\mu$ M 5, 1.4  $\mu$ M/6  $\mu$ M 13a, 0.2  $\mu$ M/0.8  $\mu$ M 13d in Cal27/Cal27CisR cells.

Compound	Cell line			
	Cal27		Cal27CisR	
	IC <sub>50</sub>	SF	IC <sub>50</sub>	SF
Cisplatin	4.36	–	42.8	–
Cisplatin + 13a	2.24	1.95	5.54	7.73
Cisplatin + 13d	1.15	3.79	3.35	12.8
Cisplatin + 5	1.47	3.00	5.12	8.36

Data shown are the mean of pooled data from at least three experiments each carried out in triplicates. The standard deviations are < 10% of the mean. All shift factors are significant (*t*-test, *p* < .05).

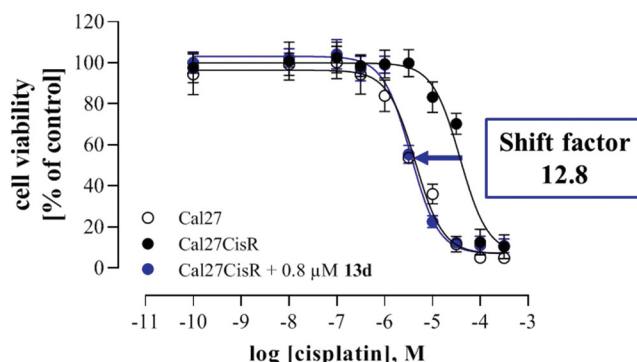


**Fig. 3.** 48 h preincubation with 13d reversed cisplatin resistance of Cal27CisR cells. Cal27 (white dots) and Cal27CisR (black dots) were incubated with cisplatin for 72 h. Preincubation of Cal27CisR with 0.8  $\mu$ M 13d 72 h prior to cisplatin incubation (blue dots) reduced the IC<sub>50</sub> value even below the IC<sub>50</sub> of the parental cell line Cal27. SF were calculated as the ratio of the IC<sub>50</sub> of cisplatin alone and the IC<sub>50</sub> of the combination of cisplatin with 13d. (For interpretation of the references to colour in this figure legend, the reader is referred to the web version of this article.)

cisplatin-sensitive Cal27 as evident by higher shift factors obtained in Cal27CisR (Table 3). The question remains whether class I HDAC inhibition or HDAC6 inhibition is responsible for the observed effect. In a previous study, we could demonstrate that inhibition of class I HDACs is responsible for the chemosensitizing effect and not HDAC6 inhibition.<sup>18</sup> However, dual inhibitors (class I and HDAC6) are not detrimental for chemosensitization as shown in our previous study<sup>18</sup> and in this study with compound 13d. This is also in accordance with literature data: Caponigro et al. have highlighted the effectiveness of class I HDAC inhibition in sensitizing oral squamous cell carcinomas to cisplatin.<sup>20</sup> In

addition, HDAC1 and HDAC2 are known as critical regulators of the DNA damage response by modulating the ATM pathway.<sup>21</sup> We thus conclude that inhibition of class I HDACs is mainly responsible for the chemosensitizing effects of the inhibitors 13a and 13d seen in this study in Cal27CisR.

#### 2.2.5. Enhancement of cisplatin-induced caspase 3/7 activation

Cancer cells can develop resistance to platinum-based anticancer agents by DNA repair mechanisms or DNA damage tolerance such as translesion synthesis (TLS). The cotreatment of cancer cells with an

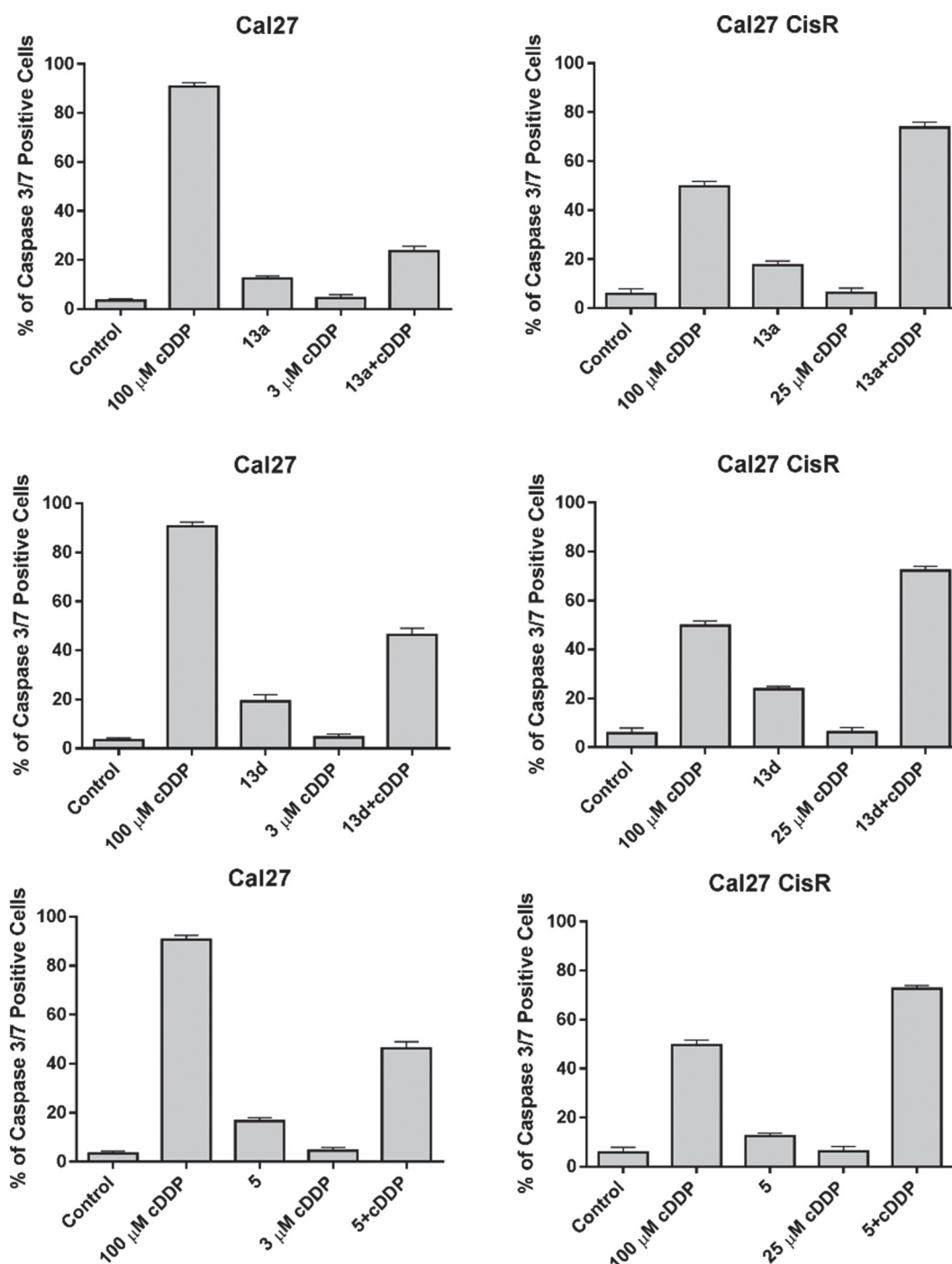


Fig. 4. Compounds 13a and 13d enhanced caspase-dependent cell death in Cal27 and Cal27CisR. Shown are the mean values of caspase 3/7 positive cells in percent  $\pm$  SEM ( $n = 3$ ). Cal27 cells were incubated with 2.8  $\mu$ M 13a, 0.4  $\mu$ M 13d or 0.8  $\mu$ M 5 prior to an additional 24 h incubation with 3  $\mu$ M Cisplatin (cDDP). Cal27CisR cells were incubated with 8  $\mu$ M 13a, 0.8  $\mu$ M 13d or 0.8  $\mu$ M 5 prior to an additional 24 h incubation with 25  $\mu$ M Cisplatin. 100  $\mu$ M Cisplatin served as positive control.

HDACi can overcome these resistance mechanisms and may therefore obtain fundamental importance for the resensitization of resistant cell lines.<sup>22</sup>

**13a** and **13d** increased the cisplatin-induced cytotoxicity significantly. This prompted us to test if the increased cytotoxic activity of the combination treatment (**13a** or **13d** with cisplatin) was mediated by apoptosis. Estimation of caspase 3/7 activation was used as marker for apoptosis induction. Because cisplatin is only incubated for 24 h in the cell-based caspase 3/7 activation assay, 2-fold higher concentrations of **13a**, **13d** and **5** were used than in the MTT shift experiments above. Results are presented in Figs. 4 and 5. **13a** and **13d** markedly enhanced caspase 3/7 activation in the combination treatment in comparison to HDACi or cisplatin alone in both, Cal27 and Cal27CisR. Both compounds are similarly effective as compound **5**. Notably, the increase in cisplatin-induced caspase activation upon combination treatment was more pronounced in the cisplatin-resistant cell line Cal27CisR than in Cal27. Since caspase activation is downstream of DNA damage and the HDACi effect is significantly larger in resistant Cal27CisR (resistant – i.e. reduced DNA damage signaling) than in sensitive Cal27 (sensitive – i.e. intact DNA damage signaling), we have a hint of enhanced DNA damage signaling induced by HDACi. This is also in accordance with data from Table 3 showing higher shift factors for Cal27CisR than for Cal27 cells. In Cal27CisR, **13a**, **13d**, and compound **5** gave even more caspase-positive cells than 100  $\mu\text{M}$  cisplatin which is an approx. 2-fold  $\text{IC}_{50}$  of cisplatin. Furthermore, the combined effects of the HDACi and cisplatin is synergistic, as the sum of HDACi- and cisplatin-induced caspase activation is significantly lower than the caspase activation by combination treatment. This is illustrated in Fig. 5 for compound **13d**: all samples (control, **13d** only, cisplatin only, **13d** plus cisplatin) contained approx. the same number of cells stained in blue

(Hoechst33342). Caspase activation only slightly increased after mono-compound treatment whereas the combination of **13d** plus cisplatin dramatically increased caspase activation shown in green.

A synergistic apoptotic effect of HDACi and cisplatin is in agreement with Zacharioudakis and coworkers.<sup>22</sup> They suggested that HDACi increase the accessibility of platinum-based anticancer agents and showed that this resulted in an accumulation of DNA-Pt adducts at particular sites in the genome. DNA-Pt adducts colocalized with the E3 ubiquitin ligase RAD18 triggering accumulation and colocalization of the polymerase Pol $\eta$  which in turn colocalized with the proliferating cell nuclear antigen (PCNA). Cotreatment of HDACi and cisplatin then resulted in the ubiquitylation of PCNA and subsequent apoptosis. The synergistic apoptotic response is either due to the inability of polymerases to efficiently bypass DNA-Pt clusters,<sup>23</sup> or HDAC inhibition caused a lesion bypass at the expense of DNA repair mechanisms.<sup>24</sup> Due to the structural similarity between SAHA and the HDACi reported in this study, a similar mode of action can be anticipated, but remains to be further investigated.

### 2.3. Molecular docking

To rationalize the observed preference of compounds **13a** and **13d** towards HDAC2 and HDAC6 and their lack of inhibitory activity towards HDAC4, both inhibitors were docked in the crystal structures of HDAC2,<sup>25</sup> HDAC4<sup>26</sup> and HDAC6<sup>27</sup> using Autodock4.2<sup>28</sup> (Fig. 6). The docking of **13a** and **13d** in HDAC4 resulted in no proper binding modes of the hydroxamic acid group with the catalytic zinc ion, which is in agreement with the enzymatic assays. In the docking performed with HDAC2 and HDAC6, the hydroxamate group of **13a** and **13d** showed bidentate interactions with the zinc metal, showing additional hydrogen bond with the catalytic Tyr782 in HDAC6 and Tyr308 in HDAC2. Additionally, the position of the alkoxyamide connecting unit of **13a** in both docked conformations suggests hydrogen bonds with Ser568 (HDAC6, 2.7 Å) and Asp104 (HDAC2, 2.3 Å) (Fig. 6A and B). In the docking of **13d** this interaction was restricted to Asp104 (2.1 Å) of HDAC2 (Fig. 6C). These residues have been previously demonstrated to be essential for the anchoring of peptide substrates<sup>27,29</sup> and in case of Asp104 to interact with the amide group, which serves as connecting unit of vorinostat.<sup>25</sup>

The di- and trimethoxyphenyl cap groups occupy a hydrophobic region of the recognition surface of HDAC2 (Fig. 6A and D orange region). These interactions are very similar to those observed in the crystal structure of HDAC2 and vorinostat<sup>25</sup> suggesting that the proposed binding modes are akin to vorinostat. The dockings in HDAC6 showed that in this isoform, the cap group of **13a** interacts with a basin present at the side of HDAC6 catalytic site (Fig. 6 B orange region). Despite this region has been shown to be essential to interaction of HDAC6 substrate recognition,<sup>30</sup> the major part of the clinically-approved HDACi including vorinostat, were shown not to interact with this region, but with the loop H25 (Fig. 6B).<sup>27</sup> This interaction, however, could only be observed in the docking of **13d** (Fig. 6D) and could be one possible explanation for the lower activity of **13a** towards HDAC6 compared to vorinostat and **13d**.

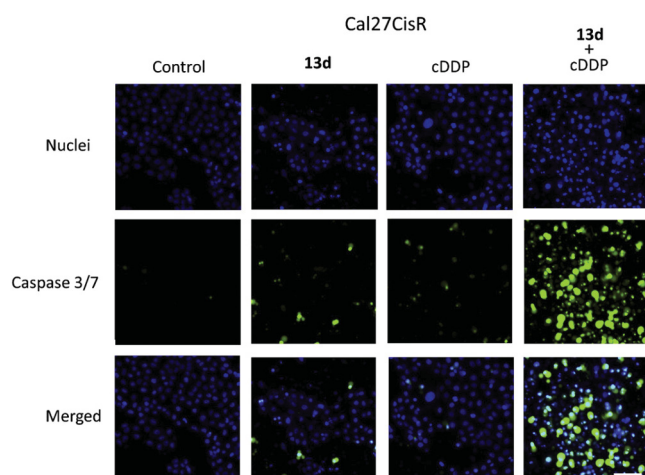


**Fig. 5.** Preincubation with 0.8  $\mu\text{M}$  **13d** led to synergistic enhancement of caspase 3/7 activation when combined with cisplatin. Exemplary pictures of nuclear stain Hoechst (blue) and active caspase 3/7 (green) of Cal27CisR incubated with 0.8  $\mu\text{M}$  **13d** or 25  $\mu\text{M}$  cisplatin alone or in combination. Scale bar, 200  $\mu\text{m}$  (applies to all images). (For interpretation of the references to colour in this figure legend, the reader is referred to the web version of this article.)

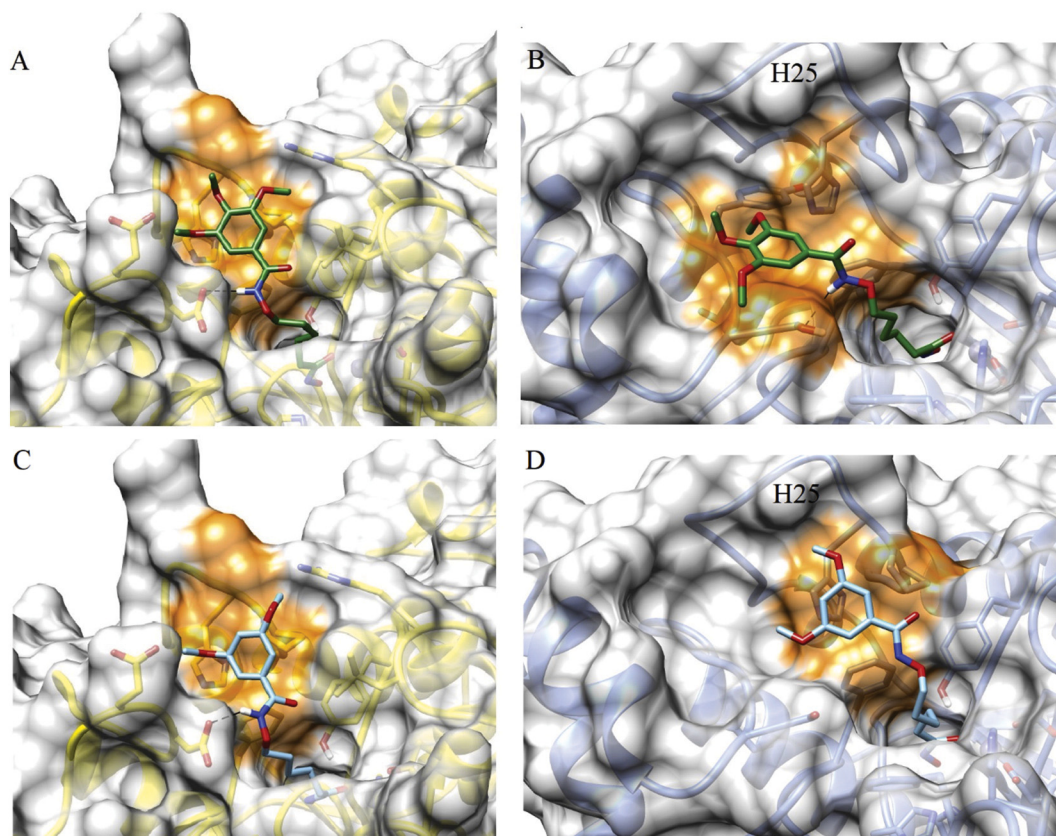


**Fig. 6.** A) Docking of **13a** (green) in HDAC2 (PDB **4LXZ**)<sup>25</sup> with the interactions highlighted in orange, hydrogen bond with Asp104 shown as a dashed line. B) Docking of **13a** (green) in HDAC6 (PDB **5EDU**)<sup>19</sup> with the interactions highlighted in orange, hydrogen bond interaction with Ser568 shown as dashed line. C) Docking of **13d** (blue) in HDAC2 (PDB **4LXZ**)<sup>25</sup> with the interactions highlighted in orange, hydrogen bond with Asp104 shown as a dashed line. D) Docking of **13d** (blue) in HDAC6 (PDB **5EDU**)<sup>19</sup> with the interactions highlighted in orange. (For interpretation of the references to colour in this figure legend, the reader is referred to the web version of this article.)

### 3. Conclusions

In this study, we evaluated structural variations of the CAP and linker group of compound **5** (LMK235), a previously introduced class I and class IIb preferential HDACi. We obtained two derivatives, **13a** and **13d** which displayed similar potency in HDAC2 and HDAC6 inhibition as compound **5**. Furthermore, **13a** and **13d** increased cisplatin potency in cisplatin-resistant cancer cells, and **13d** was slightly more effective in reversing cisplatin resistance than compound **5**. Thus, another epigenetic tool, **13d**, for evaluation in chemo-resistant cancer has been developed through this study.

### Declaration of Competing Interest

The authors declare that they have no conflict of interest.

### Acknowledgements

YA, CS, MUK, and TK gratefully acknowledge support from the Deutsche Forschungsgemeinschaft (DFG) for grant number KA 1942/1-1 to MUK and grant number KU 1577/2-1 to TK, and also the support from the DFG research training group 270650915/GRK 2158. We further acknowledge funding by the DFG for the Thermofisher Arrayscan XTI (Grant: INST 208/690-1 FUGG to MUK) and the CHDI Foundation Inc. for providing the compound CHDI-00390576-0000-004.

### Appendix A. Supplementary data

All experimental procedures and analytical data for all synthesized

compounds are provided as supplementary information. Supplementary data to this article can be found online at <https://doi.org/10.1016/j.bmc.2019.115108>.

### References

- Januar V, Saffery R, Ryan J. *Int J Epidemiol*. 2015. <https://doi.org/10.1093/ije/dyu273>.
- Fischle W, Dequiedt F, Hendzel MJ, et al. *Mol Cell*. 2002;9(1):45–57 <http://www.ncbi.nlm.nih.gov/pubmed/11804585> [Accessed March 5, 2019].
- Gryder BE, Sodji QH, Oyeler AK. *Future Med Chem*. 2012. <https://doi.org/10.4155/fmc.12.3>.
- Witt O, Deubzer HE, Milde T, Oehme I. *Cancer Lett*. 2009. <https://doi.org/10.1016/j.canlet.2008.08.016>.
- Ropero S, Esteller M. *Mol Oncol*. 2007. <https://doi.org/10.1016/j.molonc.2007.01.001>.
- Jung M. *Curr Med Chem*. 2012. <https://doi.org/10.2174/0929867013372058>.
- Melesina J, Praetorius L, Simoben CV, Robaa D, Sippl W. *Future Med Chem*. 2018. <https://doi.org/10.4155/fmc-2018-0125>.
- Bolden JE, Peart MJ, Johnstone RW. *Nat Rev Drug Discov*. 2006. <https://doi.org/10.1038/nrd2133>.
- Richon VM, Emiliani S, Verdin E, et al. *Proc Natl Acad Sci*. 1998. <https://doi.org/10.1073/PNAS.95.6.3003>.
- Hose CD, Petersen KD, Shoemaker RH, et al. *Anti-Cancer Drugs*. 2009;20(8):682–692. <https://doi.org/10.1097/cad.0b013e32832e14e1>.
- Atadja P. *Cancer Lett*. 2009. <https://doi.org/10.1016/j.canlet.2009.02.019>.
- Furumai R, Matsuyama A, Kobashi N, et al. *Cancer Res*. 2002;62(17):4916–4921.
- Kim KP, Park SJ, Kim JE, et al. *Investig New Drugs*. 2015. <https://doi.org/10.1007/s10637-015-0262-2>.
- Marek L, Hamacher A, Hansen FK, et al. *J Med Chem*. 2013. <https://doi.org/10.1021/jm301254q>.
- Kaletsch A, Pinkerneck M, Hoffmann MJ, et al. *Clin Epigenetics*. 2018;10(1):100. <https://doi.org/10.1186/s13148-018-0531-y>.
- Choi SY, Kee HJ, Jin L, et al. *Biomed Pharmacother*. 2018;101:145–154. <https://doi.org/10.1016/j.biopha.2018.02.071>.
- Alves Avelar LA, Held J, Engel JA, et al. *Arch Pharm (Weinheim)*.

- 2017;350(3–4):1–11. <https://doi.org/10.1002/ardp.201600347>.
18. Stenzel K, Hamacher A, Hansen FK, et al. *J Med Chem*. 2017;60(13):5334–5348. <https://doi.org/10.1021/acs.jmedchem.6b01538>.
19. Gosepath EM, Eckstein N, Hamacher A, et al. *Int J Cancer*. 2008;123(9):2013–2019. <https://doi.org/10.1002/ijc.23721>.
20. Caponigro F, Di Gennaro E, Ionna F, et al. *BMC Cancer*. 2016;16(1):1–10. <https://doi.org/10.1186/s12885-016-2957-y>.
21. Thurn KT, Thomas S, Raha P, Qureshi I, Munster PN. *Mol Cancer Ther*. 2013;12(10):2078–2087. <https://doi.org/10.1158/1535-7163.mct-12-1242>.
22. Zacharioudakis E, Agarwal P, Bartoli A, et al. *Angew Chemie - Int Ed*. 2017;56(23):6483–6487. <https://doi.org/10.1002/anie.201701144>.
23. Schneider S, Reißner T, Ziv O, Livneh Z, Carell T. *ChemBioChem*. 2010;11(11):1521–1524. <https://doi.org/10.1002/cbic.201000211>.
24. Koch SC, Kuper J, Gasteiger KL, et al. *Proc Natl Acad Sci U S A*. 2015;112(27):8272–8277. <https://doi.org/10.1073/pnas.1508509112>.
25. Lauffer BEL, Mintzer R, Fong R, et al. *J Biol Chem*. 2013. <https://doi.org/10.1074/jbc.M113.490706>.
26. Luckhurst CA, Breccia P, Stott AJ, et al. *ACS Med Chem Lett*. 2016. <https://doi.org/10.1021/acsmchemlett.5b00302>.
27. Hai Y, Christianson DW. *Nat Chem Biol*. 2016;12(9):741–747. <https://doi.org/10.1038/nchembio.2134>.
28. Morris G, Huey R, Lindstrom W, et al. *J Comput Chem*. 2009;28(1):2785–2791. <https://doi.org/10.1002/jcc>.
29. Watson PJ, Millard CJ, Riley AM, et al. 2016. <https://doi.org/10.1038/ncomms11262>.
30. Miyake Y, Keusch JJ, Wang L, et al. *Nat Chem Biol*. 2016;12(9):748–754. <https://doi.org/10.1038/nchembio.2140>.

## Supporting Information

### Novel alkoxyamide-based histone deacetylase inhibitors reverse cisplatin resistance in chemoresistant cancer cell lines

*Yodita Asfaha\**, *Christian Schrenk\**, *Leandro Alvares Alvelar\**, *Fritz Lange\**, *Chenyin Wang\**, *Jan J. Bandolik\**, *Alexandra Hamacher\**, *Matthias U. Kassack\*#*, *Thomas Kurz\*#*

\*Institut für Pharmazeutische und Medizinische Chemie, Heinrich-Heine-Universität Düsseldorf, Universitätsstr. 1, 40225 Düsseldorf, Germany, # MUK and TK share senior and corresponding authorship.

## 1. Experimental section

All solvents and chemicals were used as purchased without further purification. The reaction controls were carried out on Macherey Nagel precoated silica gel plates (with fluorescence indicator UV<sub>254</sub>) using ethyl acetate/ *n*-hexane and dichloromethane / methanole as solvent systems. Detection was achieved with ultraviolet irradiation (254 nm). Flash column chromatography was performed with CombiFlashRf200 (TeleDynelsco) with the solvent mixtures specified in the corresponding experiment. Proton (<sup>1</sup>H) and carbon (<sup>13</sup>C) NMR spectra were recorded on Bruker Avance III – 300, Bruker Avance DRX – 500 or Bruker Avance III – 600. Spectra were referenced to the residual non-deuterated solvent signal (<sup>1</sup>H-NMR: DMSO-*d*<sub>6</sub> (2.50), <sup>13</sup>C-NMR: DMSO-*d*<sub>6</sub> (39.52)). Chemical shifts are given in parts per million (ppm). Signal patterns are indicated as: singlet (s), doublet (d), triplet (t), quartet (q), or multiplet (m). APCI-MS was carried out using Advion expression<sup>L</sup> CMS spectrometer. Melting points were taken in open capillaries on a Büchi M-565 melting point apparatus and are uncorrected. Analytical HPLC analysis were carried out on a Knauer HPLC system comprising an Azura P 6.1L pump, an Optimas 800 autosampler, a Fast Scanning Spectrophotometer K-2600 and Knauer Reversed Phase column (SN: FK36). UV absorption was detected at 254 nm. The solvent gradient table is shown in Table 1. The purity of all final compounds was 95% or higher.

Table 1: The solvent gradient table for analytic HPLC analysis.

Time / min	Water + 0.1% TFA	ACN + 0.1% TFA
Initial	90	10
0.50	90	10
20.0	0	100
30.0	0	100
31.0	90	10
40.0	90	10

### Synthesis of 6-(aminooxy)-*N*-(benzoyloxy)hexaneamide (7)

1) 6-Bromohexanoic acid (3.90 g, 20.0 mmol, 1.00 eq) was dissolved in dry THF (80.0 mL) and cooled to -15 °C. Subsequently, *N*-methylmorpholine (2.42 mL, 22.0 mmol, 1.10 eq) and isobutyl chloroformate (2.84 mL, 22.0 eq, 1.10 eq) were added. After 15 min *O*-benzylhydroxylamine (2.84 mL, 20.0 eq, 1.00 eq) was added dropwise to the reaction mixture. The mixture was allowed to warm to rt and stirred overnight. After filtration and removing the solvent *in vacuo*, the residue was diluted in EtOAc. The organic phase was washed with saturated NaHCO<sub>3</sub> (3x 50 mL) and 10% (w/w) citric acid (3x 50 mL). The organic layer was dried over Na<sub>2</sub>SO<sub>4</sub>, filtered and the solvent was removed *in vacuo* to give the intermediate *N*-(benzloxy)-6-bromohexaneamide.

2) *N*-(benzloxy)-6-bromohexaneamide (6.21 g, 20.0 mmol, 1.00 eq) and *N*-hydroxyphthalimide (3.92 g, 24.0 mmol, 1.20 eq) were dissolved in acetonitrile (80 mL). After addition of triethylamine (5.54 mL, 40.0 mmol, 2.00 eq), the reaction mixture was refluxed for 12 h. The solvent was evaporated under reduced pressure and the residue was diluted with EtOAc, washed with saturated NaHCO<sub>3</sub> (7x 50 mL), dried over Na<sub>2</sub>SO<sub>4</sub> and filtered. The solvent was removed *in vacuo* to yield *N*-(Benzloxy)-6-((1,3-dioxoisindolin-2-yl)oxy)hexaneamide (4.57 g, 14.0 mmol, 70%) as a white powder. All spectroscopic data were in agreement with the literature.<sup>1</sup>

3) To a solution of *N*-(benzloxy)-6-((1,3-dioxoisindolin-2-yl)oxy)hexaneamide (1.01 g, 2.00 mmol, 1.00 eq) in CH<sub>2</sub>Cl<sub>2</sub> (10 mL), hydrazine monohydrate (0.20 mL, 4.00 mmol, 2.00 eq) was added dropwise. The reaction mixture was stirred overnight at rt. The resulting precipitate was filtered, and the organic layer was washed with saturated NaHCO<sub>3</sub> (3x 10 mL). After drying over Na<sub>2</sub>SO<sub>4</sub>, filtration and removing the solvent, 6-(aminooxy)-*N*-(benzoyloxy)hexaneamide (7) (0.61 g, 1.50 mmol, 75%) was obtained as a yellowish oil.

### Synthesis of 6-(aminooxy)-*N*-(trityloxy)hexanamide (9)

1) 6-Bromohexanoic acid (6.96 g, 35.7 mmol, 1.00 eq) was dissolved in dry THF (80.0 mL) and cooled to -15 °C. Subsequently, *N*-methylmorpholine (2.77 mL, 39.3 mmol, 1.10 eq) and isobutyl chloroformate (3.81 mL, 39.3 mmol, 1.10 eq) were added. After 15 min *O*-tritylhydroxylamine (9.82 g, 35.7 mmol, 1.00 eq) was added dropwise to the reaction

mixture. The mixture was allowed to warm to rt and stirred overnight. After filtration and removing the solvent *in vacuo*, the residue was diluted in EtOAc. The organic phase was washed with saturated NaHCO<sub>3</sub> (3x 50 mL), dried over Na<sub>2</sub>SO<sub>4</sub> and filtered. The solvent was removed *in vacuo* to give the intermediate 6-bromo-*N*-(trityloxy)hexanamide.

2) 6-Bromo-*N*-(trityloxy)hexanamide (6.03 g, 13.3 mmol, 1.00 eq) and *N*-hydroxyphthalimide (2.18 g, 13.3 mmol, 1.00 eq) were dissolved in acetonitrile (80 mL). After addition of triethylamine (3.70 mL, 26.6 mmol, 2.00 eq), the reaction mixture was refluxed for 12 h. The solvent was evaporated under reduced pressure and the residue was diluted in EtOAc, washed with saturated NaHCO<sub>3</sub> (7x 50 mL), dried over Na<sub>2</sub>SO<sub>4</sub> and filtered. The solvent was removed *in vacuo* to yield 6-((1,3-dioxoisindolin-2-yl)oxy)-*N*-(trityloxy)hexanamide (4.54 g, 8.48 mmol, 64%) as a brownish powder. All spectroscopic data were in agreement with the literature.<sup>2</sup>

3) To a solution of 6-((1,3-dioxoisindolin-2-yl)oxy)-*N*-(trityloxy)hexanamide (2.13 g, 4.00 mmol, 1.00 eq) in CH<sub>2</sub>Cl<sub>2</sub> (10 mL), hydrazine monohydrate (0.39 mL, 8.00 mmol, 2.00 eq) was added dropwise. The reaction mixture was stirred overnight at rt. The resulting precipitate was filtered, and the organic layer was washed with saturated NaHCO<sub>3</sub> (3x 10 mL). After drying over Na<sub>2</sub>SO<sub>4</sub> and removing the solvent, 6-(aminoxy)-*N*-(trityloxy)hexanamide (**9**) (1.22 g, 3.02 mmol, 75%) was obtained as a brownish powder.

#### **General procedure for the synthesis of 10a-e**

For the synthesis of the alkoxyamides **10a-e**, 1.00 eq of the respective carboxylic acid was dissolved in dry DMF (20 mL) and 1.00 eq HATU and 2.00 eq DIPEA were added. After stirring for 15 min the hydroxylamine **7** was added and the resulting mixture was stirred for 16h at rt. The solvent was removed, and the residue was diluted with EtOAc. The organic layer was washed with saturated NaHCO<sub>3</sub> (3x 50 mL), 10% (w/w) citric acid (3x 50 mL), dried over Na<sub>2</sub>SO<sub>4</sub> and filtered. After removing the solvent, the crude product was purified by flash column chromatography (prepacked silica cartridge, *n*-hexane/ethyl acetate) to provide the intermediates **10a-e**.

***N*-((6-(benzyloxy)amino-6-oxohexyl)oxy)-3,4,5-trimethoxybenzamide (10a)**

Colorless powder; yield:30%; mp:110 °C, <sup>1</sup>H-NMR (300 MHz, DMSO-*d*<sub>6</sub>) δ = 1.28 – 1.44 (m, 2H), 1.47 – 1.68 (m, 4H), 1.92 – 2.05 (m, 2H), 3.69 (s, 3H), 3.81 (s, 6H), 3.86 (t, *J* = 6.5 Hz, 2H), 4.78 (s, 2H), 7.09 (s, 2H), 7.29 – 7.50 (m, 5H), 10.96 (s, 1H), 11.58 (s, 1H) ppm. <sup>13</sup>C-NMR (75 MHz, DMSO-*d*<sub>6</sub>) δ = 24.7, 25.0, 27.4, 32.2, 56.0, 60.1, 75.2, 76.8, 104.5, 127.4, 128.2, 128.3, 128.8, 136.1, 140.1, 152.7, 163.6, 169.3 ppm. HPLC analysis: retention time = 10.1 min, >99%. APCI-MS(-): [M-H] = 445.8.

***N*-((6-(benzyloxy)amino-6-oxohexyl)oxy)-3,5-di-*tert*-butylbenzamide (10b)**

Colorless powder; yield:36%; mp:121 °C, <sup>1</sup>H-NMR (300 MHz, DMSO-*d*<sub>6</sub>) (600 MHz, DMSO-*d*<sub>6</sub>) δ = 1.30 (s, 18H), 1.32 – 1.42 (m, 2H), 1.50 – 1.65 (m, 4H), 1.97 (t, *J* = 7.4 Hz, 2H), 3.87 (t, *J* = 6.5 Hz, 2H), 7.55 (t, *J* = 1.9 Hz, 1H), 7.58 (d, *J* = 1.8 Hz, 2H), 8.67 (s, 1H), 10.35 (s, 1H), 11.60 (s, 1H) ppm. <sup>13</sup>C-NMR (151 MHz, DMSO-*d*<sub>6</sub>) δ = 24.9, 25.1, 27.5, 31.1, 32.2, 34.7, 75.1, 121.1, 125.2, 131.8, 150.5, 164.7, 169.0 ppm. HPLC analysis: retention time = 16.5 min, 97%. APCI-MS(-): [M-H] = 467.9.

***N*-((6-(benzyloxy)amino-6-oxohexyl)oxy)-3,5-difluorobenzamide (10c)**

Orange powder; yield:35%; mp:102 °C, <sup>1</sup>H NMR (300 MHz, DMSO-*d*<sub>6</sub>) δ = 1.26 – 1.41 (m, 2H), 1.47 – 1.65 (m, 4H), 1.97 (t, *J* = 7.2 Hz, 2H), 3.87 (t, *J* = 6.4 Hz, 2H), 4.78 (s, 2H), 7.31 – 7.42 (m, 5H), 7.42 – 7.54 (m, 3H), 10.95 (s, 1H), 11.81 (s, 1H) ppm. <sup>13</sup>C NMR (151 MHz, DMSO-*d*<sub>6</sub>) δ = 24.69, 24.92, 27.35, 32.15, 75.27, 76.76, 107.09 (t, *J* = 25.9 Hz), 110.45 (d, *J* = 5.5 Hz), 110.59 (d, *J* = 5.8 Hz), 128.19, 128.27, 128.76, 135.80 (t, *J* = 8.5 Hz), 136.10, 161.38 (d, *J* = 12.7 Hz), 161.48, 163.02 (d, *J* = 12.7 Hz), 169.28. ppm. HPLC analysis: retention time = 11.2 min, 92%. APCI-MS(-): [M-H] = 391.6.

***N*-((6-(benzyloxy)amino-6-oxohexyl)oxy)-3,5-dimethoxybenzamide (10d)**

Colorless powder; yield:42%; mp:93 °C, <sup>1</sup>H NMR (300 MHz, DMSO-*d*<sub>6</sub>) δ = 1.28 – 1.42 (m, 2H), 1.48 – 1.64 (m, 4H), 1.97 (t, *J* = 7.2 Hz, 2H), 3.77 (s, 6H), 3.85 (t, *J* = 6.4 Hz, 2H), 4.78 (s, 2H), 6.65 (t, *J* = 2.3 Hz, 1H), 6.90 (d, *J* = 2.3 Hz, 2H), 7.31 – 7.42 (m, 5H), 10.96 (s, 1H), 11.59 (s, 1H) ppm. <sup>13</sup>C NMR (151 MHz, DMSO-*d*<sub>6</sub>) δ = 25.18, 25.44, 27.87, 32.63, 55.90, 75.57, 77.23, 103.86, 105.40, 128.65, 128.74, 129.23, 134.82, 136.57, 160.82, 164.07, 169.75 ppm. HPLC analysis: retention time = 10.8 min, 96%. APCI-MS(-): [M] = 415.7.

### ***N*-((6-(benzyloxy)amino-6-oxohexyl)oxy)-3,5-bis(trifluoromethyl)benzamide (10e)**

Colorless powder; yield:40%; mp:124 °C, <sup>1</sup>H NMR (600 MHz, DMSO-*d*<sub>6</sub>) δ = 1.32 – 1.40 (m, 2H), 1.52 – 1.57 (m, 2H), 1.58 – 1.64 (m, 2H), 1.98 (t, *J* = 7.3 Hz, 2H), 3.92 (t, *J* = 6.5 Hz, 2H), 4.78 (s, 2H), 7.31 – 7.42 (m, 5H), 8.33 (s, 1H), 8.39 (s, 2H), 10.96 (s, 1H), 12.12 (s, 1H) ppm. <sup>13</sup>C NMR (151 MHz, DMSO-*d*<sub>6</sub>) δ = 24.68, 24.92, 27.38, 32.15, 75.40, 76.76, 123.46 (q, *J* = 273.0 Hz) 125.21, 127.91, 128.17, 128.26, 128.75, 130.56 (q, *J* = 33.3 Hz) 134.64, 136.10, 160.98, 169.26 ppm. HPLC analysis: retention time = 14.1 min, >99%. APCI-MS(-): [M-H] = 491.8.

### **General procedure for the synthesis of alkoxyamides 12a-c**

For the synthesis of the alkoxyamides **12a-c**, 1.00 eq of the respective acid was dissolved in dry DMF (20 mL) and 1.00 eq HATU and 2.00 eq DIPEA were added. After stirring for 15 min the hydroxylamine **9** was added and the resulting mixture was stirred for 16h at rt. The solvent was removed, and the residue was diluted with EtOAc. The organic layer was washed with saturated NaHCO<sub>3</sub> (3x 50 mL), dried over Na<sub>2</sub>SO<sub>4</sub> and filtered. After removing the solvent, the crude product was purified by flash column chromatography (prepacked silica cartridge, *n*-hexane/ethyl acetate) to provide the desired intermediates **12a-c**.

### **3,5-dibromo-*N*-((6-oxo-6-((trityloxy)amino)hexyl)oxy)benzamide(12a)**

Colorless powder; yield:48%; mp:175 °C, <sup>1</sup>H NMR (600 MHz, DMSO-*d*<sub>6</sub>) δ = 1.02 – 1.14 (m, 2H), 1.18 – 1.28 (m, 2H), 1.41 – 1.53 (m, 2H), 1.80 (t, *J* = 7.3 Hz, 2H), 3.78 (t, *J* = 6.7 Hz, 2H), 7.26 – 7.37 (m, 15H), 7.91 (d, *J* = 1.8 Hz, 2H), 8.05 (t, *J* = 1.9 Hz, 1H), 10.18 (s, 1H), 11.81 (s, 1H) ppm. <sup>13</sup>C NMR (151 MHz, DMSO-*d*<sub>6</sub>) δ = 24.49, 24.68, 27.27, 31.87, 75.22, 91.71, 122.66, 127.38, 127.49, 128.95, 129.04, 135.96, 136.26, 142.45, 161.07, 170.19 ppm. HPLC analysis: retention time = 18.6 min, >99%. APCI-MS(-): [M-2H] = 666.1.

### **2,3,5-triiodo-*N*-((6-oxo-6-((trityloxy)amino)hexyl)oxy)benzamide (12b)**

Colorless powder; yield:35%; mp:195 °C, <sup>1</sup>H NMR (600 MHz, DMSO-*d*<sub>6</sub>) δ = 1.02 – 1.10 (m, 2H), 1.19 – 1.27 (m, 2H), 1.41 – 1.51 (m, 2H), 1.79 (t, *J* = 7.3 Hz, 2H), 3.81 (t, *J* = 6.6 Hz, 2H), 7.12 – 7.43 (m, 15H), 7.56 – 7.61 (m, 1H), 8.30 (d, *J* = 2.0 Hz, 1H), 10.19 (s, 1H), 11.46 (s, 1H) ppm. <sup>13</sup>C NMR (151 MHz, DMSO-*d*<sub>6</sub>) δ = 24.52, 24.65, 27.28, 31.88, 74.94, 91.71, 95.35, 108.45, 113.54, 127.40, 127.50, 128.95, 135.16, 142.45, 144.21, 146.61, 164.32, 170.19 ppm. HPLC analysis: retention time = 18.5 min, >99%. APCI-MS(-): [M-*O*-trityl] = 628.9.

### **2,6-dichloro-*N*-((6-oxo-6-((trityloxy)amino)hexyl)oxy)benzamide (12c)**

Colorless powder; yield:30%; mp:158 °C, <sup>1</sup>H NMR (600 MHz, DMSO-*d*<sub>6</sub>) δ = 1.03 – 1.11 (m, 2H), 1.20 – 1.29 (m, 2H), 1.44 – 1.52 (m, 2H), 1.80 (t, *J* = 7.3 Hz, 2H), 3.81 (t, *J* = 6.7 Hz, 2H), 7.19 – 7.46 (m, 15H), 7.80 (s, 2H), 10.18 (s, 1H), 12.04 (s, 1H) ppm. <sup>1</sup>H NMR (600 MHz, DMSO-*d*<sub>6</sub>) δ = 1.03 – 1.11 (m, 2H), 1.20 – 1.29 (m, 2H), 1.44 – 1.52 (m, 2H), 1.80 (t, *J* = 7.3 Hz, 2H), 3.81 (t, *J* = 6.7 Hz, 2H), 7.19 – 7.46 (m, 15H), 7.80 (s, 2H), 10.18 (s, 1H), 12.04 (s, 1H) ppm. HPLC analysis: retention time = 16.8 min, 98%. APCI-MS(-): [M-2H] = 576.9.

### **General procedure for the synthesis of 13a-e, 14**

A solution of the respective *O*-benzylprotected hydroxamic acid (1.00 eq) in MeOH (30.0 mL) was hydrogenated at room temperature in the presence of a catalytic amount of Pd/C (10 wt%). After completion, the reaction mixture was filtered through celite and the filtrate was concentrated under reduced pressure. The crude products were purified by flash column chromatography (CH<sub>2</sub>Cl<sub>2</sub> / 30% MeOH in CH<sub>2</sub>Cl<sub>2</sub>).

### ***N*-((6-(hydroxyamino-6-oxohexyl)oxy)-3,4,5-trimethoxybenzamide (13a)**

Colorless powder; yield:41%; mp:165 °C, <sup>1</sup>H NMR (600 MHz, DMSO-*d*<sub>6</sub>) δ = 1.32 – 1.42 (m, 2H), 1.50 – 1.65 (m, 4H), 1.96 (t, *J* = 7.3 Hz, 2H), 3.69 (s, 3H), 3.81 (s, 6H), 3.86 (t, *J* = 6.4 Hz, 2H), 7.09 (s, 2H), 8.67 (s, 1H), 10.35 (s, 1H), 11.58 (s, 1H) ppm. <sup>13</sup>C NMR (151 MHz, DMSO-*d*<sub>6</sub>) δ = 24.9, 25.1, 27.5, 32.2, 56.0, 60.1, 75.2, 104.5, 127.4, 140.1, 152.7, 163.5, 169.0 ppm. HPLC analysis: retention time = 6.27 min, >99%. APCI-MS(-): [M-H] = 355.6.

### **3,5-di-tert-butyl-*N*-((6-(hydroxyamino-6-oxohexyl)oxy)benzamide (13b)**

Colorless powder; yield:48%; mp:165 °C, <sup>1</sup>H NMR (600 MHz, DMSO-*d*<sub>6</sub>) δ = 1.30 (s, 18H), 1.32 – 1.42 (m, 2H), 1.50 – 1.65 (m, 4H), 1.97 (t, *J* = 7.4 Hz, 2H), 3.87 (t, *J* = 6.5 Hz, 2H), 7.55 (t, *J* = 1.9 Hz, 1H), 7.58 (d, *J* = 1.8 Hz, 2H), 8.67 (s, 1H), 10.35 (s, 1H), 11.60 (s, 1H) ppm. <sup>13</sup>C NMR (151 MHz, DMSO-*d*<sub>6</sub>) δ = 24.9, 25.1, 27.5, 31.1, 32.2, 34.7, 75.1, 121.1, 125.2, 131.8, 150.5, 164.7, 169.0 ppm. HPLC analysis: retention time = 12.8 min, 97%. APCI-MS(-): [M-H] = 377.7.

### **3,5-difluoro-*N*-((6-(hydroxyamino-6-oxohexyl)oxy)benzamide (13c)**

Colorless powder; yield:36%; mp:164 °C. <sup>1</sup>H NMR (600 MHz, DMSO-*d*<sub>6</sub>) δ = 1.32 – 1.39 (m, 2H), 1.50 – 1.56 (m, 2H), 1.57 – 1.62 (m, 2H), 1.96 (t, *J* = 7.4 Hz, 2H), 3.87 (t, *J* = 6.5 Hz, 2H), 7.42 – 7.52 (m, 3H), 8.67 (s, 1H), 10.35 (s, 1H), 11.82 (s, 1H) ppm. <sup>1</sup>H NMR (600 MHz, DMSO-*d*<sub>6</sub>) δ = 1.32 – 1.39 (m, 2H), 1.50 – 1.56 (m, 2H), 1.57 – 1.62 (m, 2H), 1.96 (t, *J* = 7.4 Hz, 2H), 3.87 (t, *J* = 6.5 Hz, 2H), 7.42 – 7.52 (m, 3H), 8.67 (s, 1H), 10.35 (s, 1H), 11.82 (s, 1H) ppm. HPLC analysis: retention time = 7.07 min, 99%. APCI-MS(-): [M-H] = 301.4.

### ***N*-((6-(hydroxyamino-6-oxohexyl)oxy)-3,5-dimethoxybenzamide (13d)**

Colorless powder; yield:70%; mp:64 °C. <sup>1</sup>H NMR (300 MHz, DMSO-*d*<sub>6</sub>) δ = 1.28 – 1.41 (m, 2H), 1.46 – 1.64 (m, 4H), 1.96 (t, *J* = 7.3 Hz, 2H), 3.77 (s, 6H), 3.85 (t, *J* = 6.4 Hz, 2H), 6.65 (t, *J* = 2.3 Hz, 1H), 6.90 (d, *J* = 2.3 Hz, 2H), 8.67 (s, 1H), 10.35 (s, 1H), 11.60 (s, 1H) ppm. <sup>13</sup>C NMR (75 MHz, DMSO-*d*<sub>6</sub>) δ = 24.98, 25.16, 27.52, 32.27, 55.49, 75.20, 103.46, 104.98, 134.39, 160.43, 163.71, 169.16 ppm. HPLC analysis: retention time = 7.05 min, 97%. APCI-MS(-): [M] = 325.5.

### ***N*-((6-(hydroxyamino-6-oxohexyl)oxy)-3,5-bis(trifluoromethyl)benzamide (13e)**

Orange powder; yield:41%; mp:144 °C. <sup>1</sup>H NMR (600 MHz, DMSO-*d*<sub>6</sub>) δ = 1.32 – 1.41 (m, 2H), 1.51 – 1.57 (m, 2H), 1.59 – 1.65 (m, 2H), 1.97 (t, *J* = 7.4 Hz, 2H), 3.92 (t, *J* = 6.4 Hz, 2H), 8.34 (s, 1H), 8.39 (s, 2H), 8.66 (d, *J* = 1.8 Hz, 1H), 10.35 (s, 1H), 12.12 (s, 1H) ppm. <sup>13</sup>C NMR (151 MHz, DMSO-*d*<sub>6</sub>) δ = 24.87, 25.05, 27.41, 32.19, 75.43, 123.03 (q, *J* = 273.0 Hz), 125.23, 127.93, 130.56 (q, *J* = 33.4 Hz), 134.65, 160.99, 169.00 ppm. HPLC analysis: retention time = 10.6 min, 98%. APCI-MS(-): [M-H] = 401.6.

### ***N*-((5-(hydroxyamino-5-oxopentyl)oxy)-3,5-dimethylbenzamide (14)**

Orange powder; yield:52%; mp:158 °C. <sup>1</sup>H-NMR (600 MHz, DMSO-*d*<sub>6</sub>) δ = 1.53 – 1.65 (m, 4H), 2.00 (t, *J* = 7.0 Hz, 2H), 2.30 (s, 6H), 3.85 (d, *J* = 6.3 Hz, 2H), 7.16 (s, 1H), 7.35 (d, *J* = 1.7 Hz, 2H), 8.68 (s, 1H), 10.36 (s, 1H), 11.50 (s, 1H) ppm. <sup>13</sup>C-NMR (151 MHz, DMSO-*d*<sub>6</sub>) δ = 21.28, 22.18, 27.66, 32.38, 75.30, 125.23, 132.89, 133.22, 138.02, 164.90, 169.43 ppm. HPLC analysis: retention time = 7.45 min, 99%. APCI-MS(-): [M-H] = 279.4.

### **General procedure for the synthesis of 13f-h**

To a solution of the respective *O*-benzylprotected hydroxamic acid (1.00 eq) in CH<sub>2</sub>Cl<sub>2</sub> (10 mL), triethylsilane (10.0 eq) and trifluoroacetic acid (10.0 eq). After completion, the solvent was removed under reduced pressure. The crude products were purified by flash column chromatography (CH<sub>2</sub>Cl<sub>2</sub> / 30% MeOH in CH<sub>2</sub>Cl<sub>2</sub>).

### **3,5-dibromo-*N*-((6-(hydroxyamino)-6-oxohexyl)oxy)benzamide (13f)**

Orange powder; yield:41%; mp:151 °C. <sup>1</sup>H NMR (600 MHz, DMSO-*d*<sub>6</sub>) δ = 1.31 – 1.38 (m, 2H), 1.49 – 1.62 (m, 4H), 1.96 (t, *J* = 7.4 Hz, 2H), 3.86 (t, *J* = 6.5 Hz, 2H), 7.91 (s, 2H), 8.05 (s, 1H), 8.66 (s, 1H), 10.34 (s, 1H), 11.84 (s, 1H) ppm. <sup>13</sup>C NMR (151 MHz, DMSO-*d*<sub>6</sub>) δ = 24.87, 25.03, 27.38, 32.19, 75.28, 122.67, 129.04, 135.96, 136.25, 161.10, 168.99 ppm. HPLC analysis: retention time = 9.60 min, >99%. APCI-MS(-): [M-H] = 423.5.

### ***N*-((6-(hydroxyamino-6-oxohexyl)oxy)-2,3,5-triiodobenzamide (13g)**

White powder; yield:35%; mp:166 °C. <sup>1</sup>H NMR (300 MHz, DMSO-*d*<sub>6</sub>) δ = 1.25 – 1.39 (m, 2H), 1.46 – 1.69 (m, 4H), 1.96 (t, *J* = 7.3 Hz, 2H), 3.88 (t, *J* = 6.5 Hz, 2H), 7.59 (d, *J* = 2.0 Hz, 1H), 8.30 (d, *J* = 2.0 Hz, 1H), 8.66 (d, *J* = 1.6 Hz, 1H), 10.34 (s, 1H), 11.49 (s, 1H) ppm. <sup>13</sup>C NMR (151 MHz, DMSO-*d*<sub>6</sub>) δ = 24.90, 24.99, 27.37, 32.20, 75.00, 95.36, 108.48, 113.52, 135.18, 144.23, 146.61, 164.35, 168.99 ppm. HPLC analysis: retention time = 10.4 min, 99%. APCI-MS(-): [M] = 643.9.

### **3,5-dichloro-*N*-((6-(hydroxyamino)-6-oxohexyl)oxy)isonicotinamide (13h)**

White powder; yield:33%; mp:165 °C. <sup>1</sup>H NMR (600 MHz, DMSO-*d*<sub>6</sub>) δ = 1.31 – 1.39 (m, 2H), 1.50 – 1.56 (m, 2H), 1.57 – 1.63 (m, 2H), 1.96 (t, *J* = 7.4 Hz, 2H), 3.89 (t, *J* = 6.4 Hz, 2H), 7.80 (s, 2H), 8.66 (s, 1H), 10.34 (s, 1H), 12.05 (s, 1H) ppm. <sup>13</sup>C NMR (151 MHz, DMSO-

$d_6$ )  $\delta$  = 25.32, 25.45, 27.85, 32.65, 75.83, 121.77, 146.24, 150.32, 159.99, 169.45 ppm.  
HPLC analysis: retention time = 7.71 min, >99%. APCI-MS(-): [M-2H] = 334.4.

## 2. Computational studies

The structures of the ligands were prepared using the standard procedure of AutoDock tools version 1.5.7 (ADT)<sup>3</sup>. The structures of the proteins PDB ID 4KBX (HDAC2)<sup>4</sup>, 5A2S (HDAC4)<sup>5</sup> and 5EDU (HDAC6)<sup>6</sup> were downloaded from the Protein Data Base. Using the software UCSF Chimera<sup>7</sup>, the structure of 4KBX and 5A2S were superimposed with 5EDU to maintain the same 3D coordinates. Also, all water molecules, buffer and non-interacting ions were removed from chain A of 5EDU and chain B of 4KBX and chain A of 5A2S. The clean structures were used as input for AutoDock tools for the computation of the Gasteiger charges. After the calculation of the charges, the grid box with size 21 x 28 x 27 centered in the x, y and z coordinates 17.02, -44.55 and 101.80 with the spacing of 1.0 Å was created.<sup>8</sup> In Autodock4.2, the Lamarckian genetic algorithm was used and the search parameters were set to 100 GA runs for each ligand with a population size of 150, maximum number of  $2.5 \cdot 10^6$  energy evaluations, a maximum number of  $2.7 \cdot 10^4$  generations, a mutation rate of 0.2 and a crossover rate of 0.8 and the default dockings parameters were used. Populations of 100 docking poses were generated for each run and organized in clusters, the first pose of the cluster containing bidentate interaction between the hydroxamic acid and the zinc binding (distance of the hydroxyl and carbonyl oxygen and the zinc ion  $>3.5$  Å)<sup>9</sup> was chosen. This approach was validated by the redock of the ligand from the crystal PDB access number 5EDU, where the best conformation showed a RMSD of 2.36 Å when compared with the native one.

## 3. Biological Evaluation

### 3.1 Reagents

Cisplatin was purchased from Sigma (Germany) and dissolved in 0.9% sodium chloride solution, propidium iodide (PI) was purchased from PromoKine (Germany). Vorinostat was synthesized according to known procedures.<sup>10</sup> Stock solutions (10 mM) of the respective compounds were prepared with DMSO and diluted to the desired concentrations with the appropriate medium. All other reagents were

supplied by PAN Biotech (Germany) unless otherwise stated.

### 3.2 Cell lines and cell culture

The human ovarian carcinoma cell line A2780 was obtained from European Collection of Cell Cultures (ECACC, Salisbury, UK). The human tongue cell line Cal27 was obtained from the German Collection of Microorganisms and Cell Cultures (DSMZ, Germany). The corresponding cisplatin resistant CisR cell line Cal27CisR was generated by exposing the parental cell line to weekly cycles of cisplatin in an IC<sub>50</sub> concentration over a period of 24 - 30 weeks as described in Gosepath *et al.* and Eckstein *et al.*<sup>11,12</sup> All cell lines were grown at 37°C under humidified air supplemented with 5% CO<sub>2</sub> in RPM I 1640 (A2780) or DMEM (Cal27) containing 10% fetal calf serum, 120 IU/mL penicillin, and 120 µg/mL streptomycin. The cells were grown to 80% confluency before being used in further assays.

### 3.3 MTT cell viability assay

The rate of cell-survival under the action of test substances was evaluated by an improved MTT assay as previously described.<sup>13</sup> In brief, A2780 and Cal27 cell lines were seeded at a density of 5,000 and 2,500 cells/well in 96 well plates (Corning, Germany). After 24 h, cells were exposed to increased concentrations of the test compounds. Incubation was ended after 72 h and cell survival was determined by addition of MTT solution (Serva, Germany, 5 mg/mL in phosphate buffered saline). The formazan precipitate was dissolved in DMSO (VWR, Germany). Absorbance was measured at 544 nm and 690 nm in a FLUOstar microplate-reader (BMG LabTech, Offenburg, Germany).

To investigate the effect of **13a**, **13d**, or **5** on cisplatin-induced cytotoxicity, compounds were added 48 h before cisplatin administration. After 72 h, the cytotoxic effect was determined with a MTT cell viability assay and shift factors were calculated by dividing the IC<sub>50</sub> value of cisplatin alone by the IC<sub>50</sub> value of the drug combinations.

### 3.4 Whole-cell HDAC inhibition assay

The cellular HDAC assay was based on an assay published by Ciossek *et al.*<sup>14</sup> *cio* and

Bonfils *et al.*<sup>15</sup> with minor modifications. Briefly, human cancer cell lines Cal27 and A2780 were seeded in 96-well tissue culture plates (Corning, Germany) at a density of  $1.5 \times 10^4$  cells/well in a total volume of 90  $\mu$ L culture medium. After 24 h, cells were incubated for 18 h with increasing concentrations of test compounds. The reaction was started by adding 10  $\mu$ L of 3 mM Boc-Lys( $\epsilon$ -Ac)-AMC (Bachem, Germany) to reach a final concentration of 0.3 mM.<sup>7</sup> The cells were incubated with Boc-Lys( $\epsilon$ -Ac)-AMC for 3 h under cell culture conditions. After this incubation, 100  $\mu$ l/well stop solution (25 mM Tris-HCl (pH 8), 137 mM NaCl, 2.7 mM KCl, 1 mM MgCl<sub>2</sub>, 1% NP40, 2.0 mg/mL trypsin, 10  $\mu$ M vorinostat) was added and the reaction was developed for 3 h under cell culture conditions. Fluorescence intensity was measured at excitation of 320 nm and emission of 520 nm in a NOVOstar microplate-reader (BMG LabTech, Offenburg, Germany).

### 3.5 Caspase 3/7 activation assay

Compound-induced activation of caspases 3 and 7 was analyzed by using the CellEvent Caspase 3/7 green detection reagent (Thermo Scientific Germany) according to the manufacturer's instructions. Briefly, Cal27 and Cal27 CisR cells were seeded in 96-well-plates (Corning, Germany) at a density of 900 cells/ well. Cells were treated with **13a** or **13d** or **5** 48 h prior to cisplatin. After a further incubation period of 24 h, medium was removed and 50  $\mu$ L of CellEvent Caspase 3/7 green detection reagent (2  $\mu$ M in PBS supplemented with 5% heat inactivated FBS) was added. Cells were incubated for 30 minutes at 37°C in a humidified incubator before imaging by using the Thermo Fisher ArrayScan XTI high content screening (HCS) system (Thermo Scientific). Hoechst 33342 was used for nuclei staining. The pan caspase inhibitor QVD was used in a concentration of 20  $\mu$ M diluted in the appropriate medium and incubated 30 minutes prior to compound addition.

### 3.6 Enzyme assay

All human recombinant enzymes were purchased from Reaction Biology Corp. (Malvern, PA, USA). The HDAC activity assay of HDAC2 (catalog nr. KDA-21-277), 4 (catalog nr. KDA-21-279), 6 (catalog nr. KDA-21-213) and 8 (catalog nr. KDA-21-481) was performed in 96-well plates (Corning, Germany). Briefly 20ng of HDAC2 and HDAC8, 17.5ng of HDAC6

and 2ng of HDAC4 per reaction were used. Recombinant enzymes were diluted in assay buffer (50 mM Tris-HCL, pH 8.0, 137 mM NaCl, 2.7 mM KCl, 1 mM MgCl<sub>2</sub>, and 1 mg/ml BSA). 80 µl of this dilution was incubated with 10 µl of different concentrations of inhibitors in assay buffer. After a 5 min incubation step the reaction was started with 10 µl of 300 µM (HDAC2), 150 µM (HDAC6) Boc-Lys(Ac)-AMC (Bachem, Germany) or 100 µM (HDAC4), 60 µM (HDAC8) Boc-Lys(TFa)-AMC (Bachem, Germany). The reaction was stopped after 90 min by adding 100 µl stop solution (16mg/ml trypsin, 2 µM Panobinostat for HDAC2, HDAC6 and HDAC8, 2 µM CHDI-00390576-0000-004 (kindly provided by the CHDI Foundation Inc., New York, USA) for HDAC4 in 50 mM Tris-HCL, pH 8.0, and 100 mM NaCl. 15 min after the addition of the stop solution the fluorescence intensity was measured at excitation of 355 nm and emission of 460 nm in a NOVOstar microplate reader (BMG LabTech, Offenburg, Germany).

### **3.7 Immunoblotting**

Cells were treated with 5 µM of **13a**, 1.5 µM of **13d**, 1.5 µM of **5**, or vehicle for 24 h. The HDACi vorinostat (3 µM) was used as control. Cell pellets were dissolved with RIPA buffer (50 mM Tris-HCl pH = 8.0, 1% Triton X-100, 0.5% sodium deoxycholate, 0.1% SDS, 150 mM sodium chloride, 2 mM EDTA, supplemented with protease and phosphatase inhibitors (Pierce™ protease and phosphatase inhibitor mini tablets, Thermo Scientific) and clarified by centrifugation. Equal amounts of total protein (30 µg) were resolved by SDS-PAGE and transferred to polyvinylidene fluoride membranes (Merck Millipore). Blots were incubated with primary antibodies against acetylated α-tubulin, α-tubulin (Santa Cruz Biotechnology, Germany), histone H3, and acetyl histone H3 (Lys24) (biotechne, Germany). Immunoreactive proteins were visualized using luminol reagent (Santa Cruz Biotechnology, Germany) with an Intas Imager (Intas, Germany).

### **3.8 Data Analysis**

Concentration-effect curves were constructed with Prism 7.0 (GraphPad, San Diego, CA) by fitting the pooled data of at least three experiments performed in triplicates to the four parameter logistic equation. Statistical analysis was performed using t-test or one-way ANOVA.

#### 4. References

1. Marek L, Hamacher A, Hansen FK, et al. Histone deacetylase (HDAC) inhibitors with a novel connecting unit linker region reveal a selectivity profile for HDAC4 and HDAC5 with improved activity against chemoresistant cancer cells. *J Med Chem*. 2013;56(2):427-436. doi:10.1021/jm301254q.
2. Alves Avelar LA, Held J, Engel JA, et al. Design and Synthesis of Novel Anti-Plasmodial Histone Deacetylase Inhibitors Containing an Alkoxyamide Connecting Unit. *Arch Pharm (Weinheim)*. 2017;350(3-4):1-11. doi:10.1002/ardp.201600347.
3. Morris G Huey R Lindstrom W Sanner M Belew R et. al. AutoDock4 and AutoDockTools4: Automated docking with selective receptor flexibility. *J Comput Chem*. 2009;28(1):2785-2791. doi:10.1002/jcc.
4. Lauffer BEL, Mintzer R, Fong R, et al. Histone deacetylase (HDAC) inhibitor kinetic rate constants correlate with cellular histone acetylation but not transcription and cell viability. *J Biol Chem*. 2013. doi:10.1074/jbc.M113.490706.
5. Luckhurst CA, Breccia P, Stott AJ, et al. Potent, Selective, and CNS-Penetrant Tetrasubstituted Cyclopropane Class IIa Histone Deacetylase (HDAC) Inhibitors. *ACS Med Chem Lett*. 2016;7(1):34-39. doi:10.1021/acsmedchemlett.5b00302.
6. Hai Y, Christianson DW. Histone deacetylase 6 structure and molecular basis of catalysis and inhibition. *Nat Chem Biol*. 2016;12(9):741-747. doi:10.1038/nchembio.2134.
7. Pettersen EF, Goddard TD, Huang CC, et al. UCSF Chimera - A visualization system for exploratory research and analysis. *J Comput Chem*. 2004;25(13):1605-1612. doi:10.1002/jcc.20084.
8. Ballante F, Marshall GR. An Automated Strategy for Binding-Pose Selection and Docking Assessment in Structure-Based Drug Design. *J Chem Inf Model*. 2016;56(1):54-72. doi:10.1021/acs.jcim.5b00603.
9. Kawai K, Nagata N. Metal-ligand interactions: An analysis of zinc binding groups using the Protein Data Bank. *Eur J Med Chem*. 2012;51:271-276.

doi:10.1016/j.ejmech.2012.02.028.

10. Marek L, Hamacher A, Hansen FK, et al. Histone deacetylase (HDAC) inhibitors with a novel connecting unit linker region reveal a selectivity profile for HDAC4 and HDAC5 with improved activity against chemoresistant cancer cells. *J Med Chem*. 2013. doi:10.1021/jm301254q.
11. Gosepath EM, Eckstein N, Hamacher A, et al. Acquired cisplatin resistance in the head-neck cancer cell line Cal27 is associated with decreased DKK1 expression and can partially be reversed by overexpression of DKK1. *Int J Cancer*. 2008;123(9):2013-2019. doi:10.1002/ijc.23721.
12. Eckstein N, Servan K, Girard L, et al. Epidermal growth factor receptor pathway analysis identifies amphiregulin as a key factor for cisplatin resistance of human breast cancer cells. *J Biol Chem*. 2008;283(2):739-750. doi:10.1074/jbc.M706287200.
13. Engelke LH, Hamacher A, Proksch P, Kassack MU. Ellagic Acid and Resveratrol Prevent the Development of cisplatin Resistance in the Epithelial Ovarian Cancer Cell Line A2780. *J Cancer*. 2016;7(4):353-363. doi:10.7150/jca.13754.
14. Ciossek T, Julius H, Wieland H, Maier T, Beckers T. A homogeneous cellular histone deacetylase assay suitable for compound profiling and robotic screening. *Anal Biochem*. 2008;372(1):72-81. doi:10.1016/J.AB.2007.07.024.
15. Bonfils C, Kalita A, Dubay M, et al. Evaluation of the Pharmacodynamic Effects of MGCD0103 from Preclinical Models to Human Using a Novel HDAC Enzyme Assay. *Clin Cancer Res*. 2008;14(11):3441-3449. doi:10.1158/1078-0432.CCR-07-4427.

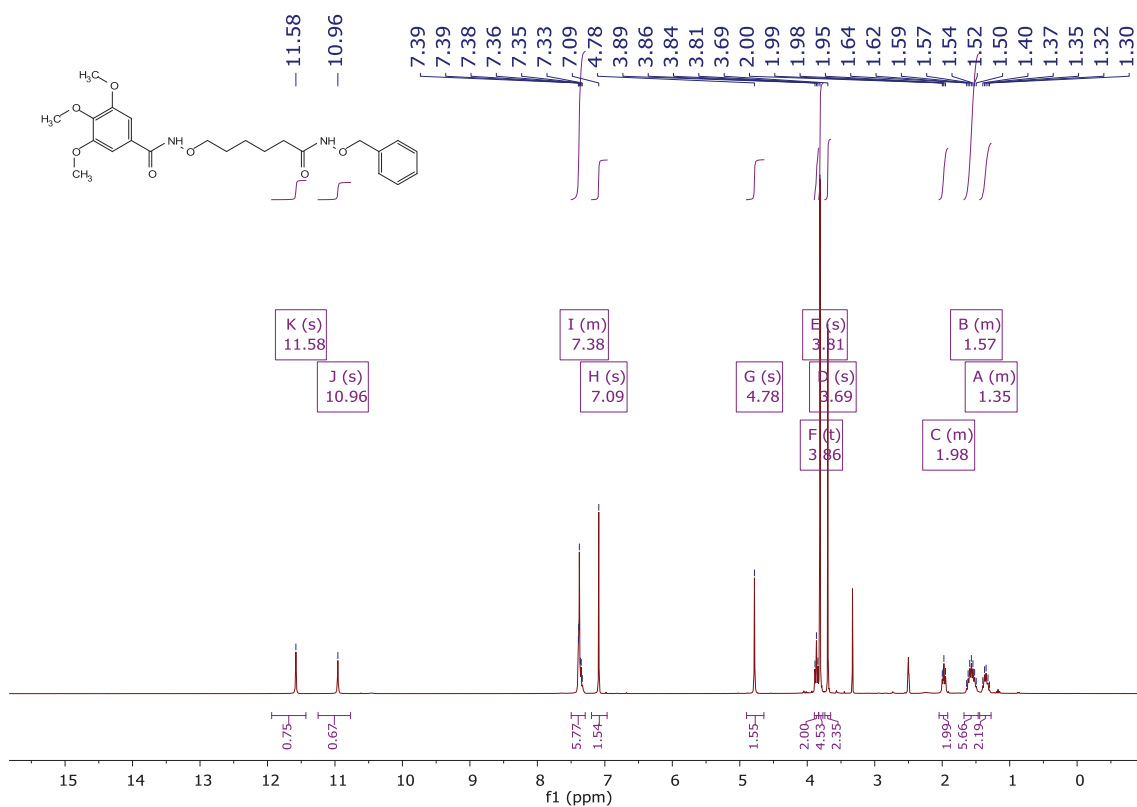
## Supporting Information 2- NMR Data

Novel alkoxyamide-based histone deacetylase inhibitors reverse  
cisplatin resistance in chemoresistant cancer cells

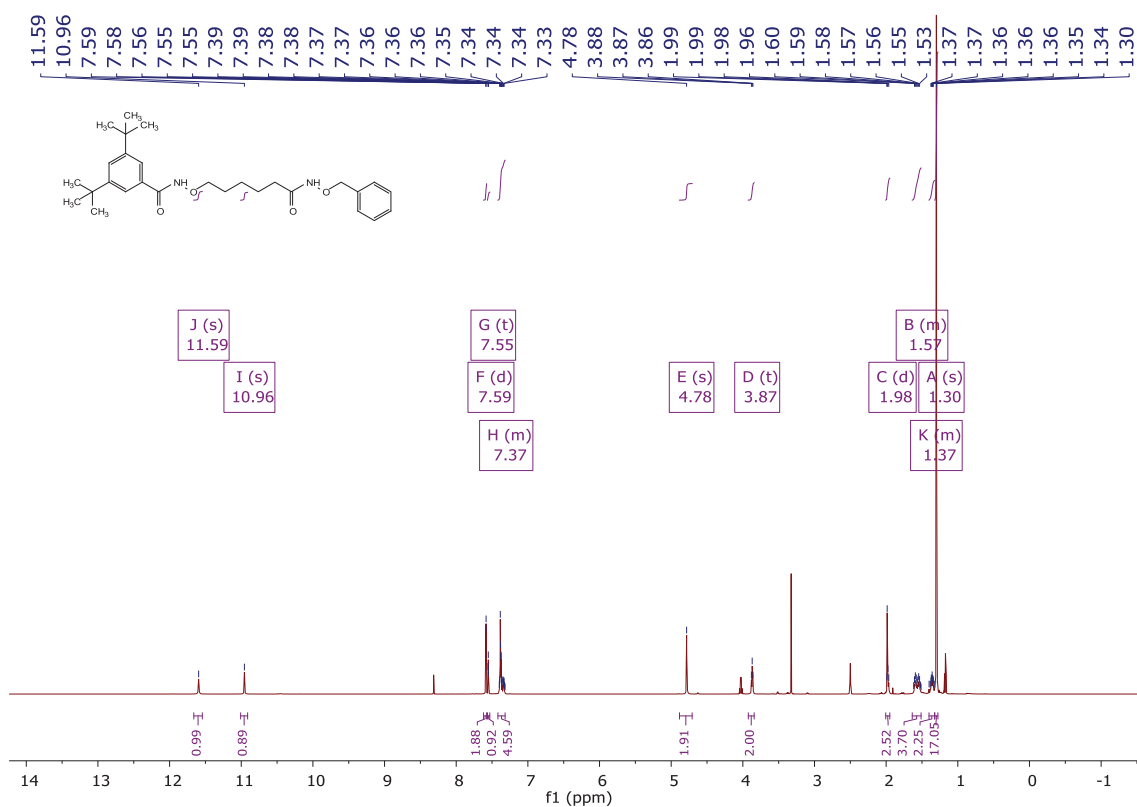
*Yodita Asfaha\**, *Christian Schrenk\**, *Leandro A. Alves Avelar\**, *Friedrich Lange\**, *Chenyin Wang\**, *Jan J. Bandolik\**, *Alexandra Hamacher\**, *Matthias U. Kassack\*#*, *Thomas Kurz\*#*

\*Institut für Pharmazeutische und Medizinische Chemie, Heinrich-Heine-Universität  
Düsseldorf, Universitätsstr. 1, 40225 Düsseldorf, Germany, # MUK and TK share senior  
and corresponding authorship

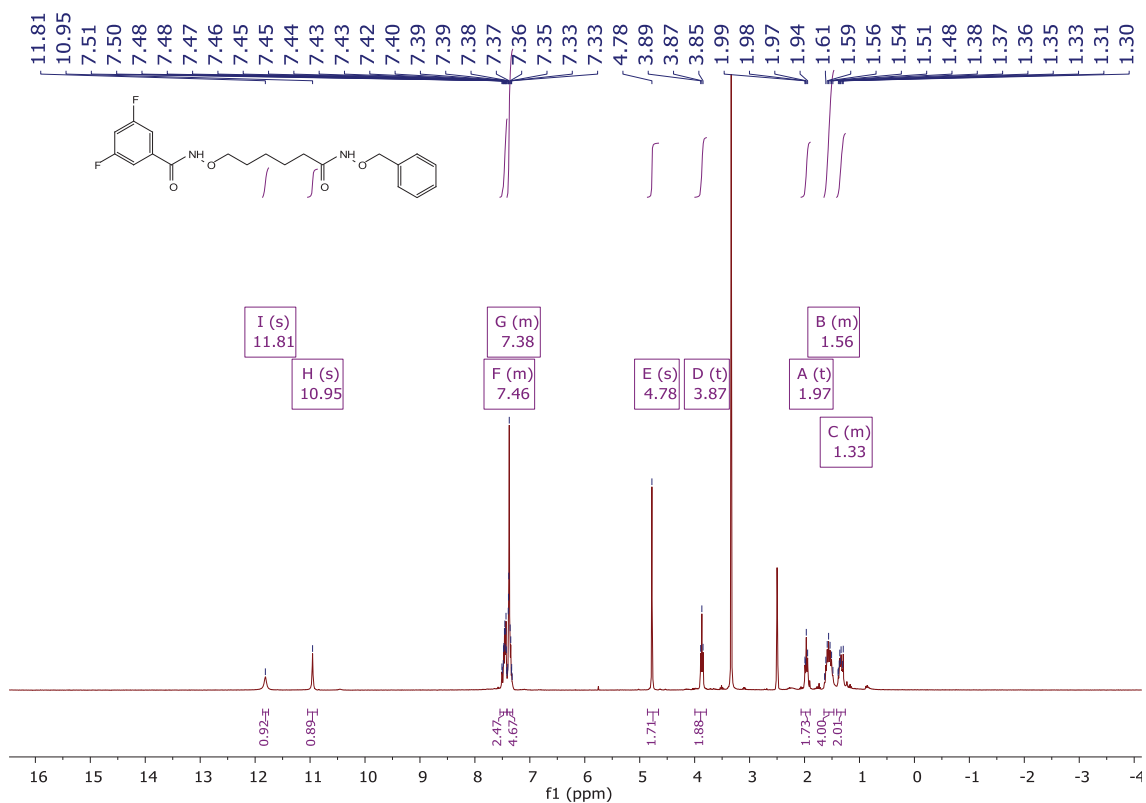
**N-((6-(benzyloxy)amino-6-oxohexyl)oxy)-3,4,5-trimethoxybenzamide (10a)**



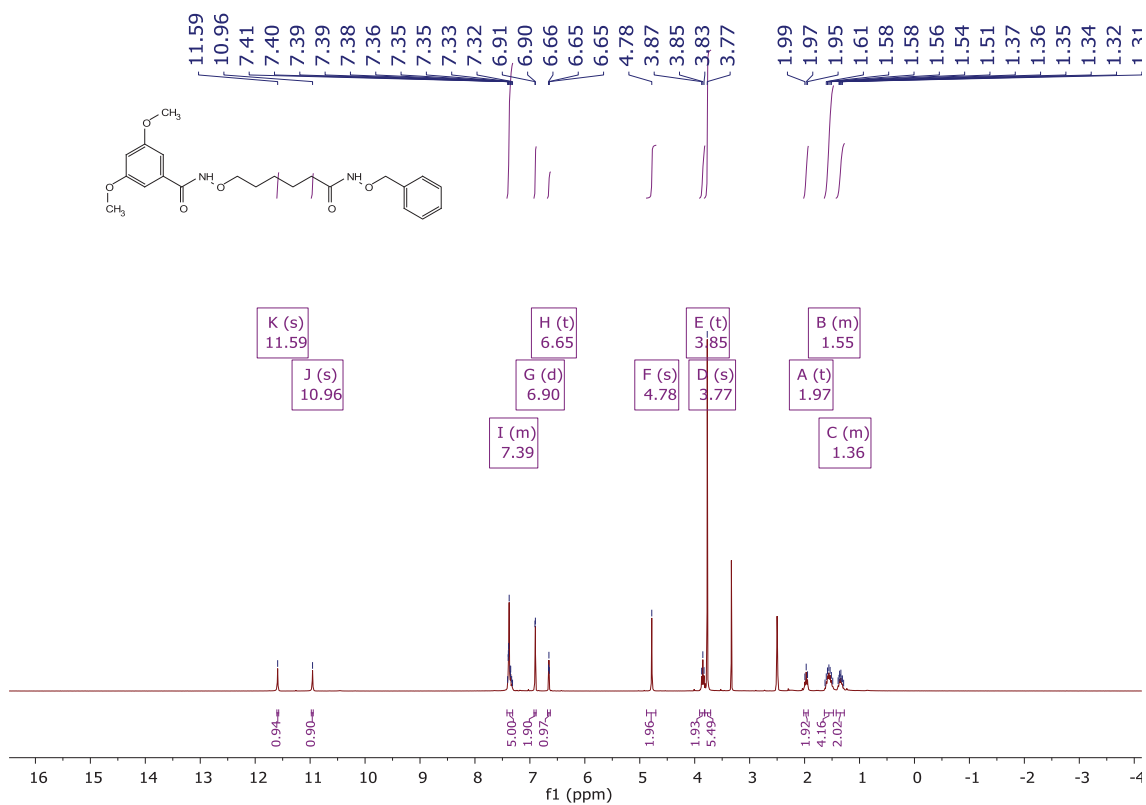
**N-((6-(benzyloxy)amino-6-oxohexyl)oxy)-3,5-di-tert-butylbenzamide (10b)**



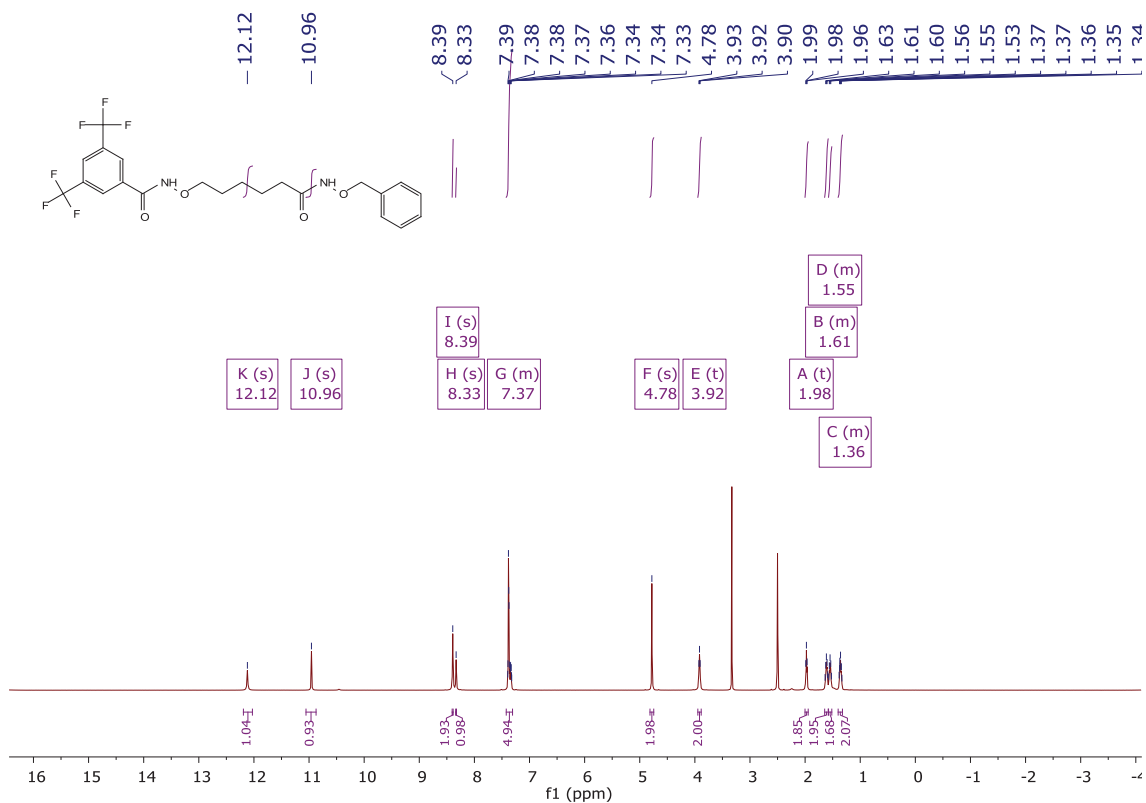
***N*-((6-(benzyloxy)amino-6-oxohexyl)oxy)-3,5-difluorobenzamide (10c)**



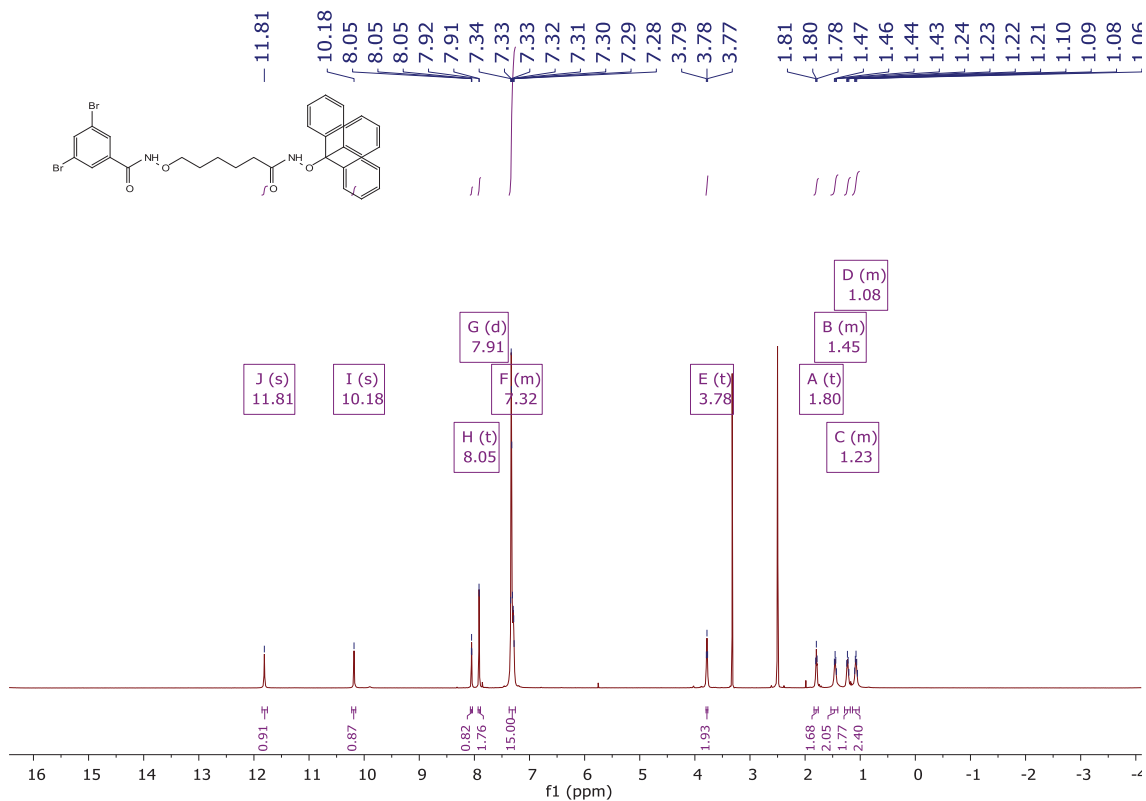
***N*-((6-(benzyloxy)amino-6-oxohexyl)oxy)-3,5-dimethoxybenzamide (10d)**



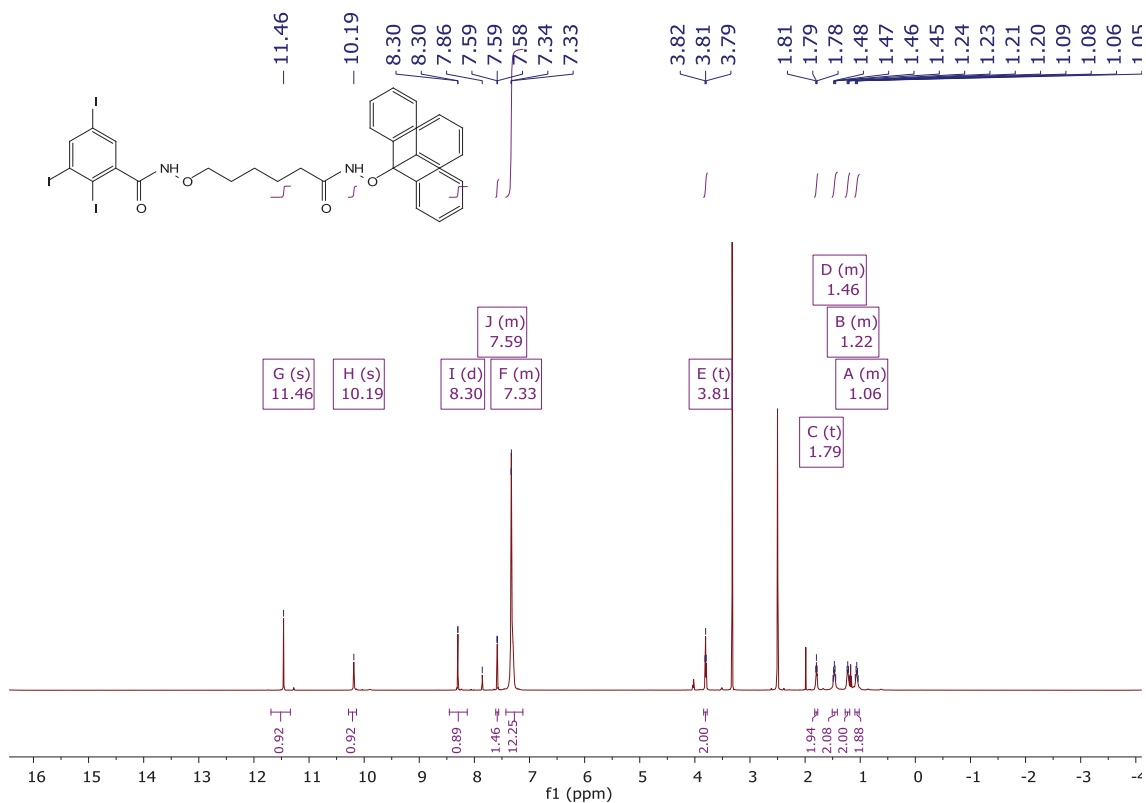
***N*-((6-(benzyloxy)amino-6-oxohexyl)oxy)-3,5-bis(trifluoromethyl)benzamide (10e)**



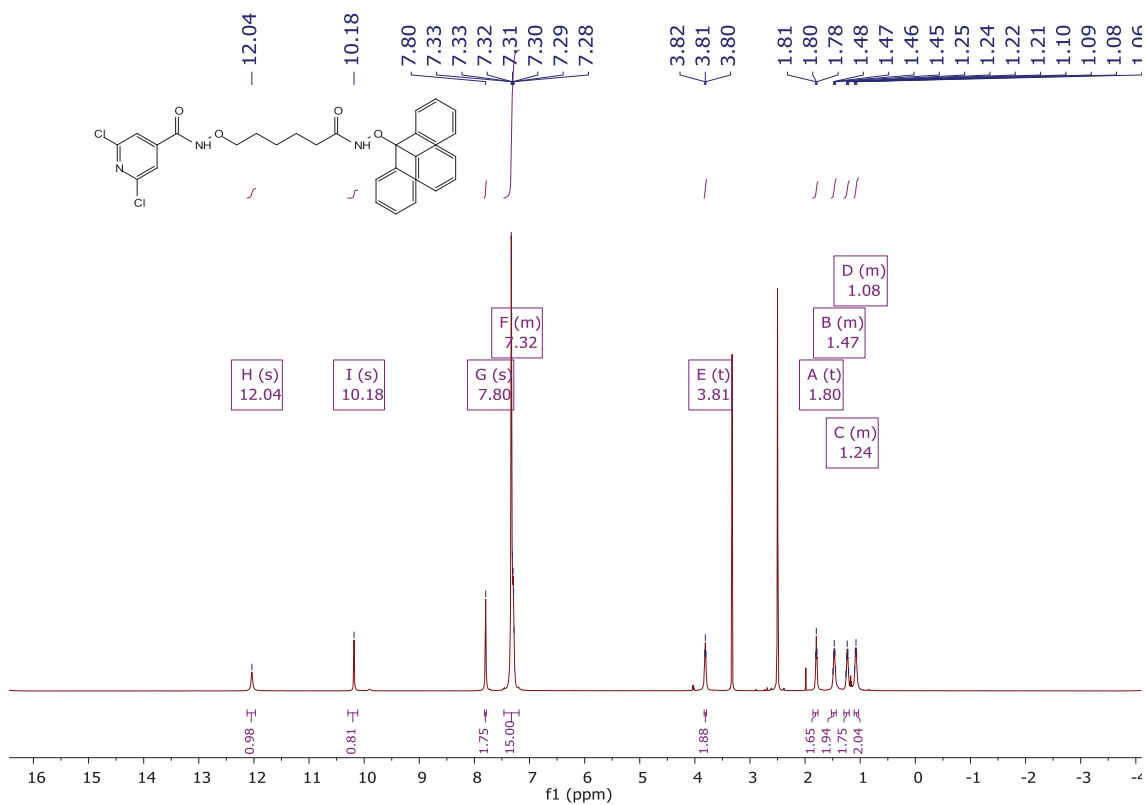
**3,5-dibromo-*N*-((6-oxo-6-((trityloxy)amino)hexyl)oxy)benzamide (12a)**



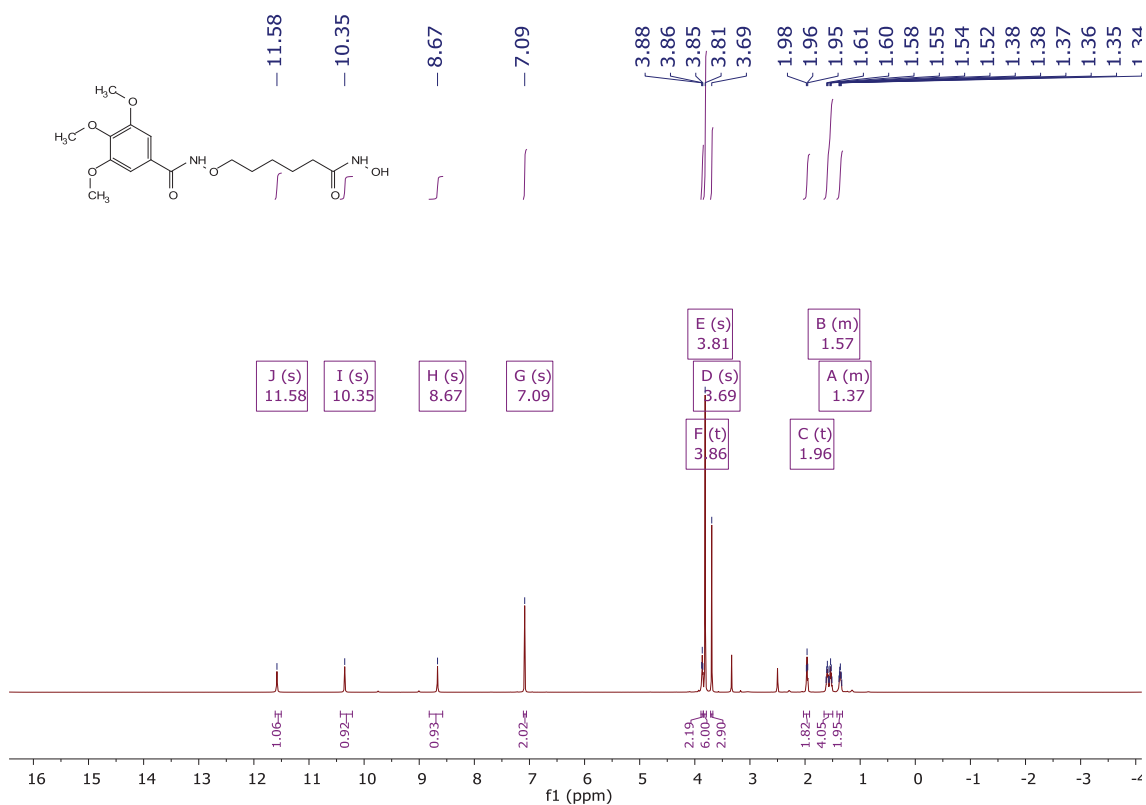
**2,3,5-triiodo-N-((6-oxo-6-((trityloxy)amino)hexyl)oxy)benzamide (12b)**



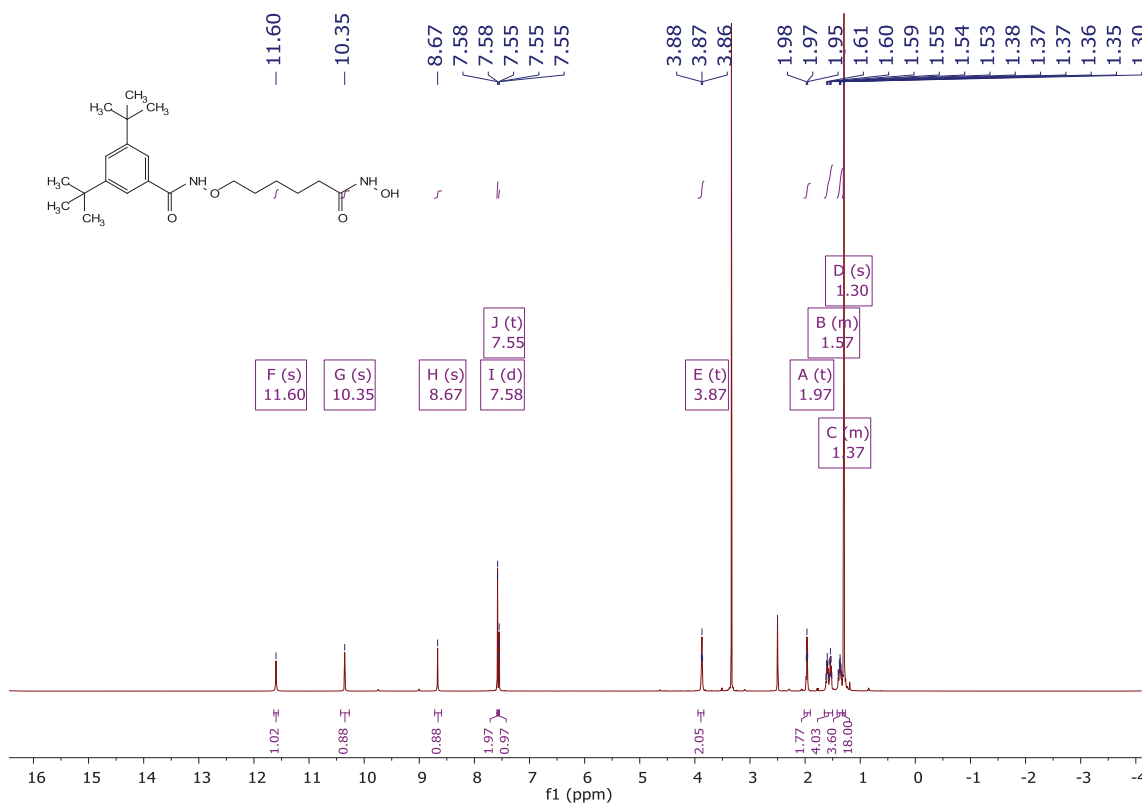
**2,6-dichloro-N-((6-oxo-6-((trityloxy)amino)hexyl)oxy)benzamide (12c)**



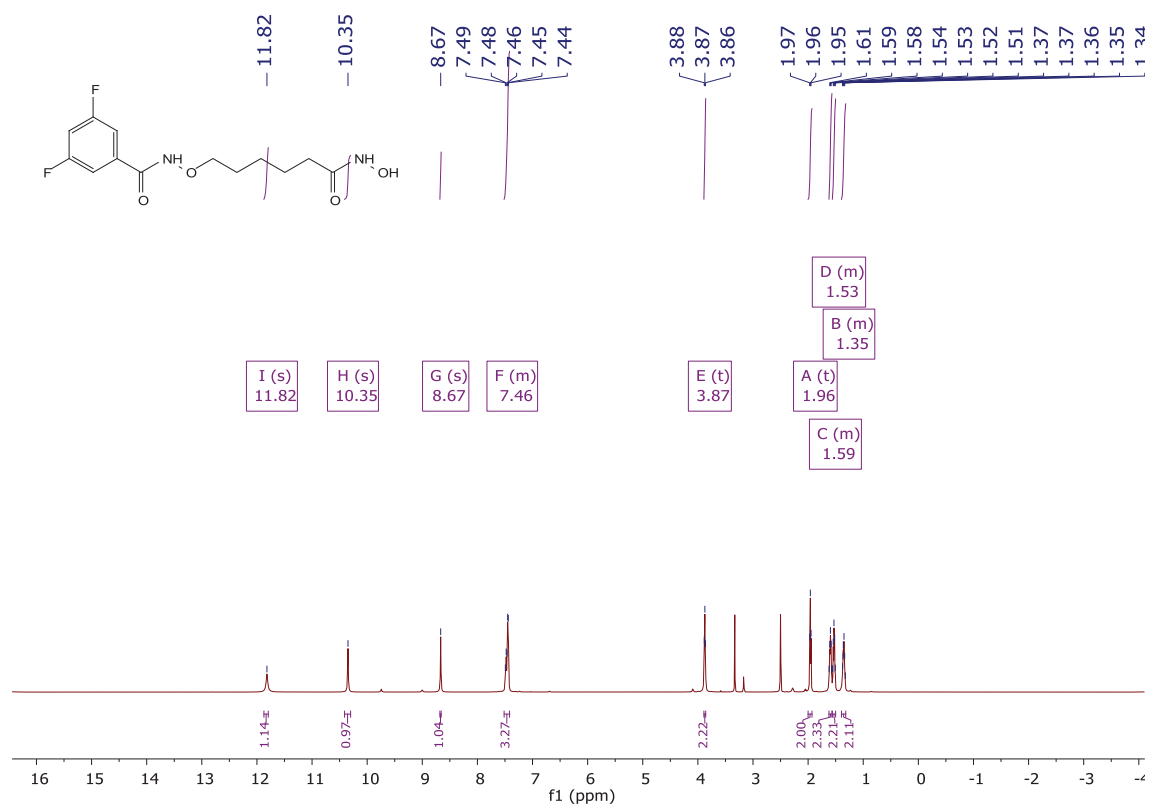
### *N*-((6-(hydroxyamino-6-oxohexyl)oxy)-3,4,5-trimethoxybenzamide (13a)



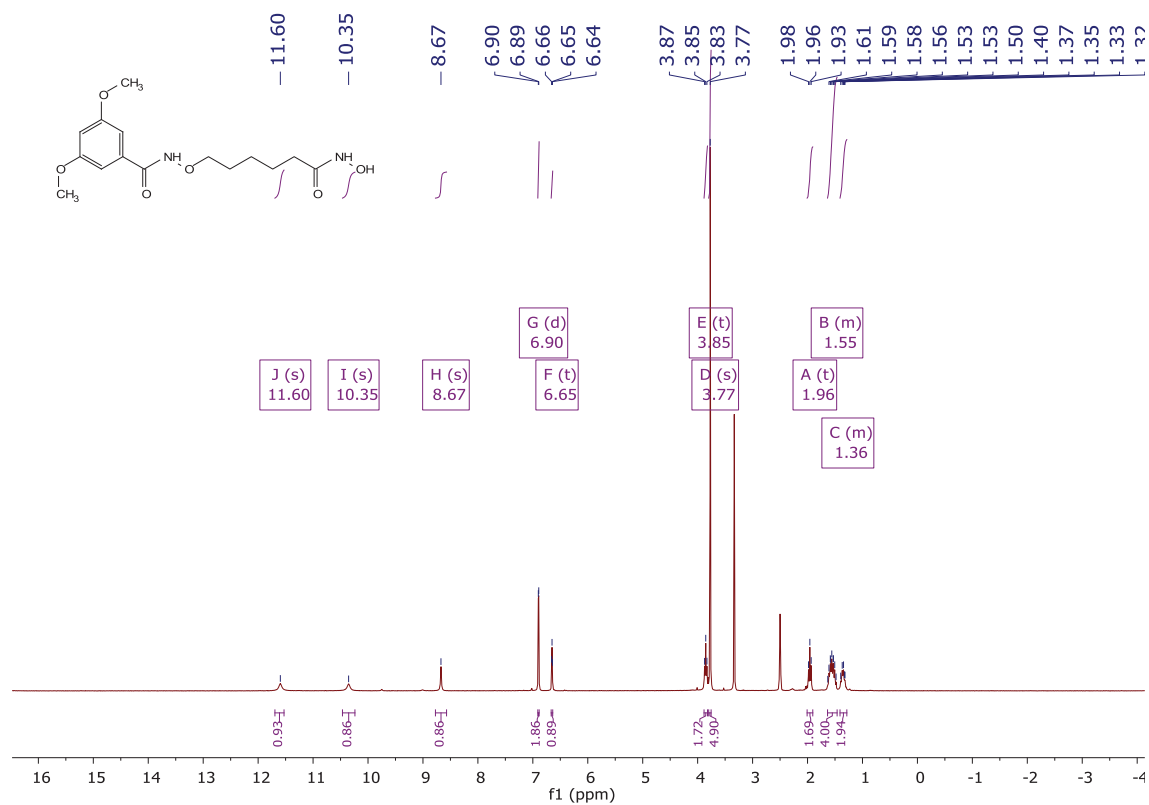
### 3,5-di-*tert*-butyl-*N*-((6-(hydroxyamino-6-oxohexyl)oxy)benzamide (13b)



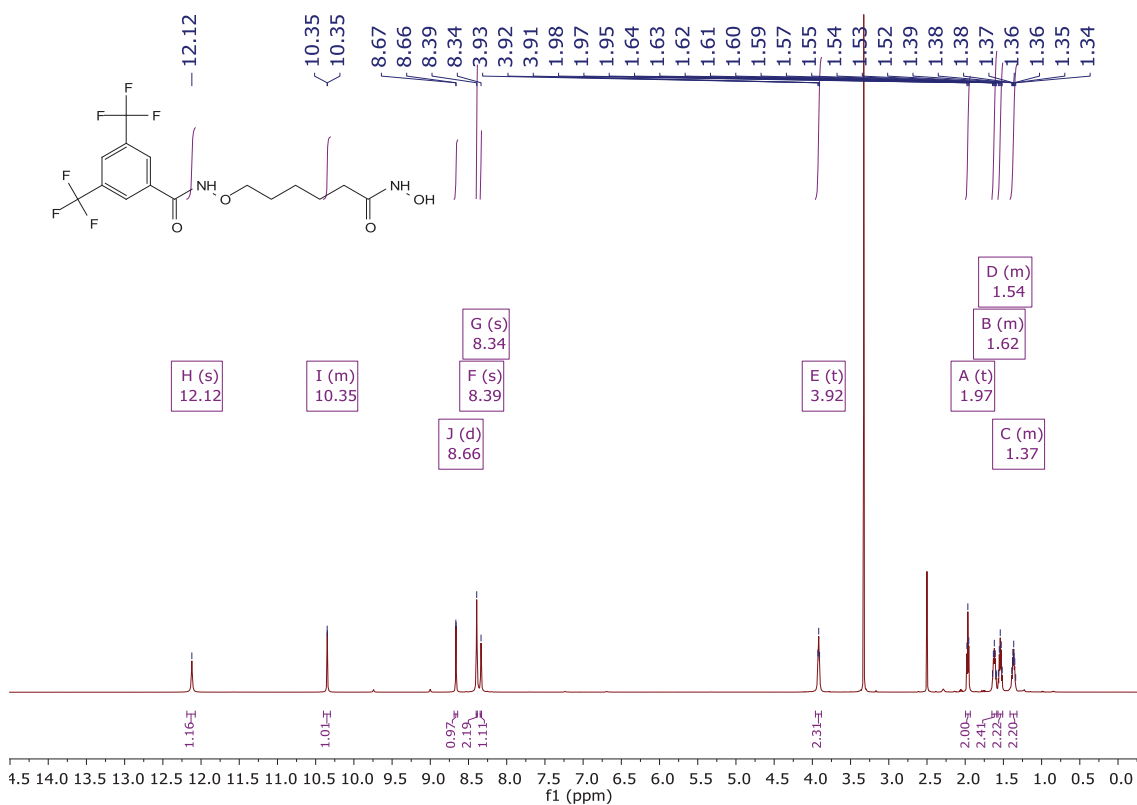
### 3,5-difluoro-N-((6-(hydroxyamino-6-oxohexyl)oxy)benzamide (13c)



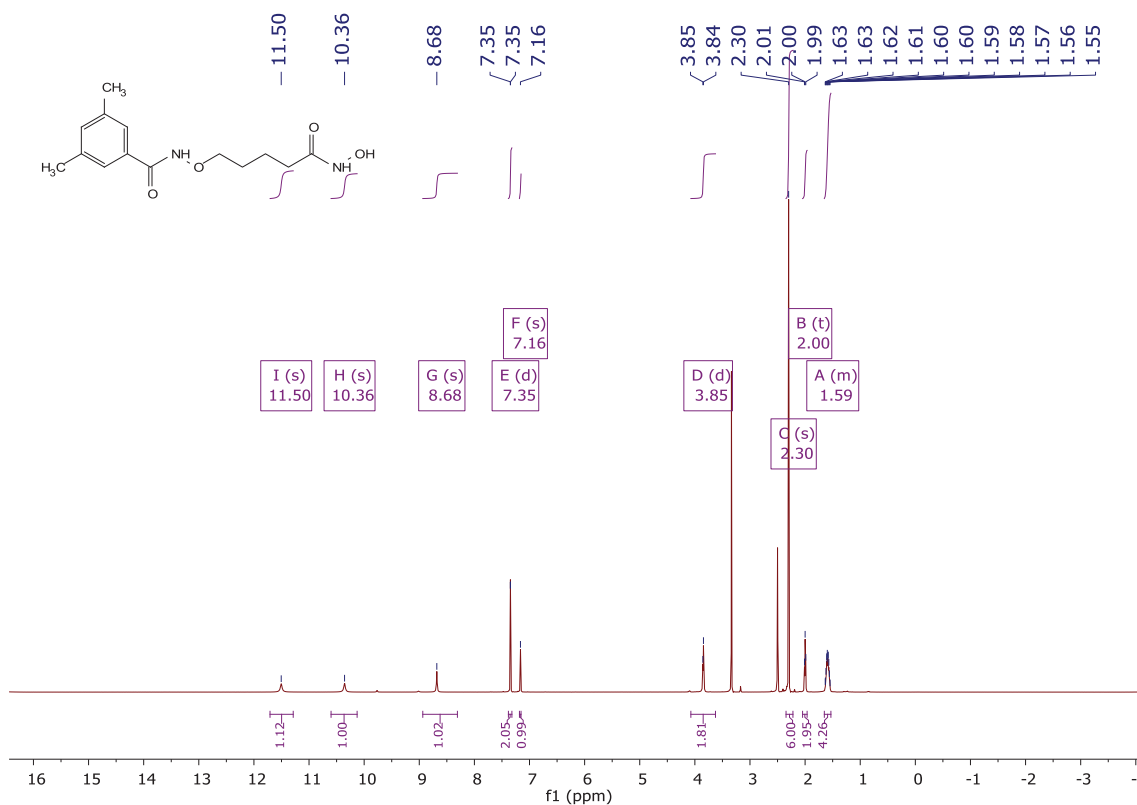
### N-((6-(hydroxyamino-6-oxohexyl)oxy)-3,5-dimethoxybenzamide (13d)



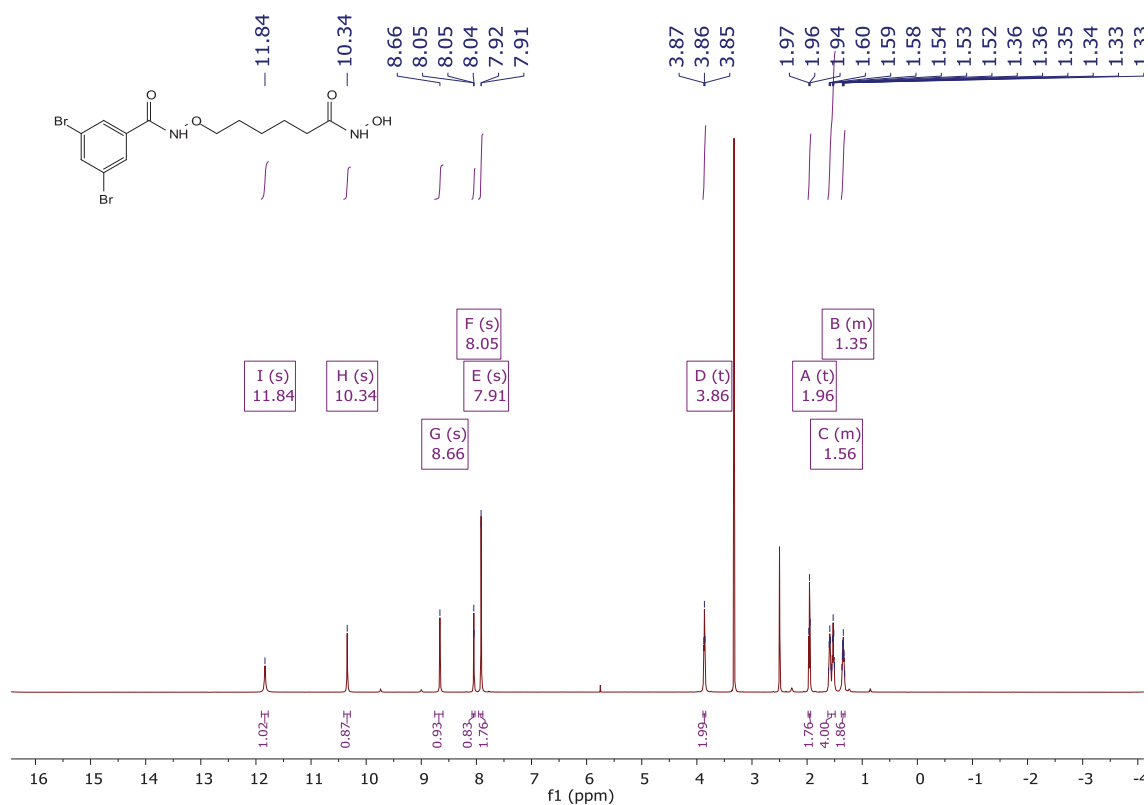
**N-((6-(hydroxyamino-6-oxohexyl)oxy)-3,5-bis(trifluoromethyl)benzamide (13e)**



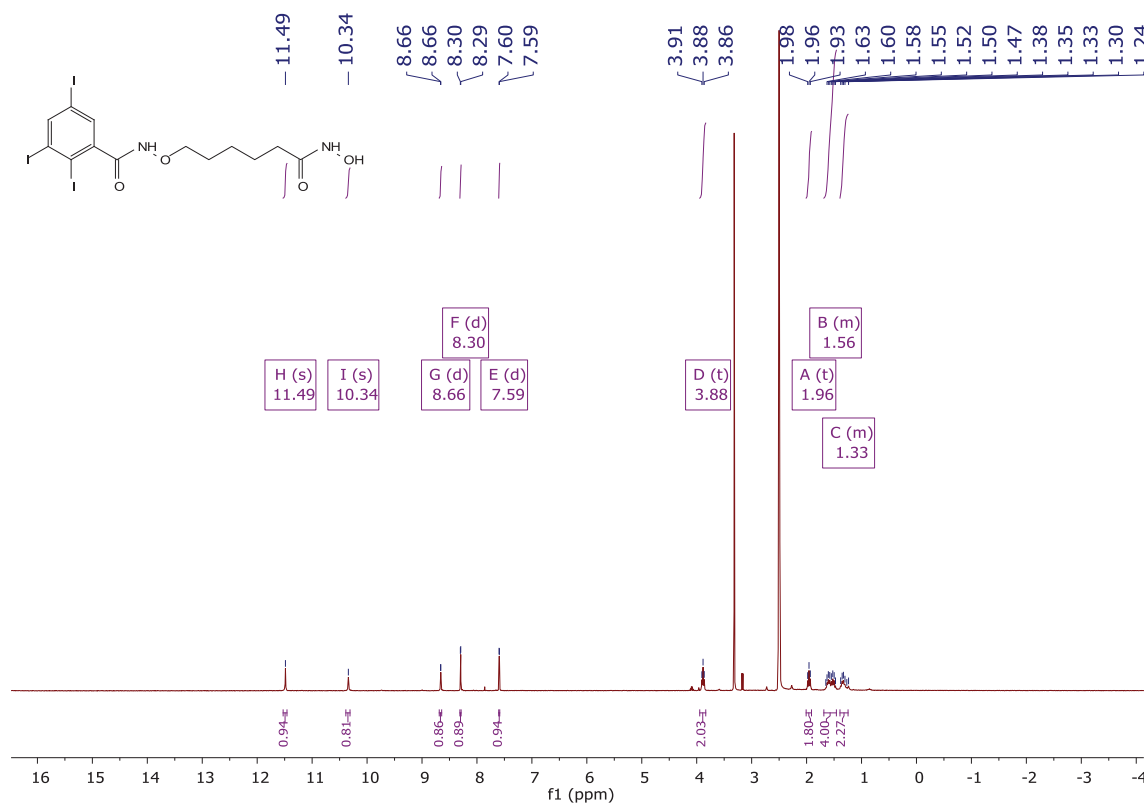
**N-((5-(hydroxyamino-5-oxopentyl)oxy)-3,5-dimethylbenzamide (14)**



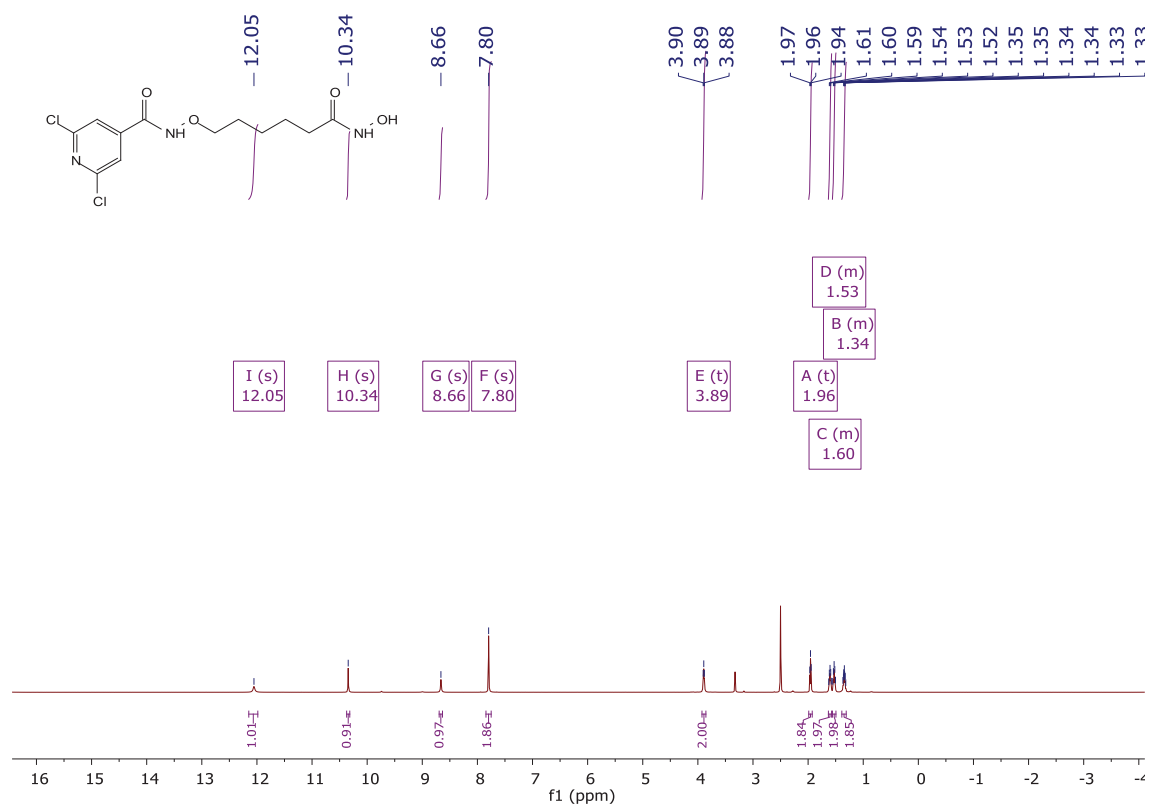
### 3,5-dibromo-*N*-((6-(hydroxyamino)-6-oxohexyl)oxy)benzamide (13f)



### *N*-((6-(hydroxyamino)-6-oxohexyl)oxy)-2,3,5-triiodobenzamide (13g)



### 3,5-dichloro-N-((6-(hydroxyamino)-6-oxohexyl)oxy)isonicotinamide (13h)



## Synthesis of thiazolyl-based hydroxamic acids as histone deacetylase inhibitors

Accepted in: Archive for Organic Chemistry

Impact Factor: 1.253 (2018)

Contribution:

- Synthesis of the compounds **9a-c**, **10**, **11**, **12a-c**, **13a-c**
- Manuscript and supporting information

## Synthesis of thiazolyl-based hydroxamic acids as histone deacetylase inhibitors

Yodita Asfaha<sup>\*#</sup>, Alexander Jan Skerhut<sup>\*#</sup>, Leandro A. Alves-Avelar<sup>\*</sup>, Nadine Horstick-Muche<sup>\*</sup>, Beate Lungerich<sup>\*</sup>, Stefan Klinken<sup>\*</sup>, Matthias U. Kassack<sup>\*#</sup>, Thomas Kurz<sup>\*#</sup>

*\*Institut für Pharmazeutische und Medizinische Chemie, Heinrich-Heine-Universität Düsseldorf, Universitätsstr.1, 40225 Düsseldorf, Germany, #YA and AJS share first authorship, MUK and TK share senior and corresponding authorship.*

Email: [thomas.kurz@hhu.de](mailto:thomas.kurz@hhu.de), [matthias.kassack@hhu.de](mailto:matthias.kassack@hhu.de)

### Dedication (optional)

Received mm-dd-yyyy

Accepted mm-dd-yyyy

Published on line mm-dd-yyyy

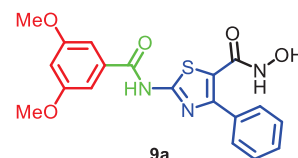
Dates to be inserted by editorial office

### Abstract

Here, we report the synthesis of 4-phenyl substituted thiazolyl-based hydroxamates as histone deacetylase inhibitors. The synthesis of the target compounds comprises of a Hantzsch-thiazole reaction, a HATU-mediated acylation and a hydroxamic acid synthesis. Preliminary docking results indicated an isozyme selectivity by addressing the lower pocket of HDAC4 with 4-phenyl thiazoles. Surprisingly, this new series of thiazolyl based hydroxamates **9a-c** revealed a moderate HDAC6 inhibitory activity in the low micromolar range. The hydroxamic acids **9a** and **9c** did not show an HDAC4 inhibition up to 100  $\mu\text{M}$ , whilst compound **9b** exhibiting a 4-pyridinyl CAP moiety displayed a moderate HDAC4 inhibitory activity in the micromolar range.



Pharmacophore model of HDAC6



IC<sub>50</sub>(HDAC6) = 3.85  $\mu\text{M}$   
SI (HDAC2/6) > 26  
SI (HDAC4/6) > 26  
SI (HDAC8/6) = 11

**Keywords:** thiazole synthesis, reaction optimization, histone deacetylase inhibitors, ester cleavage, hydroxamic acids

## Introduction

The term epigenetic refers to inheritable changes in gene expression without altering the underlying DNA sequence.<sup>1</sup> Epigenetic mechanisms are subdivided into four different classes: (1) posttranslational modifications of histones, (2) chemical modifications of DNA (3) chromatin-remodeling complexes, and (4) regulatory non-coding RNAs. An essential post-translational modification is protein acetylation/deacetylation, which is regulated by histone acetyltransferases (HATs) and histone deacetylases (HDACs). The human zinc dependent HDACs are classified into three classes: class I (HDACs 1-3, 8), class II (IIa: HDACs 4, 5, 7, 9; IIb: HDACs 6, 10) and class IV (HDAC 11).<sup>2</sup> Various studies demonstrated that HDACs are overexpressed in a broad spectrum of cancer cells.<sup>3-6</sup> Their inhibition provides a promising strategy for the development of novel epigenetic anticancer drugs. Until now, the natural product romidepsin and four trichostatin A derived HDAC inhibitors (vorinostat, belinostat, panobinostat, chidamide) are approved for the treatment of lymphoma and myeloma (Figure 1).<sup>7-12</sup> The common pharmacophore model for HDACi consists of the following four elements: a zinc binding group (ZBG), a linker and a connecting unit (CU), that interact with the substrate binding tunnel and a cap, also known as surface recognition domain.<sup>13,14</sup> According to their ZBG, HDACi can be subdivided into 4 main chemical classes: hydroxamic acids, thiols, carboxylic acids and *o*-amino anilides.<sup>15</sup>

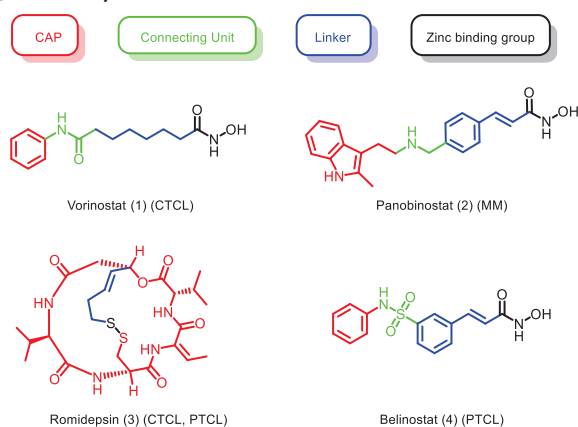


Figure 1: General pharmacophore model of HDACi and chemical structures of FDA approved HDAC inhibitors 1-4 and their indications. CTCL: cutaneous T-cell lymphoma, MM: multiple myeloma, PTCL: peripheral T-cell lymphoma.<sup>7-12</sup>

Thiazoles are privileged structures in medicinal chemistry. Its core scaffold is found in many natural products such as alkaloids, secondary metabolites and cyclopeptides.<sup>16</sup> The thiazole moiety is present in several active pharmaceutical ingredients with anti-Parkinson, anticancer, anti-inflammatory, antibacterial, CNS-regulatory and antidiuretic properties (Figure 2).<sup>17-20</sup>

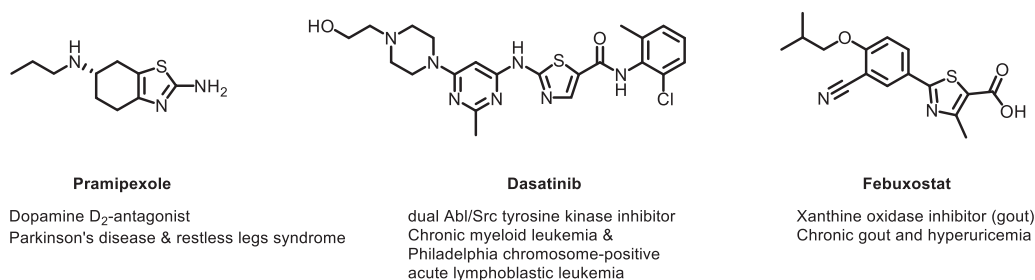


Figure 2: Selected thiazolyl-based drugs.<sup>21-23</sup>

Initial studies for the development of thiazolyl-based HDACi were performed by Anandan et al. (Figure 3).<sup>24</sup> In the reported HDACi, the thiazole moiety acts as a linker that bridges the ZBG with the cap group. These HDACi

displayed *in vitro* HDAC inhibitory activity in HeLa cell nuclear extracts and antiproliferative effects towards the breast cancer cell line MCF7 in the micromolar range.

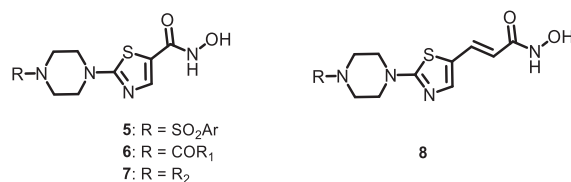
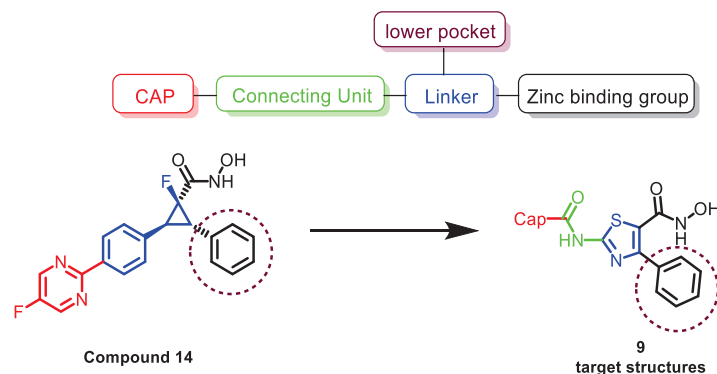


Figure 3: Thiazolyl-based hydroxamic acids HDACi **5-8**.<sup>24</sup>

## Results and Discussion

### Design of 4-phenyl substituted thiazolyl hydroxamates as HDAC inhibitors

Recent studies have shown that HDAC class IIa enzymes might be associated with neurodegenerative diseases and cancer.<sup>25–28</sup> So far, only trifluoromethyloxadiazoles (TFMO), cyclopropane hydroxamates as well as benzhydryl based class IIa HDAC inhibitors have been reported. In published crystal structures of class IIa HDACs, the so-called lower pocket was identified as a distinctive structural feature.<sup>29,30</sup> Bürli et al. and Luckhurst et al. showed that tri- and tetrasubstituted cyclopropanes, providing a scaffold with a suitable 3D-geometry that occupy the lower pocket with their phenyl moiety (Scheme 1, circled in red).<sup>25,30</sup> Here, we report the synthesis of trisubstituted thiazolyl-based hydroxamates as potential class IIa HDACi.



Scheme 1: Pharmacophore model of class IIa selective HDACi (above) and design of target structures as class IIa selective HDACi.<sup>30</sup>

In order to evaluate whether the 4-phenyl-substituent of compound **9a** might occupy the lower pocket of class IIa HDACs, we performed docking studies. Molecular docking studies of the thiazole derivative **9a**, in various HDAC-isozymes were performed using a previously validated docking protocol employing Autodock 4.2 as docking engine.<sup>31</sup> **9a**, as thiazolyl-based HDACi representative, was docked in HDAC2 (PDB 5IWG)<sup>32</sup>, HDAC8 (PDB 5CFW)<sup>33</sup>, HDAC4 (PDB 5A2S)<sup>30</sup> and HDAC6 (PDB 5EDU)<sup>34</sup>.

The analysis of the docking conformation of compound **9a** in HDAC4 suggests that, as envisioned, the hydroxamate moiety of **9a** can coordinate with the zinc cation in a bidentate manner (Figure 4). In addition, the phenyl substituent of **9a** occupied the lower pocket in a similar binding mode as the phenyl moiety of compound **14** (Figure 4). The thiazolyl-based hydroxamate **9a** did not generate valid docking poses in the other HDACs as no docking pose was observed that showed a complexation of the zinc ion by the hydroxamic acid moiety.

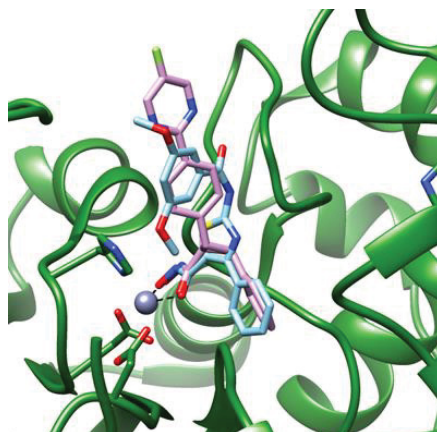
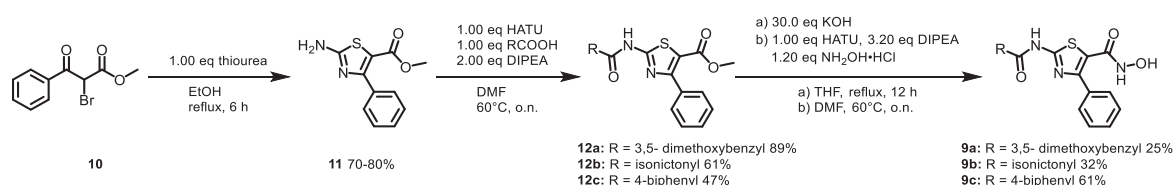


Figure 4: Proposed binding mode of compound **9a** (light blue) in HDAC4 (PDB 5A2S)<sup>30</sup>. The docking pose of compound **9a** is superimposed with the HDAC4 cocrystallised compound **14** (pink).

## Chemistry

The starting material of the Hantzsch thiazole synthesis was the  $\alpha$ -bromoester **10** that was prepared according to Borowiecki et al.<sup>35</sup> After the treatment of **10** with thiourea, the thiazole **11** was formed. In the following step, **11** and the respective carboxylic acids were coupled using HATU under basic conditions yielding the corresponding amides **12a-c**. The direct hydroxylaminolysis of the esters **12a-c** to the corresponding hydroxamic acids **9a-c** applying various literature procedures did not provide the expected products.<sup>36–40</sup> Therefore, the hydroxamic acids **9a-c** were synthesized by ester hydrolysis and subsequent conversion of the respective carboxylic acids with HATU, DIPEA and hydroxylamine hydrochloride (Scheme 2). The ester hydrolysis was achieved by the addition of an excess of potassium hydroxide. However, the same protocol was unsuccessful when applied for the cleavage of the corresponding ethyl esters. This finding underscores that the hydrolysis depends on the nature of the alkyl substituent of the ester moiety.



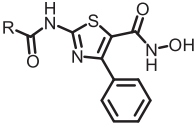
Scheme 2: Synthesis of the target structures **9a-c**.

## Biological Evaluation

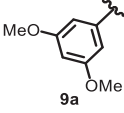
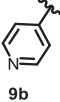
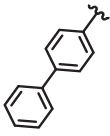
The synthesised compounds **9a-c** were assessed for their antiproliferative activity and for their HDAC inhibitory activity in the human monocytic cell line THP-1 using class-distinguishing substrates (Boc-Lys(Ac)-AMC: class I and IIb HDACs; Boc-Lys(TFAC)-AMC: class IIa, HDAC8). The results are depicted in Table 1 with vorinostat as reference compound. Among the tested compounds, **9b** exhibited the highest antiproliferative activity with 61.5% of growth inhibition at 100  $\mu\text{M}$  concentration. The introduction of a 3,5-dimethoxyphenyl (**9a**) or biphenyl (**9c**) CAP moiety led to a decreased cytotoxicity with antiproliferative effects below 50% at 100  $\mu\text{M}$ . In a whole-cell HDAC inhibition assay using the Boc-Lys(Ac)-AMC-HDAC substrate, all screened hydroxamic acids **9a-c** displayed inhibitory activities below 40% at 100  $\mu\text{M}$ . However, the cellular HDAC inhibition assay using the Boc-Lys(TFAC)-AMC-HDAC substrate revealed a slightly increased inhibition with over 45% at 100  $\mu\text{M}$  for **9a** and **9b**.

Overall there is a good correlation between the antiproliferative activity and the cellular HDAC inhibition. All tested compounds **9a-c** showed a moderate cytotoxicity and cellular HDAC inhibition.

Table 1: Cell viability (MTT assay) and whole-cell HDAC inhibition assay in the human monocytic cell line THP-1.



**9a-c**

Cpd.	cell viability (MTT)		HDAC inhibition			
			Boc-Lys(Ac)-AMC		Boc-Lys(TFAc)-AMC	
	% inhibition of 100 $\mu$ M	IC <sub>50</sub> [ $\mu$ M] (pIC <sub>50</sub> $\pm$ SEM)	% inhibition of 100 $\mu$ M	IC <sub>50</sub> [ $\mu$ M] (pIC <sub>50</sub> $\pm$ SEM)	% inhibition of 100 $\mu$ M	IC <sub>50</sub> [ $\mu$ M] (pIC <sub>50</sub> $\pm$ SEM)
 <b>9a</b>	47.1%	>100	31.2%	>100	45.2%	>100
 <b>9b</b>	61.5%	82.1 (4.09 $\pm$ 0.11)	36.9%	>100	48.1%	>100
 <b>9c</b>	44.5%	>100	38.4%	>100	37.1%	>100
<b>Vorinostat</b>	96.6%	0.18 (6.74 $\pm$ 0.06)	98%	0,75 (6.13 $\pm$ 0.054)	62%	41.43 (4.38 $\pm$ 0.04)

Presented data are calculated from at least two experiments each performed in duplicates. IC<sub>50</sub> values were calculated for compounds with an inhibition of more than 50 %. Standard deviation of percent inhibition values is less than 14 %. Vehicle control was defined as 0 % inhibition.

For further evaluation, the synthesized compounds **9a-c** were screened against recombinant human HDAC2, HDAC4, HDAC6 and HDAC8 (Table 2). Vorinostat was included as a pan-HDACi reference compound. Interestingly, the new thiazolyl-based hydroxamates **9a-c** were identified as moderate HDAC6 inhibitors in the low micromolar range. In contrast to our preliminary *in-silico* data, the hydroxamic acids **9a** and **9c** displayed no HDAC4 inhibition in the tested concentration range ( $\leq 100 \mu\text{M}$ ). However, the hydroxamic acid **9b** exhibiting a 4-pyridinyl CAP moiety demonstrated a moderate micromolar activity against HDAC4 (IC<sub>50</sub>(HDAC4) = 48.8  $\mu\text{M}$ ).

Table 2: Inhibitory activity of **9a-c** and Vorinostat on recombinant human HDAC2, HDAC4, HDAC6 and HDAC8.

**9a-c**

Cpd.	IC <sub>50</sub> [μM] (pIC <sub>50</sub> ± SEM)			
	HDAC2	HDAC4	HDAC6	HDAC8
 <b>9a</b>	>100	>100	3.85 (5.41 ± 0.04)	43.1 (4.37 ± 0.05)
 <b>9b</b>	>100	48.8 (4.31 ± 0.08)	3.6 (5.44 ± 0.04)	21.4 (4.67 ± 0.04)
 <b>9c</b>	>100	>100	9.94 (5.0 ± 0.08)	>100
<b>Vorinostat</b>	0.096 (7.02 ± 0.04)	96.5 (4.02 ± 0.05)	0.04 (7.63 ± 0.05)	4.44 (5.35 ± 0.05)

Data shown is at least from two experiments each performed at least as duplicates and the IC<sub>50</sub> value of pooled data is reported when IC<sub>50</sub> < 100 μM.

## Conclusions

Histone deacetylases are zinc-dependent metalloproteases that catalyse the removal of acetyl functional groups from lysine residues of both histone and nonhistone proteins. HDACs are involved in a multitude of biological processes e.g. in cell cycle progression, cell survival, apoptosis and differentiation. They are clinically validated targets for the treatment of cancer. Selective HDAC inhibitors may serve as important tools for elucidating the role of specific HDACs in certain diseases. Contrary to our preliminary qualitative *in-silico* screening, all synthesized compounds **9a-c** exhibited a moderate HDAC6 inhibitory activity in the low micromolar range. Nevertheless, the hydroxamic acid **9b** exhibiting a 4-pyridinyl CAP moiety displayed a moderate micromolar activity against HDAC4 (IC<sub>50</sub>(HDAC4) = 48.8 μM).

## Experimental Section

### General methods

All chemicals and solvents were purchased from commercial suppliers (Sigma Aldrich, Alfa Aesar, Fluorochem, TCI, abcr and Acros Organics) and used without further purification. All anhydrous reactions were carried out in flame-dried Schlenk-flasks and under argon atmosphere. Dry solvents were used directly from Seal® bottles from Acros Organics. Analytic Thin Layer Chromatography (TLC) was carried out with Macherey Nagel precoated silica gel plates (ALUGRAM® Xtra SIL G/UV<sub>254</sub>). Detection was achieved with ultraviolet irradiation (254 nm)

and/or staining with potassium permanganate solution (9 g  $\text{KMnO}_4$ , 60 g  $\text{K}_2\text{CO}_3$ , 15 mL of a 5% aqueous NaOH-solution, and 900 mL demineralised water). Flash column chromatography was performed with CombiFlashRf200 (TeleDyneIsc) with the solvent mixtures specified in the corresponding procedure.

## Physical data

Proton ( $^1\text{H}$ ) and carbon ( $^{13}\text{C}$ ) NMR spectra were recorded on Bruker Avance III – 300, Bruker Avance DRX – 500 or Bruker Avance III – 600. Spectra were referenced to the residual non-deuterated solvent signal ( $^1\text{H}$ -NMR:  $\text{DMSO-}d_6$  (2.50 ppm),  $^{13}\text{C}$ -NMR:  $\text{DMSO-}d_6$  (39.52 ppm);  $^1\text{H}$ -NMR:  $\text{CDCl}_3$  (7.26 ppm),  $^{13}\text{C}$ -NMR:  $\text{CDCl}_3$  (77.16 ppm)). Chemical shifts are quoted in parts per million (ppm). Signal patterns are indicated as: singlet (s), doublet (d), triplet (t), quartet (q), or multiplet (m). Coupling constants,  $J$ , are measured in Hz. Proton ( $^1\text{H}$ ) and carbon ( $^{13}\text{C}$ ) NMR spectra were recorded by the NMR-Divisions of the Department of Chemistry (Heinrich-Heine-University Düsseldorf). Electrospray Ionisation (ESI) mass spectra were carried out by the Mass spectrometry-Division of the Heinrich-Heine-University Düsseldorf, using Bruker Daltonics UHR-QTOF maXis 4G (Bruker Daltonics). Melting points (mp.) were determined using a Büchi M-565 melting point apparatus and are uncorrected.

Analytical HPLC analysis were carried out on a Knauer HPLC system comprising an Azura P 6.1L pump, an Optimas 800 autosampler, a Fast Scanning Spectro-Photometer K-2600 and Knauer Reversed Phase column (SN: FK36). UV absorption was detected at 254 nm. The solvent gradient table is shown below. The purity of all final compounds was 95% or higher.

Table 3: The solvent gradient table for analytic HPLC analysis.

Time / min	Water + 0.1% TFA	ACN + 0.1% TFA
Initial	90	10
0.50	90	10
20.0	0	100
30.0	0	100
31.0	90	10
40.0	90	10

**Synthesis of methyl 2-bromo-3-oxo-3-phenylpropanoate (10).** A solution of methyl 3-oxo-3-propanoate<sup>35</sup> (2.67 g, 15.0 mmol, 1.00 eq) in methanol (40.0 mL) was cooled to 0 °C and sodium methoxide (30 wt. % in methanol, 3.43 mL, 18.0 mmol, 1.20 eq) was added dropwise. After stirring for further 5 min, bromine (0.92 mL, 18.0 mmol, 1.20 eq) in methanol (20.0 mL) was added dropwise to the reaction. The resulting mixture was stirred overnight at rt. The solvent was removed *in vacuo*, and the crude solid was resuspended in ethyl acetate. The organic layer was washed with water (3x25 mL), dried over  $\text{Na}_2\text{SO}_4$  and filtered. After removing the solvent, the crude product was purified by flash column chromatography (prepacked silica cartridge, *n*-hexane/ethyl acetate) to provide 2-bromo-3-oxo-3-phenylpropanoate (**10**) (2.85 g, 11.1 mmol, 74%) as a yellow oil.

$^1\text{H}$  NMR (300 MHz,  $\text{DMSO-}d_6$ )  $\delta$  = 3.75 (s, 3H), 6.70 (s, 1H), 7.60 (t,  $J$  = 7.6 Hz, 2H), 7.69 – 7.78 (m, 1H), 8.04 (dd,  $J$  = 8.4, 1.3 Hz, 2H) ppm.

$^{13}\text{C}$  NMR (75 MHz,  $\text{DMSO-}d_6$ )  $\delta$  = 46.86, 53.67, 129.10, 133.08, 134.58, 165.89, 189.37 ppm.

HPLC analysis:  $R_t$  = 12.150 min, 98.2%.

HRMS (ESI+) = calcd. for  $\text{C}_{10}\text{H}_{10}\text{BrO}_3[\text{M}+\text{H}]^+$  = 256.9808, found: 256.9806.

**Synthesis of methyl 2-amino-4-phenylthiazole-5-carboxylate (11).** To a solution of methyl 2-bromo-3-oxo-3-phenylpropanoate (**10**) (2.53 g, 6.70 mmol, 1.00 eq) in methanol (40.0 mL), thiourea (0.52 g, 6.70 mmol, 1.00 eq) was added and the resulting solution was refluxed for 6 h. The solvent was evaporated under reduced pressure and the residue was dissolved in EtOAc, washed with saturated NaHCO<sub>3</sub> solution (3x 50 mL) and dried over Na<sub>2</sub>SO<sub>4</sub>. After filtration, the solvent was removed *in vacuo* to yield the crude product which was purified by flash column chromatography (prepacked silica cartridge, *n*-hexane/ethyl acetate) to provide methyl 2-amino-4-phenylthiazole-5-carboxylate (**11**) (0.70 g, 2.90 mmol, 43%) as a yellow solid.

<sup>1</sup>H NMR (300 MHz, DMSO-*d*<sub>6</sub>) δ = 3.62 (s, 3H), 7.29-7.46 (m, 3H), 7.60–7.68 (m, 2H), 7.86 (s, 2H) ppm.

<sup>13</sup>C NMR (75 MHz, DMSO-*d*<sub>6</sub>) δ = 51.40, 107.65, 127.33, 128.69, 129.58, 134.51, 159.02, 161.53, 169.89 ppm.

HPLC analysis: R<sub>t</sub> = 7.533 min, 97.2%.

HRMS (ESI+) = calcd. for C<sub>11</sub>H<sub>11</sub>N<sub>2</sub>O<sub>2</sub>S [M+H]<sup>+</sup> = 235.0536, found: 235.0535.

mp.: 183-186°C.

**General procedure 1: HATU-coupling.** For the synthesis of the amides **12a-c**, 1.00 eq of the respective carboxylic acid was dissolved in dry DMF (0.1 mmol/mL) and 1.00 eq HATU and 2.00 eq DIPEA were added. After stirring for 15 min at rt, methyl 2-amino-4-phenylthiazole-5-carboxylate (**11**) (1.00 eq) was added and the resulting mixture was stirred for 16h at 60 °C. The solvent was removed *in vacuo* and the residue was diluted with EtOAc. The organic layer was washed with saturated NaHCO<sub>3</sub> (3x 50 mL), brine (1x 50 mL), dried over Na<sub>2</sub>SO<sub>4</sub> and filtered. After the removal of the solvent, the crude product was purified by flash column chromatography (prepacked silica cartridge, *n*-hexane/ethyl acetate) to provide the amides **12a-c**.

**Synthesis of methyl 2-(3,5-dimethoxybenzamido)-4-phenyl-thiazole-5-carboxylate (12a).** 3,5-Dimethoxybenzoic acid (1.01 g, 5.50 mmol, 1.00 eq) was subjected to General Procedure 1. The crude product was purified by flash column chromatography (*n*-hexane/EtOAc) to furnish methyl 2-(3,5-dimethoxybenzamido)-4-phenyl-thiazole-5-carboxylate (**12a**) (1.95 g, 4.90 mmol, 98%) as a white solid.

<sup>1</sup>H NMR (300 MHz, DMSO-*d*<sub>6</sub>) δ = 3.74 (s, 3H), 3.83 (s, 6H), 6.76 (t, *J* = 2.2 Hz, 1H), 7.33 (d, *J* = 2.3 Hz, 2H), 7.41–7.51 (m, 3H), 7.74 (dd, *J* = 6.6, 3.0 Hz, 2H), 13.15 (s, 1H) ppm.

<sup>13</sup>C NMR (75 MHz, DMSO-*d*<sub>6</sub>) δ = 51.90, 55.59, 105.49, 106.02, 127.55, 128.91, 129.63, 133.15, 134.01, 155.96, 160.19, 160.52, 161.80, 165.33 ppm.

HPLC analysis: R<sub>t</sub> = 15.883 min, >99%.

HRMS (ESI+) = calcd. for C<sub>20</sub>H<sub>19</sub>N<sub>2</sub>O<sub>5</sub>S [M+H]<sup>+</sup> = 399.1009, found: 399.1008.

mp.: 170-174°C.

**Synthesis of methyl 2-(isonicotinamido)-4-phenylthiazole-5-carboxylate (12b).** Isonicotinic acid (373 mg, 3.00 mmol, 1.00 eq) was subjected to General Procedure 1. The crude product was purified by flash column chromatography (*n*-hexane/EtOAc) to furnish methyl 2-(isonicotinamido)-4-phenylthiazole-5-carboxylate (**12b**) (0.62 g, 1.80 mmol, 61%) as a white solid.

<sup>1</sup>H NMR (300 MHz, DMSO-*d*<sub>6</sub>) δ = 3.73 (s, 3H), 7.30-7.53 (m, 3H), 7.76 (d, *J* = 7.3 Hz, 2H), 8.01 (d, *J* = 5.2 Hz, 2H), 8.82 (d, *J* = 5.1 Hz, 2H), 9.34 (s, 1H), 11.12 (s, 1H), 13.32 (s, 1H) ppm.

<sup>13</sup>C NMR (75 MHz, DMSO-*d*<sub>6</sub>) δ = 52.03, 115.13, 121.81, 127.62, 129.04, 129.69, 133.78, 138.51, 150.46, 155.87, 159.81, 161.68, 164.67 ppm.

HPLC analysis: R<sub>t</sub> = 9.667 min, >99%.

HRMS (ESI+) = calcd. for C<sub>17</sub>H<sub>14</sub>N<sub>3</sub>O<sub>3</sub>S [M+H]<sup>+</sup> = 340.0750, found: 340.0753.

mp.: 225-229°C.

**Synthesis of methyl 2-([1,1'-biphenyl]-4-carboxamido)-4-phenylthiazole-5-carboxylate (12c).** Biphenyl-4-carboxylic acid (595 mg, 3.00 mmol, 1.00 eq) was subjected to General Procedure 1. The crude product was purified by flash column chromatography (*n*-hexane/EtOAc) to furnish methyl 2-([1,1'-biphenyl]-4-carboxamido)-4-phenylthiazole-5-carboxylate (**12c**) (0.58 g, 1.40 mmol, 47%) as a white solid.

<sup>1</sup>H NMR (600 MHz, DMSO-*d*<sub>6</sub>) δ = 3.75 (s, 3H), 7.41 – 7.47 (m, 4H), 7.51 (dd, *J* = 8.4, 6.9 Hz, 2H), 7.71 – 7.82 (m, 4H), 7.83 – 7.90 (m, 2H), 8.19 – 8.27 (m, 2H), 13.24 (s, 1H) ppm.

<sup>13</sup>C NMR (151 MHz, DMSO-*d*<sub>6</sub>) δ = 52.01, 114.70, 126.80, 126.99, 127.63, 128.43, 129.00, 129.10, 129.12, 129.70, 130.12, 134.01, 138.74, 144.40, 156.06, 160.34, 161.85, 165.56 ppm.

HPLC analysis: *R*<sub>t</sub> = 17.983 min, 98.3%.

HRMS (ESI+) = calcd. for C<sub>24</sub>H<sub>19</sub>N<sub>2</sub>O<sub>3</sub>S [M+H]<sup>+</sup> = 415.1111, found: 415.1114.

mp.: 267-270°C.

**General procedure 2: Methyl ester hydrolysis.** For the synthesis of the acids **13a-c**, 1.00 eq of the methyl ester **12a-c** was dissolved in THF (0.1 mmol/mL) and 30.0 eq potassium hydroxide was added. The resulting mixture was refluxed for 16 h. The solvent was removed *in vacuo* and the residue was resuspended with EtOAc. The organic layer was washed with saturated NaHCO<sub>3</sub> (3x 50 mL). The combined aqueous phases were acidified (pH = 2-3) and the resulting precipitate (product) was filtered off and washed with water.

**Synthesis of 2-(3,5-dimethoxybenzamido)-4-phenylthiazole-5-carboxylic acid (13a).** Methyl 2-(3,5-dimethoxybenzamido)-4-phenyl-thiazole-5-carboxylate (**12a**) (0.51 g, 1.28 mmol, 1.00 eq) was subjected to General Procedure 2. The acid **13a** (0.27 g, 0.71 mmol, 55%) was obtained as a white solid.

<sup>1</sup>H NMR (600 MHz, DMSO-*d*<sub>6</sub>) δ = 3.83 (s, 6H), 6.76 (t, *J* = 2.3 Hz, 1H), 7.33 (d, *J* = 2.3 Hz, 2H), 7.39 – 7.45 (m, 3H), 7.71 – 7.78 (m, 2H), 13.05 (s, 2H) ppm.

<sup>13</sup>C NMR (151 MHz, DMSO-*d*<sub>6</sub>) δ = 55.62, 105.46, 105.94, 116.78, 127.53, 128.73, 129.78, 133.24, 134.25, 155.10, 159.73, 160.49, 162.83, 165.22 ppm.

HPLC analysis: *R*<sub>t</sub> = 13.00 min, 96.4%.

HRMS (ESI+) = calcd. for C<sub>19</sub>H<sub>17</sub>N<sub>2</sub>O<sub>5</sub>S [M+H]<sup>+</sup> = 385.0853, found: 385.0852.

mp.: 187-191°C.

**Synthesis of 2-(isonicotinamido)-4-phenylthiazole-5-carboxylic acid (13b).** Methyl 2-(isonicotinamido)-4-phenylthiazole-5-carboxylate (**12b**) (338 mg, 1.04 mmol, 1.00 eq) was subjected to General Procedure 2. The acid **13b** (228 mg, 0.70 mmol, 67%) was obtained as a white solid.

<sup>1</sup>H NMR (300 MHz, DMSO-*d*<sub>6</sub>) δ = 1.23 (t, *J* = 7.1 Hz, 3H), 4.22 (q, *J* = 7.1 Hz, 2H), 7.40 – 7.55 (m, 3H), 7.68 – 7.81 (m, 2H), 7.98 – 8.08 (m, 2H), 8.78 – 8.90 (m, 2H), 13.50 (s, 1H) ppm.

<sup>13</sup>C NMR (75 MHz, DMSO-*d*<sub>6</sub>) δ = 13.91, 60.85, 115.62, 121.78, 127.56, 128.99, 129.71, 133.80, 138.50, 150.46, 155.66, 159.74, 161.24, 164.64 ppm.

HPLC analysis: *R*<sub>t</sub> = 6.883 min, 98.4%.

HRMS (ESI+) = calcd. for C<sub>16</sub>H<sub>12</sub>N<sub>3</sub>O<sub>3</sub>S [M+H]<sup>+</sup> = 326.0594, found: 326.0597.

mp.: 246-260 °C.

**Synthesis of 2-([1,1'-biphenyl]-4-carboxamido)-4-phenylthiazole-5-carboxylic acid (13c).** Methyl 2-([1,1'-biphenyl]-4-carboxamido)-4-phenylthiazole-5-carboxylate (**12c**) (0.35 g, 0.84 mmol, 1.00 eq) was subjected to General Procedure 2. The acid **13c** (0.31 g, 0.77 mmol, 92%) was obtained as a white solid.

<sup>1</sup>H NMR (600 MHz, DMSO-*d*<sub>6</sub>) δ = 7.40 – 7.46 (m, 4H), 7.51 (t, *J* = 7.7 Hz, 2H), 7.72 – 7.81 (m, 4H), 7.85 – 7.89 (m, 2H), 8.22 – 8.26 (m, 2H), 13.13 (s, 1H) ppm.

$^{13}\text{C}$  NMR (151 MHz,  $\text{DMSO-}d_6$ )  $\delta$  = 126.83, 127.01, 127.56, 128.44, 128.77, 129.09, 129.12, 129.81, 138.78, 144.39, 162.86, 165.44 ppm.

HPLC analysis:  $R_t$  = 14.933 min, 92.0%.

HRMS (ESI+) = calcd. for  $\text{C}_{23}\text{H}_{17}\text{N}_2\text{O}_3\text{S}$   $[\text{M}+\text{H}]^+$  = 401.0954, found: 401.0953

mp.: decomposition at 248 °C.

**General procedure 3: Hydroxamic acid formation.** For the synthesis of the hydroxamic acids **9a-c**, 1.00 eq of the respective carboxylic acid **13a-c** was dissolved in dry DMF (0.1 mmol/mL), 1.00 eq HATU and 3.20 eq DIPEA were added. After stirring for 15 min at rt, 1.20 eq hydroxylamine hydrochloride was then added and the resulting mixture was stirred for further 16 h at 60 °C. The reaction mixture was then poured into water and the resulting participate was then filtered and washed with aqueous HCl-solution (pH = 4) and water. The crude product was purified by flash column chromatography (prepacked silica cartridge, DCM/30% methanol in DCM) to provide the corresponding hydroxamic acids.

**Synthesis of 2-(3,5-dimethoxybenzamido)-N-hydroxy-4-phenylthiazole-5-carboxamide (9a).** 2-(3,5-dimethoxybenzamido)-4-phenylthiazole-5-carboxylic acid (**13a**) (199 mg, 0.50 mmol, 1.00 eq) was subjected to General Procedure 3. The hydroxamic acid **9a** (50.0 mg, 0.12 mmol, 25%) was obtained as a white solid.

$^1\text{H}$  NMR (300 MHz,  $\text{DMSO-}d_6$ )  $\delta$  = 3.84 (s, 6H), 6.76 (s, 1H), 7.34 (d,  $J$  = 2.2 Hz, 2H), 7.38 – 7.52 (m, 3H), 7.77 (d,  $J$  = 6.8 Hz, 2H), 9.28 (s, 1H), 11.07 (s, 1H), 12.98 (s, 1H) ppm.

$^{13}\text{C}$  NMR (75 MHz,  $\text{DMSO-}d_6$ )  $\delta$  = 55.61, 105.35, 105.96, 128.13, 128.28, 128.70, 129.70, 129.71, 133.40, 134.10, 154.81, 160.52, 161.78, 165.01.

HPLC analysis :  $R_t$  = t = 10.383 min, 95.0%.

HRMS (ESI+) = calcd. for  $\text{C}_{19}\text{H}_{18}\text{N}_3\text{O}_5\text{S}$   $[\text{M}+\text{H}]^+$  = 400.0962, found: 400.0960.

mp.: decomposition at 225 °C.

**Synthesis of N-hydroxy-2-(isonicotinamido)-4-phenylthiazole-5-carboxamide (9b).** 2-(Isonicotinamido)-4-phenylthiazole-5-carboxylic acid (**13b**) (595 mg, 1.83 mmol, 1.00 eq) was subjected to General Procedure 3. The hydroxamic acid **9b** (0.200 g, 0.59 mmol, 32%) was obtained as an orange solid.

$^1\text{H}$  NMR (300 MHz,  $\text{DMSO-}d_6$ )  $\delta$  = 7.42 (dq,  $J$  = 13.5, 6.8 Hz, 3H), 7.76 (d,  $J$  = 7.3 Hz, 2H), 8.01 (d,  $J$  = 5.2 Hz, 2H), 8.82 (d,  $J$  = 5.1 Hz, 2H), 9.34 (s, 1H), 11.12 (s, 1H) ppm.

$^{13}\text{C}$  NMR (75 MHz,  $\text{DMSO-}d_6$ )  $\delta$  = 117.92, 121.95, 128.40, 128.59, 133.95, 138.88, 150.59, 156.94, 164.49 ppm.

HPLC analysis:  $R_t$  = 4.817 min, 97.3%.

HRMS (ESI+) = calcd. for  $\text{C}_{16}\text{H}_{13}\text{N}_4\text{O}_3\text{S}$   $[\text{M}+\text{H}]^+$  = 341.0703, found: 304.0706.

mp.: 210-214 °C.

**Synthesis of 2-([1,1'-biphenyl]-4-carboxamido)-N-hydroxy-4-phenylthiazole-5-carboxamide (9c).** 2-([1,1'-biphenyl]-4-carboxamido)-4-phenylthiazole-5-carboxylic acid (**13c**) (260 mg, 0.65 mmol, 1.00 eq) was subjected to General Procedure 3. The hydroxamic acid **9c** (0.165 g, 0.40 mmol, 61%) was obtained as a white solid.

$^1\text{H}$  NMR (600 MHz,  $\text{DMSO-}d_6$ )  $\delta$  = 7.38 – 7.47 (m, 4H), 7.52 (t,  $J$  = 7.6 Hz, 2H), 7.79 (d,  $J$  = 7.6 Hz, 4H), 7.88 (d,  $J$  = 8.0 Hz, 2H), 8.25 (d,  $J$  = 8.1 Hz, 2H), 9.29 (s, 1H), 11.09 (s, 1H), 13.05 (s, 1H) ppm.

$^{13}\text{C}$  NMR (151 MHz,  $\text{DMSO-}d_6$ )  $\delta$  = 126.81, 127.00, 127.55, 128.22, 128.32, 128.41, 129.02, 129.11, 130.26, 134.05, 138.79, 144.30, 148.59, 157.20, 159.67, 165.16 ppm.

HPLC analysis :  $R_t$  = t = 12.633 min, 95.7%.

HRMS (ESI+) = calcd. for  $\text{C}_{23}\text{H}_{18}\text{N}_3\text{O}_3\text{S O}_3$   $[\text{M}+\text{H}]^+$  = 416.1063, found: 416.1055.

mp.: decomposition at 225 °C.

## Acknowledgements

YA, AJS, MUK, and TK gratefully acknowledge support from the Deutsche Forschungsgemeinschaft (DFG) for grant number KA 1942/1-1 to MUK and grant number KU 1577/2-1 to TK, and the support from the DFG research training group 270650915/GRK 2158. We further acknowledge the CHDI Foundation Inc. for providing the compound CHDI-00390576-0000-004.

## Supplementary Material

The performed docking studies and the experimental procedures for the biological evaluation are provided as supplementary material.

## References

- 1 Bird, A., *Nature* **2007**, *447* (7143), 396–398.  
<https://doi.org/10.1038/nature05913>
- 2 Fischle, W.; Dequiedt, F.; Hendzel, M. J.; Guenther, M. G.; Lazar, M. A.; Voelter, W.; Verdin, E., *Mol. Cell* **2002**, *9*, 45–57.  
[https://10.1016/s1097-2765\(01\)00429-4](https://10.1016/s1097-2765(01)00429-4)
- 3 Gryder, B. E.; Sodji, Q. H.; Oyelere, A. K., *Future Med. Chem.* **2012**, *4*, 505–524.  
<https://doi.org/10.4155/fmc.12.3>
- 4 Witt, O.; Deubzer, H. E.; Milde, T.; Oehme, I., *Cancer Lett.* **2009**, *277*, 8–21.  
<https://doi.org/10.1016/j.canlet.2008.08.016>
- 5 Ropero, S.; Esteller, M., *Mol. Oncol.* **2007**, *1*, 19–25.  
<https://doi.org/10.1016/j.molonc.2007.01.001>
- 6 Jung, M., *Curr. Med. Chem.* **2001**, *8*, 1505–1511.  
<https://doi.org/10.2174/0929867013372058>
- 7 Marks, P. A.; Breslow, R., *Nat. Biotechnol.* **2007**, *25*, 84–90.  
<https://doi.org/10.1038/nbt1272>
- 8 Duvic, M.; Talpur, R.; Ni, X.; Zhang, C.; Hazarika, P.; Kelly, C.; Chiao, J. H.; Reilly, J. F.; Ricker, J. L.; Richon, V. M.; Frankel, S. R., *Blood* **2007**, *109*, 31–39.  
<https://doi.org/10.1182/blood-2006-06-025999>
- 9 Minucci, S.; Pelicci, P. G., *Nat. Rev. Cancer* **2006**, *6*, 38–51.  
<https://doi.org/10.1038/nrc1779>
- 10 Richon, V. M.; Emiliani, S.; Verdin, E.; Webb, Y.; Breslow, R.; Rifkind, R. A.; Marks, P. A., *Proc. Natl. Acad. Sci.* **1998**, *95*, 3003–3007.  
<https://doi.org/10.1073/pnas.95.6.3003>
- 11 Hose, C. D.; Petersen, K. D.; Shoemaker, R. H.; Kondapaka, S.; Pezzoli, P.; Monforte, J.; Monks, A.; Sehested, M.; Vansant, G., *Anticancer. Drugs* **2009**, *20*, 682–692.  
<https://doi.org/10.1097/cad.0b013e32832e14e1>
- 12 Atadja, P., *Cancer Lett.* **2009**, *280*, 233–241.  
<https://doi.org/10.1016/j.canlet.2009.02.019>

- 13 Melesina, J.; Praetorius, L.; Simoben, C. V.; Robaa, D.; Sippl, W., *Future Med. Chem.* **2018**, *10*, 1537–1540.  
<https://doi.org/10.4155/fmc-2018-0125>
- 14 Bolden, J. E.; Peart, M. J.; Johnstone, R. W., *Nat. Rev. Drug Discov.* **2006**, *5*, 769–784.  
<https://doi.org/10.1038/nrd2133>
- 15 Seidel, C.; Schnekenburger, M.; Dicato, M.; Diederich, M., *Genes Nutr.* **2012**, *7* (3), 357–367.  
<https://doi.org/10.1007/s12263-012-0283-9>
- 16 Mishra, R.; Sharma, P. K.; Verma, P. K.; Tomer, I.; Mathur, G.; Dhakad, P. K., *J. Heterocycl. Chem.* **2017**, *54*, 2103–2116.  
<https://doi.org/10.1002/jhet.2827>
- 17 Rashad, A. E.; Mahmoud, A. E.; Ali, M. M., *Eur. J. Med. Chem.* **2011**, *46*, 1019–1026.  
<https://doi.org/10.1016/j.ejmech.2011.01.013>
- 18 Karegoudar, P.; Karthikeyan, M. S.; Prasad, D. J.; Mahalinga, M.; Holla, B. S.; Kumari, N. S., *Eur. J. Med. Chem.* **2008**, *43*, 261–267.  
<https://doi.org/10.1016/j.ejmech.2007.03.014>
- 19 Cukurovali, A.; Yilmaz, I.; Gur, S.; Kazaz, C., *Eur. J. Med. Chem.* **2006**, *41*, 201–207.  
<https://doi.org/10.1016/j.ejmech.2005.01.013>
- 20 Wu, X.; Kassie, F.; Mersch-Sundermann, V., *Mutat. Res. - Rev. Mutat. Res.* **2005**, *589*, 81–102.  
<https://doi.org/10.1016/j.mrrev.2004.11.001>
- 21 Barone, P.; Poewe, W.; Albrecht, S.; Debievre, C.; Massey, D.; Rascol, O.; Tolosa, E.; Weintraub, D., *Lancet Neurol.* **2010**, *9*, 573–580.  
[https://doi.org/10.1016/S1474-4422\(10\)70106-X](https://doi.org/10.1016/S1474-4422(10)70106-X)
- 22 Mukaihara, K.; Tanabe, Y.; Kubota, D.; Akaike, K.; Hayashi, T.; Mogushi, K.; Hosoya, M.; Sato, S.; Kobayashi, E.; Okubo, T.; Kim, Y.; Kohsaka, S.; Saito, T.; Kaneko, K.; Suehara, Y., *PLoS One* **2017**, *12*, e0185321.  
<https://doi.org/10.1371/journal.pone.0185321>
- 23 White, W. B.; Chohan, S.; Dabholkar, A.; Hunt, B.; Jackson, R., *Am. Heart J.* **2012**, *164*, 14–20.  
<https://doi.org/10.1016/j.ahj.2012.04.011>
- 24 Anandan, S.; Ward, J. S.; Broxk, R. D.; Denny, T.; Bray, M. R.; Patel, D. V.; Xiao, X., *Bioorg. Med. Chem. Lett.* **2007**, *17*, 5995–5999.  
<https://doi.org/10.1016/j.bmcl.2007.07.050>
- 25 Bürli, R. W.; Luckhurst, C. A.; Aziz, O.; Matthews, K. L.; Yates, D.; Lyons, K. A.; Beconi, M.; McAllister, G.; Breccia, P.; Stott, A. J.; et al., *J. Med. Chem.* **2013**, *56*, 9934–9954.  
<https://doi.org/10.1021/jm4011884>
- 26 Hobara, T.; Uchida, S.; Otsuki, K.; Matsubara, T.; Funato, H.; Matsuo, K.; Suetsugi, M.; Watanabe, Y., *J. Psychiatr. Res.* **2010**, *44* (5), 263–270. <https://doi.org/10.1016/j.jpsychires.2009.08.015>
- 27 Sung, Y. M.; Lee, T.; Yoon, H.; DiBattista, A. M.; Song, J. M.; Sohn, Y.; Moffat, E. I.; Turner, R. S.; Jung, M.; Kim, J.; Hoe, H.-S., *Exp. Neurol.* **2013**, *239*, 192–201.  
<https://doi.org/10.1016/j.expneurol.2012.10.005>
- 28 Tsankova, N.; Renthal, W.; Kumar, A.; Nestler, E. J., *Nat. Rev. Neurosci.* **2007**, *8*, 355–367.  
<https://doi.org/10.1038/nrn2132>
- 29 Lobera, M.; Madauss, K. P.; Pohlhaus, D. T.; Wright, Q. G.; Trocha, M.; Schmidt, D. R.; Baloglu, E.; Trump, R. P.; Head, M. S.; Hofmann, G. A.; Murray-Thompson, M.; Schwartz, B.; Chakravorty, S.; Wu, Z.; Mander, P. K.; Kruidenier, L.; Reid, R. A.; Burkhardt, W.; Turunen, B. J.; Rong, J. X.; Wagner, C.; Moyer, M. B.; Wells,

- C.; Hong, X.; Moore, J. T.; Williams, J. D.; Soler, D.; Ghosh, S.; Nolan, M. A., *Nat. Chem. Biol.* **2013**, *9*, 319–325.  
<https://doi.org/10.1038/nchembio.1223>
- 30 Luckhurst, C. A.; Breccia, P.; Stott, A. J.; Aziz, O.; Birch, H. L.; Bürli, R. W.; Hughes, S. J.; Jarvis, R. E.; Lamers, M.; Leonard, P. M.; Matthews, K. L.; McAllister, G.; Pollack, S.; Saville-Stones, E.; Wishart, G.; Yates, D.; Dominguez, C., *ACS Med. Chem. Lett.* **2016**, *7*, 34–39.  
<https://doi.org/10.1021/acsmchemlett.5b00302>
- 31 Asfaha, Y.; Schrenk, C.; Alves Avelar, L. A.; Lange, F.; Wang, C.; Bandolik, J. J.; Hamacher, A.; Kassack, M. U.; Kurz, T., *Bioorg. Med. Chem.* **2020**, *28*, 115108.  
<https://doi.org/10.1016/j.bmc.2019.115108>
- 32 Wagner, F. F.; Weïwer, M.; Steinbacher, S.; Schomburg, A.; Reinemer, P.; Gale, J. P.; Campbell, A. J.; Fisher, S. L.; Zhao, W.-N.; Reis, S. A.; et al., *Bioorg. Med. Chem.* **2016**, *24*, 4008–4015.  
<https://doi.org/10.1016/j.bmc.2016.06.040>
- 33 Chekler, E. L. P.; Pellegrino, J. A.; Lanz, T. A.; Denny, R. A.; Flick, A. C.; Coe, J.; Langille, J.; Basak, A.; Liu, S.; Stock, I. A.; Sahasrabudhe, P.; Bonin, P. D.; Lee, K.; Pletcher, M. T.; Jones, H. L., *Chem. Biol.* **2015**, *22*, 1588–1596. <https://doi.org/10.1016/j.chembiol.2015.10.013>
- 34 Hai, Y.; Christianson, D. W., *Nat. Chem. Biol.* **2016**, *12*, 741–747. <https://doi.org/10.1038/nchembio.2134>
- 35 Borowiecki, P.; Bretner, M., *Tetrahedron Asymmetry* **2013**, *24*, 925–936.  
<https://doi.org/10.1016/j.tetasy.2013.06.004>
- 36 Gradilone, S. A.; LaRusso, N. F. Treatment of polycystic diseases with an HDAC6 inhibitor. US2015/0119413A1, 2015.
- 37 Diedrich, D.; Hamacher, A.; Gertzen, C. G. W.; Alves Avelar, L. A.; Reiss, G. J.; Kurz, T.; Gohlke, H.; Kassack, M. U.; Hansen, F. K., *Chem. Commun.* **2016**, 3219–3222.  
<https://doi.org/10.1039/C5CC10301K>
- 38 Marson, C. M.; Savy, P.; Rioja, A. S.; Mahadevan, T.; Mikol, C.; Veerupillai, A.; Nsubuga, E.; Chahwan, A.; Joel, S. P., *J. Med. Chem.* **2006**, *49*, 800–805. <https://doi.org/10.1021/jm051010j>
- 39 Liguori, A.; Sindona, G.; Romeo, G.; Uccella, N., *Synthesis (Stuttg)*. **1987**, 168–168.  
<https://doi.org/10.1055/s-1987-27874>
- 40 Dines, J. A.; Marson, C. M., *Tetrahedron* **2016**, *72*, 8584–8592. <https://doi.org/10.1016/j.tet.2016.11.039>

This paper is an open access article distributed under the terms of the Creative Commons Attribution (CC BY) license (<http://creativecommons.org/licenses/by/4.0/>)

## Supporting Information

### **Synthesis of thiazolyl-based hydroxamic acids as histone deacetylase inhibitors**

**Yodita Asfaha\*\***, **Alexander Jan Skerhut\*\***, **Leandro A. Alves-Avelar\***, **Nadine Horstick-Muche\***, **Beate Lungerich\***, **Stefan Klinken\***, **Matthias U. Kassack\*\***, **Thomas Kurz\*\***

*\*Institut für Pharmazeutische und Medizinische Chemie, Heinrich-Heine-Universität  
Düsseldorf, Universitätsstr.1, 40225 Düsseldorf, Germany, # YA and AJS share first  
authorship, MUK and TK share senior and corresponding authorship.*

*Email: [thomas.kurz@hhu.de](mailto:thomas.kurz@hhu.de), [matthias.kassack@hhu.de](mailto:matthias.kassack@hhu.de)*

## Docking studies

The structures of the ligands were prepared using the software ChemDraw 16.0 and Discovery studio and used as input for AutoDock tools version 1.5.7 (ADT). The crystal structures of the proteins HDAC2 (PDB: 5IWG)<sup>1</sup>, HDAC4 (PDB: 5A2S)<sup>2</sup>, HDAC6 (PDB: 5EDU)<sup>3</sup> and HDAC8 (PDB: 5FCW)<sup>4</sup> were downloaded from the Protein Data Base. All water molecules, buffer and non-interacting ions were removed with Autodock 4.2. The cleaned protein structures were used for the grid box generation. Using Autodock 4.2, a Lamarckian genetic algorithm was applied and the search parameters were set to 100 GA runs for each ligand with a population size of 150, maximum number of  $2.5 \cdot 10^6$  energy evaluations, a maximum number of  $2.7 \cdot 10^4$  generations, a mutation rate of 0.2 and a crossover rate of 0.8 and the default docking parameters. Populations of 100 docking poses were generated for each run and organized in clusters and the first pose of the cluster demonstrating coordinative interactions between the hydroxamic acid and the zinc ion (distance  $< 3.5 \text{ \AA}$ ) was selected.

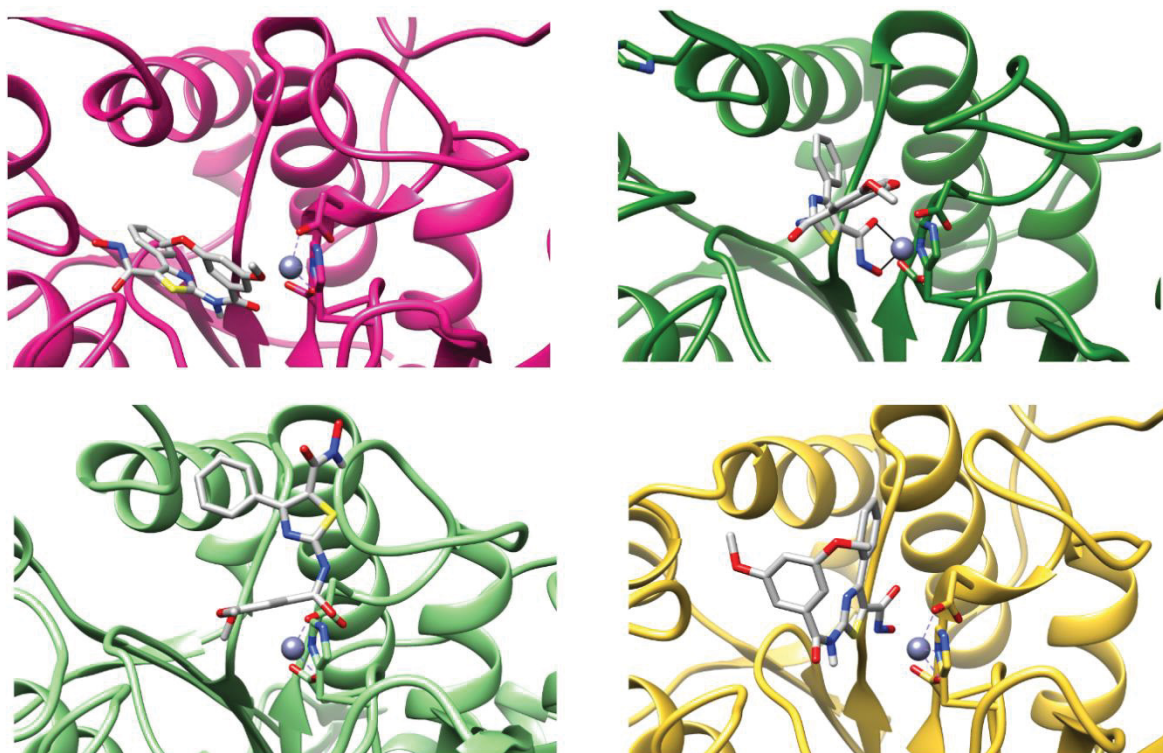


Figure 1: A) Docking of **9a** in the crystal structure of HDAC2 B) Docking of **9a** in the crystal structure of HDAC4 C) Docking of **9a** in the crystal structure of HDAC6 D) Docking of **9a** in the crystal structure of HDAC8.

## Biological evaluation

### Reagents

Cisplatin was purchased from Sigma (Munich, Germany) and dissolved in 0.9% sodium chloride solution. Stock solutions (10 mM) of vorinostat (Selleckchem, Houston, Texas, USA), Panobinostat, CHDI-00390576-000-004 (kindly provided by the CHDI Foundation Inc., New York, USA) and the respective compounds were prepared with DMSO and diluted to the desired concentrations with the appropriate medium.

### Cell lines and cell culture

The human peripheral blood monocytic cell line THP-1 was kindly provided by Prof. Dr Hanenberg (Heinrich-Heine-University, Duesseldorf, Germany). It was cultured in RPMI 1640 containing 10 % heat inactivated fetal calf serum 120 IU/mL penicillin and 120 µg/mL streptomycin at 37 °C in a humidified atmosphere of 5 % CO<sub>2</sub>.

### MTT Cell Viability Assay

MTT assay was performed as previously described.<sup>5-7</sup> Cells were seeded at a density of 15 000 cells/well in 96-well plates (Corning, Kaiserslautern, Germany) in 90 µl culture medium. After 24h preincubation, cells were incubated with the test compounds. After 72 h, MTT solution (5 mg/mL in phosphate buffered saline) was added. The precipitate was dissolved in acidic isopropanol solution (165 µL concentrated HCl (VWR, Langenfeld, Germany) in 50 mL isopropanol (VWR, Langenfeld, Germany). Absorbance was measured at 595 nm and 690 nm in a NOVOstar microplate-reader (BMG LabTech, Offenburg, Germany).

### Whole-Cell HDAC Inhibition Assay

The cellular HDAC assay is based on an assay published by Heltweg and Jung<sup>8</sup>, Ciossek et al.<sup>9</sup>, and Bonfils et al.<sup>10</sup> with minor modifications as described in Marek et al.<sup>5</sup>. Cells were seeded at a density of 50 000 cells/well in 96-well plates (Corning, Kaiserslautern, Germany) in 90 µl of culture medium. After 24 h, cells were incubated for 18 h with the test compounds. 10 µl of 3 mM HDAC substrate in DMSO (VWR, Langenfeld, Germany) of either Boc-Lys(ε-Ac)-AMC (Bachem, Bubendorf, Switzerland) or Boc-Lys(ε-TfAc)-AMC (Bachem, Bubendorf, Switzerland) was incubated for 3h under cell culture conditions. 100 µl/well of the stop solution (25 mM Tris-HCl (pH 8), 137 mM NaCl, 2.7 mM KCl, 1 mM MgCl<sub>2</sub>, 1% NP40, 2.0 mg/mL trypsin and 10 µM vorinostat for Boc-Lys(ε-Ac)-AMC and 10 µM panobinostat for Boc-Lys(ε-TfAc)-AMC) was added and incubated for 3 h. Fluorescence intensity was measured at an excitation of 320 nm and emission of 520 nm in a NOVOstar microplate reader (BMG LabTech, Offenburg, Germany).

### **Enzyme HDAC Inhibition Assay**

All human recombinant enzymes were purchased from Reaction Biology Corp. (Malvern, PA, USA). The HDAC activity assays for HDAC2 (cat nr. KDA-21-277), HDAC4 (cat nr. KDA-21-279), HDAC6 (cat nr. KDA-21-213), and HDAC8 (cat nr. KDA-21-481) were performed in 96-well-plates (Corning, Kaiserslautern, Germany). Briefly, 20 ng of HDAC2/8, 17.5 ng of HDAC6 and 2 ng of HDAC4 per reaction were used. Recombinant enzymes were diluted in assay buffer (50 mM Tris-HCl, pH 8.0, 137 mM NaCl, 2.7 mM KCl, 1 mM MgCl<sub>2</sub>, and 1 mg/mL BSA). After a 5 min incubation step the reaction was started with 10 µL of 300 µM (HDAC2), 150 µM (HDAC6) Boc-Lys(ε-Ac)-AMC (Bachem, Bubendorf, Switzerland) or 100 µM (HDAC4), 60 µM (HDAC8) Boc-Lys-(ε-TFAC)-AMC (Bachem, Bubendorf, Switzerland). The reaction was stopped after 90 min by adding 100 µL stop solution (16 mg/mL trypsin, 2 µM vorinostat for HDAC2/6/8, 4 µM CHDI-00390576-000-004 for HDAC4 in 50 mM Tris-HCl, pH 8.0, and 100 mM NaCl. 15 min after the addition of the stop solution the fluorescence intensity was measured at excitation of 355 nm and emission of 460 nm in a NOVOstar microplate reader (BMG LabTech, Offenburg, Germany).

## References

- (1) Wagner, F. F.; Weïwer, M.; Steinbacher, S.; Schomburg, A.; Reinemer, P.; Gale, J. P.; Campbell, A. J.; Fisher, S. L.; Zhao, W.-N.; Reis, S. A.; et al., *Bioorg. Med. Chem.* **2016**, *24* (18), 4008–4015. <https://doi.org/10.1016/j.bmc.2016.06.040>.
- (2) Luckhurst, C. A.; Breccia, P.; Stott, A. J.; Aziz, O.; Birch, H. L.; Bürli, R. W.; Hughes, S. J.; Jarvis, R. E.; Lamers, M.; Leonard, P. M.; et al., *ACS Med. Chem. Lett.* **2016**, *7* (1), 34–39. <https://doi.org/10.1021/acsmchemlett.5b00302>.
- (3) Hai, Y.; Christianson, D. W., *Nat. Chem. Biol.* **2016**, *12* (9), 741–747. <https://doi.org/10.1038/nchembio.2134>.
- (4) Tabackman, A. A.; Frankson, R.; Marsan, E. S.; Perry, K.; Cole, K. E., *J. Struct. Biol.* **2016**, *195* (3), 373–378. <https://doi.org/10.1016/j.jsb.2016.06.023>.
- (5) Marek, L.; Hamacher, A.; Hansen, F. K.; Kuna, K.; Gohlke, H.; Kassack, M. U.; Kurz, T., *J. Med. Chem.* **2013**, *56* (2), 427–436. <https://doi.org/10.1021/jm301254q>.
- (6) Stenzel, K.; Hamacher, A.; Hansen, F. K.; Gertzen, C. G. W.; Senger, J.; Marquardt, V.; Marek, L.; Marek, M.; Romier, C.; Remke, M.; et al., *J. Med. Chem.* **2017**, *60* (13), 5334–5348. <https://doi.org/10.1021/acs.jmedchem.6b01538>.
- (7) Engelke, L. H.; Hamacher, A.; Proksch, P.; Kassack, M. U., *J. Cancer* **2016**, *7* (4), 353–363. <https://doi.org/10.7150/jca.13754>.
- (8) Heltweg, B.; Jung, M. A, *Anal. Biochem.* **2002**, *302* (2), 175–183. <https://doi.org/10.1006/abio.2001.5542>.
- (9) Ciossek, T.; Julius, H.; Wieland, H.; Maier, T.; Beckers, T., *Anal. Biochem.* **2008**, *372* (1), 72–81. <https://doi.org/10.1016/j.ab.2007.07.024>.
- (10) Bonfils, C.; Kalita, A.; Dubay, M.; Siu, L. L.; Carducci, M. A.; Reid, G.; Martell, R. E.; Besterman, J. M.; Li, Z., *Clin. Cancer Res.* **2008**, *14* (11), 3441–3449. <https://doi.org/10.1158/1078-0432.CCR-07-4427>.

## **Are thioether-based hydroxamic acids HDAC8 or class IIa HDAC selective inhibitors?**

Unpublished

Contribution:

- Synthesis of the compounds **10a-k, 13, 14a-k, 20a,b, 21a,b; 23-26, 27a,b** and **28 a,b**
- Manuscript and supporting information

## **Are thioether-based hydroxamic acids HDAC8 or class IIa HDAC selective inhibitors?**

*Yodita Asfaha<sup>\*#</sup>, Alexander Jan Skerhut<sup>\*#</sup>, Leandro A. Alves-Avelar<sup>\*</sup>, Nadine Horstick-Muche<sup>\*</sup>, Matthias U. Kassack<sup>\*#</sup>, Thomas Kurz<sup>\*#</sup>*

\*Institut für Pharmazeutische und Medizinische Chemie, Heinrich-Heine-Universität Düsseldorf, Universitätsstr. 1, 40225 Düsseldorf, Germany. # YA and AJS share first authorship, MUK and TK share senior and corresponding authorship.

## Abstract

Histone deacetylases (HDACs) are important epigenetic regulators that govern numerous biological processes such as proliferation, migration, differentiation, and programmed cell death. HDAC8, a Zn<sup>2+</sup>-dependent class I HDAC, provides an attractive target for the treatment of various diseases including specific cancer subtypes (e.g. T-cell lymphoma, neuroblastoma). The development and design of selective HDAC8 inhibitors provides a promising strategy for the target-specific treatment of diseases. Here, we describe the synthesis and biological evaluation of thioether-based hydroxamates as HDAC8 inhibitors. Among the tested compounds, compound **10k** was identified as the most potent and selective HDAC8 inhibitor in the nanomolar range (IC<sub>50</sub>(HDAC8) = 0.28 μM) with a ≥356-fold selectivity over HDAC2 and a 35/21-fold preference over HDAC4/6.

## 1. Introduction

Acetylation at ε-amino groups is an essential post-translational modification of proteins including histones, transcription factors, and cytoskeletal elements. Two types of antagonistic enzymes regulate the dynamic acetylation state of client proteins: the histone acetyltransferases (HATs) and the histone deacetylases (HDACs).<sup>[1]</sup> Lysine acetylation of histones induces a relaxation of the chromatin structure that augments the accessibility of the transcriptional machinery. In contrast, the removal of acetyl groups increases the condensation state of chromatin and, therefore, a repression of gene transcription.<sup>[2]</sup> Until now, 18 human HDACs have been identified and summarized into four classes based on their homology to yeast deacetylases. Class I (HDACs 1-3, 8) share a high degree of homology with Rpd3, class II (IIa: HDACs 4, 5, 7, 9; IIb: HDACs 6, 10) are homologous to Hda1, class III are related to Sir2 and class IV (HDAC 11) share common characteristics with both Rpd3 and Hda1.<sup>[3]</sup> Class I, II and IV are zinc-dependent enzymes, whereas the class III, commonly known as sirtuins, depends on the cofactor NAD<sup>+</sup>.<sup>[4,5]</sup> Class IIa HDACs are crucial regulators in specific developmental and differentiation processes, and their dysregulation is associated with a broad range of diseases such as Morbus Huntington.<sup>[6,7]</sup> However, the participation of class IIa HDACs in maintaining the homeostasis in healthy cells or in pathological processes is, currently, not well understood. It has been shown that the catalytic activity of class IIa HDACs is

intrinsically much lower compared to class I HDACs (approx.1000 fold) due to a Tyr to His switch in the active site. Their repressive transcriptional activity is hypothesized to depend on their association with class I enzymes and on their capability to suppress transcription factors by e.g. protein-protein interaction. [8–11] Class IIa HDACs have been proposed as potential targets for the treatment of cardiovascular diseases, neurodegenerative disorders, viral infections, diabetes, and cancer. Moreover, their inhibition is assumed to result in clinically relevant immunomodulation. [12–16] Selective HDAC inhibitors may serve as important tools for elucidating the role of class IIa HDACs in the aforementioned diseases. In published crystal structures of class IIa HDACs the so-called lower pocket was identified as a distinctive structural feature. [17,18] The pharmacophore model for class IIa selective HDACi consists of the following four elements: a zinc-binding group (ZBG), a linker that interacts with the substrate-binding tunnel, a lower pocket (LP)-group that occupies the distinct pocket and a cap, also known as surface recognition domain (Figure 1).[19]

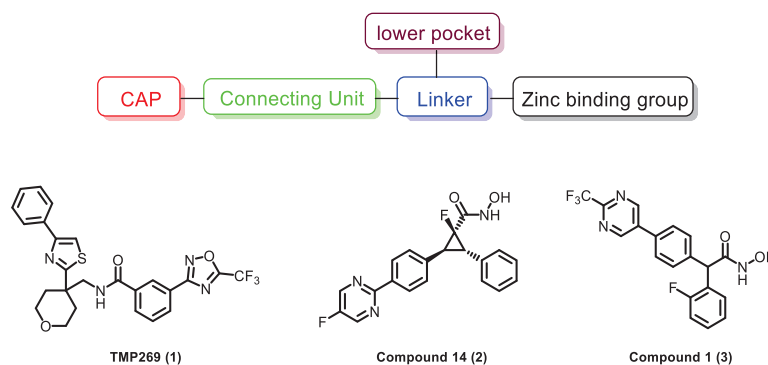


Figure 1: Selected class IIa selective HDACi **1-3**. [17,18,20]

Besides class IIa HDACs, HDAC8, a Zn<sup>2+</sup>-dependent class I HDAC, was identified as a druggable target for the treatment of specific cancer subtypes (e.g. T-cell lymphoma, neuroblastoma) and several X-linked intellectual disabilities. Furthermore, the employment of HDAC8 selective inhibitors is a promising approach for the treatment of parasitic infections e.g. by targeting *Schistosoma mansoni* HDAC8 (smHDAC8) in the parasitic disease schistosomiasis. [21–24] HDAC8 differs from the prototypical class I enzymes in several respects: a) independence of cofactors for activity b) absence of the C-terminal protein-binding domain c) mainly cytoplasmic localization d) binding of diverse cations including Fe<sup>2+</sup> and K<sup>+</sup> to its active site e) negative regulation of its deacetylase activity by phosphorylation of Ser39 by cyclic-AMP-dependent protein

kinase (PKA).<sup>[25–30]</sup> Furthermore, HDAC8 exhibits characteristic structural features in the catalytic domain, including conformational flexibility in close proximity to the active site, which allows the design of HDAC8 selective inhibitors. (loop L1 mediated). One particularly feature is the so-called *foot-pocket* (acetate release channel) which is also observed in HDAC1, 2 and 3. However, the *foot-pocket* of HDAC8 is opened by the movement of the gatekeeper residue W141 instead of the leucine residue presents in the other class I HDACs. Another distinctive feature is the formation of the *side-pocket* due to a different conformation of the loop L6. This cavity has not been detected in other HDACs, so far.<sup>[31]</sup> Although, the design of specific HDACi is challenging, the unique active site of HDAC8 permits the development of HDAC8-selective inhibitors (Figure 2). PCI-34051 (**4**) is one of the most widely used selective HDAC8-inhibitor in research. This hydroxamic acid **4** inhibits HDAC8 in the nanomolar range and displays a >200-fold selectivity over HDAC1 and 6 and >1000 fold over HDAC 2/3/10.<sup>[21]</sup> It was demonstrated that PCI-34051 (**4**) induces caspase-dependent apoptosis in T cell-derived tumors, but not in hematopoietic or solid tumor cell lines. In contrast to pan-inhibitors, this inhibitor **4** does not induce detectable histone or tubulin acetylation. The induction of apoptosis is partly the results of calcium flux in a PLC $\gamma$ 1 mediated manner.<sup>[21]</sup> Nevertheless, it remains controversial if isozyme-specific inhibitors are superior to pan-HDAC inhibitors as anticancer drugs in regard to their clinical efficacy and potency.

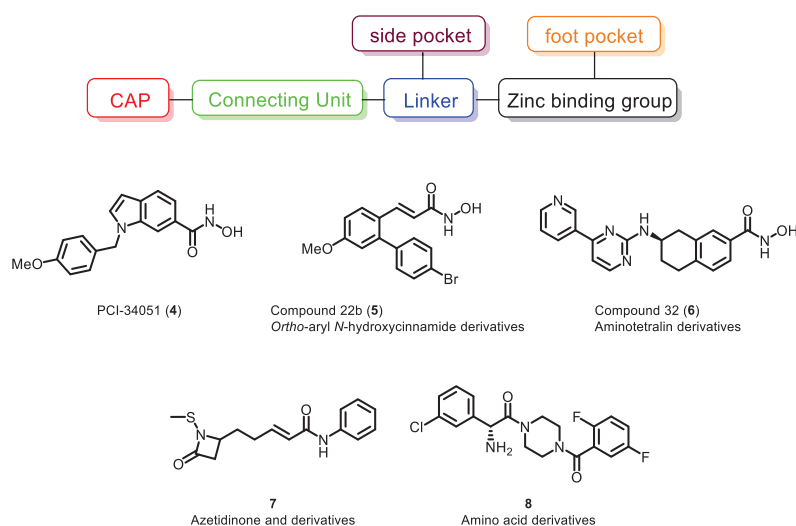


Figure 2: Selected HDAC8-specific inhibitors **4-8**.<sup>[21,32–35]</sup>

However, novel HDAC selective inhibitors may present beneficial properties that reduce side effects in personalized medicine, which could result in higher patient compliance, a

reduced likelihood of the occurrence of resistances and, therefore, more effective active pharmaceutical ingredients. Sulfur-containing functional groups are present in a wide spectrum of pharmaceutical and natural products. The significance of sulfur in drug development is demonstrated by approximately 360 sulfur-containing FDA approved drugs. Amongst the sulfur-containing drug, thioethers rank third with roughly 9%.<sup>[36]</sup> Tessier *et al.* introduced thioether-based hydroxamates **9** as HDACi (Figure 3).<sup>[37]</sup> The inhibitors **9** displayed an IC<sub>50</sub> value less than or equal to 15 μM against one or more of HDAC4, HDAC5, HDAC6, HDAC7, HDAC8, HDAC9, HDAC10 and HDAC11. A specific range was not reported.

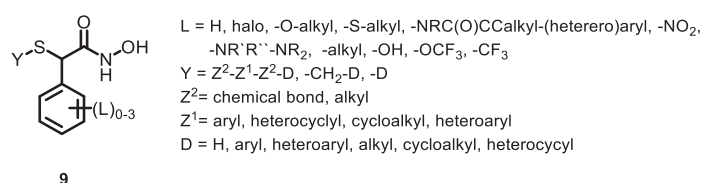


Figure 3: General structure of the previously reported thioether-based hydroxamates **9** as HDACi.<sup>[37]</sup>

However, the specific enzyme inhibition data were not reported. Here, we present the development of novel thioether-based hydroxamates and their investigation in regard to their HDAC inhibition profile as well as their potential as anticancer agents.

## 2. Results and Discussion

### 2.1. Rational design

In order to assess the HDAC isozyme selectivity profile of thioether-based hydroxamates, we performed an *in-silico* screening with *N*-hydroxy-2-phenyl-2-(phenylthio)acetamide (**10a**) as lead structure from Tessier *et al.* (Figure 4).<sup>[37]</sup>

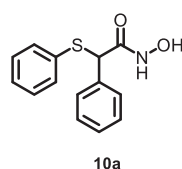


Figure 4: The lead structure **10a**.<sup>[37]</sup>

The compound was docked into HDAC2 (PDB: 4LXZ)<sup>[38]</sup>, HDAC8 (PDB: 5FCW)<sup>[39]</sup>, HDAC4 (PDB: 5A2S)<sup>[18]</sup> and HDAC6 (PDB: 5EDU)<sup>[40]</sup> according to Asfaha *et al.*<sup>[41]</sup> The thioether-based hydroxamate **10a** did not produce valid docking poses in HDAC2 and

HDAC6 with the complexation of the zinc ion by the hydroxamic acid moiety. However, valid binding modes were predicted for HDAC4 and HDAC8. The preliminary docking results indicated the occupation of their specific pockets (lower pocket: HDAC4; side pocket: HDAC8) with either the thioether or phenyl moiety of **10a** (Figure 5).

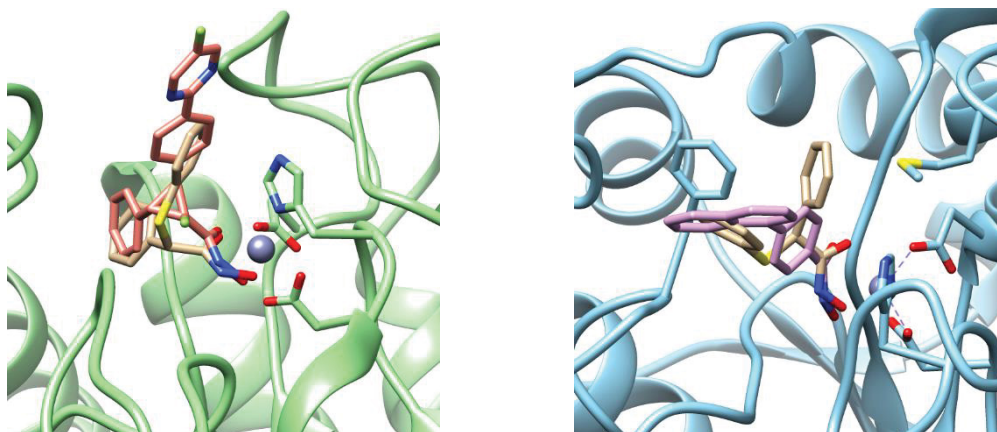


Figure 5: Superposition of **10a** and Compound 14 (**2**) in HDAC4 (PDB: 5A2S)<sup>[18]</sup> (left). Superposition of **10a** and PCI-34051 (**4**) in HDAC8 (PDB: 5EDU)<sup>[39]</sup> (right).

Based on this qualitative *in-silico* screening, the evaluated compound **10a** suggested a potential HDAC4 and HDAC8 preference. Here, we report the derivatization of the lead structure **10a** (Figure 6) in order to evaluate its selectivity for class IIa HDACs and HDAC8.

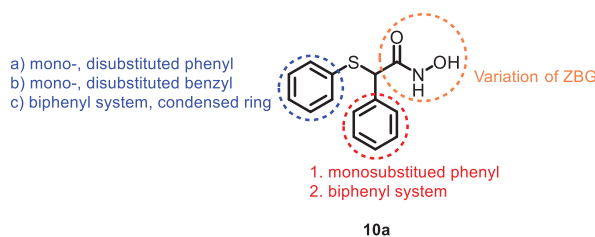
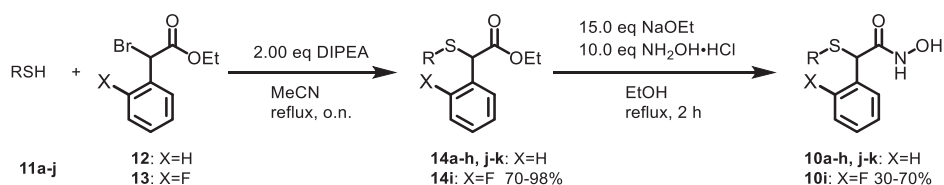


Figure 6: Derivatization of the lead structure **10a**.

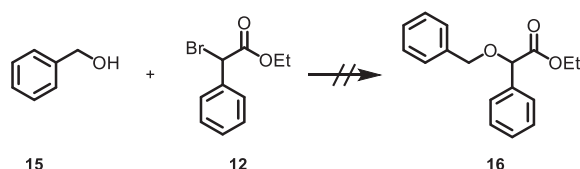
## 2.2. Chemistry

The synthesis of the first set of thioether-based HDACi **10a-k** was performed according to Tessier *et al.* (Scheme 1).<sup>[37]</sup> The respective bromo derivative **12** or **13** was converted with various commercially available thiols **11a-j** under basic conditions into the respective thioethers **14a-k**. Subsequently, the hydroxamic acids **10a-k** were prepared by a hydroxylaminolysis of the ethyl esters **14a-k**. The screened reaction conditions for the *O*-alkylation are depicted in Table 1 and Table 2. However, neither the Palladium-catalyzed cross-coupling nor the triflation of the hydroxyl group of **15** or the Mitsunobu - and Finkelstein reaction with **17** resulted in the respective product **16**.



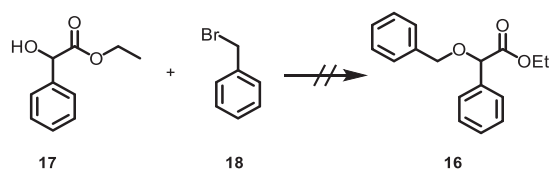
Scheme 1: Synthesis of thioether-based hydroxamates **10a-k**.

Table 1: Screened reaction conditions for the formation of the oxa analog **16**. All reactions were carried out overnight.



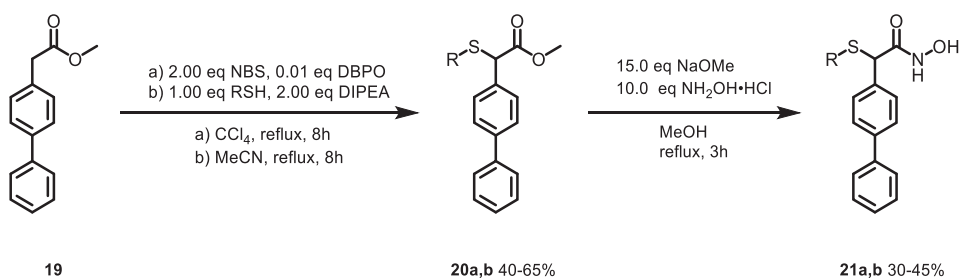
No.	Reagents	Solvent	Base	T / °C	Yield
1	0.10 eq Pd[OAc] <sub>2</sub> , 0.30 eq Xantphos	toluene	5.00 eq Cs <sub>2</sub> CO <sub>3</sub>	100	-
2	1.10 eq Tf <sub>2</sub> O	CH <sub>2</sub> Cl <sub>2</sub>	2.00 eq pyridine	-20 - rt	-
3	-	THF	1.10 eq NaH	rt	-

Table 2: Attempted Mitsunobu- and Finkelstein reaction for the synthesis of **16**. All reactions were carried out overnight.



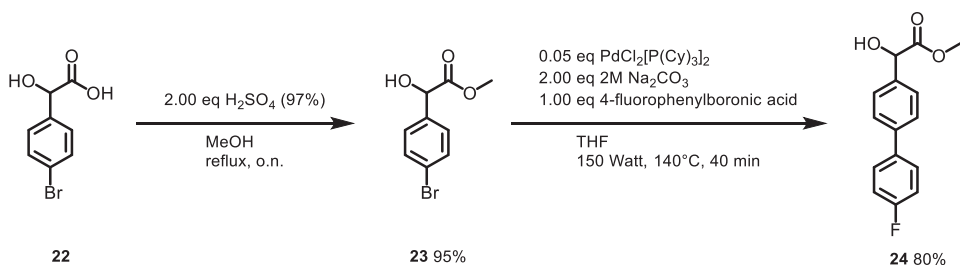
No.	Reagents	Solvent	Base	T / °C	Yield
1	1.20 eq PPh <sub>3</sub> , 1.20 eq DIAD	THF	-	0-rt	-
2	0.10 eq KI	acetone	5.00 eq K <sub>2</sub> CO <sub>3</sub>	reflux	-

Considering the qualitative docking studies and the symmetry of the lead compound **10a**, the  $\alpha$ -thioether or the  $\alpha$ -phenyl substituent might intrude into the lower pocket. Therefore, the second set of HDACi contains  $\alpha$ -biphenyl substituents (**21a,b**) in order to direct the biphenyl moiety into the entrance tunnel of the active site of class IIa HDACs. The synthesis of these inhibitors **21a,b** is summarized in Scheme 2. In the first step, the  $\alpha$ -bromo ester is generated via radical bromination of **19**, followed by the conversion with the respective thiol. Finally, the methyl esters **20a,b** were transformed into their hydroxamic acids **21a,b**.



Scheme 2: Synthesis of the  $\alpha$ -biphenyl substituted thioether derivatives **21a,b**.

For the installation of the mono-fluoro-substituted biphenyl moiety, the carboxylic acid **22** was first esterified and the subsequent Suzuki-coupling was performed (1.00 eq methyl ester, 0.05 eq  $\text{PdCl}_2[\text{P}(\text{Cy})_3]_2$ , 2.00 eq 2 M  $\text{Na}_2\text{CO}_3$ ) in a microwave-assisted reaction (Scheme 3). The screened reaction conditions for the Pd-catalyzed reaction are shown in Table 3. The employment of bis(tricyclohexylphosphine)palladium(II) dichloride proved to be the most suitable catalyst amongst the tested reaction conditions (Table 3, entry 5). Various solvents e.g. alcohols, dipolar aprotic solvents, ethers, toluene can be applied for the Suzuki-coupling.<sup>[42]</sup> The solvent of choice was THF, as the electron donation properties of ether containing solvents can contribute significantly to the stability of the organometallic species.<sup>[42]</sup>

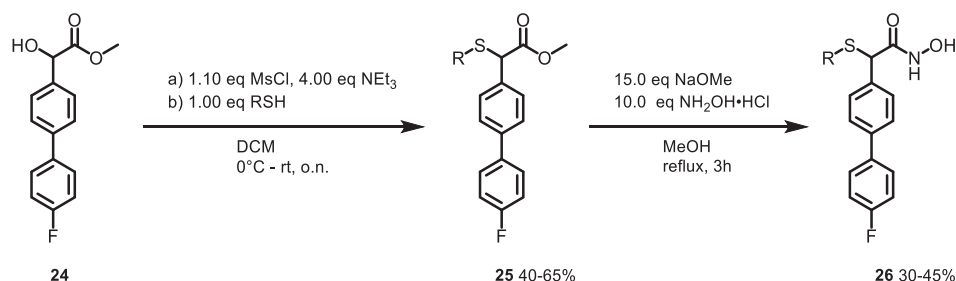


Scheme 3: Installation of the substituted biphenyl moiety to **23**.

Table 3: Screened reaction conditions for the Suzuki-coupling. All reactions were carried out at 140 °C.

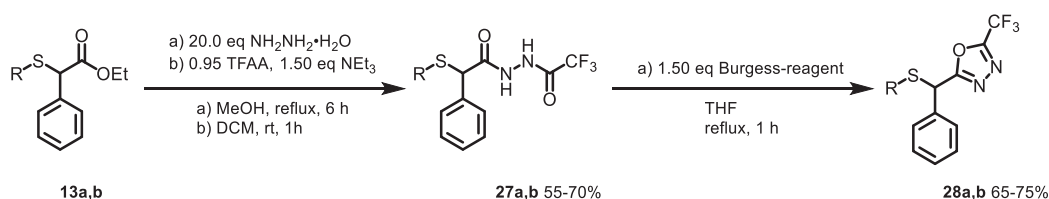
No.	Cat. / 0.05 eq	Solvent	Base / 2.00 eq	P / Watt	t / min	Yield
1	$\text{PdCl}_2[\text{P}(\text{Cy})_3]_2$	MeCN/EtOH 2:1	2M $\text{Na}_2\text{CO}_3$	150	20	-
2	$\text{PdCl}_2[\text{P}(\text{Cy})_3]_2$	DME/EtOH 2:1	2M $\text{Na}_2\text{CO}_3$	150	20	-
3	$\text{Pd}(\text{OAc})_2 + \text{Xantphos}$	toluene/ $\text{H}_2\text{O}$ 9:1	$\text{Cs}_2\text{CO}_3$	100	20	-
4	$\text{PdCl}_2[\text{P}(\text{Cy})_3]_2$	dioxane/EtOH 6:1	2M $\text{Na}_2\text{CO}_3$	150	20	18%
5	$\text{PdCl}_2[\text{P}(\text{Cy})_3]_2$	THF	2M $\text{Na}_2\text{CO}_3$	100	40	80%

In the next step, the hydroxyl group of **24** was mesylated under basic conditions, followed by the displacement of the mesylate group with the respective thiol. The obtained thioether **25** was then converted into the hydroxamic acid **26** by hydroxylaminolysis (Scheme 4).



Scheme 4: Synthesis of the hydroxamic acid **26**.

In our endeavor to develop selective class IIa HDACi, we further evaluated the influence of different zinc-binding groups. Lobera *et al.* introduced the trifluoromethyloxadiazolyl moiety (TFMO) as a novel ZBG.<sup>[17]</sup> It was demonstrated that compounds exhibiting this ZBG showed a 150-1000-fold higher selectivity towards class IIa HDACs than the respective hydroxamates. In order to investigate the influence of 2-(trifluoromethyl)-1,3,4-oxadiazole as ZBG, we envisioned a modification of the hydroxamic acid with the 2-(trifluoromethyl)-1,3,4-oxadiazole moiety as ZBG. The synthesis was performed according to Scheme 5.<sup>[43]</sup> Firstly, the ethyl esters **13a,b** were transformed into the corresponding *N*-acyl hydrazides **27a,b**. Secondly, the cyclization was successfully achieved by dehydration (Burgess-reagent), providing the final products **28a,b**.



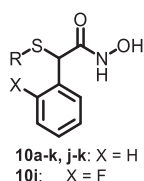
Scheme 5: Synthesis of the inhibitors **28a,b**.

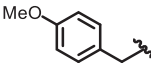
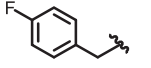
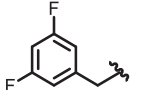
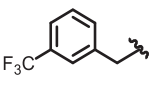
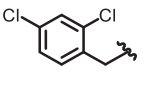
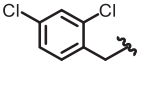
### 2.3 Biological evaluation

The synthesized compounds **10a-k**, **21a-b**, **26**, **28a-b** were assessed for their antiproliferative activity and for their HDAC inhibitory activity in the human monocytic cell line THP-1 using class-distinguishing substrates (Boc-Lys(Ac)-AMC: class I and IIb

HDACs; Boc-Lys(TFAc)-AMC: class IIa, HDAC8). The results are depicted in Table 4, Table 5 and Table 6 with CHDI-00390576 and TMP269 as reference compounds. Among the tested compounds **10a-k**, compound **10g** exhibited the strongest antiproliferative activity with 99% growth inhibition at 100  $\mu$ M concentration. In particular, the halogen-substituted thioether derivatives (**10e-k**) displayed an increased cytotoxicity with antiproliferative effects between 76-99% at 100  $\mu$ M in comparison to the unsubstituted thioether derivatives **10a-c** (63-72% at 100  $\mu$ M). The employment of the 2-(trifluoromethyl)-1,3,4-oxadiazole ZBG (**28a-b**) led to a significant diminished cytotoxicity (17-27% growth inhibition at 100  $\mu$ M). Furthermore, the  $\alpha$ -biphenyl derivatives **21a-b** and **26** showed a decreased cytotoxicity with antiproliferative activities below 47% at 100  $\mu$ M, compared to **10a-k**. In the performed whole-cell HDAC inhibition assay using the Boc-Lys(Ac)-AMC-HDAC substrate, all screened hydroxamic acids **10a-k**, **21a-b**, **26** displayed inhibitory activities below 69% at 100  $\mu$ M. However, the cellular HDAC inhibition assay with the Boc-Lys(TFAc)-AMC-HDAC substrate revealed that **10j** exhibited the strongest cellular inhibition with 82% at 100  $\mu$ M. In particular, the halogen-substituted thioether derivatives (**10e-k**) showed an increased cellular HDAC inhibition with 53-82% at 100  $\mu$ M in comparison to the unsubstituted thioether derivatives **10a-c** (41-66% at 100  $\mu$ M). Additionally, the employment of an  $\alpha$ -biphenyl moiety in the case of **21a-b** and **26** did not significantly impact the cellular HDAC inhibition (45-78% at 100  $\mu$ M). However, the introduction of the 2-(trifluoromethyl)-1,3,4-oxadiazole as ZBG (**28a-b**) resulted in a significant decreased HDAC inhibition in both performed cellular HDAC inhibition assay ( $\leq 40\%$  HDAC inhibition at 100  $\mu$ M).

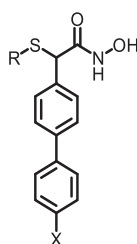
Table 4: Cell viability (MTT assay) and whole-cell HDAC inhibition assay in the human monocytic cell line THP-1.



Cpd.	R	X	Cell viability		HDAC inhibition			
			% inhibition of 100 $\mu$ M	IC <sub>50</sub> [ $\mu$ M] (pIC <sub>50</sub> $\pm$ SEM)	Boc-Lys(Ac)-AMC		Boc-Lys(TFAc)-AMC	
					% inhibition of 100 $\mu$ M	IC <sub>50</sub> [ $\mu$ M] (pIC <sub>50</sub> $\pm$ SEM)	% inhibition of 100 $\mu$ M	IC <sub>50</sub> [ $\mu$ M] (pIC <sub>50</sub> $\pm$ SEM)
10a		H	63%	59.77 (4.22 $\pm$ 0.21)	31%	n.d.	41%	n.d.
10b		H	72%	n.d.	49%	n.d.	66%	64.5 (4.19 $\pm$ 0.11)
10c		H	67%	59.69 (4.22 $\pm$ 0.34)	26%	n.d.	54%	88.6 (4.05 $\pm$ 0.16)
10d		H	65%	27.1 (4.57 $\pm$ 0.24)	61%	67.5 (4.17 $\pm$ 0.08)	75%	45.6 (4.34 $\pm$ 0.17)
10e		H	91%	29.22 (4.53 $\pm$ 0.28)	52%	92.8 (4.03 $\pm$ 0.05)	60%	91.8 (4.04 $\pm$ 0.18)
10f		H	86%	47.54 (4.32 $\pm$ 1.25)	43%	n.d.	53%	90.6 (4.04 $\pm$ 0.22)
10g		H	99%	16.7 (4.78 $\pm$ 0.11)	60%	52.9 (4.28 $\pm$ 0.15)	63%	91.3 (4.04 $\pm$ 0.87)
10h		H	76%	54.0 (4.27 $\pm$ 0.07)	64%	69.6 (4.16 $\pm$ 0.20)	56%	68.1 (4.17 $\pm$ 0.12)
10i		F	84%	41.5 (4.38 $\pm$ 0.59)	64%	68.8 (4.16 $\pm$ 0.20)	61%	69.2 (4.16 $\pm$ 0.28)
10j		H	81%	37.2 (4.43 $\pm$ 0.23)	62%	67.3 (4.17 $\pm$ 0.18)	82%	56.2 (4.25 $\pm$ 0.35)
10k		H	76%	45.4 (4.34 $\pm$ 0.61)	63%	67.0 (4.17 $\pm$ 0.20)	77%	54.5 (4.26 $\pm$ 0.17)
	CHDI-00390576		100%	30.4 (4.52 $\pm$ 0.04)	42%	n.d.	100%	0.02 (7.69 $\pm$ 0.10)
	TMP269		70%	58.54 (4.23 $\pm$ 0.0039)	13%	n.d.	39%	n.d.

Presented data are calculated from at least two experiments each performed in duplicates. IC<sub>50</sub> values were calculated for compounds with an inhibition of more than 50 %. Standard deviation of percent inhibition values is less than 14 %. Vehicle control was defined as 0 % inhibition. n.d. = not determined.

Table 5: Cell viability (MTT assay) and whole-cell HDAC inhibition assay in the human monocytic cell line THP-1.

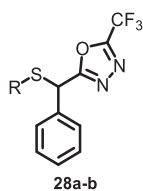


21a-b: X = H  
26: X = F

Cpd.	R	X	Cell viability		HDAC inhibition			
			% inhibition of 100 $\mu$ M	IC <sub>50</sub> [ $\mu$ M] (pIC <sub>50</sub> $\pm$ SEM)	% inhibition of 100 $\mu$ M	IC <sub>50</sub> [ $\mu$ M] (pIC <sub>50</sub> $\pm$ SEM)	% inhibition of 100 $\mu$ M	IC <sub>50</sub> [ $\mu$ M] (pIC <sub>50</sub> $\pm$ SEM)
21a		H	47%	n.d.	45%	n.d.	78%	53.5 (4.27 $\pm$ 0.15)
21b		H	3%	n.d.	59%	85.2 (4.07 $\pm$ 0.06)	72%	51.8 (4.29 $\pm$ 0.17)
26		F	29%	n.d.	69%	59.4 (4.23 $\pm$ 0.04)	45%	n.d.
	CHDI-00390576		100%	30.4 (4.52 $\pm$ 0.04)	42%	n.d.	100%	0.02 (7.69 $\pm$ 0.10)
	TMP269		70%	58.54 (4.23 $\pm$ 0.0039)	13%	n.d.	39%	n.d.

Presented data are calculated from at least two experiments each performed in duplicates. IC<sub>50</sub> values were calculated for compounds with an inhibition of more than 50 %. Standard deviation of percent inhibition values is less than 14 %. Vehicle control was defined as 0 % inhibition. n.d. = not determined.

Table 6: Cell viability (MTT assay) and whole-cell HDAC inhibition assay in the human monocytic cell line THP-1.



Cpd.	R	Cell viability		HDAC inhibition			
		% inhibition of 100 $\mu$ M	IC <sub>50</sub> [ $\mu$ M] (pIC <sub>50</sub> $\pm$ SEM)	Boc-Lys(Ac)-AMC % inhibition of 100 $\mu$ M	IC <sub>50</sub> [ $\mu$ M] (pIC <sub>50</sub> $\pm$ SEM)	Boc-Lys(TFAc)-AMC % inhibition of 100 $\mu$ M	IC <sub>50</sub> [ $\mu$ M] (pIC <sub>50</sub> $\pm$ SEM)
28a		27%	n.d.	34%	n.d.	28%	n.d.
28b		17%	n.d.	40%	n.d.	12%	n.d.
CHDI-00390576		100%	30.4 (4.52 $\pm$ 0.04)	42%	n.d.	100%	0.02 (7.69 $\pm$ 0.10)
TMP269		70%	58.54 (4.23 $\pm$ 0.0039)	13%	n.d.	39%	n.d.

Presented data are calculated from at least two experiments each performed in duplicates. IC<sub>50</sub> values were calculated for compounds with an inhibition of more than 50 %. Standard deviation of percent inhibition values is less than 14 %. Vehicle control was defined as 0 % inhibition. n.d. = not determined.

#### 2.4 Inhibitory activity on HDAC2, HDAC4, HDAC6 and HDAC8

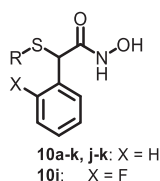
For further evaluation, the synthesized compounds **10a-k**, **21a-b**, **26** and **28a-b** were tested against recombinant human HDAC2, HDAC4, HDAC6 and HDAC8 (Table 7, Table 8 and Table 9). CHDI-00390576 and TMP269 were included as class IIa selective HDACi reference compounds. Due to the poor water-solubility of TMP269, the literature IC<sub>50</sub> values are displayed as references. The lead structure **10a** displayed a low micromolar inhibition of HDAC8 (IC<sub>50</sub>(HDAC8) = 3.47  $\mu$ M) with a >29/11/5-fold stronger preference over HDAC2/4/6. The introduction of a methylene group in the cap region (**10b**) to the lead structure **10a** resulted in a slightly decreased HDAC8 inhibition in the low micromolar range (IC<sub>50</sub>(HDAC8) = 5.81  $\mu$ M) with a >17-fold preference over HDAC2. Moreover, **10b** did not discriminate between HDAC4 (IC<sub>50</sub>(HDAC4) = 12.6  $\mu$ M) and HDAC6 (IC<sub>50</sub>(HDAC6) = 12.7  $\mu$ M). The substitution of the phenyl (**10b**) with the cyclohexyl moiety in case of **10c** did not have a significant influence on the HDAC

isozyme inhibition profile and resulted in a slightly stronger HDAC8 inhibition ( $IC_{50}(\text{HDAC8}) = 3.19 \mu\text{M}$ ) compared to **10b**. The modification of the hydroxamic acids **10a,b** to the TFMO-isomers **28a,b** led to a complete loss of HDAC inhibition which is in agreement with the cellular data of these compounds. The introduction of substituents (OMe: **10d** and F:**10e**) in the *para*-position of **10b** did not have a significant impact on the HDAC isozyme inhibition profile compared to **10b**. In case of **10d**, no direct discrimination between HDAC4 ( $IC_{50}(\text{HDAC4}) = 5.38 \mu\text{M}$ ) and HDAC8 ( $IC_{50}(\text{HDAC8}) = 7.98 \mu\text{M}$ ) was observed. The employment of the monofluorinated biphenyl moiety (**26**) to **10e** demonstrated a significant loss of HDAC8 inhibitory activity ( $IC_{50}(\text{HDAC8}) = 56.3 \mu\text{M}$ ) compared to **10e**. Furthermore, the introduction of two fluoro substituents in *meta*-position (**10f**) to **10b** revealed a similar HDAC8 inhibition and selectivity profile compared to **10b**. Interestingly, the employment of substituents (Cl: **10j** and Br: **10k**) in the *ortho*-position of **10b** displayed a nanomolar inhibition of HDAC8. **10k** was identified as the most potent HDAC8 inhibitor ( $IC_{50}(\text{HDAC8}) = 0.28 \mu\text{M}$ ) with a  $\geq 356$ -fold selectivity over HDAC2 and a 35/21-fold preference over HDAC4/6. In comparison, the chlorine-derivative **10j** exhibited a decreased HDAC8 inhibitory activity ( $IC_{50}(\text{HDAC8}) = 0.393 \mu\text{M}$ ) and diminished preference over the other HDACs (SI(HDAC2/HDAC8): 184, SI(HDAC4/HDAC8): 15, SI(HDAC6/HDAC8): 11). Surprisingly, the  $\alpha$ -biphenyl substituent derivative **21b** showed a 10-fold reduced HDAC8 inhibitory activity compared to compound **10k** and neither HDAC2, HDAC4 nor HDAC6 inhibitions were detected. The employment of an additional chlorine atom in the *para*-position (**10h**) to **10j**, resulted in a diminished HDAC8 inhibition in the low micromolar range ( $IC_{50}(\text{HDAC8}) = 1.15 \mu\text{M}$ ) with a  $>10/14/7$ -fold preference over HDAC2/4/6. Interestingly, the introduction of the 2-fluorophenyl moiety (**10i**) to **10h** exhibited an increased HDAC8 inhibition in the nanomolar range ( $IC_{50}(\text{HDAC8}) = 0.70 \mu\text{M}$ ) with a more pronounced preference for HDAC6 (SI(HDAC6/8) = 29) compared to **10h**. The exchange of the phenyl of **10h** to a biphenyl moiety (**21a**) exhibited a 26-fold diminished HDAC8 inhibition ( $IC_{50}(\text{HDAC8}) = 29.9 \mu\text{M}$ ) compared to **10h**.

In summary, we have identified a new series of thioether-based hydroxamates as potent and selective HDAC8 inhibitors. Initial SAR-studies revealed that *ortho*-substitution of

the thioether moiety in case of **10j** and **10k** are preferable over *para*- and *meta*-substitutions (**10d-g**) for HDAC8 inhibition. Furthermore, a biphenyl system (**21a-b**, **26**) resulted in a diminished HDAC8 inhibition in the micromolar range. The ZBG variation in case of **28a-b** demonstrated that hydroxamates **10a-k** are more potent and selective towards HDAC8, compared to **28a-b**. Among the tested substances **10a-k**, **21a-b**, **26** and **28a-b**, the compound **10k** was identified as a nanomolar HDAC8 inhibitor ( $IC_{50}(\text{HDAC8}) = 0.28 \mu\text{M}$ ) with a  $\geq 356$ -fold selectivity over HDAC2 and a 35/21-fold preference over HDAC4/6.

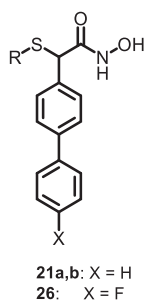
Table 7: Inhibitory activity of **10a-k**, CHDI-00390576 and TMP269 on recombinant human HDAC2, HDAC4, HDAC6 and HDAC8.



Cpd.	R	X	IC <sub>50</sub> [μM] (pIC <sub>50</sub> ± SEM)			
			HDAC2	HDAC4	HDAC6	HDAC8
10a		H	>100	39.2 (4.41 ± 0.1)	16.1 (4.79 ± 0.05)	3.47 (5.46 ± 0.034)
10b		H	>100	12.6 (4.9 ± 0.06)	12.7 (4.9 ± 0.04)	5.81 (5.24 ± 0.12)
10c		H	47.3 (4.33 ± 0.05)	15.3 (4.82 ± 0.09)	12.3 (4.91 ± 0.08)	3.19 (5.5 ± 0.027)
10d		H	>100	5.38 (5.27 ± 0.06)	11.6 (4.94 ± 0.039)	7.98 (5.10 ± 0.07)
10e		H	>100	15.7 (4.8 ± 0.06)	16.9 (4.77 ± 0.03)	4.94 (5.31 ± 0.14)
10f		H	>100	12.93 (4.89 ± 0.06)	11.7 (4.93 ± 0.04)	3.24 (5.49 ± 0.022)
10g		H	>100	10.76 (4.97 ± 0.065)	15.34 (4.81 ± 0.04)	9.45 (5.03 ± 0.05)
10h		H	>100	15.7 (4.81 ± 0.04)	7.90 (5.1 ± 0.04)	1.15 (5.94 ± 0.02)
10i		F	>100	8.06 (5.09 ± 0.04)	20.42 (4.69 ± 0.05)	0.70 (6.16 ± 0.05)
10j		H	72.35 (4.14 ± 0.05)	5.75 (5.24 ± 0.08)	4.28 (5.37 ± 0.05)	0.393 (6.41 ± 0.04)
10k		H	>100	9.87 (5.01 ± 0.074)	5.76 (5.24 ± 0.05)	0.281 (6.55 ± 0.05)
	CHDI-00390576		>100	0.097 (7.01 ± 0.03)	5.98 (5.22 ± 0.04)	24.77 (4.61 ± 0.02)
	TMP269*		>100	0.157	8.2	4.2

Data shown is at least from two experiments each performed at least as duplicates and the IC<sub>50</sub> value of pooled data is reported when IC<sub>50</sub> < 100 μM. \*Data taken from Lobera et al.<sup>[17]</sup>

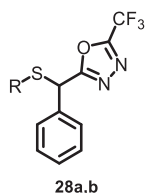
Table 8: Inhibitory activity of **21a,b**, **26**, CHDI-00390576 and TMP269 on recombinant human HDAC2, HDAC4, HDAC6 and HDAC8.



Cpd.	R	X	IC <sub>50</sub> [μM] (pIC <sub>50</sub> ± SEM)			
			HDAC2	HDAC4	HDAC6	HDAC8
<b>21a</b>		H	>100	>100	>100	29.9 (4.52 ± 0.031)
<b>21b</b>		H	>100	>100	>100	2.73 (5.56 ± 0.038)
<b>26</b>		F	>100	>100	48.89 (4.31 ± 0.037)	56.3 (4.25 ± 0.04)
	CHDI-00390576		>100	0.097 (7.01 ± 0.03)	5.98 (5.22 ± 0.04)	24.77 (4.61 ± 0.02)
	TMP269*		>100	0.157	8.2	4.2

Data shown is at least from two experiments each performed at least as duplicates and the IC<sub>50</sub> value of pooled data is reported when IC<sub>50</sub> < 100 μM. \*Data taken from Lobera et al.<sup>[17]</sup>

Table 9: Inhibitory activity of **28a,b**, CHDI-00390576 and TMP269 on recombinant human HDAC2, HDAC4, HDAC6 and HDAC8.



Cpd.	R	IC <sub>50</sub> [μM] (pIC <sub>50</sub> ± SEM)			
		HDAC2	HDAC4	HDAC6	HDAC8
<b>28a</b>		>100	>100	>100	>100
<b>28b</b>		>100	>100	>100	>100
	CHDI-00390576	>100	0.097 (7.01 ± 0.03)	5.98 (5.22 ± 0.04)	24.77 (4.61 ± 0.02)
	TMP269*	>100	0.157	8.2	4.2

Data shown is at least from two experiments each performed at least as duplicates and the IC<sub>50</sub> value of pooled data is reported when IC<sub>50</sub> < 100 μM. \*Data taken from Lobera et al.<sup>[17]</sup>

### 3. Conclusions

Histone deacetylase 8 (HDAC8) is a unique zinc-dependent class I HDAC and provides an attractive therapeutic anticancer target. Besides catalyzing the removal of acetyl functional groups from lysine residues of both histone and nonhistone proteins, HDAC8 also mediates signaling via scaffolding functions. Dysregulated expression and/or aberrant interactions with transcription factors are crucial in HDAC8-associated cancers. The employment of HDAC8 selective inhibitors presents a promising strategy for anticancer treatment, as they are expected to have a lower degree of pan-HDAC inhibitors associated side effects. So far, only a limited number of selective and potent HDAC8 inhibitors have been reported as anticancer agents. Here, we report the synthesis and biological evaluation of thioether-based hydroxamates as HDAC8 inhibitors. Among the tested compounds **10a-k**, **21a-b**, **26**, **28a-b**, we have identified **10k** as the most potent and selective HDAC8 inhibitor in the nanomolar range ( $IC_{50}(\text{HDAC8}) = 0.28 \mu\text{M}$ ) with a  $\geq 356$ -fold selectivity over HDAC2 and a 35/21-fold preference over HDAC4/6. Further studies will focus on the structural optimization of compound **10k** to improve e.g. the HDAC8 selectivity, water solubility and pharmacokinetic properties. Furthermore, the elucidation of the binding mode of **10k** within the catalytic pocket of HDAC8 via crystallization studies is subject of future research.

## **Acknowledgements**

YA, AJS, MUK, and TK gratefully acknowledge support from the Deutsche Forschungsgemeinschaft (DFG) for grant number KA 1942/1-1 to MUK and grant number KU 1577/2-1 to TK, and the support from the DFG research training group GRK2158 (270650915/GRK2158). We further acknowledge the CHDI Foundation Inc. for providing the compound CHDI-00390576-0000-004.

## **Supplementary information**

Experimental procedures and analytical data for compounds **10a-k**, **13**, **14a-k**, **20a,b**, **21a,b**; **23-26**, **27a,b** and **28 a,b** are provided as supplementary information.

## References

- [1] M. Bantscheff, C. Hopf, M. M. Savitski, A. Dittmann, P. Grandi, A. M. Michon, J. Schlegl, Y. Abraham, I. Becher, G. Bergamini, et al., *Nat. Biotechnol.* **2011**, *29*, 255–268.
- [2] M. Haberland, R. L. Montgomery, E. N. Olson, *Nat. Rev. Genet.* **2011**, *10*, 32–42.
- [3] X.-J. Yang, E. Seto, *Nat. Rev. Mol. Cell Biol.* **2008**, *9*, 206–218.
- [4] A. J. Guise, R. A. Mathias, E. A. Rowland, F. Yu, I. M. Cristea, *Proteomics* **2014**, *14*, 2156–2166.
- [5] P. Cohen, *Trends Biochem. Sci.* **2000**, *25*, 596–601.
- [6] M. Martin, R. Kettmann, F. Dequiedt, *Oncogene* **2007**, *26*, 5450–5467.
- [7] A. S. Carvalho, H. Ribeiro, P. Voabil, D. Penque, O. N. Jensen, H. Molina, R. Matthiesen, *Mol. Cell. Proteomics* **2014**, *13*, 3294–3307.
- [8] W. Fischle, F. Dequiedt, M. J. Hendzel, M. G. Guenther, M. A. Lazar, W. Voelter, E. Verdin, *Mol. Cell* **2002**, *9*, 45–57.
- [9] A. Lahm, C. Paolini, M. Pallaoro, M. C. Nardi, P. Jones, P. Neddermann, S. Sambucini, M. J. Bottomley, P. Lo Surdo, A. Carfi, et al., *Proc. Natl. Acad. Sci.* **2007**, *104*, 17335–17340.
- [10] P. Jones, S. Altamura, R. De Francesco, P. Gallinari, A. Lahm, P. Neddermann, M. Rowley, S. Serafini, C. Steinkühler, *Bioorganic Med. Chem. Lett.* **2008**, *18*, 1814–1819.
- [11] W. Fischle, V. Kiermer, F. Dequiedt, E. Verdin, *Biochem. Cell Biol.* **2001**, *79*, 337–348.
- [12] C. L. Zhang, T. A. McKinsey, E. N. Olson, *Mol. Cell. Biol.* **2002**, *22*, 7302–7312.
- [13] A. Clocchiatti, C. Florean, C. Brancolini, *J. Cell. Mol. Med.* **2011**, *15*, 1833–1846.
- [14] K. S. Keedy, N. M. Archin, A. T. Gates, A. Espeseth, D. J. Hazuda, D. M. Margolis, *J. Virol.* **2009**, *83*, 4749–4756.
- [15] M. M. Mihaylova, D. S. Vasquez, K. Ravnskjaer, P. D. Denechaud, R. T. Yu, J. G. Alvarez, M. Downes, R. M. Evans, M. Montminy, R. J. Shaw, *Cell* **2011**, *145*, 607–621.
- [16] M. Mielcarek, C. Landles, A. Weiss, A. Bradaia, T. Seredenina, L. Inuabasi, G. F. Osborne, K. Wadel, C. Touller, R. Butler, et al., *PLoS Biol.* **2013**, *11*, e1001717.
- [17] M. Lobera, K. P. Madauss, D. T. Pohlhaus, Q. G. Wright, M. Trocha, D. R. Schmidt, E. Baloglu, R. P. Trump, M. S. Head, G. A. Hofmann, et al., *Nat. Chem. Biol.* **2013**, *9*, 319–325.
- [18] C. A. Luckhurst, P. Breccia, A. J. Stott, O. Aziz, H. L. Birch, R. W. Bürli, S. J. Hughes, R. E. Jarvis, M. Lamers, P. M. Leonard, et al., *ACS Med. Chem. Lett.* **2016**, *7*, 34–39.

- [19] J. Melesina, L. Praetorius, C. V. Simoben, D. Robaa, W. Sippl, *Future Med. Chem.* **2018**, *10*, 1537–1540.
- [20] C. A. Luckhurst, O. Aziz, V. Beaumont, R. W. Bürli, P. Breccia, M. C. Maillard, A. F. Haughan, M. Lamers, P. Leonard, K. L. Matthews, et al., *Bioorg. Med. Chem. Lett.* **2019**, *29*, 83–88.
- [21] S. Balasubramanian, J. Ramos, W. Luo, M. Sirisawad, E. Verner, J. J. Buggy, *Leukemia* **2008**, *22*, 1026–1034.
- [22] I. Oehme, H. E. Deubzer, M. Lodrini, T. Milde, O. Witt, *Expert Opin. Investig. Drugs* **2009**, *18*, 1605–1617.
- [23] M. Harakalova, M.-J. van den Boogaard, R. Sinke, S. van Lieshout, M. C. van Tuil, K. Duran, I. Renkens, P. A. Terhal, C. de Kovel, I. J. Nijman, et al., *J. Med. Genet.* **2012**, *49*, 539–543.
- [24] M. Marek, S. Kannan, A.-T. Hauser, M. Moraes Mourão, S. Caby, V. Cura, D. A. Stolf, K. Schmidtkunz, J. Lancelot, L. Andrade, et al., *PLoS Pathog.* **2013**, *9*, e1003645.
- [25] D. Waltregny, W. Glénisson, S. L. Tran, B. J. North, E. Verdin, A. Colige, V. Castronovo, *FASEB J.* **2005**, *19*, 966–968.
- [26] H. Lee, N. Sengupta, A. Villagra, N. Rezai-Zadeh, E. Seto, *Mol. Cell. Biol.* **2006**, *26*, 5259–5269.
- [27] H. Lee, N. Rezai-Zadeh, E. Seto, *Mol. Cell. Biol.* **2004**, *24*, 765–773.
- [28] I. Van den Wyngaert, W. de Vries, A. Kremer, J.-M. Neefs, P. Verhasselt, W. H. M. L. Luyten, S. U. Kass, *FEBS Lett.* **2000**, *478*, 77–83.
- [29] E. Hu, Z. Chen, T. Fredrickson, Y. Zhu, R. Kirkpatrick, G.-F. Zhang, K. Johanson, C.-M. Sung, R. Liu, J. Winkler, *J. Biol. Chem.* **2000**, *275*, 15254–15264.
- [30] J. J. Buggy, M. L. Sideris, P. Mak, D. D. Lorimer, B. McIntosh, J. M. Clark, *Biochem. J.* **2000**, *350 Pt 1*, 199–205.
- [31] J. Melesina, D. Robaa, R. J. Pierce, C. Romier, W. Sippl, *J. Mol. Graph. Model.* **2015**, *62*, 342–361.
- [32] W.-J. Huang, Y.-C. Wang, S.-W. Chao, C.-Y. Yang, L.-C. Chen, M.-H. Lin, W.-C. Hou, M.-Y. Chen, T.-L. Lee, P. Yang, et al., *ChemMedChem* **2012**, *7*, 1815–1824.
- [33] G. Tang, J. C. Wong, W. Zhang, Z. Wang, N. Zhang, Z. Peng, Z. Zhang, Y. Rong, S. Li, M. Zhang, et al., *J. Med. Chem.* **2014**, *57*, 8026–8034.
- [34] P. Galletti, A. Quintavalla, C. Ventrici, G. Giannini, W. Cabri, S. Penco, G. Gallo, S. Vincenti, D. Giacomini, *ChemMedChem* **2009**, *4*, 1991–2001.
- [35] L. Whitehead, M. R. Dobler, B. Radetich, Y. Zhu, P. W. Atadja, T. Claiborne, J. E. Grob, A. McRiner, M. R. Pancost, A. Patnaik, et al., *Bioorg. Med. Chem.* **2011**, *19*, 4626–4634.
- [36] E. A. Ilardi, E. Vitaku, J. T. Njardarson, *J. Med. Chem.* **2014**, *57*, 2832–2842.

- [37] P. Tessier, S. Leit, D. Smil, R. Déziel, A. Ajamian, A. Chantigny, Yves, C. Dominguez, *Inhibitors of Histone Deacetylase*, **2008**, WO2008/122115 A1.
- [38] B. E. L. Lauffer, R. Mintzer, R. Fong, S. Mukund, C. Tam, I. Zilberleyb, B. Flicke, A. Ritscher, G. Fedorowicz, R. Vallero, et al., *J. Biol. Chem.* **2013**, *288*, 26926–26943.
- [39] A. A. Tabackman, R. Frankson, E. S. Marsan, K. Perry, K. E. Cole, *J. Struct. Biol.* **2016**, *195*, 373–378.
- [40] Y. Hai, D. W. Christianson, *Nat. Chem. Biol.* **2016**, *12*, 741–747.
- [41] Y. Asfaha, C. Schrenk, L. A. Alves Avelar, F. Lange, C. Wang, J. J. Bandolik, A. Hamacher, M. U. Kassack, T. Kurz, *Bioorg. Med. Chem.* **2020**, *28*, 115108.
- [42] J. Sherwood, J. H. Clark, I. J. S. Fairlamb, J. M. Slattery, *Green Chem.* **2019**, *21*, 2164–2213.
- [43] J. Lee, Y. Han, Y. Kim, J. Min, M. Bae, D. Kim, S. Jin, J. Kyung, *1,3,4-Oxadiazole Sulfamide Derivative Compounds as Histone Deacetylase 6 Inhibitor, and the Pharmaceutical Composition Comprising the Same*, **2018**, US2018/0230113 A1.

## Supporting Information

### **Are thioether-based hydroxamic acids HDAC8 or class IIa HDAC selective inhibitors?**

*Yodita Asfaha<sup>\*#</sup>, Alexander Jan Skerhut<sup>\*#</sup>, Leandro A. Alves-Avelar<sup>\*</sup>, Nadine Horstick-Muche<sup>\*</sup>,  
Matthias U. Kassack<sup>\*#</sup>, Thomas Kurz<sup>\*#</sup>*

<sup>\*</sup>Institut für Pharmazeutische und Medizinische Chemie, Heinrich-Heine-Universität  
Düsseldorf, Universitätsstr. 1, 40225 Düsseldorf, Germany. <sup>#</sup>YA and AJS share first authorship,  
MUK and TK share senior and corresponding authorship.

## Experimental section

### General methods

All chemicals and solvents were purchased from commercial suppliers (Sigma Aldrich, Alfa Aesar, Fluorochem, TCI, abcr and Acros Organics) and used without further purification. All anhydrous reactions were carried out in flame-dried Schlenk-flasks and under argon atmosphere. Dry solvents were used directly from Seal<sup>®</sup> bottles from Acros Organics. Analytic Thin Layer Chromatography (TLC) was carried out with Macherey Nagel precoated silica gel plates (ALUGRAM<sup>®</sup> Xtra SIL G/UV<sub>254</sub>). Detection was achieved with ultraviolet irradiation (254 nm) and/or staining with potassium permanganate solution (9 g KMnO<sub>4</sub>, 60 g K<sub>2</sub>CO<sub>3</sub>, 15 mL of a 5% aqueous NaOH-solution, and 900 mL demineralised water). Flash column chromatography was performed with CombiFlashRf200 (TeleDyneIsco) with the solvent mixtures specified in the corresponding procedure.

### Physical data

Proton (<sup>1</sup>H) and carbon (<sup>13</sup>C) NMR spectra were recorded on Bruker Avance III – 300, Bruker Avance DRX – 500 or Bruker Avance III – 600. Spectra were referenced to the residual non-deuterated solvent signal (<sup>1</sup>H-NMR: DMSO-*d*<sub>6</sub> (2.50 ppm), <sup>13</sup>C-NMR: DMSO-*d*<sub>6</sub> (39.52 ppm); <sup>1</sup>H-NMR: CDCl<sub>3</sub> (7.26 ppm), <sup>13</sup>C-NMR: CDCl<sub>3</sub> (77.16 ppm)). Chemical shifts are quoted in parts per million (ppm). Signal patterns are indicated as: singlet (s), doublet (d), triplet (t), quartet (q), or multiplet (m). Coupling constants, *J*, are measured in Hz. Proton (<sup>1</sup>H) and carbon (<sup>13</sup>C) NMR spectra were recorded by the NMR-Divisions of the Department of Chemistry (Heinrich Heine University Duesseldorf). Electrospray Ionisation (ESI) mass spectra were carried out by the Mass spectrometry-Division of the Heinrich Heine University Duesseldorf, using Bruker Daltonics UHR-QTOF maXis 4G (Bruker Daltonics). Melting points (mp.) were determined using a Büchi M-565 melting point apparatus and are uncorrected.

Analytical HPLC analysis were carried out on a Knauer HPLC system comprising an Azura P 6.1L pump, an Optimas 800 autosampler, a Fast Scanning Spectro-Photometer K-2600 and a Knauer Reversed Phase column (SN: FK36). UV absorption was detected at 254 nm. The solvent gradient table is shown below. The purity of all final compounds was 95% or higher.

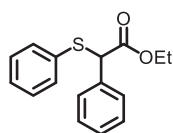
Table 1: The solvent gradient table for analytic HPLC analysis.

Time / min	Water + 0.1% TFA	ACN + 0.1% TFA
Initial	90	10
0.50	90	10
20.0	0	100
30.0	0	100
31.0	90	10
40.0	90	10

### General procedure 1: Formation of thioethers

For the synthesis of the thioethers **14a-k** and **20a-b**, 1.00 eq of the respective bromo derivative (**12** or **13**), 2.00 eq  $\text{NEt}_3$  and 1.00 eq of the thiol were dissolved in MeCN (0.1 mmol/mL). The resulting reaction mixture was refluxed for 8 h. Upon completion of the reaction, the solvent was removed *in vacuo* and the residue was diluted with EtOAc. The organic layer was washed with saturated  $\text{NaHCO}_3$  (3x 50 mL), brine (1x 50 mL), dried over  $\text{Na}_2\text{SO}_4$  and filtered. After removing the solvent under reduced pressure, the crude product was purified by flash chromatography (prepacked silica cartridge, *n*-hexane/ethyl acetate) furnishing the products.

### Synthesis of ethyl 2-phenyl-2-(phenylthio)acetate (**14a**)



[272.36]

Following the General procedure 1, ethyl  $\alpha$ -bromophenylacetate (**12**) (1.80 mL, 10.0 mmol, 1.00 eq) and benzenethiol (**11a**) (1.03 mL, 10.0 mmol, 1.00 eq) provided the compound **14a** (2.34 g, 8.60 mmol, 86%) as a clear oil.

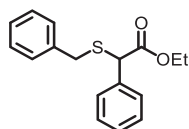
$^1\text{H}$  NMR (600 MHz,  $\text{DMSO}-d_6$ )  $\delta$  = 1.05 (t,  $J$  = 7.1 Hz, 3H), 3.99 – 4.11 (m, 2H), 5.34 (s, 1H), 7.24 – 7.29 (m, 1H), 7.29 – 7.38 (m, 5H), 7.38 – 7.42 (m, 2H), 7.46 – 7.50 (m, 2H) ppm.

$^{13}\text{C}$  NMR (151 MHz,  $\text{DMSO}-d_6$ )  $\delta$  = 13.81, 53.96, 61.33, 127.52, 128.25, 128.32, 128.40, 128.61, 129.03, 131.09, 133.52, 135.49, 169.87 ppm.

HPLC analysis:  $R_t$  = 16.050 min, >99%.

HRMS (ESI+) = calcd. for  $\text{C}_{16}\text{H}_{17}\text{O}_2\text{S}$   $[\text{M}+\text{H}]^+$  = 273.0944, found: 273.0947.

### Synthesis of ethyl 2-(benzylthio)-2-phenylacetate (**14b**)



[286.39]

Ethyl  $\alpha$ -bromophenylacetate (**12**) (1.80 mL, 10.0 mmol, 1.00 eq) and benzyl mercaptan (**11b**) (1.17 mL, 10.0 mmol, 1.00 eq) were subjected to General procedure 1. Purification by flash

chromatography (*n*-hexane/EtOAc) furnished the thioether **14b** (2.75 g, 9.59 mmol, 96%) as a clear oil.

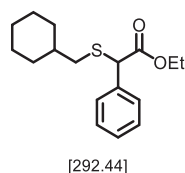
<sup>1</sup>H NMR (600 MHz, DMSO-*d*<sub>6</sub>) δ = 1.15 (t, *J* = 7.1 Hz, 3H), 3.67 – 3.84 (m, 2H), 4.00 – 4.15 (m, 2H), 4.63 (s, 1H), 7.22 – 7.28 (m, 3H), 7.29 – 7.34 (m, 3H), 7.34 – 7.41 (m, 4H) ppm.

<sup>13</sup>C NMR (151 MHz, DMSO-*d*<sub>6</sub>) δ = 13.90, 35.64, 51.06, 61.27, 127.09, 128.04, 128.27, 128.45, 128.63, 128.86, 136.10, 137.27, 170.19 ppm.

HPLC analysis: *R*<sub>t</sub> = 16.267 min, 97.1%.

HRMS (ESI+) = calcd. for C<sub>17</sub>H<sub>19</sub>O<sub>2</sub>S [M+H]<sup>+</sup> = 287.1100, found: 287.1100.

### Synthesis of ethyl 2-((cyclohexylmethyl)thio)-2-phenylacetate (**14c**)



Following the General procedure 1, ethyl α-bromophenylacetate (**12**) (1.80 mL, 10.0 mmol, 1.00 eq) and cyclohexanethiol (**11c**) (1.30 mL, 10.0 mmol, 1.00 eq) furnished the title compound **14c** (1.01 g, 3.61 mmol, 36%) as a colorless oil.

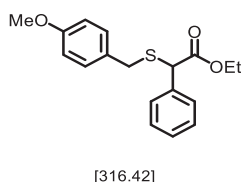
<sup>1</sup>H NMR (300 MHz, DMSO-*d*<sub>6</sub>) δ = 1.35 – 1.03 (m, 9H), 1.56 – 1.41 (m, 1H), 1.74 – 1.56 (m, 2H), 1.86 (t, *J* = 12.2 Hz, 2H), 2.68 (tt, *J* = 10.0, 4.4 Hz, 1H), 4.22 – 3.98 (m, 2H), 4.83 (s, 1H), 7.40 – 7.24 (m, 3H), 7.51 – 7.41 (m, 2H) ppm.

<sup>13</sup>C NMR (75 MHz, DMSO-*d*<sub>6</sub>) δ = 3.80, 25.09, 25.15, 32.79, 32.82, 43.55, 49.71, 60.97, 127.68, 128.18, 128.31, 129.10, 136.90, 170.65 ppm.

HPLC analysis: *R*<sub>t</sub> = 17.667 min, 96.2%.

HRMS (ESI+) = calcd. for C<sub>16</sub>H<sub>23</sub>O<sub>2</sub>S [M+CH<sub>3</sub>OH+H]<sup>+</sup> = 323.0912, found: 323.0916.

### Synthesis of ethyl 2-((4-methoxybenzyl)thio)-2-phenylacetate (**14d**)



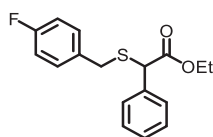
Following the General procedure 1, ethyl α-bromophenylacetate (**12**) (1.80 mL, 10.0 mmol, 1.00 eq) and (4-methoxyphenyl)methanethiol (**11d**) (1.41 mL, 10.0 mmol, 1.00 eq) gave the title compound **14d** (1.58 g, 50.1 mmol, 50%) as a yellowish oil.

$^1\text{H}$  NMR (300 MHz,  $\text{DMSO-}d_6$ )  $\delta$  = 1.15 (t,  $J$  = 7.1 Hz, 3H), 3.63 – 3.71 (m, 2H), 3.73 (s, 4H), 3.98 – 4.20 (m, 2H), 4.60 (s, 1H), 6.85 – 6.92 (m, 2H), 7.13 – 7.22 (m, 2H), 7.25 – 7.42 (m, 5H) ppm.  
 $^{13}\text{C}$  NMR (75 MHz,  $\text{DMSO-}d_6$ )  $\delta$  = 13.92, 35.07, 50.96, 55.05, 61.27, 113.87, 128.01, 128.28, 128.62, 128.93, 130.03, 136.16, 158.34, 170.26 ppm.

HPLC analysis:  $R_t$  = 17.150 min, >99%.

HRMS (ESI+) = calcd. for  $\text{C}_{18}\text{H}_{24}\text{NO}_3\text{S}$   $[\text{M}+\text{NH}_4]^+$  = 334.1471, found: 334.1474.

### Synthesis of ethyl 2-((4-fluorobenzyl)thio)-2-phenylacetate (**14e**)



[304.38]

Ethyl  $\alpha$ -bromophenylacetate (**12**) (0.54 mL, 3.00 mmol, 1.00 eq) and 4-fluorobenzyl mercaptan (**11e**) (0.38 mL, 3.00 mmol, 1.00 eq) were subjected to General procedure 1. The crude product was purified by flash chromatography (*n*-hexane/EtOAc) yielding the thioether **14e** (0.81 g, 2.67 mmol, 89%) as a clear oil.

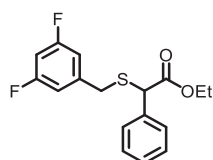
$^1\text{H}$  NMR (300 MHz,  $\text{DMSO-}d_6$ )  $\delta$  = 1.14 (t,  $J$  = 7.1 Hz, 3H), 3.68 – 3.83 (m, 2H), 3.98 – 4.15 (m, 2H), 4.63 (s, 1H), 7.05 – 7.19 (m, 2H), 7.25 – 7.44 (m, 7H) ppm.

$^{13}\text{C}$  NMR (151 MHz,  $\text{DMSO-}d_6$ )  $\delta$  = 13.88, 34.84, 51.05, 61.29, 115.20 (d,  $J$  = 21.4 Hz), 128.04, 128.26, 128.62, 130.78 (d,  $J$  = 8.2 Hz), 133.58 (d,  $J$  = 3.3 Hz), 136.07, 160.41, 162.02, 170.18 ppm.

HPLC analysis:  $R_t$  = 16.233 min, >99%.

HRMS (ESI+) = calcd. for  $\text{C}_{17}\text{H}_{18}\text{FO}_2\text{S}$   $[\text{M}+\text{H}]^+$  = 305.1006, found: 305.1008.

### Synthesis of ethyl 2-((3,5-difluorobenzyl)thio)-2-phenylacetate (**14f**)



[322.37]

Ethyl  $\alpha$ -bromophenylacetate (**12**) (0.90 mL, 5.00 mmol, 1.00 eq) and (3,5-difluorophenyl)methanethiol (**11f**) (817 mg, 5.00 mmol, 1.00 eq) were subjected to General

procedure 1. Purification by flash chromatography (*n*-hexane/EtOAc) provided the thioether **14f** (1.45 g, 4.50 mmol, 90%) as a clear oil.

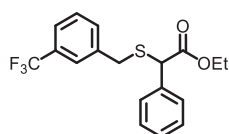
$^1\text{H}$  NMR (300 MHz, DMSO- $d_6$ )  $\delta$  = 1.14 (t,  $J$  = 7.1 Hz, 3H), 3.82 (d,  $J$  = 1.7 Hz, 2H), 3.96 – 4.14 (m, 2H), 4.71 (s, 1H), 6.92 – 7.03 (m, 2H), 7.09 (tt,  $J$  = 9.4, 2.4 Hz, 1H), 7.26 – 7.42 (m, 5H) ppm.

$^{13}\text{C}$  NMR (75 MHz, DMSO- $d_6$ )  $\delta$  = 13.69, 35.00, 51.24, 61.17, 102.34 (t,  $J$  = 25.8 Hz), 111.39 – 112.03 (m), 127.92, 128.13, 128.46, 135.90, 142.33 (t,  $J$  = 9.3 Hz), 160.45 (d,  $J$  = 13.4 Hz), 163.72 (d,  $J$  = 13.3 Hz), 169.95 ppm.

HPLC analysis:  $R_t$  = 16.550 min, 98.7%.

HRMS (ESI+) = calcd. for  $\text{C}_{17}\text{H}_{18}\text{BrO}_2\text{S}$   $[\text{M}+\text{H}]^+$  = 365.0205, found: 365.0209.

### Synthesis of ethyl 2-phenyl-2-((3-(trifluoromethyl)benzyl)thio)acetate (**14g**)



[354.39]

Following the General procedure 1, ethyl  $\alpha$ -bromophenylacetate (**12**) (1.80 mL, 10.0 mmol, 1.00 eq) and (3-(trifluoromethyl)phenyl)methanethiol (**11g**) (1.96 g, 10.0 mmol, 1.00 eq) gave the title compound **14g** (2.53 g, 71.4 mmol, 71%) as a clear oil.

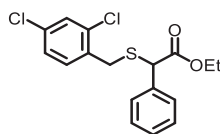
$^1\text{H}$  NMR (600 MHz, DMSO- $d_6$ )  $\delta$  = 1.12 (t,  $J$  = 7.1 Hz, 3H), 3.85 – 3.95 (m, 2H), 3.97 – 4.08 (m, 2H), 4.68 (s, 1H), 7.27 – 7.41 (m, 5H), 7.52 – 7.64 (m, 4H) ppm.

$^{13}\text{C}$  NMR (151 MHz, DMSO- $d_6$ )  $\delta$  = 13.80, 35.22, 51.28, 61.31, 123.77 (q,  $J$  = 3.8 Hz), 124.13 (q,  $J$  = 272.3 Hz), 125.32 (q,  $J$  = 3.8 Hz), 128.08, 128.24, 128.64, 129.08 (q,  $J$  = 31.4 Hz), 129.50, 132.98, 136.00, 139.21, 170.14 ppm.

HPLC analysis:  $R_t$  = 17.200 min, 93.2%.

HRMS (ESI+) = calcd. for  $\text{C}_{18}\text{H}_{18}\text{F}_3\text{O}_2\text{S}$   $[\text{M}+\text{H}]^+$  = 355.0974, found: 355.0974.

### Synthesis of ethyl 2-((2,4-dichlorobenzyl)thio)-2-phenylacetate (**14h**)



[355.27]

Ethyl  $\alpha$ -bromophenylacetate (**12**) (1.80 mL, 10.0 mmol, 1.00 eq) and 2,4-dichlorobenzyl mercaptan (**11h**) (1.50 mL, 10.0 mmol, 1.00 eq) were subjected to General procedure 1. The crude product was purified by flash chromatography (*n*-hexane/EtOAc) to afford the thioether **14h** (1.74 g, 4.91 mmol, 49%) as a clear oil.

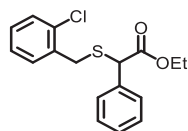
$^1\text{H}$  NMR (300 MHz, DMSO- $d_6$ )  $\delta$  = 1.14 (t,  $J$  = 7.1 Hz, 3H), 3.85 (s, 2H), 4.07 (qd,  $J$  = 7.1, 4.2 Hz, 2H), 4.77 (s, 1H), 7.26 – 7.45 (m, 7H), 7.59 (dd,  $J$  = 1.5, 1.0 Hz, 1H) ppm.

$^{13}\text{C}$  NMR (75 MHz, DMSO- $d_6$ )  $\delta$  = 35.59, 50.21, 52.49, 121.14, 126.99, 128.32, 128.74, 130.39, 131.43, 135.52, 136.99, 170.23 ppm.

HPLC analysis:  $R_t$  = 19.883 min, 95.1%.

HRMS (ESI+) = calcd. for  $\text{C}_{17}\text{H}_{17}\text{Cl}_2\text{O}_2\text{S}$   $[\text{M}+\text{H}]^+$  = 355.0321, found: 355.0324.

### Synthesis of ethyl 2-((2-chlorobenzyl)thio)-2-phenylacetate (**14j**)



[320.83]

Ethyl  $\alpha$ -bromophenylacetate (**12**) (1.80 mL, 10.0 mmol, 1.00 eq) and 2-chlorobenzenemethanethiol (**11i**) (1.62 g, 10.0 mmol, 1.00 eq) were subjected to General procedure 1. Purification by flash chromatography (*n*-hexane/EtOAc) afforded the product **14j** (2.65 g, 8.24 mmol, 82%) as a clear oil.

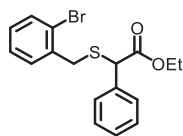
$^1\text{H}$  NMR (300 MHz, DMSO- $d_6$ )  $\delta$  = 1.15 (t,  $J$  = 7.1 Hz, 3H), 3.86 (s, 2H), 4.08 (qd,  $J$  = 7.1, 5.0 Hz, 2H), 4.76 (s, 1H), 7.26 – 7.46 (m, 9H) ppm.

$^{13}\text{C}$  NMR (75 MHz, DMSO- $d_6$ )  $\delta$  = 13.75, 33.33, 51.41, 61.20, 127.13, 127.92, 128.17, 128.47, 128.93, 129.39, 130.96, 132.98, 134.85, 135.92, 169.96 ppm.

HPLC analysis:  $R_t$  = 16.983 min, 98.4%.

HRMS (ESI+) = calcd. for  $\text{C}_{17}\text{H}_{18}\text{ClO}_2\text{S}$   $[\text{M}+\text{H}]^+$  = 321.0711, found: 321.0707.

## Synthesis of ethyl 2-((2-bromobenzyl)thio)-2-phenylacetate (**14k**)



[365.29]

Following the General procedure 1, ethyl  $\alpha$ -bromophenylacetate (**12**) (0.44 mL, 2.50 mmol, 1.00 eq) and 2-bromobenzyl mercaptan (**11j**) (0.34 mL, 2.50 mmol, 1.00 eq) gave the title compound **14k** (0.80 g, 2.19 mmol, 88%) as a clear oil.

$^1\text{H}$  NMR (300 MHz, DMSO- $d_6$ )  $\delta$  = 1.15 (t,  $J$  = 7.1 Hz, 3H), 3.86 (s, 2H), 3.99 – 4.17 (m, 2H), 4.77 (s, 1H), 7.20 (ddd,  $J$  = 7.9, 6.6, 2.5 Hz, 1H), 7.28 – 7.46 (m, 7H), 7.56 – 7.63 (m, 1H) ppm.

$^{13}\text{C}$  NMR (75 MHz, DMSO- $d_6$ )  $\delta$  = 13.76, 36.01, 51.40, 61.20, 123.69, 127.71, 127.92, 128.18, 128.46, 129.13, 130.96, 132.69, 135.91, 136.49, 169.95 ppm.

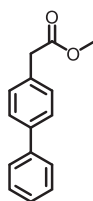
HPLC analysis:  $R_t$  = 17.233 min, >99%.

HRMS (ESI+) = calcd. for  $\text{C}_{17}\text{H}_{18}\text{BrO}_2\text{S}$   $[\text{M}+\text{H}]^+$  = 365.0205, found: 365.0209.

### General procedure 2: Formation of methyl ester

Following the procedure of Lu *et al.*,<sup>[1]</sup> 1.00 eq of the respective acid and concentrated sulfuric acid (95%, 3.00 eq) were dissolved in methanol (0.1 mmol/ mL). The mixture was heated to reflux for 8 h. Subsequently, the solvent was removed under reduced pressure and the residue was diluted with EtOAc. The organic layer was washed with saturated  $\text{NaHCO}_3$ -solution (3x), brine (1x) and dried over  $\text{Na}_2\text{SO}_4$ . Subsequent filtration and concentrating *in vacuo* yielded the corresponding methyl esters **19** and **23**.

### Synthesis of methyl 2-([1,1'-biphenyl]-4-yl)acetate (**19**)



[226.28]

Following the General procedure 2, 4-biphenylacetic acid (2.12 g, 10.0 mmol, 1.00 eq) and concentrated sulfuric acid (95%, 1.68 mL, 3.00 eq) furnished the methyl ester **19** (2.15 g, 9.50 mmol, 95%) as a clear oil.

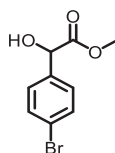
$^1\text{H}$  NMR (300 MHz,  $\text{DMSO-}d_6$ )  $\delta$  = 3.63 (s, 3H), 3.73 (s, 2H), 7.37 (dd,  $J$  = 7.7, 3.1 Hz, 3H), 7.46 (t,  $J$  = 7.5 Hz, 2H), 7.58 – 7.69 (m, 4H) ppm.

$^{13}\text{C}$  NMR (151 MHz,  $\text{DMSO-}d_6$ )  $\delta$  = 39.75, 51.70, 126.46, 126.58, 126.67, 127.36, 128.91, 129.93, 133.59, 138.77, 139.87, 171.57 ppm.

HPLC analysis:  $R_t$  = 14.683 min, >99%.

HRMS (ESI+) = calcd. for  $\text{C}_{15}\text{H}_{14}\text{N}_2\text{O}_2$   $[\text{M}+\text{H}]^+$  = 227.1067, found: 227.1065.

### Synthesis of methyl 2-([1,1'-biphenyl]-4-yl)acetate (**23**)



[245.07]

4-Bromo-DL-mandelic acid (**22**) (2.41 g, 10.0 mmol, 1.00 eq) and concentrated sulfuric acid (95%, 1.68 mL, 3.00 eq) were subjected to General procedure 2 yielding the methyl ester **23** (2.20 g, 8.96 mmol, 90%) as a clear oil.

$^1\text{H}$  NMR (300 MHz,  $\text{DMSO-}d_6$ )  $\delta$  = 7.59 – 7.51 (m, 2H), 7.41 – 7.31 (m, 2H), 6.19 (d,  $J$  = 5.3 Hz, 1H), 5.16 (d,  $J$  = 5.1 Hz, 1H), 3.61 (s, 3H) ppm.

$^{13}\text{C}$  NMR (75 MHz,  $\text{DMSO-}d_6$ )  $\delta$  = 51.82, 71.73, 121.01, 128.79, 131.14, 139.02, 172.53 ppm.

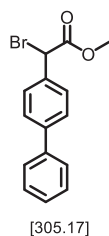
Elemental analysis: calcd.: C: 44.11%, H:3.70%; found: C: 44.18%, H:3.75%;

HRMS (ESI+) = calcd. for  $\text{C}_9\text{H}_9\text{BrNaO}_3$   $[\text{M}+\text{Na}]^+$  = 266.9627, found: 266.9626.

### General procedure 3: Radical bromination

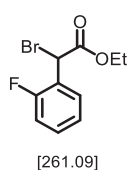
Following the procedure of Inguibert *et al.*,<sup>[2]</sup> a mixture of the respective methyl ester (1.00 eq), *N*-bromosuccinimide (2.00 eq) and a catalytic amount of benzoyl peroxide (0.01 eq) in dried CCl<sub>4</sub> (0.1 mmol/mL) was refluxed for 8 h. Afterwards, the precipitate was filtered off using celite and the filtrate was washed with a 1M sodium thiosulfate solution (3x) and brine (1x). After drying over Na<sub>2</sub>SO<sub>4</sub>, filtration and removing the solvent *in vacuo*, the crude product was purified by flash column chromatography (prepacked silica cartridge, *n*-hexane/ethyl acetate) yielding the corresponding bromo derivative.

### Synthesis of methyl 2-([1,1'-biphenyl]-4-yl)-2-bromoacetate (**29**)



Methyl 2-([1,1'-biphenyl]-4-yl)acetate (**19**) (905 mg, 4.00 mmol, 1.00 eq) was subjected to General procedure 3 yielding the title compound **29** (1.19 g, 3.90 mmol, 89%) as a yellowish oil. All spectroscopic data were in agreement with the literature.<sup>[2]</sup>

### Synthesis of ethyl 2-bromo-2-(2-fluorophenyl)acetate (**13**)



Ethyl 2-(2-fluorophenyl)acetate (920 mg, 5.00 mmol, 1.00 eq) was subjected to General procedure 3 to furnish the bromo derivative **13** (796 mg, 3.05 mmol, 61%) as a colorless oil.

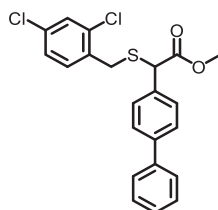
<sup>1</sup>H NMR (300 MHz, DMSO-*d*<sub>6</sub>)  $\delta$  = 1.17 (t, *J* = 7.1 Hz, 3H), 4.20 (q, *J* = 7.1 Hz, 2H), 6.13 (s, 1H), 7.13 – 7.40 (m, 3H), 7.39 – 7.65 (m, 2H) ppm.

<sup>13</sup>C NMR (75 MHz, DMSO-*d*<sub>6</sub>)  $\delta$  = 13.66, 13.83, 41.42 (d, *J* = 3.1 Hz), 60.46, 62.34, 66.56 (d, *J* = 3.1 Hz), 115.11 (d, *J* = 21.6 Hz), 115.75 (d, *J* = 20.9 Hz), 124.29 (d, *J* = 3.5 Hz), 124.79 (d, *J* = 3.6 Hz), 128.74 (d, *J* = 4.1 Hz), 129.83 (d, *J* = 8.3 Hz), 130.45 (d, *J* = 2.8 Hz), 131.34 (d, *J* = 8.6 Hz), 157.72, 161.02, 166.78 ppm.

HPLC analysis:  $R_t = 13.681$  min, 97.4%.

HRMS (ESI+) = calcd. for  $C_{10}H_{11}BrFO_2$   $[M+H]^+ = 260.9921$ , found: 260.9924.

### Synthesis of methyl 2-([1,1'-biphenyl]-4-yl)-2-((2,4-dichlorobenzyl)thio)-acetate (**20a**)



[417.36]

Following the General procedure 1, methyl 2-([1,1'-biphenyl]-4-yl)-2-bromoacetate (**29**) (763 mg, 2.50 mmol, 1.00 eq) and 2,4-dichlorobenzyl mercaptan (**11h**) (0.35 mL, 2.50 mmol, 1.00 eq) furnished the title compound **20a** (942 mg, 2.26 mmol, 90%) as a colorless oil.

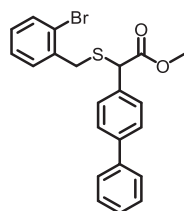
$^1H$  NMR (300 MHz,  $DMSO-d_6$ )  $\delta = 3.63$  (s, 3H), 3.88 (s, 2H), 4.87 (s, 1H), 7.32 – 7.51 (m, 7H), 7.55 – 7.70 (m, 5H) ppm.

$^{13}C$  NMR (75 MHz,  $DMSO-d_6$ )  $\delta = 33.02, 51.06, 52.75, 126.75, 127.01, 127.44, 127.71, 128.98, 129.03, 132.40, 132.68, 134.11, 134.36, 135.05, 139.55, 140.08, 170.63$  ppm.

HPLC analysis:  $R_t = 19.498$  min, 99.0%.

HRMS (ESI+) = calcd. for  $C_{22}H_{22}Cl_2NO_2S$   $[M+NH_4]^+ = 434.0743$ , found: 434.0734.

### Synthesis of methyl 2-([1,1'-biphenyl]-4-yl)-2-((2-bromobenzyl)thio)-acetate (**20b**)



[427.36]

Methyl 2-([1,1'-biphenyl]-4-yl)-2-bromoacetate (**29**) (1.49 g, 4.90 mmol, 1.00 eq) and 2-bromobenzyl mercaptan (**11j**) (0.66 mL, 4.90 mmol, 1.00 eq) were subjected to General procedure 1. The crude product was purified by flash chromatography (*n*-hexane/EtOAc) to afford the thioether **20b** (1.63 g, 3.81 mmol, 78%) as a yellowish oil.

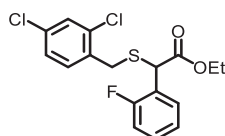
$^1H$  NMR (300 MHz,  $DMSO-d_6$ )  $\delta = 3.65$  (s, 3H), 3.89 (s, 2H), 4.86 (s, 1H), 7.21 (ddd,  $J = 7.9, 7.0, 2.1$  Hz, 1H), 7.30 – 7.42 (m, 3H), 7.43 – 7.54 (m, 4H), 7.59 – 7.69 (m, 5H) ppm.

$^{13}\text{C}$  NMR (75 MHz,  $\text{DMSO-}d_6$ )  $\delta$  = 36.18, 50.99, 52.70, 123.90, 126.61, 126.71, 126.98, 127.66, 127.88, 128.98, 129.34, 129.96, 131.16, 132.88, 135.09, 136.61, 139.53, 140.00, 170.64 ppm.

HPLC analysis:  $R_t$  = 18.634 min, 97.8%.

HRMS (ESI+) = calcd. for  $\text{C}_{22}\text{H}_{23}\text{Br}_3\text{NO}_2\text{S}$   $[\text{M}+\text{NH}_4]^+$  = 444.0627, found: 444.0633.

### Synthesis of ethyl 2-((2,4-dichlorobenzyl)thio)-2-(2-fluorophenyl)acetate (**14i**)



[373.27]

Following the General procedure 1, ethyl 2-bromo-2-(2-fluorophenyl)acetate (**13**) (522 mg, 2.00 mmol, 1.00 eq) and 2,4-dichlorobenzyl mercaptan (**11h**) (0.28 mL, 2.00 mmol, 1.00 eq) yielded the thioether **14i** (549 mg, 1.47 mmol, 74%) as a colorless oil.

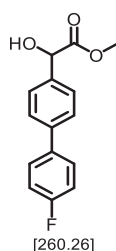
$^1\text{H}$  NMR (300 MHz,  $\text{DMSO-}d_6$ )  $\delta$  = 1.14 (t,  $J$  = 7.1 Hz, 3H), 3.93 (s, 2H), 4.10 (qd,  $J$  = 7.1, 0.6 Hz, 2H), 4.96 (s, 1H), 7.15 – 7.25 (m, 2H), 7.29 – 7.53 (m, 4H), 7.59 (d,  $J$  = 2.0 Hz, 1H) ppm.

$^{13}\text{C}$  NMR (75 MHz,  $\text{DMSO-}d_6$ )  $\delta$  = 13.81, 32.98, 44.74, 61.60, 115.48 (d,  $J$  = 21.6 Hz), 123.39 (d,  $J$  = 14.0 Hz), 124.67 (d,  $J$  = 3.5 Hz), 127.38, 128.95, 129.89 (d,  $J$  = 3.0 Hz), 130.16 (d,  $J$  = 8.3 Hz), 132.26, 132.68, 134.06 (d,  $J$  = 3.6 Hz), 157.83, 161.09, 169.29 ppm.

HPLC analysis:  $R_t$  = 18.211 min, >99%.

HRMS (ESI+) = calcd. for  $\text{C}_{17}\text{H}_{16}\text{Cl}_2\text{FO}_2\text{S}$   $[\text{M}+\text{H}]^+$  = 373.0227, found: 373.0228.

### Synthesis of methyl 2-(4'-fluoro-[1,1'-biphenyl]-4-yl)-2-hydroxyacetate (**24**)



[260.26]

To a stirred solution of methyl 2-([1,1'-biphenyl]-4-yl)acetate (**23**) (245 mg, 1.00 mmol, 1.00 eq) and 4-fluorophenylboronic acid (140 mg, 1.00 mmol, 1.00 eq) in THF (3 mL) was added  $\text{PdCl}_2[\text{P}(\text{Cy})_3]_2$  (38.3 mg, 0.05 mmol, 0.05 eq). The mixture was degassed with argon for 5 min, treated with 2 M aqueous  $\text{Na}_2\text{CO}_3$ -solution (1.00 mL, 2.00 mmol, 2.00eq) and heated at 140 °C for 40 min under microwave irradiation (150 Watt). After cooling at rt, the mixture

was acidified with 4 M HCl in dioxane (pH = 3 – 4) and filtered through celite. The filtrate was concentrated *in vacuo* and the crude product was purified by flash chromatography (prepacked silica cartridge, *n*-hexane/ethyl acetate) to furnish the product **24** (204 mg, 0.79 mmol, 79%) as a white solid.

$^1\text{H}$  NMR (300 MHz, DMSO- $d_6$ )  $\delta$  = 3.63 (s, 3H), 5.20 (s, 1H), 6.13 (s, 1H), 7.18 – 7.38 (m, 2H), 7.41 – 7.54 (m, 2H), 7.58 – 7.77 (m, 4H) ppm.

$^{13}\text{C}$  NMR (75 MHz, DMSO- $d_6$ )  $\delta$  = 51.66, 72.05, 115.41, 115.70, 126.43, 127.13, 128.51 (d,  $J$  = 8.1 Hz), 136.17 (d,  $J$  = 3.0 Hz), 138.66, 160.18, 163.42, 172.80 ppm.

HPLC analysis:  $R_t$  = 12.033 min, 97.3%.

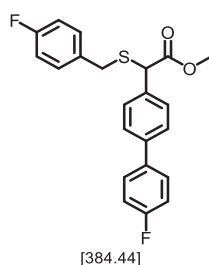
HRMS (ESI+) = calcd. for  $\text{C}_{15}\text{H}_{13}\text{FNaO}_3$  [ $\text{M}+\text{Na}$ ] $^+$  = 283.0741, found: 283.0741.

mp.: 111.7 °C.

#### General procedure 4: Functionalization of the $\alpha$ -hydroxy methyl ester

A solution of methyl 2-(4'-fluoro-[1,1'-biphenyl]-4-yl)-2-hydroxyacetate (**24**) (1.00 eq) and 3.00 eq  $\text{NEt}_3$  in anhydrous  $\text{CH}_2\text{Cl}_2$  (1 mmol/mL) was cooled to 0 °C. 1.10 eq methanesulfonyl chloride was added dropwise and the mixture was stirred for 30 min at 0 °C. Subsequently, the respective thiol/mercaptan (1.00 eq) was added and the reaction mixture was stirred overnight at room temperature. It was then diluted with  $\text{CH}_2\text{Cl}_2$ , washed with water (3x), dried over  $\text{Na}_2\text{SO}_4$  and filtered. After removing the solvent, the crude product was purified by flash chromatography (prepacked silica cartridge, *n*-hexane/ethyl acetate) to afford the product **25**.

#### Synthesis of methyl 2-(4'-fluoro-[1,1'-biphenyl]-4-yl)-2-((4-fluorobenzyl)thio)-acetate (**25**)



Methyl 2-(4'-fluoro-[1,1'-biphenyl]-4-yl)-2-hydroxyacetate (**24**) (601 mg, 2.31 mmol, 1.00 eq) and 4-fluorobenzyl mercaptan (**11e**) (346 mg, 2.31 mmol, 1.00 eq) were subjected to General

procedure 4. The crude product was purified by flash chromatography (*n*-hexane/EtOAc) yielding the thioether **25** (571 g, 1.49 mmol, 64%) as a yellowish oil.

<sup>1</sup>H NMR (600 MHz, DMSO-*d*<sub>6</sub>) δ = 3.57 (d, *J* = 13.4 Hz, 1H), 3.71 (d, *J* = 13.4 Hz, 1H), 4.34 (s, 1H), 7.11 – 7.17 (m, 2H), 7.24 – 7.31 (m, 4H), 7.49 – 7.53 (m, 2H), 7.60 – 7.64 (m, 2H), 7.68 – 7.73 (m, 2H), 9.05 (d, *J* = 1.5 Hz, 1H), 10.87 (d, *J* = 1.6 Hz, 1H) ppm.

<sup>13</sup>C NMR (151 MHz, DMSO-*d*<sub>6</sub>) δ = 34.91, 50.64, 52.62, 115.23 (d, *J* = 21.3 Hz), 115.77 (d, *J* = 21.2 Hz), 126.94, 128.71 (d, *J* = 8.1 Hz), 128.93, 130.84 (d, *J* = 8.0 Hz), 133.59 (d, *J* = 3.0 Hz), 135.17, 136.00 (d, *J* = 3.2 Hz), 138.91, 161.25 (d, *J* = 243.0 Hz), 161.98 (d, *J* = 244.8 Hz), 170.69 ppm.

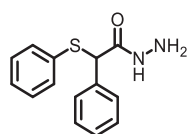
HPLC analysis: *R*<sub>t</sub> = 13.617 min, 98.4%.

HRMS (ESI+) = calcd. for C<sub>22</sub>H<sub>22</sub>F<sub>2</sub>NO<sub>2</sub>S [M+NH<sub>4</sub>]<sup>+</sup> = 402.1334, found: 402.1336.

### General procedure 5 Formation of the hydrazides

Following the procedure of Lee et al.,<sup>[3]</sup> 1.00 eq of the respective ethyl ester **13a-b** and 20.0 eq of hydrazine monohydrate were dissolved in EtOH (0.1 mmol/mL). The resulting mixture was refluxed for 10 h. Upon completion of the reaction, the reaction mixture was concentrated under reduced pressure yielding the corresponding hydrazides **30a-b**.

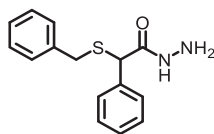
### Synthesis of 2-phenyl-2-(phenylthio)acetohydrazide (**30a**)



[258.34]

Ethyl 2-phenyl-2-(phenylthio)acetate (**13a**) (2.29 g, 8.41 mmol, 1.00 eq) and hydrazine monohydrate (8.32 mL, 168 mmol, 20.0 eq) were subjected to General procedure 5. The product **30a** was used directly for the next step without further purification.

## Synthesis of 2-(benzylthio)-2-phenylacetohydrazide (**30b**)



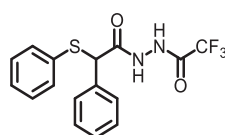
[272.37]

Ethyl 2-(benzylthio)-2-phenylacetate (**13b**) (1.72 g, 6.00 mmol, 1.00 eq) and hydrazine monohydrate (5.94 mL, 120 mmol, 20.0 eq) were converted according General procedure 5. The product **30b** was used directly for the next step without further purification.

## General procedure 6 *N*-acylation of hydrazides

Following the procedure of Lee et al.,<sup>[3]</sup> 1.00 eq of the respective hydrazide **30a-b** and 2.00 eq of NEt<sub>3</sub> were dissolved in dry CH<sub>2</sub>Cl<sub>2</sub> (1 mmol/mL). 0.95 eq Trifluoroacetic anhydride was added dropwise and the resulting mixture was stirred at rt overnight. Upon completion of the reaction, the reaction mixture was concentrated under reduced pressure and the residue was resuspended in water. The aqueous layer was extracted with CH<sub>2</sub>Cl<sub>2</sub> (3x). The combined organic layers were dried over Na<sub>2</sub>SO<sub>4</sub> and filtered. After removing the solvent *in vacuo*, the crude product was purified by flash column chromatography (prepacked silica cartridge, *n*-hexane/ethyl acetate) yielding the corresponding products **27a-b**.

## Synthesis of 2,2,2-trifluoro-*N'*-(2-phenyl-2-(phenylthio)acetyl)-aceto-hydrazide (**27a**)



[354.35]

Following the General procedure 6, 2-phenyl-2-(phenylthio)acetohydrazide (**30a**) (1.29 g, 5.00 mmol, 1.00 eq) yielded the product **27a** (864 mg, 2.44 mmol, 37%) as a white solid.

<sup>1</sup>H NMR (600 MHz, DMSO-*d*<sub>6</sub>) δ = 5.16 (s, 1H), 7.23 – 7.28 (m, 1H), 7.29 – 7.38 (m, 7H), 7.46 – 7.51 (m, 2H), 10.81 (s, 1H), 11.64 (s, 1H) ppm.

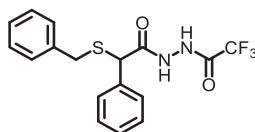
<sup>13</sup>C NMR (151 MHz, DMSO-*d*<sub>6</sub>) δ = 53.67, 115.98 (q, *J* = 288.3 Hz), 127.21, 128.15, 128.31, 128.47, 128.57, 129.18, 130.19, 134.31, 136.52, 155.44 (q, *J* = 36.2 Hz), 167.63 ppm.

HPLC analysis: *R*<sub>t</sub> = 12.600 min, 96.0%.

HRMS (ESI+) = calcd. for C<sub>16</sub>H<sub>14</sub>F<sub>3</sub>N<sub>2</sub>O<sub>2</sub>S [M+H]<sup>+</sup> = 355.0723, found: 355.0722.

mp.: 158.9 °C.

### Synthesis of *N'*-(2-(benzylthio)-2-phenylacetyl)-2,2,2-trifluoroaceto-hydrazide (**27b**)



[368.37]

2-(Benzylthio)-2-phenylacetohydrazide (**30b**) (1.81 g, 6.66 mmol, 1.00 eq) was converted according to General procedure 6. The crude product was purified by flash column chromatography (prepacked silica cartridge, *n*-hexane/ethyl acetate) yielding the product **27a** (681 mg, 1.85 mmol, 28%) as a white solid.

<sup>1</sup>H NMR (600 MHz, DMSO-*d*<sub>6</sub>) δ = 3.68 (d, *J* = 13.0 Hz, 1H), 3.78 (d, *J* = 13.0 Hz, 1H), 4.59 (s, 1H), 7.23 – 7.39 (m, 8H), 7.43 – 7.50 (m, 2H), 10.71 (s, 1H), 11.58 (s, 1H) ppm.

<sup>13</sup>C NMR (151 MHz, DMSO-*d*<sub>6</sub>) δ = 5.18, 50.44, 115.74 (q, *J* = 288.2 Hz), 127.09, 128.01, 128.34, 128.52, 128.91, 136.39, 137.52, 155.60 (q, *J* = 36.3 Hz), 168.21 ppm.

HPLC analysis: *R*<sub>t</sub> = 13.033 min, 96.2%.

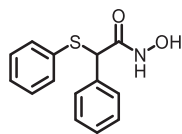
HRMS (ESI+) = calcd. for C<sub>17</sub>H<sub>16</sub>F<sub>3</sub>N<sub>2</sub>O<sub>2</sub>S [M+H]<sup>+</sup> = 369.0879, found: 369.0881.

mp.: 128.0 °C.

### General procedure 7: Formation of the hydroxamic acids

To a solution of the respective ester **14a-k**, **20a,b** and **25** (1.00 eq) and alkali metal alkoxide (15.0 eq) in MeOH or EtOH (1 mmol/mL), hydroxylamine hydrochloride (10.0 eq) was added. The reaction mixture was refluxed for 2-3 h and the solvent was then removed under reduced pressure. The residue was resuspended in 1 M aqueous HCl-solution and extracted into EtOAc (3x). The combined organic phases were dried over Na<sub>2</sub>SO<sub>4</sub>, filtered and evaporated *in vacuo*. The crude product was purified by flash chromatography (prepacked silica cartridge, CH<sub>2</sub>Cl<sub>2</sub> /15% MeOH in CH<sub>2</sub>Cl<sub>2</sub>) and a following recrystallisation (*n*-hexane/ethyl acetate) furnished the corresponding hydroxamic acids **10a-k**, **21a-b** and **26**.

### Synthesis of *N*-hydroxy-2-phenyl-2-(phenylthio)acetamide (**10a**)



[259.32]

Following the General procedure 7, ethyl 2-phenyl-2-(phenylthio)acetate (**14a**) (498 mg, 1.83 mmol, 1.00 eq), sodium ethoxide (1.95 g, 27.5 mmol, 15.0 eq) and hydroxylamine hydrochloride (1.27 g, 18.3 mmol, 10.0 eq) gave the title compound **10a** (303 mg, 1.17 mmol, 64%) as a white solid.

$^1\text{H}$  NMR (600 MHz, DMSO- $d_6$ )  $\delta$  = 4.91 (s, 1H), 7.20 – 7.25 (m, 1H), 7.26 – 7.35 (m, 7H), 7.46 – 7.50 (m, 2H), 9.05 – 9.13 (m, 1H), 10.93 (s, 1H) ppm.

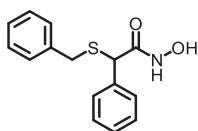
$^{13}\text{C}$  NMR (151 MHz, DMSO- $d_6$ )  $\delta$  = 52.98, 127.03, 127.89, 128.16, 128.39, 129.10, 130.11, 134.58, 137.34, 165.71 ppm.

HPLC analysis:  $R_t$  = 9.883 min, 97.9%.

HRMS (ESI+) = calcd. for  $\text{C}_{14}\text{H}_{14}\text{NO}_2\text{S}$   $[\text{M}+\text{H}]^+$  = 260.0740, found: 260.0742.

mp.: 121.7 °C.

### Synthesis of 2-(benzylthio)-*N*-hydroxy-2-phenylacetamide (**10b**)



[273.35]

Ethyl 2-(benzylthio)-2-phenylacetate (**14b**) (573 mg, 2.00 mmol, 1.00 eq), sodium ethoxide (2.13 g, 30.0 mmol, 15.0 eq) and hydroxylamine hydrochloride (1.39 g, 20.0 mmol, 10.0 eq) were converted according to General procedure 7 yielding the hydroxamic acid **10b** (119 mg, 0.44 mmol, 22%) as a white solid.

$^1\text{H}$  NMR (300 MHz, DMSO- $d_6$ )  $\delta$  = 3.53 (d,  $J$  = 13.1 Hz, 1H), 3.67 (d,  $J$  = 13.1 Hz, 1H), 4.33 (s, 1H), 7.18 – 7.39 (m, 7H), 7.41 – 7.48 (m, 2H), 9.02 (d,  $J$  = 1.5 Hz, 1H), 10.86 (d,  $J$  = 1.5 Hz, 1H) ppm.

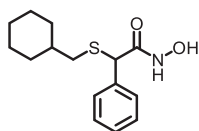
$^{13}\text{C}$  NMR (75 MHz, DMSO- $d_6$ )  $\delta$  = 35.01, 49.87, 126.84, 127.53, 128.15, 128.18, 128.32, 128.65, 137.41, 137.62, 166.00 ppm.

HPLC analysis:  $R_t$  = 10.383 min, >99%.

HRMS (ESI+) = calcd. for C<sub>15</sub>H<sub>16</sub>NO<sub>2</sub>S [M+H]<sup>+</sup> = 274.0896, found: 274.0899.

mp.: 134.5 °C.

### Synthesis of 2-((cyclohexylmethyl)thio)-*N*-hydroxy-2-phenylacetamide (**10c**)



[265.38]

Following the General procedure 7, ethyl 2-((cyclohexylmethyl)thio)-2-phenylacetate (**14c**) (557 mg, 2.00 mmol, 1.00 eq), sodium ethoxide (2.13 g, 30.0 mmol, 15.0 eq) and hydroxylamine hydrochloride (1.39 g, 20.0 mmol, 10.0 eq) afforded the title compound **10c** (244 mg, 0.92 mmol, 46%) as a white solid.

<sup>1</sup>H NMR (300 MHz, DMSO-*d*<sub>6</sub>) δ = 1.23 (q, *J* = 9.2, 7.4 Hz, 5H), 1.42 – 2.01 (m, 5H), 2.56 (q, *J* = 4.1 Hz, 1H), 4.48 (s, 1H), 7.15 – 7.37 (m, 3H), 7.39 – 7.55 (m, 2H), 9.01 (d, *J* = 1.6 Hz, 1H), 10.83 (d, *J* = 1.6 Hz, 1H) ppm.

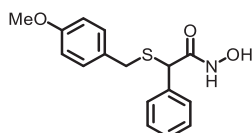
<sup>13</sup>C NMR (75 MHz, DMSO-*d*<sub>6</sub>) δ = 25.18, 32.80, 32.97, 43.02, 48.40, 127.31, 128.04, 138.33, 166.56 ppm.

HPLC analysis: R<sub>t</sub> = 10.983 min, >99.9%.

HRMS (ESI+) = calcd. for C<sub>14</sub>H<sub>20</sub>NO<sub>2</sub>S [M+H]<sup>+</sup> = 266.1209, found: 266.1211.

mp.: 137.1 °C.

### Synthesis of *N*-hydroxy-2-((4-methoxybenzyl)thio)-2-phenylacetamide (**10d**)



[303.38]

Following the General procedure 7, ethyl 2-((4-methoxybenzyl)thio)-2-phenylacetate (**14d**) (633 mg, 2.00 mmol, 1.00 eq), sodium ethoxide (2.13 g, 30.0 mmol, 15.0 eq) and hydroxylamine hydrochloride (1.39 g, 20.0 mmol, 10.0 eq) afforded the title compound **10d** (177 mg, 0.58 mmol, 29%) as a white solid.

$^1\text{H}$  NMR (300 MHz,  $\text{DMSO-}d_6$ )  $\delta$  = 3.41 – 3.66 (m, 2H), 3.73 (s, 3H), 4.30 (s, 1H), 6.77 – 6.93 (m, 2H), 7.09 – 7.22 (m, 2H), 7.25 – 7.52 (m, 5H), 9.01 (s, 1H), 10.84 (s, 1H) ppm.

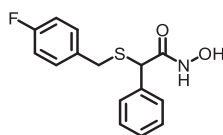
$^{13}\text{C}$  NMR (75 MHz,  $\text{DMSO-}d_6$ )  $\delta$  = 34.43, 49.79, 54.98, 113.79, 127.48, 128.13, 128.17, 129.32, 129.78, 137.49, 158.20, 166.06 ppm.

HPLC analysis:  $R_t$  = 10.367 min, >99%.

HRMS (ESI+) = calcd. for  $\text{C}_{16}\text{H}_{18}\text{NO}_3\text{S}$   $[\text{M}+\text{H}]^+$  = 304.1002, found: 304.1001.

mp.: 128.5 °C.

### Synthesis of 2-((4-fluorobenzyl)thio)-*N*-hydroxy-2-phenylacetamide (10e)



[291.35]

Ethyl 2-((4-fluorobenzyl)thio)-2-phenylacetate (**14e**) (457 mg, 1.50 mmol, 1.00 eq), sodium ethoxide (1.60 g, 22.5 mmol, 15.0 eq) and hydroxylamine hydrochloride (1.04 g, 15.0 mmol, 10.0 eq) were subjected to General procedure 7 yielding the hydroxamic acid **10e** (98.0 mg, 0.34 mmol, 22%) as a white solid.

$^1\text{H}$  NMR (300 MHz,  $\text{DMSO-}d_6$ )  $\delta$  = 3.47 – 3.75 (m, 2H), 4.29 (s, 1H), 7.05 – 7.55 (m, 9H), 9.02 (d,  $J$  = 1.2 Hz, 1H), 10.81 – 10.91 (m, 1H) ppm.

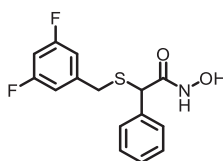
$^{13}\text{C}$  NMR (151 MHz,  $\text{DMSO-}d_6$ )  $\delta$  = 34.21, 49.78, 115.23 (d,  $J$  = 21.3 Hz), 127.74, 128.31 (d,  $J$  = 6.6 Hz), 130.71 (d,  $J$  = 8.1 Hz), 133.99, 134.01, 137.44, 160.40, 162.01, 166.05 ppm.

HPLC analysis:  $R_t$  = 10.683 min, >99.9%.

HRMS (ESI+) = calcd. for  $\text{C}_{15}\text{H}_{15}\text{FN O}_2\text{S}$   $[\text{M}+\text{H}]^+$  = 292.0802, found: 292.0801.

mp.: 136.6 °C.

### Synthesis of 2-((3,5-difluorobenzyl)thio)-*N*-hydroxy-2-phenylacetamide (10f)



[309.34]

Following the General procedure 7, ethyl 2-((3,5-difluorobenzyl)thio)-2-phenylacetate (**14f**) (645 mg, 2.00 mmol, 1.00 eq), sodium ethoxide (2.13 g, 30.0 mmol, 15.0 eq) and hydroxylamine hydrochloride (1.39 g, 20.0 mmol, 10.0 eq) gave the title compound **10f** (302 mg, 0.98 mmol, 49%) as a white solid.

$^1\text{H}$  NMR (300 MHz, DMSO- $d_6$ )  $\delta$  = 3.51 – 3.78 (m, 2H), 4.30 (s, 1H), 6.88 – 6.99 (m, 2H), 7.10 (tt,  $J$  = 9.4, 2.4 Hz, 1H), 7.24 – 7.38 (m, 3H), 7.39 – 7.48 (m, 2H), 9.04 (s, 1H), 10.86 (s, 1H) ppm.

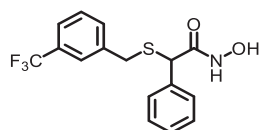
$^{13}\text{C}$  NMR (75 MHz, DMSO- $d_6$ )  $\delta$  = 34.30, 34.33, 34.36, 102.30 (t,  $J$  = 25.8 Hz), 111.73 (d,  $J$  = 24.9 Hz), 111.73 (d,  $J$  = 9.1 Hz), 127.62, 128.15, 128.18, 137.21, 142.72 (t,  $J$  = 9.3 Hz), 160.50 (d,  $J$  = 13.4 Hz), 163.76 (d,  $J$  = 13.3 Hz), 165.82 ppm.

HPLC analysis:  $R_t$  = 11.117 min, >99.9%.

HRMS (ESI+) = calcd. for  $\text{C}_{15}\text{H}_{14}\text{F}_2\text{NO}_2\text{S}$   $[\text{M}+\text{H}]^+$  = 310.0708, found: 310.0711.

mp.: 124.0 °C.

#### Synthesis of *N*-hydroxy-2-phenyl-2-((3-(trifluoromethyl)benzyl)thio)-acetamide (**10g**)



[341.35]

Ethyl 2-phenyl-2-((3-(trifluoromethyl)benzyl)thio)acetate (**14g**) (709 mg, 2.00 mmol, 1.00 eq), sodium ethoxide (2.13 g, 30.0 mmol, 15.0 eq) and hydroxylamine hydrochloride (1.39 g, 20.0 mmol, 10.0 eq) were subjected to General procedure 7 providing the hydroxamic acid **10g** (252 mg, 0.74 mmol, 37%) as a white solid.

$^1\text{H}$  NMR (300 MHz, DMSO- $d_6$ )  $\delta$  = 3.57 – 3.89 (m, 2H), 4.31 (s, 1H), 7.22 – 7.37 (m, 3H), 7.36 – 7.47 (m, 2H), 7.49 – 7.65 (m, 4H), 9.03 (s, 1H), 10.86 (s, 1H) ppm.

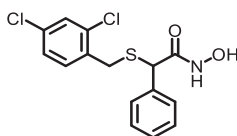
$^{13}\text{C}$  NMR (75 MHz, DMSO- $d_6$ )  $\delta$  = 34.49, 49.95, 123.56 (q,  $J$  = 3.9 Hz), 124.05 (d,  $J$  = 272.3 Hz), 125.12 (q,  $J$  = 3.9 Hz), 127.60, 128.16, 128.87, 129.36, 132.75, 132.77, 137.26, 139.43, 165.89 ppm.

HPLC analysis:  $R_t$  = 12.083 min, >99.9%.

HRMS (ESI+) = calcd. for  $\text{C}_{16}\text{H}_{15}\text{F}_3\text{NO}_2\text{S}$   $[\text{M}+\text{H}]^+$  = 342.0770, found: 342.0770.

mp.: 118.4 °C.

### Synthesis of 2-((2,4-dichlorobenzyl)thio)-*N*-hydroxy-2-phenylacetamide (**10h**)



[342.25]

Ethyl 2-((2,4-dichlorobenzyl)thio)-2-phenylacetate (**14h**) (711 mg, 2.00 mmol, 1.00 eq), sodium ethoxide (2.13 g, 30.0 mmol, 15.0 eq) and hydroxylamine hydrochloride (1.39 g, 20.0 mmol, 10.0 eq) were subjected to General procedure 7 yielding the hydroxamic acid **10h** (240 mg, 0.70 mmol, 35%) as a white solid.

$^1\text{H}$  NMR (300 MHz, DMSO- $d_6$ )  $\delta$  = 3.59 – 3.78 (m, 2H), 4.36 (s, 1H), 7.22 – 7.40 (m, 5H), 7.41 – 7.48 (m, 2H), 7.58 (d,  $J$  = 2.0 Hz, 1H), 9.04 (s, 1H), 10.88 (s, 1H) ppm.

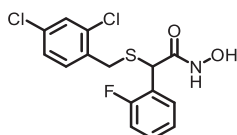
$^{13}\text{C}$  NMR (75 MHz, DMSO- $d_6$ )  $\delta$  = 32.21, 50.09, 127.27, 127.61, 128.15, 128.19, 128.81, 132.07, 132.37, 133.91, 134.54, 137.17, 165.82 ppm.

HPLC analysis:  $R_t$  = 12.650 min, 99.0%.

HRMS (ESI+) = calcd. for  $\text{C}_{15}\text{H}_{14}\text{Cl}_2\text{NO}_2\text{S}$   $[\text{M}+\text{H}]^+$  = 342.0117, found: 342.0114.

mp.: 138.3 °C.

### Synthesis of ethyl 2-((2,4-dichlorobenzyl)thio)-2-(2-fluorophenyl)acetate (**10i**)



[360.24]

Following the General procedure 7, ethyl 2-((2,4-dichlorobenzyl)thio)-2-(2-fluorophenyl)acetate (**14i**) (1.24 g, 3.32 mmol, 1.00 eq), sodium ethoxide (3.53 g, 49.8 mmol, 15.0 eq) and hydroxylamine hydrochloride (2.31 g, 33.2 mmol, 10.0 eq) afforded the title compound **10i** (484 mg, 1.34 mmol, 41%) as a white solid.

$^1\text{H}$  NMR (300 MHz, DMSO- $d_6$ )  $\delta$  = 3.65 – 3.99 (m, 2H), 4.71 (s, 1H), 7.11 – 7.22 (m, 2H), 7.30 – 7.39 (m, 3H), 7.56 (t,  $J$  = 1.3 Hz, 1H), 7.74 (td,  $J$  = 7.7, 1.8 Hz, 1H), 9.10 (d,  $J$  = 1.5 Hz, 1H), 10.99 (d,  $J$  = 1.5 Hz, 1H) ppm.

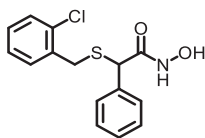
$^{13}\text{C}$  NMR (75 MHz, DMSO- $d_6$ )  $\delta$  = 32.65, 41.86 (d,  $J$  = 2.5 Hz), 114.91, 115.20, 124.02, 124.20, 124.44 (d,  $J$  = 3.5 Hz), 127.39, 128.91, 129.69 (d,  $J$  = 8.6 Hz), 130.19 (d,  $J$  = 2.9 Hz), 132.10, 132.56, 134.02, 134.31, 157.68, 160.94, 165.11 ppm.

HPLC analysis:  $R_t$  = 12.727 min, >99.9%.

HRMS (ESI+) = calcd. for C<sub>15</sub>H<sub>13</sub>Cl<sub>2</sub>FNO<sub>2</sub>S [M+H]<sup>+</sup> = 360.0023, found: 360.0019.

mp.: 126.2 °C.

### Synthesis of ethyl 2-((2-chlorobenzyl)thio)-2-phenylacetate (**10j**)



[307.80]

Following the General procedure 7, ethyl 2-((2-chlorobenzyl)thio)-2-phenylacetate (**14j**) (642 mg, 2.00 mmol, 1.00 eq), sodium ethoxide (2.13 g, 30.0 mmol, 15.0 eq) and hydroxylamine hydrochloride (1.39 g, 20.0 mmol, 10.0 eq) afforded the title compound **10j** (235 mg, 0.76 mmol, 38%) as a white solid.

<sup>1</sup>H NMR (300 MHz, DMSO-*d*<sub>6</sub>) δ = 3.70 (q, *J* = 13.2 Hz, 2H), 4.40 (s, 1H), 7.25 – 7.38 (m, 6H), 7.39 – 7.52 (m, 3H), 9.05 (d, *J* = 1.5 Hz, 1H), 10.91 (d, *J* = 1.6 Hz, 1H) ppm.

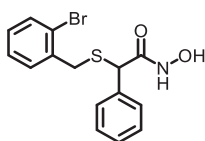
<sup>13</sup>C NMR (75 MHz, DMSO-*d*<sub>6</sub>) δ = 32.80, 50.22, 127.16, 127.61, 128.16, 128.21, 128.82, 129.39, 130.87, 132.98, 135.24, 137.28, 165.94 ppm.

HPLC analysis: *R*<sub>t</sub> = 11.183 min, 99.7%.

HRMS (ESI+) = calcd. for C<sub>15</sub>H<sub>15</sub>ClNO<sub>2</sub>S [M+H]<sup>+</sup> = 308.0507, found: 308.0510.

mp.: 139.3 °C.

### Synthesis of 2-((2-bromobenzyl)thio)-*N*-hydroxy-2-phenylacetamide (**10k**)



[352.25]

Ethyl 2-((2-bromobenzyl)thio)-2-phenylacetate (**14k**) (548 mg, 1.50 mmol, 1.00 eq), sodium ethoxide (1.60 g, 22.5 mmol, 15.0 eq) and hydroxylamine hydrochloride (1.04 g, 15.0 mmol, 10.0 eq) were subjected to General procedure 7 furnishing the hydroxamic acid **10k** (80.0 mg, 0.23 mmol, 15%) as a white solid.

$^1\text{H}$  NMR (300 MHz,  $\text{DMSO-}d_6$ )  $\delta$  = 3.61 – 3.82 (m, 2H), 4.40 (s, 1H), 7.12 – 7.42 (m, 6H), 7.47 (dt,  $J$  = 6.0, 1.6 Hz, 2H), 7.59 (dd,  $J$  = 7.9, 1.2 Hz, 1H), 9.04 (d,  $J$  = 1.5 Hz, 1H), 10.86 – 10.96 (m, 1H) ppm.

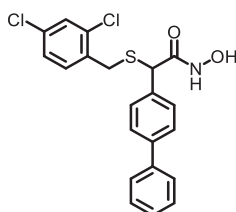
$^{13}\text{C}$  NMR (75 MHz,  $\text{DMSO-}d_6$ )  $\delta$  = 35.49, 50.21, 123.72, 127.59, 127.73, 128.15, 128.21, 129.02, 130.86, 132.68, 136.87, 137.27, 165.91 ppm.

HPLC analysis:  $R_t$  = 11.433 min, 98.2%.

HRMS (ESI+) = calcd. for  $\text{C}_{15}\text{H}_{15}\text{BrNO}_2\text{S}$   $[\text{M}+\text{H}]^+$  = 352.0001, found: 352.0000.

mp.: 138.3 °C.

### Synthesis of 2-([1,1'-biphenyl]-4-yl)-2-((2,4-dichlorobenzyl)thio)-*N*-hydroxyacetamid (**21a**)



[418.33]

Methyl 2-([1,1'-biphenyl]-4-yl)-2-((2,4-dichlorobenzyl)thio)-acetate (**20a**) (872 mg, 2.09 mmol, 1.00 eq), sodium methoxide (5.4 M in MeOH, 5.81 mL, 31.3 mmol, 15.0 eq) and hydroxylamine hydrochloride (1.45 g, 20.9 mmol, 10.0 eq) were subjected to General procedure 7 providing the hydroxamic acid **21a** (461 mg, 1.10 mmol, 53%) as a white solid.

$^1\text{H}$  NMR (300 MHz,  $\text{DMSO-}d_6$ )  $\delta$  = 3.65 – 3.83 (m, 2H), 4.43 (s, 1H), 7.29 – 7.72 (m, 12H), 9.07 (s, 1H), 10.92 (s, 1H) ppm.

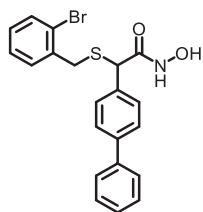
$^{13}\text{C}$  NMR (75 MHz,  $\text{DMSO-}d_6$ )  $\delta$  = 32.29, 49.84, 126.60, 126.66, 127.37, 127.52, 128.85, 128.92, 128.95, 132.22, 132.47, 134.02, 134.64, 136.44, 139.67, 139.69, 165.84 ppm.

HPLC analysis:  $R_t$  = 16.019 min, >99.9%.

HRMS (ESI+) = calcd. for  $\text{C}_{21}\text{H}_{17}\text{Cl}_2\text{NNaO}_2\text{S}$   $[\text{M}+\text{Na}]^+$  = 440.0249, found: 440.0249.

mp.: 140.9 °C.

### Synthesis of 2-([1,1'-biphenyl]-4-yl)-2-((2-bromobenzyl)thio)-*N*-hydroxy-acetamide (**21b**)



[428.34]

Following the General procedure 7, methyl 2-([1,1'-biphenyl]-4-yl)-2-((2-bromobenzyl)thio)acetate (**20b**) (1.41 g, 3.31 mmol, 1.00 eq), sodium methoxide (5.4 M in MeOH, 9.18 mL, 49.6 mmol, 15.0 eq) and hydroxylamine hydrochloride (2.30 g, 33.1 mmol, 10.0 eq) gave the title compound **21b** (483 mg, 1.13 mmol, 34%) as a white solid.

$^1\text{H}$  NMR (600 MHz, DMSO- $d_6$ )  $\delta$  = 3.68 – 3.80 (m, 2H), 4.46 (s, 1H), 7.20 (ddd,  $J$  = 7.6, 5.2, 3.7 Hz, 1H), 7.30 – 7.40 (m, 3H), 7.41 – 7.50 (m, 2H), 7.53 – 7.71 (m, 7H), 9.07 (s, 1H), 10.94 (s, 1H) ppm.

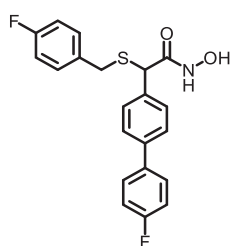
$^{13}\text{C}$  NMR (151 MHz, DMSO- $d_6$ )  $\delta$  = 35.57, 49.95, 123.88, 126.63, 126.66, 127.53, 127.86, 128.90, 128.95, 129.18, 131.01, 132.84, 136.54, 136.98, 139.63, 139.69, 165.93 ppm.

HPLC analysis:  $R_t$  = 14.821 min, >99.9%.

HRMS (ESI+) = calcd. for  $\text{C}_{21}\text{H}_{19}\text{BrNO}_2\text{S}$  [ $\text{M}+\text{H}$ ] $^+$  = 428.0314, found: 428.0312.

mp.: 144.7 °C.

### Synthesis of 2-(4'-fluoro-[1,1'-biphenyl]-4-yl)-2-((4-fluorobenzyl)thio)-*N*-hydroxy-acetamide (**26**)



[385.43]

Following the General procedure 7, methyl 2-(4'-fluoro-[1,1'-biphenyl]-4-yl)-2-((4-fluorobenzyl)thio)acetate (**25**) (384 mg, 1.00 mmol, 1.00 eq), sodium methoxide (5.4 M in MeOH, 2.78 mL, 15.0 mmol, 15.0 eq) and hydroxylamine hydrochloride (695 mg, 10.0 mmol, 10.0 eq) yielded the title compound **26** (210 mg, 0.55 mmol, 55%) as a white solid.

$^1\text{H}$  NMR (300 MHz,  $\text{DMSO-}d_6$ )  $\delta$  = 3.49 – 3.77 (m, 2H), 4.34 (s, 1H), 7.04 – 7.18 (m, 2H), 7.29 (ddd,  $J$  = 8.9, 7.3, 1.8 Hz, 4H), 7.48 – 7.56 (m, 2H), 7.55 – 7.66 (m, 2H), 7.67 – 7.78 (m, 2H), 9.06 (s, 1H), 10.88 (s, 1H) ppm.

$^{13}\text{C}$  NMR (75 MHz,  $\text{DMSO-}d_6$ )  $\delta$  = 34.26, 49.50, 115.51 (dd,  $J$  = 39.1, 21.3 Hz), 126.62, 128.68 (d,  $J$  = 8.2 Hz), 128.90, 130.76 (d,  $J$  = 8.2 Hz), 134.01 (d,  $J$  = 3.0 Hz), 136.20 (d,  $J$  = 3.0 Hz), 136.65, 138.59, 159.98 (d,  $J$  = 53.2 Hz), 163.21 (d,  $J$  = 54.8 Hz), 166.01 ppm.

HPLC analysis:  $R_t$  = 14.203 min, 98.8%.

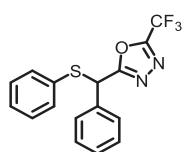
HRMS (ESI+) = calcd. for  $\text{C}_{21}\text{H}_{18}\text{F}_2\text{NO}_2\text{S}$   $[\text{M}+\text{H}]^+$  = 386.1021, found: 386.1015.

mp.: 144.8 °C.

### General procedure 8: Cyclisation

Following the procedure of Lee et al.,<sup>[3]</sup> a solution of the respective *N*-acyl hydrazide **27a-b** (1.00 eq) and methyl *N*-(triethylammoniumsulfonyl)carbamate (Burgess reagent, 1.50 eq) in THF (0.05 mmol/mL) was refluxed for 8 h. The reaction mixture was then concentrated under reduced pressure and the residue was resuspended in water. The aqueous layer was extracted with  $\text{CH}_2\text{Cl}_2$  (3x). The combined organic phases were dried over  $\text{Na}_2\text{SO}_4$ , filtered and evaporated *in vacuo*. The crude product was purified by flash chromatography (prepacked silica cartridge, *n*-hexane/ethyl acetate) yielding the products **28a-b**.

### Synthesis of 2-(phenyl(phenylthio)methyl)-5-(trifluoromethyl)-1,3,4-oxadiazole (28a)



[336.34]

Following the General procedure 8, 2,2,2-trifluoro-*N'*-(2-phenyl-2-(phenylthio)acetyl)-acetohydrazide (**27a**) (262 mg, 0.74 mmol, 1.00 eq) and the Burgess-reagent (273 mg, 1.11 mmol, 1.50 eq) yielded the title compound **28a** (151 mg, 0.45 mmol, 61%) as a white solid.

$^1\text{H}$  NMR (600 MHz,  $\text{DMSO-}d_6$ )  $\delta$  = 6.36 (s, 1H), 7.27 – 7.50 (m, 9H), 7.55 – 7.63 (m, 2H) ppm.

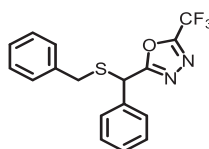
$^{13}\text{C}$  NMR (151 MHz,  $\text{DMSO-}d_6$ )  $\delta$  = 40.06, 45.85, 115.93 (q,  $J$  = 271.3 Hz), 128.65, 128.71, 128.76, 128.79, 128.82, 128.88, 129.23, 131.55, 132.91, 134.40, 154.49 (q,  $J$  = 43.6 Hz), 167.85 ppm.

HPLC analysis:  $R_t = 16.338$  min, >99.9%.

HRMS (ESI+) = calcd. for  $C_{16}H_{12}F_3N_2O_2S$   $[M+H]^+ = 337.0617$ , found: 337.0620.

mp.: 51.2 °C.

### Synthesis of *N'*-(2-(benzylthio)-2-phenylacetyl)-2,2,2-trifluoroaceto-hydrazide (**28b**)



[350.36]

*N'*-(2-(benzylthio)-2-phenylacetyl)-2,2,2-trifluoroaceto-hydrazide (**20b**) (386 mg, 1.00 mmol, 1.00 eq) and the Burgess-reagent (273 mg, 1.11 mmol, 1.50 eq) were subjected to General procedure 8 providing the product **28b** (203 mg, 0.58 mmol, 58%) as a yellowish oil.

$^1H$  NMR (300 MHz,  $DMSO-d_6$ )  $\delta = 3.93$  (d,  $J = 0.9$  Hz, 2H), 5.75 (s, 1H), 7.19 – 7.33 (m, 5H), 7.33 – 7.53 (m, 5H) ppm.

$^{13}C$  NMR (151 MHz,  $DMSO-d_6$ )  $\delta = 36.09, 42.72, 115.95$  (d,  $J = 271.3$  Hz), 127.16, 128.29, 128.46, 128.51, 128.61, 128.77, 129.01, 135.06, 136.88, 153.98 – 154.97 (m), 168.09 ppm.

HPLC analysis:  $R_t = 16.600$  min, 95.7%.

HRMS (ESI+) = calcd. for  $C_{17}H_{14}F_3N_2O_2S$   $[M+H]^+ = 351.0773$ , found: 351.0773.

## References

- [1] A. Lu, X. Ji, B. Zhou, Z. Wu, Y. Zhang, *Angew. Chemie - Int. Ed.* **2018**, *57*, 3233–3237.
- [2] N. Inguibert, P. Coric, H. Poras, H. Meudal, F. Teffot, M. C. Fournié-Zaluski, B. P. Roques, *J. Med. Chem.* **2002**, *45*, 1477–1486.
- [3] J. Lee, Y. Han, Y. Kim, J. Min, M. Bae, D. Kim, S. Jin, J. Kyung, *1,3,4-Oxadiazole Sulfamide Derivative Compounds as Histone Deacetylase 6 Inhibitor, and the Pharmaceutical Composition Comprising the Same*, **2018**, US2018/0230113 A1.

## **Alkoxyamide-based TFMO-derivatives: Potent and Selective Class IIa Histone Deacetylase Inhibitors**

Unpublished

Contribution:

- Synthesis of the compounds **2a-c**, **3a-g**, **4**, **5**, **6a-f**, **9**, **10**, **14**, **15** and **20a-f**
- Manuscript and supporting information

**Alkoxyamide-based TFMO-derivatives:  
Potent and Selective  
Class IIa Histone Deacetylase Inhibitors**

*Yodita Asfaha<sup>\*#</sup>, Alexander Jan Skerhut<sup>\*#</sup>, Leandro A. Alves-Avelar<sup>\*</sup>, Nadine Horstick-Muche<sup>\*</sup>, Matthias U. Kassack<sup>\*#</sup>, Thomas Kurz<sup>\*#</sup>*

\*Institut für Pharmazeutische und Medizinische Chemie, Heinrich-Heine-Universität Düsseldorf, Universitätsstr. 1, 40225 Düsseldorf, Germany. # YA and AJS share first authorship, MUK and TK share senior and corresponding authorship.

.

## Abstract

Histone deacetylases (HDACs) are clinically validated targets for the treatment of cancer. However, resistances to the currently approved HDAC inhibitors (HDACi) are often detected and they suffer from severe side effects such as cardiac toxicity or neutropenia and their limited therapeutic efficacy against solid tumors as single therapeutic agents. In regard to the distinct tissue distribution and cellular localization of individual HDACs as well as their various implication in different cancer types, isozyme-selective HDACi may overcome these limitations. The therapeutic advantages of isozyme-selective HDACs are not yet clinically confirmed and are still matter of current research. Here, we report the synthesis and biological evaluation of *meta*- and *para*-substituted TFMO-derivatives **2a-c** and **3a-g** exhibiting an alkoxyamide moiety as connecting unit. We have designed and synthesized the five potent and selective HDAC4 inhibitors **3a-e** with an HDAC4 inhibitory activity in the nanomolar range. The most potent and selective HDAC4 inhibitors was the *para*-substituted oxazole compound **3a** ( $IC_{50}(\text{HDAC4}) = 0.12 \mu\text{M}$ ) with a more than 800-fold selectivity over HDAC2/6/8. Furthermore, the class IIa HDAC selective inhibitor **3a** displayed a 115-fold stronger HDAC4 inhibition than the lead structure TMP269. Although **3a** was less potent than CHDI-00390576, it demonstrated a 14-/3-fold higher HDAC6/HDAC4 and HDAC8/HDAC4 selectivity indices than CHDI-00390576.

## 1. Introduction

Histone deacetylases (HDACs) regulate numerous cellular processes, including cell cycle progression, differentiation, and apoptosis.<sup>[1,2]</sup> It has been demonstrated that nuclear HDACs promote transcriptional repression and gene silencing<sup>[3,4]</sup> However, non-histone proteins (cell receptors, chaperones, and cytoskeletal proteins) are also addressed by HDACs.<sup>[5]</sup> So far, 11 human zinc-dependent HDACs have been identified and are categorized into three classes based on their homology to yeast deacetylases: Class I (HDACs 1-3, 8), class II (IIa: HDACs 4, 5, 7, 9; IIb: HDACs 6, 10) and class IV (HDAC 11).<sup>[6]</sup> Class IIa Histone deacetylases (HDAC4, 5, 7, 9) were discovered in the early 2000s.<sup>[7-14]</sup> Class IIa HDACs possess unique features that distinguish them from the other classes as

they do not “erase” acetylated lysins and are rarely associate with histone tails.<sup>[15–17]</sup> These enzymes contain a well-conserved extended *N*-terminus which bears multiple bindings sites for various transcription factors such as MEF2, SRF, and Runx2.<sup>[11,14,18–20]</sup> The *N*-terminal domain exhibits also conserved serine residues that undergo signal-dependent phosphorylation. When class IIa HDACs are unphosphorylated they are located in the nucleus. Their transcriptional repressive activity is proposed to be a result of their interaction either with transcription factors or with class I HDAC enzymes. However, these interactions are disrupted if class IIa HDACs are phosphorylated in response to specific signals e.g. activation of CaMK, PDK, and MARK kinases via extracellular stimuli. This stimulates their export to the cytoplasm and a derepression of their targets occurs.<sup>[21]</sup> One of the most important features of this class is their tissue-specific expression pattern (cardiovascular, musculoskeletal, nervous and immune system), where they have essential roles in cell development and differentiation. Compared to class I HDACs, the catalytic activity of class IIa HDACs is intrinsically much lower (approx.1000 fold) due to a Tyr to His switch in their active site.<sup>[15,16,22]</sup> The mechanisms regulating class IIa HDACs functions in health and disease remains insufficiently understood. The prevailing hypothesis is that the catalytic domain serves as a recognition domain for the interaction with *N*-acetyl lysine residues of various proteins.<sup>[23,24]</sup> Class IIa HDACs are potential targets for the treatment of cardiovascular diseases, viral infections, diabetes, neurodegenerative disease, and cancer. <sup>[25–29]</sup> The molecular mechanism and therapeutic potential of class IIa HDACs could be elucidated by the employment of potent and selective class IIa HDAC inhibitors (HDACi). In published crystal structures of class IIa HDACs, the so-called lower pocket was revealed as a structural feature in the catalytic domain of this class. <sup>[30,31]</sup> The pharmacophore model for class IIa selective HDACi contains the following four elements: a zinc-binding group (ZBG), a linker that interacts with the substrate-binding tunnel, a lower pocket group (LP-group) that occupies the selectivity pocket and a cap, also known as surface recognition domain.<sup>[32]</sup> In 2013, Lobera *et al.* and Novartis discovered simultaneously class IIa selective HDACi, revealing a trifluoromethyloxadiazolyl moiety (TFMO) as a novel ZBG. Lobera *et al.* demonstrated that inhibitors that exhibit this novel ZBG showed an up to 10,000-fold higher selectivity towards class IIa HDACs compared to their corresponding hydroxamates.<sup>[30]</sup> A

crystallographic analysis confirmed that the TFMO group acts as a non-chelating ZBG via the coordination of the fluorine atoms and its oxygen to the zinc ion in the catalytic center. It is proposed that their class IIa selectivity arises from the bulkiness but modest zinc-binding ability of the TFMO moiety as well as the *U*-shaped conformation of these inhibitors. Lobera *et al.* reported that the TFMO-based HDACi display an improved pharmacokinetic profile compared to hydroxamates.<sup>[30]</sup> Furthermore, it is presumed that the TFMO series has fewer pan-inhibitor associated off-targets effects.

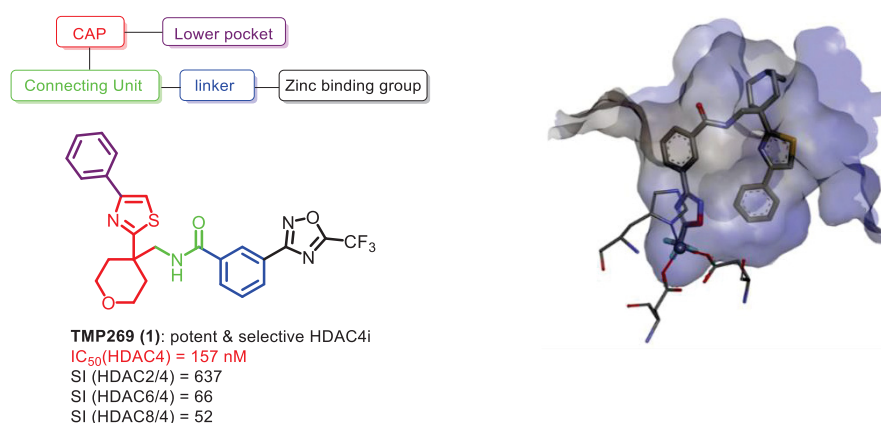


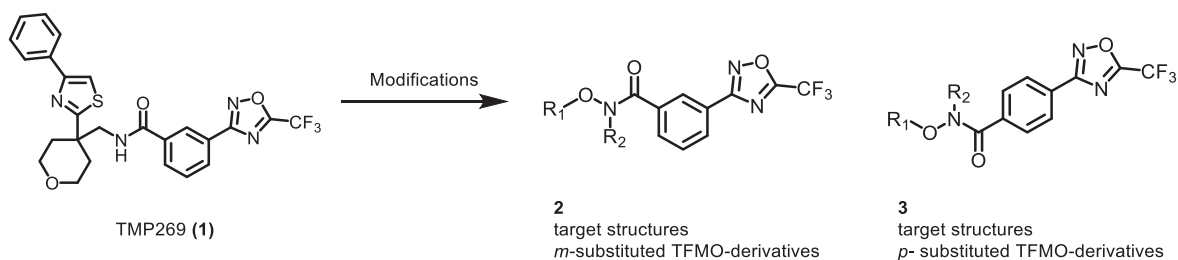
Figure 1: Pharmacophore model of class IIa HDAC inhibitors. Chemical structure of TMP269 (**1**). Binding mode of TMP269 (**1**) in the binding pocket of HDAC7 (PDB:3ZNR).<sup>[30]</sup>

Here, we report the synthesis and biological evaluation of *meta*- and *para*-substituted TFMO-derivatives exhibiting an alkoxyamide moiety as a connecting unit.

## 2. Results and Discussion

### 2.1 Rational design

Our aim was to design selective HDAC class IIa inhibitors by using selectivity directing ZBGs like the 5-trifluoromethyl-1,2,4-oxadiazole (TFMO) moiety. The lead structure TMP269 (**1**) was modified in its connecting unit (CU) and its cap region to deduce structure-activity relationships (Scheme 1).



Scheme 1: Modification of TMP269 (**1**) in its CU and its cap region.

In order to assess the HDAC isozyme selectivity profile of TFMO-derivatives exhibiting an alkoxyamide as CU, we performed an *in-silico* screening with *N*-((2-phenyloxazol-4-yl)methoxy)-3-(5-(trifluoromethyl)-1,2,4-oxadiazol-3-yl)benzamide (**2a**) and its *para* derivative **3a** as target structures. The compounds were docked in HDAC7 (PDB:3ZNR)<sup>[30]</sup> using AutoDock Vina and further superimposed with the co-crystallized ligand TMP269 (**1**) (Figure 2).

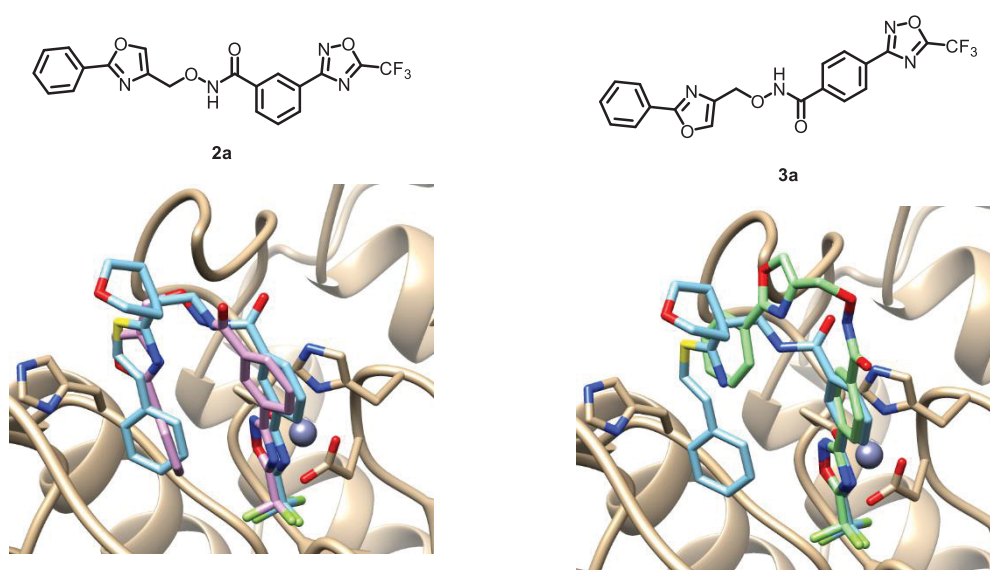
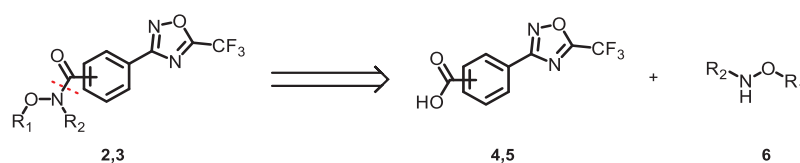


Figure 2: Superposition of **2a** (purple, left) and its *para*-derivative **3a** (right) with TMP269 (**1**) (cyan) in HDAC7 (PDB:3ZNR).<sup>[30]</sup>

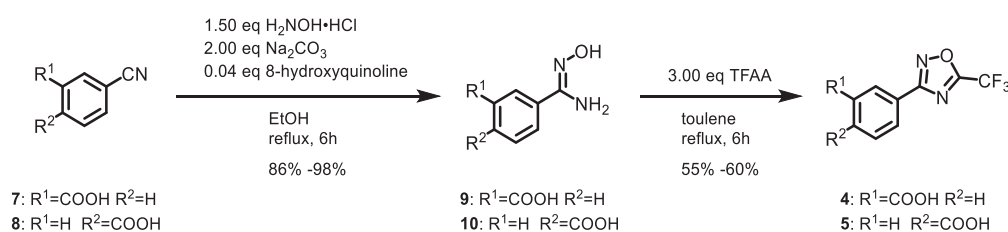
The docking results suggested that **2a** and **3a** assume a similar TFMO-zinc coordination mode to TMP269 (**1**). The preliminary docking results indicate a U-shape conformation of the *meta*-derivative **2a** in the active site of HDAC7 and the occupation of the lower pocket with the 2-phenyloxazolyl moiety. In contrast, the *para*-substituted analog **3a** exhibits a rather J-shaped conformation. Based on this preliminary qualitative *in-silico* screening, the compounds **2a** and **3a** might display a potential class IIa HDACs inhibition. Here, we report the derivatization of the proposed structures **2a** and **3a** in order to evaluate their HDAC isozyme inhibition profile. The *meta*- and *para*-substituted TFMO-derivatives **2** and **3** were synthesized from the building blocks **4** or **5** and **6**.



Scheme 2: Retrosynthetic analysis of the *meta*- and *para*-substituted TFMO-derivatives **2,3**.

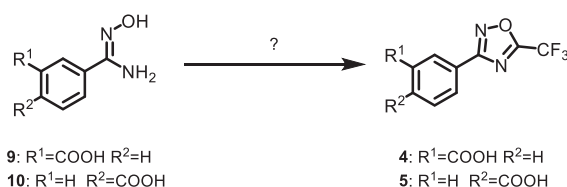
## 2.2 Chemistry

The first building blocks **4** and **5** were synthesized according to Scheme 3. Following the procedure of Lobera et al.,<sup>[30]</sup> the respective nitrile **7/8** was treated with a catalytic amount of 8-hydroxyquinoline and 2.00 eq hydroxylamine hydrochloride under basic conditions furnishing the corresponding Z-configured amidoximes **9** and **10**. The subsequent ring-closing reaction was unsuccessful applying literature procedures. Therefore, a reaction optimization was performed (Table 1). From the tested procedures, the reaction with 3.00 eq TFAA in toluene resulted in the highest yields. After recrystallisation, a yield of 60% was obtained for **4** which was 2-fold higher than the reported literature yield.



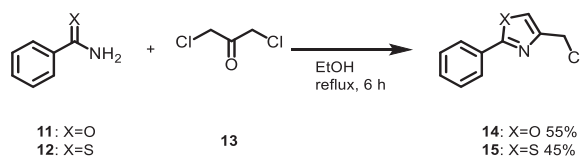
Scheme 3: Synthesis of **4** and **5**.

Table 1: Screened reaction conditions for the ring-closing reaction.



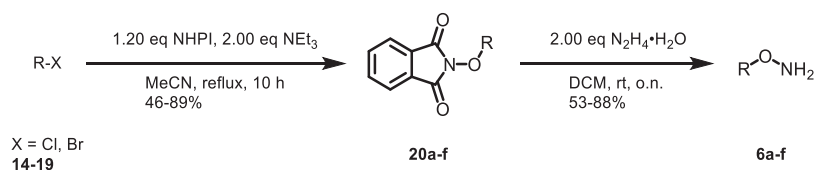
No.	Solvent	TFAA / eq	T / °C	t / h	P / Watt	Yield
<b>1</b> <sup>[30]</sup>	pyridine	3.00	50	3	-	-
<b>2</b>	pyridine	3.00	reflux	4	-	-
<b>3</b>	2.00 eq DIPEA / toluene	3.00	reflux	4	-	-
<b>4</b>	2.00 eq DIPEA / toluene	2.00	reflux	4	120	-
<b>5</b>	toluene	3.00	reflux	6	-	55-60%

The second required building blocks were the respective hydroxylamines **6a-f**. The first step of the hydroxylamine synthesis was the formation of the oxazole **14** and the thiazole **15** according to Scheme 4. The starting materials **11** and **12** were converted with 1,3-dichloroacetone (**13**) in an analogous Hantzsch-thiazole reaction providing the heterocycles **14** and **15** in moderate yields.



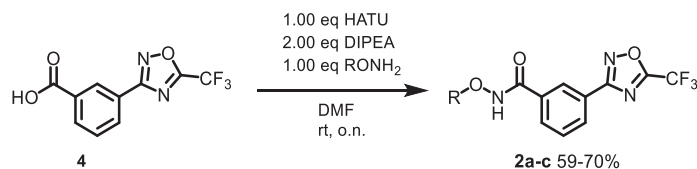
Scheme 4: Synthesis of heterocycles **14** and **15**.

The synthesized heterocycles **14** and **15** as well as the commercially available alkylating reagents **16-19** were then converted with *N*-hydroxyphthalimide (NHPI) to compounds **20a-f**. Subsequently, the deprotection was performed with 2.00 eq of hydrazine monohydrate yielding the *O*-substituted hydroxylamines **6a-f**.

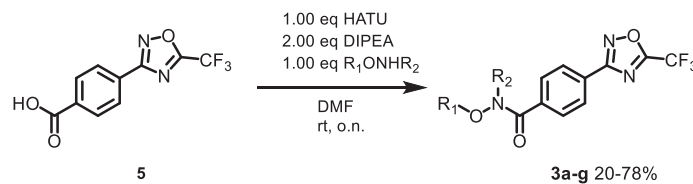


Scheme 5: Synthesis of hydroxylamines **6a-f**.

The TFMO-based HDACi **2a-c** and **3a-g** were obtained, via a HATU-mediated coupling of the respective acid **4** or **5** with the *O*-substituted hydroxylamines **6a-f**, in moderate yields (Scheme 6, Scheme 7).



Scheme 6: Synthesis of *meta*-substituted TFMO-based HDACi **2a-c**.

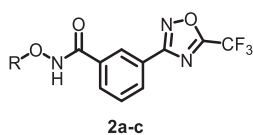


Scheme 7: Synthesis of *para*-substituted TFMO-based HDACi **3a-g**.

## 2.1 Biological Evaluation

The synthesized compounds **2a-c** and **3a-g** were assessed for their antiproliferative activity and their HDAC inhibitory activity in the human monocytic cell line THP-1 using class-distinguishing substrates (Boc-Lys(Ac)-AMC: class I and IIb HDACs; Boc-Lys(TFAc)-AMC: class IIa, HDAC8). The results are depicted in Table 2 and Table 3 with CHDI-00390576 and TMP269 as reference compounds. Among the tested compounds **2a-c**, the *meta*-substituted TFMO-derivative **2a** exhibited the strongest antiproliferative activity with 51.6% of growth inhibition at 100  $\mu$ M concentration. The modification of **2a** with a thiazolyl (**2b**) and a biphenyl moiety (**2c**) led to a decreased cytotoxicity with antiproliferative effects below 34% at 100  $\mu$ M. In comparison, the *para*-substituted TFMO-derivatives **3a-f** displayed moderate antiproliferative activities between 44.5 – 50.8% at 100  $\mu$ M. Interestingly, the introduction of the propylbenzyl moiety (**3g**) in the CAP region led to a significantly diminished cytotoxicity with an antiproliferative effect of 6.9% at 100  $\mu$ M. In the performed whole-cell HDAC inhibition assay using the Boc-Lys(Ac)-AMC-HDAC substrate, the *meta*-substituted TFMO derivatives **2a-c** revealed weak cellular HDAC inhibition below 6% at 100  $\mu$ M. Among the *para*-substituted TFMO-derivatives **3a-g**, the piperidine derivative **3b** exhibited the most pronounced HDAC inhibition with an inhibitory activity of 70% at 100  $\mu$ M. The cellular HDAC inhibition assay with the Boc-Lys(TFAc)-AMC-HDAC substrate identified the *para*-substituted TFMO-compounds, **3b** and **3c**, as the most potent inhibitors with a cellular HDAC inhibition in the nanomolar range. Both compounds, **3b** and **3c**, displayed a stronger cellular HDAC inhibition than the lead structure TMP269. However, the reference compound CHDI-00390576 demonstrated a more pronounced cellular HDAC inhibition than the compounds **3b** and **3c**. To sum up, the *para*-substituted TFMO-derivatives **3a-g** displayed stronger HDAC inhibitory activities (using the Boc-Lys(TFAc)-AMC-HDAC substrate) (69-100% at 100  $\mu$ M) than the corresponding *meta*-substituted compounds **2a-c** (below 38% at 100  $\mu$ M).

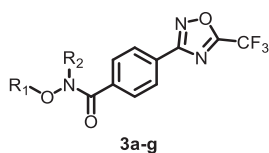
Table 2: Cell viability (MTT assay) and whole-cell HDAC inhibition assay in the human monocytic cell line THP-1.



Cpd.	R	cell viability (MTT)		HDAC inhibition			
		% inhibition of 100 $\mu$ M	IC <sub>50</sub> [ $\mu$ M] (pIC <sub>50</sub> $\pm$ SEM)	% inhibition of 100 $\mu$ M	IC <sub>50</sub> [ $\mu$ M] (pIC <sub>50</sub> $\pm$ SEM)	% inhibition of 100 $\mu$ M	IC <sub>50</sub> [ $\mu$ M] (pIC <sub>50</sub> $\pm$ SEM)
2a		51.6%	95.84 (4.02 $\pm$ 60.94)	n.a.	n.d.	38%	n.d.
2b		29.8%	n.d.	6%	n.d.	33%	n.d.
2c		34.0%	n.d.	n.a.	n.d.	13%	n.d.
	CHDI-00390576	100%	30.4 (4.52 $\pm$ 0.04)	42%	n.d.	100%	(7.69 $\pm$ 0.10)
	TMP269	70%	58.54 (4.23 $\pm$ 0.039)	13%	n.d.	39%	n.d.

Presented data are calculated from at least two experiments each performed in duplicates. IC<sub>50</sub> values were calculated for compounds with an inhibition of more than 50 %. Standard deviation of percent inhibition values is less than 14 %. Vehicle control was defined as 0 % inhibition. n.d. = not determined. n.a. = not active.

Table 3: Cell viability (MTT assay) and whole-cell HDAC inhibition assay in the human monocytic cell line THP-1.



Cpd.	R <sub>1</sub>	R <sub>2</sub>	cell viability (MTT)		HDAC inhibition			
			% inhibition of 100 μM	IC <sub>50</sub> [μM] (pIC <sub>50</sub> ± SEM)	Boc-Lys(Ac)-AMC		Boc-Lys(TFAc)-AMC	
					% inhibition of 100 μM	IC <sub>50</sub> [μM] (pIC <sub>50</sub> ± SEM)	% inhibition of 100 μM	IC <sub>50</sub> [μM] (pIC <sub>50</sub> ± SEM)
<b>3a</b>	H		46.9%	n.d.	n.a.	n.d.	76%	38.05 (4.42 ± 0.16)
<b>3b</b>	H		44.9%	n.d.	70%	36.5 (4.44 ± 0.1)	100%	0.6 (6.23 ± 0.06)
<b>3c</b>	H		46.6%	n.d.	41%	n.d.	100%	0.43 (6.37 ± 0.06)
<b>3d</b>	H		44.5%	n.d.	n.a.	n.d.	69%	33.63 (4.47 ± 0.21)
<b>3e</b>	Me		50.5%	98.72 (4.01 ± 70.04)	3%	n.d.	74%	32.11 (4.49 ± 0.11)
<b>3f</b>	H		50.8%	103.5 (3.99 ± 0.04)	14%	n.d.	91%	3.41 (5.47 ± 0.26)
<b>3g</b>	H		6.9%	n.d.	6%	n.d.	81%	33.6 (4.47 ± 0.13)
		CHDI-00390576	100%	30.4 (4.52 ± 0.04)	42%	n.d.	100%	0.02 (7.69 ± 0.10)
		TMP269	70%	58.54 (4.23 ± 0.039)	13%	n.d.	39%	n.d.

Presented data are calculated from at least two experiments each performed in duplicates. IC<sub>50</sub> values were calculated for compounds with an inhibition of more than 50 %. Standard deviation of percent inhibition values is less than 14 %. Vehicle control was defined as 0 % inhibition. n.d. = not determined. n.a. = not active.

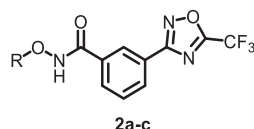
## 2.2. Inhibitory activity on HDAC2, HDAC4, HDAC6 and HDAC8

For further evaluation, the synthesized compounds **2a-c** and **3a-g** were tested against recombinant human HDAC2, HDAC4, HDAC6, and HDAC8 (Table 4 and Table 5). CHDI-00390576 and TMP269 were included as class IIa selective HDACi reference compounds. Due to the poor water-solubility of TMP269, the literature IC<sub>50</sub> values are displayed as references. Among the tested *meta*-substituted TFMO-derivatives **2a-c**, **2a** displayed an HDAC4 inhibition in the micromolar range (IC<sub>50</sub>(HDAC4) = 33.6 μM) with an approximately 3-fold preference over the other HDACs. Interestingly, the introduction of the thiazolyl moiety (**2b**) in the CAP region led to a complete loss of HDAC isozyme inhibition. The *para*-substituted TFMO-derivative **3a** displayed a 285-fold increased inhibitory activity towards HDAC4 (IC<sub>50</sub>(HDAC4) = 0.118 μM) in comparison to its *meta*-derivative **2a**. Furthermore, **3b** and **3c** have been also identified as potent HDAC4 inhibitors in the nanomolar range. However, **3a** exhibits a significantly higher HDAC4 selectivity (SI (HDAC2/HDAC4) ≥ 847, SI (HDAC6/HDAC4) ≥ 847; SI (HDAC8/HDAC4) ≥ 847) than the morpholine derivative **3c** (SI (HDAC2/HDAC4) = 299, SI (HDAC6/HDAC4) = 129; SI (HDAC8/HDAC4) = 51) as well as the piperidine derivative **3b** (SI (HDAC2/HDAC4) = 264, SI (HDAC6/HDAC4) = 104; SI (HDAC8/HDAC4) = 94). The introduction of the ethylbenzyl moiety (**3d**) in the cap region led to a slightly decreased HDAC4 isozyme inhibition (IC<sub>50</sub>(HDAC4) = 0.33 μM), but increased selectivity (SI ≥ 303 over HDAC2/6/8) over the other HDAC isozymes compared to **3b** and **3c**. Moreover, the employment of a benzyl (**3f**) and propylbenzyl group (**3g**) were not well tolerated in respect to HDAC4 inhibition, resulting in an inhibition in the low micromolar range. However, the *N*-methylated derivative **3e** was 3-fold more potent against HDAC4 than the demethylated compound **3f**.

In summary, the *para*-substituted TFMO-derivatives **3a-g** demonstrating an alkoxyamide moiety as CU showed a stronger inhibition against HDAC4 than the corresponding *meta*-substituted TFMO-derivatives **2a-c**. Compound **3a** was identified as the most potent and selective HDAC4 inhibitor. **3a** exhibited an HDAC4 inhibitory activity in the nanomolar range (IC<sub>50</sub>(HDAC4) = 0.118 μM) with an at least 847-fold higher selectivity over HDAC2/6/8. In addition, the class IIa selective inhibitor **3a** displayed a 1.3-fold stronger HDAC4 inhibition than the lead structure TMP269. Although **3a** was

less potent than CHDI-00390576, it demonstrated a 14-/3-fold higher HDAC6/HDAC4 and HDAC8/HDAC4 selectivity indices than CHDI-00390576. Due to the limited antiproliferative activity and cellular HDAC inhibition of **3a**, subject of future research will focus on the structural optimization of compound **3a** in order to improve its potency, water solubility and pharmacokinetic properties.

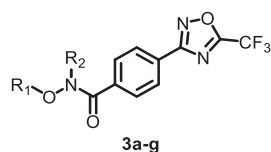
Table 4: Inhibitory activity of **2a-c**, CHDI-00390576 and TMP269 on recombinant human HDAC2, HDAC4, HDAC6 and HDAC8.



Cpd.	R	IC <sub>50</sub> [μM] (pIC <sub>50</sub> ± SEM)			
		HDAC2	HDAC4	HDAC6	HDAC8
<b>2a</b>		>100	33.6 (4.47 ± 0.05)	>100	>100
<b>2b</b>		>100	>100	>100	>100
<b>2c</b>		>100	>100	>100	>100
CHDI-00390576		>100	0.097 (7.01 ± 0.03)	5.98 (5.22 ± 0.04)	24.77 (4.61 ± 0.02)
TMP269*		>100	0.157	8.2	4.2

Data shown is at least from two experiments each performed at least as duplicates and the IC<sub>50</sub> value of pooled data is reported when IC<sub>50</sub> < 100 μM. \*Data taken from Lobera et al.<sup>[30]</sup>

Table 5: Inhibitory activity of **3a-g**, CHDI-00390576 and TMP269 on recombinant human HDAC2, HDAC4, HDAC6 and HDAC8.



Cpd.	R <sub>1</sub>	R <sub>2</sub>	IC <sub>50</sub> [μM] (pIC <sub>50</sub> ± SEM)			
			HDAC2	HDAC4	HDAC6	HDAC8
<b>3a</b>	H		>100	0.118 (6.93 ± 0.04)	>100	>100
<b>3b</b>	H		29.0 (4.54 ± 0.03)	0.11 (6.95 ± 0.03)	11.4 (4.94 ± 0.12)	10.3 (4.99 ± 0.08)
<b>3c</b>	H		41.9 (4.38 ± 0.04)	0.14 (6.85 ± 0.03)	18.12 (4.74 ± 0.069)	7.13 (5.15 ± 0.11)
<b>3d</b>	H		>100	0.33 (6.49 ± 0.04)	>100	>100
<b>3e</b>	Me		>100	0.48 (6.31 ± 0.03)	>100	>100
<b>3f</b>	H		>100	1.32 (5.88 ± 0.11)	>100	>100
<b>3g</b>	H		>100	1.80 (5.74 ± 0.04)	>100	>100
		CHDI-00390576	>100	0.097 (7.01 ± 0.03)	5.98 (5.22 ± 0.04)	24.77 (4.61 ± 0.02)
		TMP269*	>100	0.157	8.2	4.2

Data shown is at least from two experiments each performed at least as duplicates and the IC<sub>50</sub> value of pooled data is reported when IC<sub>50</sub> < 100 μM. \*Data taken from Lobera et al.<sup>[30]</sup>

### 3 Conclusions

Histone deacetylases (HDACs) are known for their capability of removing acetyl groups of conserved lysine residues from histones and nonhistone proteins. These enzymes govern numerous cellular processes, including cell cycle progression, differentiation, and apoptosis. Class IIa HDACs (HDAC4, 5, 7, and 9) have unique features that distinguish them from the other classes as they do not “erase” acetylated lysines and are rarely associated at histone tails. Recent studies revealed that class IIa enzymes are associated with neurodegenerative diseases and cancer. Only a few class IIa HDAC inhibitors have been identified due to the conserved structure of zinc-dependent HDACs. Here, we report the synthesis and biological evaluation of *meta*- and *para*-substituted TFMO-derivatives **2a-c** and **3a-g** exhibiting an alkoxy amide as a connecting unit. The *para*-substituted TFMO-derivatives **3a-g** displayed an increased HDAC4 inhibition in comparison to the corresponding *meta*-substituted TFMO-derivatives **2a-c**. We have identified five potent and selective HDAC4 inhibitors **3a-e** with an HDAC4 inhibitory activity in the high nanomolar range. The most potent and selective HDAC4 inhibitor was the *para*-substituted oxazole compound **3a** ( $IC_{50}(\text{HDAC4}) = 0.118 \mu\text{M}$ ) with a more than 800-fold higher preference over HDAC2/6/8. Furthermore, the class IIa HDAC selective inhibitor **3a** displayed a 1.3-fold stronger HDAC4 inhibition than the lead structure TMP269. Although **3a** was less potent than CHDI-00390576, it demonstrated a 14-/3-fold higher HDAC6/HDAC4 and HDAC8/HDAC4 selectivity indices than CHDI-00390576. Due to the limited antiproliferative activity and cellular HDAC inhibition of **3a**, further studies will focus on the structural optimization of **3a** in its linker and cap region to improve its potency, water solubility and metabolic stability. Further biological evaluation will investigate the combination of our class IIa selective HDACi with proteasome inhibitors in the leukemia cell lines HL-60 and RPM-8226 as well as in the human tongue squamous carcinoma cell line Cal27 and the human ovarian cancer cell line A2780.

## **Acknowledgements**

YA, AJS, MUK, and TK gratefully acknowledge support from the Deutsche Forschungsgemeinschaft (DFG) for grant number KA 1942/1-1 to MUK and grant number KU 1577/2-1 to TK, and the support from the DFG research training group 270650915/GRK 2158. We further acknowledge the CHDI Foundation Inc. for providing the compound CHDI-00390576.

## **Supplementary information**

Experimental procedures and analytical data for compounds **2a-c**, **3a-g**, **4**, **5**, **6a-f**, **9**, **10**, **14**, **15** and **20a-f** are provided as supplementary information.

## References

- [1] I. Berger, C. Bieniossek, C. Schaffitzel, M. Hassler, E. Santelli, T. J. Richmond, *J. Biol. Chem.* **2003**, *278*, 17625–17635.
- [2] M. N. Melo-Braga, M. Schulz, Q. Liu, A. Swistowski, G. Palmisano, K. Engholm-Keller, L. Jakobsen, X. Zeng, M. R. Larsen, *Mol. Cell. Proteomics* **2014**, *13*, 311–328.
- [3] W. D. Cress, E. Seto, *J. Cell. Physiol.* **2000**, *184*, 1–16.
- [4] C. M. Grozinger, S. L. Schreiber, *Chem. Biol.* **2002**, *9*, 3–16.
- [5] P. Joshi, T. M. Greco, A. J. Guise, Y. Luo, F. Yu, A. I. Nesvizhskii, I. M. Cristea, *Mol. Syst. Biol.* **2013**, *9*, 1–21.
- [6] X.-J. Yang, E. Seto, *Nat. Rev. Mol. Cell Biol.* **2008**, *9*, 206–218.
- [7] C. M. Grozinger, C. A. Hassig, S. L. Schreiber, *Proc. Natl. Acad. Sci. U. S. A.* **1999**, *96*, 4868–4873.
- [8] A. H. Wang, N. R. Bertos, M. Vezmar, N. Pelletier, M. Crosato, H. H. Heng, J. Th'ng, J. Han, X. J. Yang, *Mol. Cell. Biol.* **1999**, *19*, 7816–27.
- [9] H. Y. Kao, M. Downes, P. Ordentlich, R. M. Evans, *Genes Dev.* **2000**, *14*, 55–66.
- [10] U. Mahlknecht, S. Schnittger, J. Will, N. Cicek, D. Hoelzer, *Biochem. Biophys. Res. Commun.* **2002**, *293*, 182–191.
- [11] F. Dequiedt, H. Kasler, W. Fischle, V. Kiermer, M. Weinstein, B. G. Herndier, E. Verdin, *Immunity* **2003**, *18*, 687–98.
- [12] W. Fischle, F. Dequiedt, M. Fillion, M. J. Hendzel, W. Voelter, E. Verdin, *J. Biol. Chem.* **2001**, *276*, 35826–35835.
- [13] X. Zhou, P. A. Marks, R. A. Rifkind, V. M. Richon, *Proc. Natl. Acad. Sci. U. S. A.* **2001**, *98*, 10572–10577.
- [14] E. A. Miska, C. Karlsson, E. Langley, S. J. Nielsen, J. Pines, T. Kouzarides, *EMBO J.* **1999**, *18*, 5099–5107.
- [15] W. Fischle, F. Dequiedt, M. J. Hendzel, M. G. Guenther, M. A. Lazar, W. Voelter, E. Verdin, *Mol. Cell* **2002**, *9*, 45–57.
- [16] A. Lahm, C. Paolini, M. Pallaoro, M. C. Nardi, P. Jones, P. Neddermann, S. Sambucini, M. J. Bottomley, P. Lo Surdo, A. Carfi, et al., *Proc. Natl. Acad. Sci.* **2007**, *104*, 17335–17340.

- [17] E. Di Giorgio, E. Gagliostro, C. Brancolini, *Cell. Mol. Life Sci.* **2015**, DOI 10.1007/s00018-014-1727-8.
- [18] C. Lemerrier, A. Verdel, B. Galloo, S. Curtet, M. P. Brocard, S. Khochbin, *J. Biol. Chem.* **2000**, *275*, 15594–15599.
- [19] T. A. McKinsey, C.-L. Zhang, J. Lu, E. N. Olson, *Nature* **2000**, *408*, 106–111.
- [20] U. Dressel, P. J. Bailey, S. C. M. Wang, M. Downes, R. M. Evans, G. E. O. Muscat, *J. Biol. Chem.* **2001**, *276*, 17007–17013.
- [21] M. Parra, *FEBS J.* **2015**, *282*, 1736–1744.
- [22] P. Jones, S. Altamura, R. De Francesco, P. Gallinari, A. Lahm, P. Neddermann, M. Rowley, S. Serafini, C. Steinkühler, *Bioorganic Med. Chem. Lett.* **2008**, *18*, 1814–1819.
- [23] J. E. Bradner, N. West, M. L. Grachan, E. F. Greenberg, S. J. Haggarty, T. Warnow, R. Mazitschek, *Nat. Chem. Biol.* **2010**, *6*, 238–243.
- [24] W. Fischle, V. Kiermer, F. Dequiedt, E. Verdin, *Biochem. Cell Biol.* **2001**, *79*, 337–348.
- [25] C. L. Zhang, T. A. McKinsey, E. N. Olson, *Mol. Cell. Biol.* **2002**, *22*, 7302–7312.
- [26] A. Clocchiatti, C. Florean, C. Brancolini, *J. Cell. Mol. Med.* **2011**, *15*, 1833–1846.
- [27] K. S. Keedy, N. M. Archin, A. T. Gates, A. Espeseth, D. J. Hazuda, D. M. Margolis, *J. Virol.* **2009**, *83*, 4749–4756.
- [28] M. M. Mihaylova, D. S. Vasquez, K. Ravnskjaer, P. D. Denechaud, R. T. Yu, J. G. Alvarez, M. Downes, R. M. Evans, M. Montminy, R. J. Shaw, *Cell* **2011**, *145*, 607–621.
- [29] M. Mielcarek, C. Landles, A. Weiss, A. Bradaia, T. Seredenina, L. Inuabasi, G. F. Osborne, K. Wadel, C. Touller, R. Butler, et al., *PLoS Biol.* **2013**, *11*, e1001717.
- [30] M. Lobera, K. P. Madauss, D. T. Pohlhaus, Q. G. Wright, M. Trocha, D. R. Schmidt, E. Baloglu, R. P. Trump, M. S. Head, G. A. Hofmann, et al., *Nat. Chem. Biol.* **2013**, *9*, 319–325.
- [31] C. A. Luckhurst, P. Breccia, A. J. Stott, O. Aziz, H. L. Birch, R. W. Bürli, S. J. Hughes, R. E. Jarvis, M. Lamers, P. M. Leonard, et al., *ACS Med. Chem. Lett.* **2016**, *7*, 34–39.
- [32] J. Melesina, L. Praetorius, C. V. Simoben, D. Robaa, W. Sippl, *Future Med. Chem.* **2018**, *10*, 1537–1540.

Supporting Information

**Alkoxyamide-based TFMO-derivatives:  
Potent and Selective  
Class IIa Histone Deacetylase Inhibitors**

*Yodita Asfaha<sup>\*#</sup>, Alexander Jan Skerhut<sup>\*#</sup>, Leandro A. Alves-Avelar<sup>\*</sup>, Nadine Horstick-Muche<sup>\*</sup>,  
Matthias U. Kassack<sup>\*#</sup>, Thomas Kurz<sup>\*#</sup>*

\*Institut für Pharmazeutische und Medizinische Chemie, Heinrich-Heine-Universität  
Düsseldorf, Universitätsstr. 1, 40225 Düsseldorf, Germany. #YA and AJS share first authorship,  
MUK and TK share senior and corresponding authorship.

## Experimental section

### General methods

All chemicals and solvents were purchased from commercial suppliers (Sigma Aldrich, Alfa Aesar, Fluorochem, TCI, abcr and Acros Organics) and used without further purification. All anhydrous reactions were carried out in flame-dried Schlenk-flasks and under argon atmosphere. Dry solvents were used directly from Seal<sup>®</sup> bottles from Acros Organics. Analytic Thin Layer Chromatography (TLC) was carried out with Macherey Nagel precoated silica gel plates (ALUGRAM<sup>®</sup> Xtra SIL G/UV<sub>254</sub>). Detection was achieved with ultraviolet irradiation (254 nm) and/or staining with potassium permanganate solution (9 g KMnO<sub>4</sub>, 60 g K<sub>2</sub>CO<sub>3</sub>, 15 mL of a 5% aqueous NaOH-solution, and 900 mL demineralised water). Flash column chromatography was performed with CombiFlashRf200 (TeleDynelisco) with the solvent mixtures specified in the corresponding procedure.

### Physical data

Proton (<sup>1</sup>H) and carbon (<sup>13</sup>C) NMR spectra were recorded on Bruker Avance III – 300, Bruker Avance DRX – 500 or Bruker Avance III – 600. Spectra were referenced to the residual non-deuterated solvent signal (<sup>1</sup>H-NMR: DMSO-*d*<sub>6</sub> (2.50 ppm), <sup>13</sup>C-NMR: DMSO-*d*<sub>6</sub> (39.52 ppm); <sup>1</sup>H-NMR: CDCl<sub>3</sub> (7.26 ppm), <sup>13</sup>C-NMR: CDCl<sub>3</sub> (77.16 ppm)). Chemical shifts are quoted in parts per million (ppm). Signal patterns are indicated as: singlet (s), doublet (d), triplet (t), quartet (q), or multiplet (m). Coupling constants, *J*, are measured in Hz. Proton (<sup>1</sup>H) and carbon (<sup>13</sup>C) NMR spectra were recorded by the NMR-Divisions of the Department of Chemistry (Heinrich Heine University Duesseldorf). Electrospray Ionisation (ESI) mass spectra were carried out by the Mass spectrometry-Division of the Heinrich Heine University Duesseldorf, using Bruker Daltonics UHR-QTOF maXis 4G (Bruker Daltonics). Melting points (mp.) were determined using a Büchi M-565 melting point apparatus and are uncorrected.

Analytical HPLC analysis were carried out on a Knauer HPLC system comprising an Azura P 6.1L pump, an Optimas 800 autosampler, a Fast Scanning Spectro-Photometer K-2600 and a Knauer Reversed Phase column (SN: FK36). UV absorption was detected at 254 nm. The solvent gradient table is shown below. The purity of all final compounds was 95% or higher.

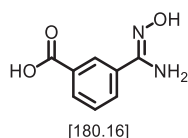
Table 1: The solvent gradient table for analytic HPLC analysis.

Time / min	Water + 0.1% TFA	ACN + 0.1% TFA
Initial	90	10
0.50	90	10
20.0	0	100
30.0	0	100
31.0	90	10
40.0	90	10

### General procedure 1: Formation of amidoxime

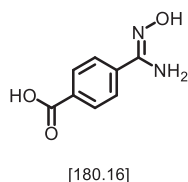
Following the procedure of Lobera et al.,<sup>[1]</sup> 1.00 eq of the respective nitrile **7,8** and 0.4 mol% 8-hydroxyquinoline were dissolved in EtOH (10 mL/mmol). To this reaction mixture, 2.00 eq hydroxylamine hydrochloride in water (2.0 mL/mmol) and 1.60 eq sodium carbonate in water (1 mL/mmol) were added. The mixture was heated at reflux for 6 h. The solvent was then removed *in vacuo*. The residue was diluted with water and the aqueous phase was acidified to pH = 3. The formed yellow precipitate was then filtered, washed with water and acetone to furnish the corresponding amidoxime **9** and **10**.

### Synthesis of 3-(*N'*-hydroxycarbamimidoyl)benzoic acid (**9**)



3-Cyanobenzoic acid (**7**) (2.94 g, 20.0 mmol, 1.00 eq) was subjected to General procedure 1. The amidoxime **9** (3.10 g, 17.2 mmol, 86%) was obtained as a white solid. All spectroscopic data were in agreement with the literature.<sup>[1]</sup>

### Synthesis of 4-(*N'*-hydroxycarbamimidoyl)benzoic acid (**10**)



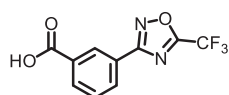
4-Cyanobenzoic acid (**8**) (4.50 g, 30.0 mmol, 1.00 eq) was subjected to General procedure 1 to provide the amidoxime **10** (4.68 g, 26.0 mmol, 87%) as a yellow solid. All spectroscopic data were in agreement with the literature.<sup>[2]</sup>

### General procedure 2: Formation of the TFMO-moiety

A solution of corresponding amidoxime **9,10** (1.00 eq) in anhydrous toluene (1 mmol/mL) was cooled to 0 °C and 3.00 eq trifluoroacetic anhydride was added dropwise. The reaction mixture was slowly allowed to warm to rt and then refluxed for further 8 h. The solvent was removed *in vacuo*, and the crude solid diluted with ethyl acetate. The organic layer was

washed with brine (3x25 mL), dried over Na<sub>2</sub>SO<sub>4</sub>, filtered and the solvent was then removed under reduced pressure. The crude product was purified by recrystallization (ethyl acetate/*n*-hexane) to yield the products **4** and **5**.

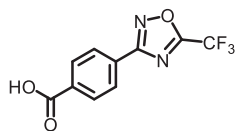
#### Synthesis of 3-(5-(trifluoromethyl)-1,2,4-oxadiazol-3-yl)benzoic acid (**4**)



[258.16]

3-(*N*'-Hydroxycarbamimidoyl)benzoic acid (**9**) (979 mg, 5.43 mmol, 1.00 eq) was subjected to General procedure 2 to furnish the product **4** (624 mg, 2.42 mmol, 45%) as a white solid. All spectroscopic data were in agreement with the literature. <sup>[1]</sup>

#### Synthesis of 4-(5-(trifluoromethyl)-1,2,4-oxadiazol-3-yl)benzoic acid (**5**)



[258.16]

4-(*N*'-hydroxycarbamimidoyl)benzoic acid (**10**) (1.80 g, 10.0 mmol, 1.00 eq) was subjected to General procedure 2 to afford 3-(5-(trifluoromethyl)-1,2,4-oxadiazol-3-yl)benzoic acid (**5**) (1.55 g, 6.00 mmol, 60%) as a white solid.

<sup>1</sup>H NMR (300 MHz, DMSO-*d*<sub>6</sub>) δ = 8.08 – 8.24 (m, 4H), 13.38 (s, 1H) ppm.

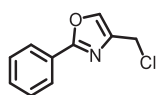
<sup>13</sup>C NMR (75 MHz, DMSO) δ = 115.65 (q), 127.56, 128.04, 130.20, 134.20, 165.47, 165.24 (q), 167.86 ppm.

HPLC analysis: *R*<sub>t</sub> = 12.483 min, 95.8%.

HRMS (ESI+) = calcd. for C<sub>12</sub>H<sub>8</sub>F<sub>3</sub>N<sub>3</sub>O<sub>3</sub> [M+ACN]<sup>+</sup> = 299.0518, found: 299.2219.

mp.: 251°C.

### Synthesis of 4-(chloromethyl)-2-phenyloxazole (**14**)



[193.63]

A mixture of benzamide (**11**) (1.82 g, 15.0 mmol, 1.00 eq) and 1,3-dichloroacetone (**13**) (3.81 g, 30.0 mmol, 2.00 eq) in toluene (80 mL) was refluxed for 6 h. The solvent was evaporated under reduced pressure and the crude product was purified by flash chromatography (prepacked silica cartridge, *n*-hexane/ethyl acetate) yielding the product **14** (1.54 g, 7.96 mmol, 53%) as a white solid.

$^1\text{H}$  NMR (300 MHz, DMSO- $d_6$ )  $\delta$  = 4.75 (d,  $J$  = 0.8 Hz, 2H), 7.51 – 7.59 (m, 3H), 7.95 – 8.03 (m, 2H), 8.27 – 8.28 (m, 1H) ppm.

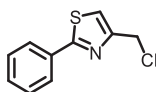
$^{13}\text{C}$  NMR (75 MHz, DMSO- $d_6$ )  $\delta$  = 37.13, 125.93, 126.44, 129.07, 130.79, 137.80, 138.26, 161.02 ppm.

HPLC analysis:  $R_t$  = 12.467 min, 99.9%.

HRMS (ESI+) = calcd. for  $\text{C}_{10}\text{H}_9\text{ClNO}$   $[\text{M}+\text{H}]^+$  = 194.0367, found: 194.0371.

mp.: 55 °C.

### Synthesis of 4-(chloromethyl)-2-phenylthiazole (**15**)



[209.69]

A mixture of thiobenzamide (**12**) (686 mg, 5.00 mmol, 1.00 eq) and 1,3-dichloroacetone (**13**) (698 mg, 5.50 mmol, 1.10 eq) in ethanol (40 mL) was refluxed for 6 h. The solvent was evaporated under reduced pressure and the residue was diluted with EtOAc, washed with saturated  $\text{NaHCO}_3$  solution (3x30 mL), dried over  $\text{Na}_2\text{SO}_4$  and filtered. After removing the solvent *in vacuo*, the crude product was purified by flash chromatography (prepacked silica cartridge, *n*-hexane/ethyl acetate) to provide the product **15** (420 mg, 2.00 mmol, 40%) as an orange oil.

$^1\text{H}$  NMR (600 MHz, DMSO- $d_6$ )  $\delta$  = 4.88 (s, 2H), 7.49 – 7.54 (m, 3H), 7.81 (s, 1H), 7.93 – 7.96 (m, 2H) ppm.

$^{13}\text{C}$  NMR (75 MHz,  $\text{DMSO-}d_6$ )  $\delta$  = 37.24, 126.01, 126.48, 129.22, 130.93, 137.96, 138.30, 161.09 ppm.

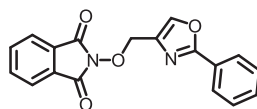
HPLC analysis:  $R_t$  = 13.833 min, 99.2%.

HRMS (ESI+) = calcd. for  $\text{C}_{10}\text{H}_9\text{ClNS}$   $[\text{M}+\text{H}]^+$  = 210.0139, found: 210.0137.

### General procedure 3: Conversion with NHPI

Following the procedure of Asfaha et al.,<sup>[3]</sup> 1.00 eq of the respective halide derivative **14-19** and 1.20 eq *N*-hydroxyphthalimide (NHPI) were dissolved in acetonitrile (4 mL/mmol). After the addition of 2.00 eq triethylamine, the resulting solution was refluxed for 12 h. The solvent was evaporated under reduced pressure and the residue was diluted with EtOAc, washed with saturated  $\text{NaHCO}_3$  solution (7x 50 mL), dried over  $\text{Na}_2\text{SO}_4$  and filtered. The solvent was removed *in vacuo* to yield the crude product which was purified as stated.

### Synthesis of 2-((2-phenyloxazol-4-yl)methoxy)isoindoline-1,3-dione (**20a**)



[320.30]

4-(Chloromethyl)-2-phenyloxazole (**14**) (395 mg, 2.42 mmol, 1.00 eq) was subjected to General procedure 3. The crude product was purified by flash chromatography (*n*-hexane/EtOAc) to provide **20a** (418 mg, 1.31 mmol, 59%) as a white solid.

$^1\text{H}$  NMR (300 MHz,  $\text{DMSO-}d_6$ )  $\delta$  = 5.15 (s, 2H), 7.47 – 7.58 (m, 3H), 7.82 – 7.93 (m, 6H), 8.40 (s, 1H) ppm.

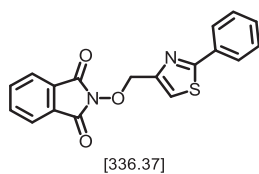
$^{13}\text{C}$  NMR (75 MHz,  $\text{DMSO-}d_6$ )  $\delta$  = 69.66, 123.14, 125.85, 126.46, 128.45, 129.02, 130.72, 134.68, 135.56, 140.17, 160.85, 162.97 ppm.

HPLC analysis:  $R_t$  = 13.833 min, 99.2%.

HRMS (ESI+) = calcd. for  $\text{C}_{18}\text{H}_{13}\text{N}_2\text{O}_4$   $[\text{M}+\text{H}]^+$  = 321.0870, found: 321.0869.

mp.: 152 °C.

### Synthesis of 2-((2-phenylthiazol-4-yl)methoxy)isoindoline-1,3-dione (**20b**)



4-(Chloromethyl)-2-phenylthiazole (**15**) (359 mg, 2.20 mmol, 1.00 eq) was subjected to General procedure 3. The crude product was purified by flash chromatography (*n*-hexane/EtOAc) to furnish **20b** (434 mg, 1.29 mmol, 65%) as a white solid.

<sup>1</sup>H NMR (300 MHz, DMSO-*d*<sub>6</sub>) δ = 5.28 (s, 2H), 7.38 – 7.50 (m, 3H), 7.71 – 7.79 (m, 2H), 7.82 – 7.89 (m, 4H), 7.96 (s, 1H) ppm.

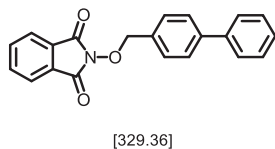
<sup>13</sup>C NMR (75 MHz, DMSO-*d*<sub>6</sub>) δ = 72.78, 122.19, 123.25, 126.00, 128.52, 129.15, 130.36, 132.66, 134.78, 150.47, 163.01, 167.29 ppm.

HPLC analysis: *R*<sub>t</sub> = 13.800 min, 99.9%.

HRMS (ESI+) = calcd. for C<sub>18</sub>H<sub>13</sub>N<sub>2</sub>O<sub>3</sub>S [M+H]<sup>+</sup> = 337.0641, found: 337.0643.

mp.: 131 °C.

### Synthesis of 2-([1,1'-biphenyl]-4-ylmethoxy)isoindoline-1,3-dione (**20c**)



4-Bromomethylbiphenyl (**16**) (1.44 g, 8.80 mmol, 1.00 eq) was subjected to General procedure 3. The crude product was purified by flash chromatography (*n*-hexane/EtOAc) to furnish **20c** (1.20 g, 3.64 mmol, 46%) as a white solid.

<sup>1</sup>H NMR (300 MHz, DMSO-*d*<sub>6</sub>) δ = 5.22 (s, 2H), 7.34 – 7.42 (m, 1H), 7.44 – 7.52 (m, 2H), 7.58 – 7.64 (m, 2H), 7.66 – 7.76 (m, 4H), 7.83 – 7.90 (m, 4H) ppm.

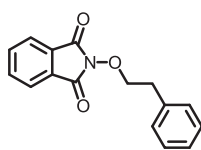
<sup>13</sup>C NMR (75 MHz, DMSO-*d*<sub>6</sub>) δ = 78.95, 123.28, 126.69, 126.72, 127.72, 128.55, 128.99, 130.25, 133.37, 134.83, 139.50, 140.74, 163.14 ppm.

HPLC analysis: *R*<sub>t</sub> = 16.500 min, >99%.

HRMS (ESI+) = calcd. for C<sub>21</sub>H<sub>16</sub>NO<sub>3</sub> [M+H]<sup>+</sup> = 330.1125, found: 330.1124.

mp.: 195 °C.

### Synthesis of 2-phenethoxyisoindoline-1,3-dione (**20d**)



[267,28]

(2-Bromoethyl)benzene (**17**) (1.85 g, 10.0 mmol, 1.00 eq) was subjected to General procedure 3. The crude product was purified by flash chromatography (*n*-hexane/EtOAc) to obtain **20d** (1.94 g, 8.85 mmol, 89%) as a brown solid.

$^1\text{H}$  NMR (300 MHz, DMSO- $d_6$ )  $\delta$  = 3.04 (t,  $J$  = 7.0 Hz, 2H), 4.37 (t,  $J$  = 7.0 Hz, 2H), 7.14 – 7.37 (m, 5H), 7.85 (s, 4H) ppm.

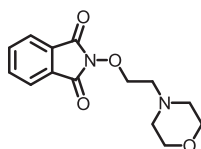
$^{13}\text{C}$  NMR (75 MHz, DMSO- $d_6$ )  $\delta$  = 34.05, 77.82, 123.20, 126.35, 128.33, 128.65, 128.84, 134.73, 137.44, 163.28 ppm.

HPLC analysis:  $R_t$  = 13.533 min, 95.8%.

HRMS (ESI+) = calcd. for  $\text{C}_{16}\text{H}_{14}\text{NO}_3$   $[\text{M}+\text{H}]^+$  = 268.0968, found: 268.0970.

mp.: 92.8°C.

### Synthesis of 2-(2-morpholinoethoxy)isoindoline-1,3-dione (**20e**)



[276,29]

4-(2-Chloroethyl)morpholine hydrochloride (**18**) (837 mg, 4.50 mmol, 1.00 eq) was subjected to General procedure 3. The crude product was purified by flash chromatography (*n*-hexane/EtOAc/0.1%  $\text{NEt}_3$ ) to furnish **20e** (589 mg, 2.13 mmol, 47%) as a white solid.

$^1\text{H}$  NMR (300 MHz, DMSO- $d_6$ )  $\delta$  = 2.36 (dd,  $J$  = 5.7, 3.6 Hz, 4H), 2.63 – 2.71 (m, 2H), 3.34 – 3.39 (m, 5H), 4.22 – 4.28 (m, 2H), 7.87 (s, 4H) ppm.

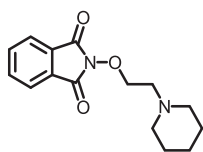
$^{13}\text{C}$  NMR (75 MHz, DMSO- $d_6$ )  $\delta$  = 53.13, 56.53, 65.89, 73.56, 123.06, 128.61, 134.62, 163.01 ppm.

HPLC analysis:  $R_t$  = 5.223 min, 98%.

HRMS (ESI+) = calcd. for  $\text{C}_{14}\text{H}_{17}\text{N}_2\text{O}_4$   $[\text{M}+\text{H}]^+$  = 277.1183, found: 277.1181.

mp.: 98.2 °C.

### Synthesis of 2-(2-(piperidin-1-yl)ethoxy)isoindoline-1,3-dione (**20f**)



[274.32]

1-(2-Chloroethyl)piperidine hydrochloride (**19**) (1.11 g, 6.00 mmol, 1.00 eq) was subjected to General procedure 3. The crude product was purified by flash chromatography (*n*-hexane/EtOAc/0.1% NEt<sub>3</sub>) to afford **20f** (850 mg, 3.10 mmol, 52%) as a yellow solid.

<sup>1</sup>H NMR (300 MHz, DMSO-*d*<sub>6</sub>) δ = 1.18 – 1.31 (m, 6H), 2.27 (d, *J* = 4.6 Hz, 4H), 2.57 – 2.68 (m, 2H), 4.19 – 4.28 (m, 2H), 7.86 (s, 4H) ppm.

<sup>13</sup>C NMR (75 MHz, DMSO-*d*<sub>6</sub>) δ = 23.67, 25.23, 53.90, 57.03, 73.48, 123.01, 128.66, 134.56, 163.00 ppm.

HPLC analysis: R<sub>t</sub> = 6.291 min, 92%.

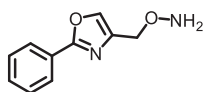
HRMS (ESI+) = calcd. for C<sub>16</sub>H<sub>23</sub>N<sub>2</sub>O<sub>4</sub> [M+H]<sup>+</sup> = 307.1652, found: 307.1653

mp.: 91.1 °C.

### General procedure 4: Formation of *O*-hydroxylamines

To a solution of the respective NHPI-derivative **20a-f** (1.00 eq) in CH<sub>2</sub>Cl<sub>2</sub> (20 mL/mmol), 2.00 eq hydrazine monohydrate was added dropwise. The reaction mixture was stirred overnight at rt. The resulting precipitate was filtered and the organic layer was washed with saturated NaHCO<sub>3</sub> solution (3x 10 mL). After drying over Na<sub>2</sub>SO<sub>4</sub> and filtration, the solvent was removed *in vacuo* providing the hydroxylamines **6a-f**.

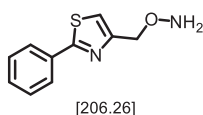
### Synthesis of *O*-((2-phenylthiazol-4-yl)methyl)hydroxylamine (**6a**)



[190.20]

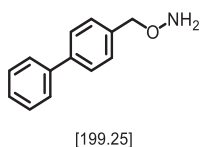
2-((2-Phenylthiazol-4-yl)methoxy)isoindoline-1,3-dione (**20a**) (442 mg, 1.38 mmol, 1.00 eq) was subjected to General procedure 4. The hydroxylamine **6a** (218 mg, 1.15 mmol, 83%) was used directly for the next step without any further purification.

### Synthesis of *O*-((2-phenylthiazol-4-yl)methyl)hydroxylamine (**6b**)



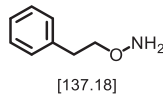
2-((2-Phenylthiazol-4-yl)methoxy)isoindoline-1,3-dione (**20b**) (673 mg, 2.00 mmol, 1.00 eq) was subjected to General procedure 4. The product **6b** (368 mg, 1.78 mmol, 89%) was then used directly for the next step without any further purification.

### Synthesis of *O*-([1,1'-biphenyl]-4-ylmethyl)hydroxylamine (**6c**)



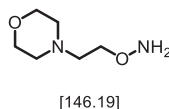
2-([1,1'-Biphenyl]-4-ylmethoxy)isoindoline-1,3-dione (**20c**) (494 mg, 1.50 mmol, 1.00 eq) was subjected to General procedure 4. The hydroxylamine **6c** (263 mg, 1.32 mmol, 88%) was used directly for the next step without any further purification.

### Synthesis of *O*-phenethylhydroxylamine (**6d**)



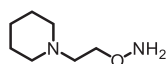
2-Phenethoxyisoindoline-1,3-dione (**20d**) (553 mg, 2.00 mmol, 1.00 eq) was subjected to General procedure 4. The product **6d** (192 mg, 1.40 mmol, 70%) was then used directly for the next step without any further purification.

### Synthesis of *O*-(2-morpholinoethyl)hydroxylamine (**6e**)



2-(2-Morpholinoethoxy)isoindoline-1,3-dione (**20e**) (553 mg, 2.00 mmol, 1.00 eq) was subjected to General procedure 4. The hydroxylamine **6e** (240 mg, 1.64 mmol, 82%) was then used directly for the further step without any further purification.

### Synthesis of *O*-(2-(piperidin-1-yl)ethyl)hydroxylamine (**6f**)



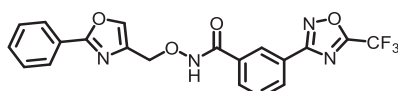
[144.22]

2-(2-(Piperidin-1-yl)ethoxy)isoindoline-1,3-dione (**20f**) (686 mg, 2.50 mmol, 1.00 eq) was subjected to General procedure 4. The hydroxylamine **6f** (190 mg, 1.32 mmol, 53%) was then used directly for the next step without any further purification.

### General procedure 5: HATU-coupling

For the synthesis of the alkoxyamides **2a-c** and **3a-g**, 1.00 eq of the corresponding carboxylic acid **4,5** was dissolved in dry DMF (0.1 mmol/mL) and 1.00 eq HATU and 2.00 eq DIPEA were added. After stirring for 15 min at rt, the respective hydroxylamine (1.00 eq) was then added and the resulting mixture was stirred for further 16h at rt. The solvent was removed *in vacuo* and the residue was diluted with EtOAc. The organic layer was washed with saturated NaHCO<sub>3</sub> (3x 50 mL), brine (1x 50 mL), dried over Na<sub>2</sub>SO<sub>4</sub> and filtered. After removing the solvent, the crude product was purified as stated.

### Synthesis of *N*-((2-phenyloxazol-4-yl)methoxy)-3-(5-(trifluoromethyl)-1,2,4-oxadiazol-3-yl)benzamide (**2a**)



[430.34]

3-(5-(Trifluoromethyl)-1,2,4-oxadiazol-3-yl)benzoic acid (**4**) (297 mg, 1.15 mmol, 1.00 eq) was converted with *O*-((2-phenyloxazol-4-yl)methyl)hydroxylamine (**6a**) (297 mg, 1.15 mmol, 1.00 eq) according to General procedure 5. The crude product was purified by flash chromatography (*n*-hexane/EtOAc) to afford **2a** (292 mg, 0.68 mmol, 59%) as a beige solid.

<sup>1</sup>H NMR (300 MHz, DMSO-*d*<sub>6</sub>) δ = 4.95 (s, 2H), 7.51 – 7.58 (m, 3H), 7.73 (t, *J* = 7.8 Hz, 1H), 7.97 – 8.07 (m, 3H), 8.23 (d, *J* = 7.8 Hz, 1H), 8.35 (s, 1H), 8.45 (s, 1H), 12.07 (s, 1H) ppm.

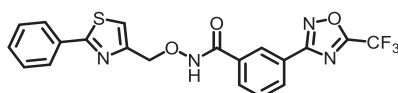
<sup>13</sup>C NMR (151 MHz, DMSO-*d*<sub>6</sub>) δ = 68.16, 115.73 (q, *J* = 273.3 Hz), 124.75, 125.93, 126.12, 126.76, 129.17, 129.91, 130.27, 130.75, 131.11, 133.46, 136.70, 139.46, 160.82, 163.18, 165.18 (q, *J* = 43.5 Hz), 167.97 ppm.

HPLC analysis: *R*<sub>t</sub> = 14.667 min, 98.7%.

HRMS (ESI+) = calcd. for C<sub>20</sub>H<sub>14</sub>F<sub>3</sub>N<sub>4</sub>O<sub>4</sub> [M+H]<sup>+</sup> = 431.0962, found: 431.0961.

mp.: 122 °C.

### Synthesis of *N*-((2-phenylthiazol-4-yl)methoxy)-3-(5-(trifluoromethyl)-1,2,4-oxadiazol-3-yl)benzamide (**2b**)



[446.40]

3-(5-(Trifluoromethyl)-1,2,4-oxadiazol-3-yl)benzoic acid (**4**) (461 mg, 1.78 mmol, 1.00 eq) was coupled with *O*-((2-phenylthiazol-4-yl)methyl)hydroxylamine (**6b**) (368 mg, 1.78 mmol, 1.00 eq) according to General procedure 5. The crude product was purified by flash chromatography (*n*-hexane/EtOAc) to furnish **2b** (557 mg, 1.25 mmol, 70%) as a white solid.

<sup>1</sup>H NMR (300 MHz, DMSO-*d*<sub>6</sub>) δ = 5.10 (s, 2H), 7.46 – 7.54 (m, 3H), 7.73 (t, *J* = 7.8 Hz, 1H), 7.86 (s, 1H), 7.91 – 7.99 (m, 2H), 8.04 (dt, *J* = 7.9, 1.5 Hz, 1H), 8.23 (d, *J* = 7.8 Hz, 1H), 8.44 (s, 1H), 12.11 (s, 1H) ppm.

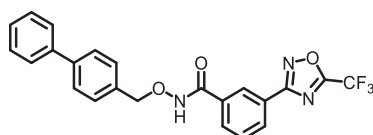
<sup>13</sup>C NMR (151 MHz, DMSO-*d*<sub>6</sub>) δ = 71.95, 99.50, 115.73 (q, *J* = 273.2 Hz), 120.31, 124.75, 126.11, 129.23, 129.91, 130.31, 131.09, 132.91, 133.46, 152.04, 163.18, 165.18 (q, *J* = 131.5, 43.6 Hz), 165.61, 167.19, 167.96 ppm.

HPLC analysis: *R*<sub>t</sub> = 15.433 min, 98.7%.

HRMS (ESI+) = calcd. for C<sub>20</sub>H<sub>14</sub>F<sub>3</sub>N<sub>4</sub>O<sub>3</sub>S [M+H]<sup>+</sup> = 447.0733, found: 447.0740.

mp.: 140 °C.

### Synthesis of *N*-([1,1'-biphenyl]-4-ylmethoxy)-3-(5-(trifluoromethyl)-1,2,4-oxadiazol-3-yl)benzamide (**2c**)



[439.39]

3-(5-(Trifluoromethyl)-1,2,4-oxadiazol-3-yl)benzoic acid (**4**) (341 mg, 1.32 mmol, 1.00 eq) was coupled with *O*-([1,1'-biphenyl]-4-ylmethyl)hydroxylamine (**6c**) (263 mg, 1.32 mmol, 1.00 eq)

according to General procedure 5. The crude product was purified by flash chromatography (*n*-hexane/EtOAc) to provide **2c** (341 mg, 0.78 mmol, 59%) as a white solid.

<sup>1</sup>H NMR (300 MHz, DMSO-*d*<sub>6</sub>) δ = 5.01 (s, 2H), 7.34 – 7.42 (m, 1H), 7.44 – 7.51 (m, 2H), 7.53 – 7.60 (m, 2H), 7.65 – 7.78 (m, 5H), 8.05 (d, *J* = 8.0, 1.4 Hz, 1H), 8.24 (d, *J* = 7.5 Hz, 1H), 8.44 (s, 1H), 12.10 (s, 1H) ppm.

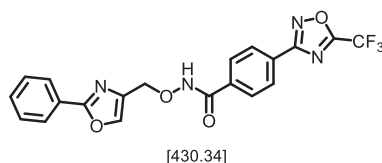
<sup>13</sup>C NMR (151 MHz, DMSO-*d*<sub>6</sub>) δ = 76.73, 116.65 (q,), 124.77, 126.02, 126.63, 126.67, 127.56, 128.95, 129.63, 129.96, 130.27, 131.08, 131.10, 133.48, 135.04, 139.74, 140.19, 163.16, 165.20 (q, *J* = 43.9 Hz), 167.97 ppm.

HPLC analysis: *R*<sub>t</sub> = 17.083 min, >99%.

HRMS (ESI+) = calcd. for C<sub>23</sub>H<sub>17</sub>F<sub>3</sub>N<sub>3</sub>O<sub>3</sub> [M+H]<sup>+</sup> = 440.1217, found: 440.1210.

mp.: 173 °C.

### Synthesis of *N*-((2-phenyloxazol-5-yl)methoxy)-4-(5-(trifluoromethyl)-1,2,4-oxadiazol-3-yl)benzamide (**3a**)



4-(5-(Trifluoromethyl)-1,2,4-oxadiazol-3-yl)benzoic acid (**5**) (767 mg, 2.97 mmol, 1.00 eq) was treated with *O*-((2-phenyloxazol-4-yl)methyl)hydroxylamine (**6a**) (565 mg, 2.97 mmol, 1.00 eq) according to General procedure 5. The crude product was purified by flash chromatography (*n*-hexane/EtOAc) to afford **3a** (250 mg, 0.58 mmol, 20%) as a white solid.

<sup>1</sup>H NMR (300 MHz, DMSO-*d*<sub>6</sub>) δ = 4.95 (s, 2H), 7.55 (p, *J* = 3.8, 3.4 Hz, 3H), 7.87 – 8.08 (m, 4H), 8.15 (d, *J* = 8.2 Hz, 2H), 8.34 (s, 1H), 12.00 (s, 1H) ppm.

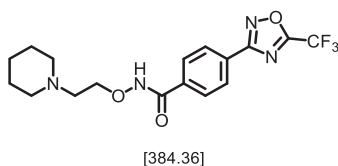
<sup>13</sup>C NMR (151 MHz, DMSO-*d*<sub>6</sub>) δ = 68.26, 116.65 (q), 125.95, 126.77, 127.13, 127.52, 128.40, 129.21, 130.78, 135.78, 136.68, 139.46, 160.84, 163.45, 165.23 (d, *J* = 43.7 Hz), 167.88 ppm.

HPLC analysis: *R*<sub>t</sub> = 14.050 min, 99.6%.

HRMS (ESI+) = calcd. for C<sub>20</sub>H<sub>14</sub>F<sub>3</sub>N<sub>4</sub>O<sub>4</sub> [M+H]<sup>+</sup> = 431.0962, found: 431.0958.

mp.: 199 °C.

### Synthesis of *N*-(2-(piperidin-1-yl)ethoxy)-4-(5-(trifluoromethyl)-1,2,4-oxadiazol-3-yl)benzamide (**3b**)



3-(5-(Trifluoromethyl)-1,2,4-oxadiazol-3-yl)benzoic acid (**5**) (341 mg, 1.32 mmol, 1.00 eq) was coupled with *O*-(2-(piperidin-1-yl)ethyl)hydroxylamine (**6f**) (190 mg, 1.32 mmol, 1.00 eq) according to General procedure 5. The crude product was purified by flash chromatography (CH<sub>2</sub>Cl<sub>2</sub>/30% MeOH in CH<sub>2</sub>Cl<sub>2</sub>/ 0.1% NEt<sub>3</sub>) to furnish **3b** (273 mg, 0.71 mmol, 54%) as a yellowish solid.

<sup>1</sup>H NMR (300 MHz, DMSO-*d*<sub>6</sub>) δ = 1.41 (q, *J* = 6.0 Hz, 2H), 1.55 (p, *J* = 5.5 Hz, 4H), 2.57 (t, *J* = 5.3 Hz, 4H), 2.71 (t, *J* = 5.5 Hz, 2H), 4.06 (t, *J* = 5.5 Hz, 2H), 7.95 – 8.01 (m, 2H), 8.12 – 8.20 (m, 2H) ppm.

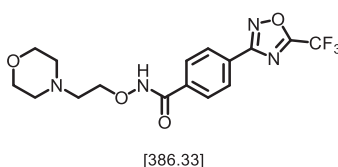
<sup>13</sup>C NMR (75 MHz, DMSO-*d*<sub>6</sub>) δ = 23.39, 24.95, 53.82, 56.02, 72.27, 115.70 (d, *J* = 273.2 Hz), 126.91, 127.47, 128.18, 135.88, 163.10, 165.18 (d, *J* = 43.7 Hz), 167.86 ppm.

HPLC analysis: *R*<sub>t</sub> = 10.321 min, 96.2%.

HRMS (ESI+) = calcd. for C<sub>17</sub>H<sub>20</sub>F<sub>3</sub>N<sub>4</sub>O<sub>3</sub> [M+H]<sup>+</sup> = 385.1482, found: 385.1482

mp.: 131 °C.

### Synthesis of *N*-(2-morpholinoethoxy)-4-(5-(trifluoromethyl)-1,2,4-oxadiazol-3-yl)benzamide (**3c**)



3-(5-(Trifluoromethyl)-1,2,4-oxadiazol-3-yl)benzoic acid (**5**) (423 mg, 1.64 mmol, 1.00 eq) was converted with *O*-(2-morpholinoethyl)hydroxylamine (**6e**) (240 mg, 1.64 mmol, 1.00 eq) according to General procedure 5. The crude product was purified by flash chromatography (CH<sub>2</sub>Cl<sub>2</sub>/30% MeOH in CH<sub>2</sub>Cl<sub>2</sub>/ 0.1% NEt<sub>3</sub>) to provide **3c** (457 mg, 1.18 mmol, 72%) as a yellowish solid.

$^1\text{H}$  NMR (300 MHz,  $\text{DMSO-}d_6$ )  $\delta$  = 2.55 (t,  $J$  = 4.4 Hz, 4H), 2.69 (t,  $J$  = 5.3 Hz, 2H), 3.60 (t,  $J$  = 4.7 Hz, 4H), 4.06 (t,  $J$  = 5.4 Hz, 2H), 7.94 – 8.00 (m, 2H), 8.14 – 8.20 (m, 2H) ppm.

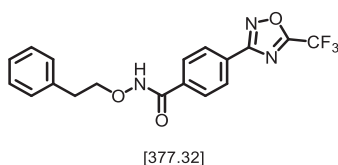
$^{13}\text{C}$  NMR (126 MHz,  $\text{DMSO-}d_6$ )  $\delta$  = 3.26, 55.99, 65.89, 72.67, 115.70 (q,  $J$  = 273.2 Hz), 127.02, 127.51, 128.17, 135.68, 162.90, 165.19 (q,  $J$  = 44.0 Hz), 167.88 ppm.

HPLC analysis:  $R_t$  = 15.637 min, 95.2%.

HRMS (ESI+) = calcd. for  $\text{C}_{16}\text{H}_{18}\text{F}_3\text{N}_4\text{O}_4$   $[\text{M}+\text{H}]^+$  = 387.1275, found: 387.1279.

mp.: 75 °C.

### Synthesis of *N*-phenethoxy-4-(5-(trifluoromethyl)-1,2,4-oxadiazol-3-yl)benzamide (**3d**)



3-(5-(Trifluoromethyl)-1,2,4-oxadiazol-3-yl)benzoic acid (**5**) (258 mg, 1.00 mmol, 1.00 eq) was coupled with *O*-phenethylhydroxylamine (**6d**) (137 mg, 1.00 mmol, 1.00 eq) according to General procedure 5. The crude product was purified by flash chromatography ( $\text{CH}_2\text{Cl}_2$ /30% MeOH in  $\text{CH}_2\text{Cl}_2$ / 0.1%  $\text{NEt}_3$ ) to furnish **3d** (256 mg, 0.68 mmol, 68%) as a white solid.

$^1\text{H}$  NMR (600 MHz,  $\text{DMSO-}d_6$ )  $\delta$  = 2.97 (t,  $J$  = 6.7 Hz, 2H), 4.15 (t,  $J$  = 6.8 Hz, 2H), 7.18 – 7.26 (m, 1H), 7.32 (dt,  $J$  = 14.9, 7.6 Hz, 4H), 7.97 (d,  $J$  = 8.2 Hz, 2H), 8.15 (d,  $J$  = 8.1 Hz, 2H), 11.96 (s, 1H) ppm.

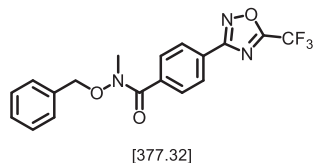
$^{13}\text{C}$  NMR (75 MHz, DMSO)  $\delta$  = 34.07, 39.40, 75.88, 115.78 (d,  $J$  = 273.2 Hz), 126.24, 127.12, 127.57, 128.34, 128.36, 128.91, 135.87, 138.36, 163.40, 165.28 (d,  $J$  = 43.8 Hz), 167.93 ppm.

HPLC analysis:  $R_t$  = 14.509 min, >99%.

HRMS (ESI+) = calcd. for  $\text{C}_{18}\text{H}_{15}\text{F}_3\text{N}_3\text{O}_3$   $[\text{M}+\text{H}]^+$  = 378.1060, found: 378.1059.

mp.: 109 °C.

### Synthesis of *N*-(benzyloxy)-*N*-methyl-4-(5-(trifluoromethyl)-1,2,4-oxadiazol-3-yl)benzamide (**3e**)



3-(5-(Trifluoromethyl)-1,2,4-oxadiazol-3-yl)benzoic acid (**5**) (258 mg, 1.00 mmol, 1.00 eq) was treated with *O*-benzyl-*N*-methylhydroxylamine<sup>[4]</sup> (138 mg, 1.00 mmol, 1.00 eq) according to General procedure 5. The crude product was purified by flash chromatography (*n*-hexane/EtOAc) to furnish **3e** (296 mg, 0.78 mmol, 78%) as a white solid.

<sup>1</sup>H NMR (600 MHz, CDCl<sub>3</sub>) δ = 3.34 (s, 3H), 4.62 (s, 2H), 6.99 (d, *J* = 7.4 Hz, 2H), 7.16 – 7.28 (m, 3H), 7.64 – 7.71 (m, 2H), 8.03 – 8.09 (m, 2H) ppm.

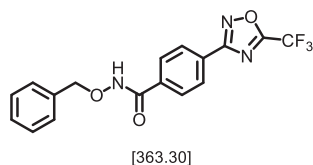
<sup>13</sup>C NMR (151 MHz, CDCl<sub>3</sub>) δ = 34.64, 76.31, 115.96 (q, *J* = 273.8 Hz), 126.51, 127.25, 128.60, 129.03, 129.17, 129.46, 133.68, 137.94, 166.04 (q, *J* = 44.4 Hz), 168.87 ppm.

HPLC analysis: *R*<sub>t</sub> = 9.111 min, 98.5%.

HRMS (ESI+) = calcd. for C<sub>18</sub>H<sub>15</sub>F<sub>3</sub>N<sub>3</sub>O<sub>3</sub> [M+H]<sup>+</sup> = 378.1060, found: 378.1059.

mp.: 74 °C.

### Synthesis of *N*-(benzyloxy)-4-(5-(trifluoromethyl)-1,2,4-oxadiazol-3-yl)benzamide (**3f**)



3-(5-(Trifluoromethyl)-1,2,4-oxadiazol-3-yl)benzoic acid (**5**) (258 mg, 1.00 mmol, 1.00 eq) was coupled with *O*-benzylhydroxylamine<sup>[3]</sup> (123 mg, 1.00 mmol, 1.00 eq) according to General procedure 5. The crude product was purified by flash chromatography (*n*-hexane/EtOAc) to furnish **3f** (144 mg, 0.40 mmol, 40%) as a white solid.

<sup>1</sup>H NMR (300 MHz, DMSO-*d*<sub>6</sub>) δ = 4.96 (s, 2H), 7.28 – 7.54 (m, 5H), 7.88 – 8.02 (m, 2H), 8.16 (d, *J* = 8.2 Hz, 2H), 12.02 (s, 1H) ppm.

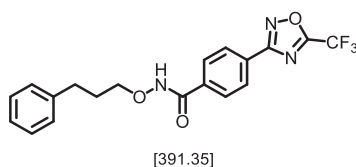
<sup>13</sup>C NMR (75 MHz, DMSO-*d*<sub>6</sub>) δ = 77.12, 115.75 (d, *J* = 273.1 Hz), 127.12, 127.57, 128.31, 128.36, 128.96, 135.81, 163.41, 164.95, 165.53, 167.91 ppm.

HPLC analysis: *R*<sub>t</sub> = 13.879 min, 98.9%.

HRMS (ESI+) = calcd. for C<sub>17</sub>H<sub>13</sub>F<sub>3</sub>N<sub>3</sub>O<sub>3</sub> [M+H]<sup>+</sup> = 364.0905, found: 354.0905.

mp.: 199 °C.

**Synthesis of *N*-(3-phenylpropoxy)-4-(5-(trifluoromethyl)-1,2,4-oxadiazol-3-yl)-benzamide (3g)**



3-(5-(Trifluoromethyl)-1,2,4-oxadiazol-3-yl)benzoic acid (**5**) (258 mg, 1.00 mmol, 1.00 eq) was converted with *O*-(3-phenylpropyl)hydroxylamine<sup>[5]</sup> (151 mg, 1.00 mmol, 1.00 eq) according to General procedure 5. The crude product was purified by flash chromatography (*n*-hexane/EtOAc) to furnish **3g** (296 mg, 0.78 mmol, 78%) as a white solid.

<sup>1</sup>H NMR (300 MHz, DMSO-*d*<sub>6</sub>) δ = 1.80 – 2.03 (m, 2H), 2.73 (dd, *J* = 8.8, 6.6 Hz, 2H), 3.93 (t, *J* = 6.4 Hz, 2H), 7.13 – 7.38 (m, 5H), 7.92 – 8.05 (m, 2H), 8.11 – 8.22 (m, 2H), 11.90 (s, 1H) ppm.

<sup>13</sup>C NMR (75 MHz, DMSO-*d*<sub>6</sub>) δ = 29.61, 31.43, 74.69, 115.73 (d, *J* = 273.2 Hz), 125.79, 127.05, 127.53, 128.30, 128.37, 135.89, 141.56, 163.25, 165.22 (d, *J* = 43.9 Hz), 167.88 ppm.

HPLC analysis: *R*<sub>t</sub> = 15.154 min, 99.1%.

HRMS (ESI+) = calcd. for C<sub>19</sub>H<sub>17</sub>F<sub>3</sub>N<sub>3</sub>O<sub>3</sub> [M+H]<sup>+</sup> = 392.1217, found: 392.1218.

mp.: 140 °C.

## References

- [1] M. Lobera, K. P. Madauss, D. T. Pohlhaus, Q. G. Wright, M. Trocha, D. R. Schmidt, E. Baloglu, R. P. Trump, M. S. Head, G. A. Hofmann, et al., *Nat. Chem. Biol.* **2013**, *9*, 319–325.
- [2] K. Liu, H. Lu, L. Hou, Z. Qi, C. Teixeira, F. Barbault, B.-T. Fan, S. Liu, S. Jiang, L. Xie, *J. Med. Chem.* **2008**, *51*, 7843–7854.
- [3] Y. Asfaha, C. Schrenk, L. A. Alves Avelar, F. Lange, C. Wang, J. J. Bandolik, A. Hamacher, M. U. Kassack, T. Kurz, *Bioorg. Med. Chem.* **2020**, *28*, 115108.
- [4] E. Olshvang, A. Szebesczyk, H. Kozłowski, Y. Hadar, E. Gumienna-Kontecka, A. Shanzer, *Dalt. Trans.* **2015**, *44*, 20850–20858.
- [5] B. Mavunkel, W. Rzeszotarski, P. Kaplita, D. DeHaven-Hudkins, *Eur. J. Med. Chem.* **1994**, *29*, 659–666.

## **The Second Generation of Potent and Selective Class IIa Histone Deacetylase Inhibitors**

Unpublished

Contribution:

- Synthesis of the compounds **1a-t** and **4-7**
- Manuscript and supporting information

# **The Second Generation of Potent and Selective Class IIa Histone Deacetylase Inhibitors**

*Yodita Asfaha\*\**, *Alexander Jan Skerhut\*\**, *Leandro A. Alves-Avelar\**, *Nadine Horstick-Muche\**, *Matthias U. Kassack\*\**, *Thomas Kurz\*\**

\*Institut für Pharmazeutische und Medizinische Chemie, Heinrich-Heine-Universität Düsseldorf, Universitätsstr. 1, 40225 Düsseldorf, Germany. # YA and AJS share first authorship, MUK and TK share senior and corresponding authorship.

## Abstract

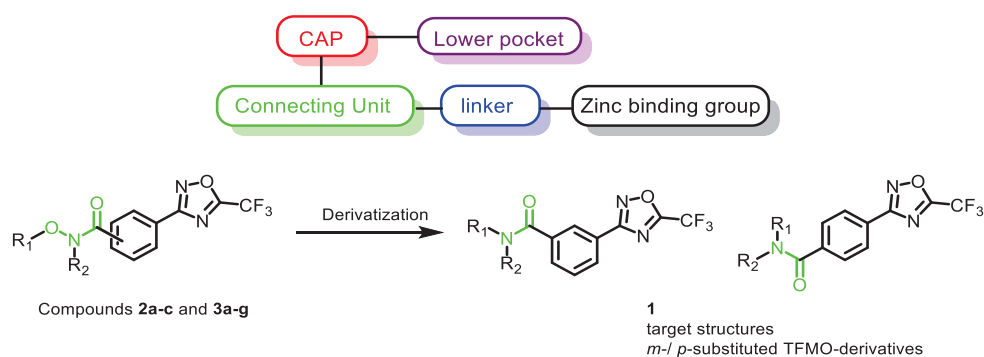
The causation and progression of cancer is not only regulated via genetic alterations, but also via epigenetic processes. Acetylation of histones plays a crucial role in the epigenetic regulation of gene expression and is catalyzed by the balance between histone acetyltransferases (HATs) and histone deacetylases (HDACs). HDAC inhibitors provide powerful epigenetic modulators with tremendous therapeutic potential and have multiple effects at the cellular and systemic level. Currently, HDAC inhibitors are evaluated for a broad range of disorders e.g. hematologic malignancies, psychiatric disorders and are currently in clinical trials for several other diseases. In addition to altering gene expression, HDAC enzymes also influence the activity of numerous non-histone proteins. However, the first-generation HDAC inhibitors target multiple HDAC isozymes (pan-inhibitors) which might lead to the observed severe side effects. Therefore, the development of class selective HDAC inhibitors provides an attractive approach to improve the risk-benefit profiles compared to pan-HDACi. Here, we report the discovery of seven potent and selective HDAC class IIa inhibitors with inhibitory activities in the nanomolar range. The most potent and selective HDAC class IIa inhibitor was compound **11** ( $IC_{50}(\text{HDAC4}) = 12 \text{ nM}$ ) with a 511/482/355-fold selectivity over HDAC2/6/8. These selective HDAC inhibitors present valuable pharmacological tools to elucidate the functions of class IIa HDACs in health and cancer.

## 1. Introduction

Histone deacetylases (HDACs) are classically known for their capability of removing acetyl groups from conserved lysine residues of histones and non-histone proteins.<sup>[1,2]</sup> HDACs have been extensively studied in regards to gene transcription and the epigenetic control of cells.<sup>[3]</sup> It has been shown that HDACs promote chromatin condensation and repression of gene transcription by deacetylation of histones. The 11 human zinc-dependent HDACs are subdivided into three classes based on phylogenetic analyses and their sequence similarities to yeast deacetylases: class I (HDACs 1-3, 8), class II (IIa: HDACs 4, 5, 7, 9; IIb: HDACs 6, 10) and class IV (HDAC 11).<sup>[4]</sup> HDACs have been implicated in regulating numerous cellular processes such as proliferation, migration, differentiation and apoptosis.<sup>[5-7]</sup> Despite their nomenclature and classic functions, recent studies proposed that non-deacetylase roles exist for class IIa HDACs. Moreover, several features distinguish this class from the other HDAC classes. In contrast to class I HDACs, class IIa HDACs are not ubiquitously expressed.<sup>[2,8]</sup> HDAC4, 5 and 9 are mainly expressed in the heart, brain and skeletal muscle. HDAC7 is primarily found in endothelial cells of the vascular system, heart, lung and skeletal muscle.<sup>[9,10]</sup> Within a cell, these enzymes shuttle between the cytoplasm and the nucleus which is regulated by intrinsic nuclear import and export signals. They contain an extended *N*-terminus with highly conserved serine residues that undergo signal-dependent phosphorylation. Upon phosphorylation, these residues bind to the 14-3-3 protein, resulting in the nuclear export and cytoplasmic retention of the class IIa HDACs<sup>[11,12]</sup> The *N*-terminus also bears binding sites for transcription factors and chromatin modulators including class I HDACs.<sup>[13-15]</sup> It is assumed that their transcriptional repressive activity is due to their association to multiprotein complexes with other transcription factors or class I HDACs.<sup>[16-19]</sup> In addition, the catalytic activity of class IIa HDACs is much lower compared to class I and class IIb HDACs due to a Tyr/His switch in their active site. In particular, this replacement reveals the so-called lower pocket as a unique structural feature of this class.<sup>[17,18]</sup> Because of their extremely low deacetylase activity, it is proposed that they operate as “readers” with the catalytic domain as a recognition domain for *N*-acetylated lysine residues of proteins.<sup>[20,21]</sup> Class IIa HDACs are involved in a broad range of biological processes and their dysregulation has been associated with cardiovascular diseases,

diabetes, neurodegenerative diseases, muscle-atrophy disorders and certain cancers.<sup>[22–28]</sup> However, the signalling pathways and mechanisms controlling class IIa HDACs functions in health and disease remain poorly understood. Therefore, the therapeutic potential of this class could be evaluated by the application of potent and selective class IIa HDAC inhibitors (HDACi).

We previously reported the design, synthesis and biological evaluation of TFMO-based class IIa selective HDACi. We now describe the structural optimization of these compounds by the replacement of the alkoxyamide connecting unit (CU) (green) with an amide CU (Scheme 1).

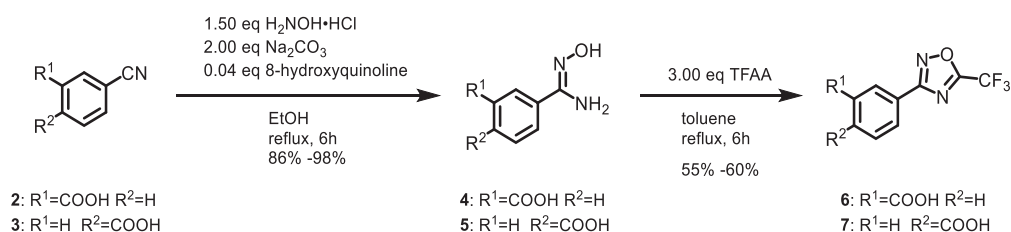


Scheme 1: Pharmacophore model of class IIa selective HDAC inhibitors. Derivatization of the alkoxyamide-based TFMO compounds **2a-c** and **3a-g**.

## 2. Results and Discussion

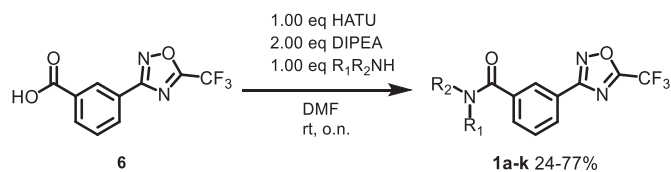
### 2.1. Chemistry

Following the optimized procedure of Asfaha et al., the TFMO derivatives **6** and **7** were synthesized according to Scheme 2. The generated amidoximes **4** and **5** were treated with an excess of trifluoroacetic anhydride in toluene providing the heterocycles **6** and **7** in moderate yields.

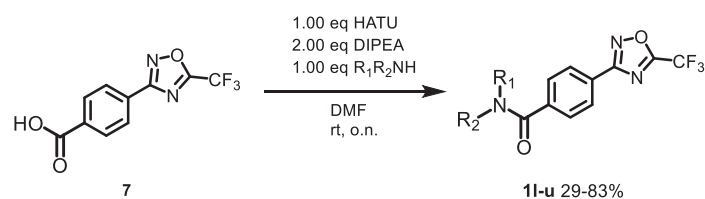


Scheme 2: Synthesis of **6** and **7**.

The *meta*- and *para* substituted TFMO-derivatives were furnished via a HATU-mediated acylation with commercially available amines, in moderate to good yields (Scheme 3 and Scheme 4).



Scheme 3: Synthesis of *meta*-substituted TFMO-based HDACi **1a-j**.

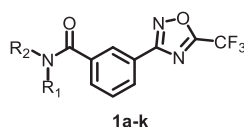


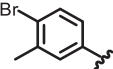
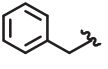
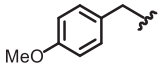
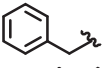
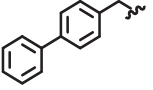
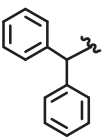
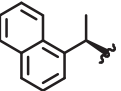
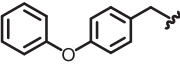
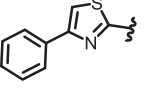
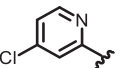
Scheme 4: Synthesis of *para*-substituted TFMO-based HDACi **1l-u**.

## 2.2. Biological evaluation

The synthesized compounds **1a-t** were assessed for their antiproliferative activity and for their HDAC inhibitory activity in the human monocytic cell line THP-1 using class-distinguishing substrates (Boc-Lys(Ac)-AMC: class I and IIb HDACs; Boc-Lys(TFAc)-AMC: class IIa, HDAC8). The results are depicted in Table 1 and Table 2 with CHDI-00390576 and TMP269 as reference compounds. The *meta*-substituted TFMO-derivatives **1a-k** displayed low to moderate cytotoxicity with antiproliferative effects below 78.2% growth inhibition at 100  $\mu$ M. Among the tested *para*-substituted TFMO-derivatives **1l-t**, compound **1l** exhibited the strongest antiproliferative effect in the low micromolar range and demonstrated a 6/3-fold increased cytotoxicity compared to the HDAC class IIa selective compounds TMP269 and CHDI-00390576. In the performed whole-cell HDAC inhibition assay using the Boc-Lys(Ac)-AMC-HDAC substrate, all screened *meta*-substituted TFMO-derivatives **1a-k** displayed inhibitory activities below 38% at 100  $\mu$ M. However, the cellular HDAC inhibition assay with the Boc-Lys(TFAc)-AMC-HDAC substrate revealed that compound **1k** exhibited the strongest cellular HDAC inhibition with 71% at 100  $\mu$ M. Among the tested *para*-substituted TFMO-derivatives **1l-t**, in the performed whole-cell HDAC inhibition assay using the Boc-Lys(Ac)-AMC-HDAC substrate, compound **1l** showed the most pronounced HDAC cellular inhibition with an inhibitory activity in the nanomolar range ( $IC_{50} = 0.7 \mu$ M). The cellular HDAC inhibition assay with the Boc-Lys(TFAc)-AMC-HDAC substrate revealed that the *para*-substituted TFMO-derivatives **1l-t** are more potent than the corresponding *meta*-substituted TFMO-derivatives **1a-k** with inhibitory activities between 18-100%. To sum up, the most potent compound in the cellular HDAC assay (using the Boc-Lys(TFAc)-AMC-HDAC substrate) was **1l** showing an  $IC_{50}$  value of 0.08  $\mu$ M, which is in the same order of magnitude as the class IIa selective hydroxamate-based HDAC inhibitor CHDI-00390576.

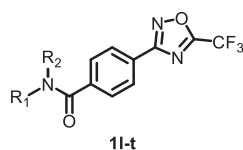
Table 1: Cell viability (MTT assay) and whole-cell HDAC inhibition assay in the human monocytic cell line THP-1.



Cpd.	R <sub>1</sub>	R <sub>2</sub>	cell viability (MTT)		HDAC inhibition			
					Boc-Lys(Ac)-AMC		Boc-Lys(TFAc)-AMC	
			% inhibition of 100 μM IC <sub>50</sub> [μM]	IC <sub>50</sub> [μM] (pIC <sub>50</sub> ± SEM)	% inhibition of 100 μM	IC <sub>50</sub> [μM] (pIC <sub>50</sub> ± SEM)	% inhibition of 100 μM	IC <sub>50</sub> [μM] (pIC <sub>50</sub> ± SEM)
<b>1a</b>	Me		36.2%	n.d.	9%	n.d.	58%	81.35 (4.09 ± 0.04)
<b>1b</b>	H		39.6%	n.d.	10%	n.d.	26%	n.d.
<b>1c</b>	H		78.2%	13.0 (4.89 ± 0.11)	20%	n.d.	59%	70.55 (4.15 ± 0.09)
<b>1d</b>	H		34.7%	n.d.	30%	n.d.	66%	45.09 (4.35 ± 0.08)
<b>1e</b>	Benzyl		31.5%	n.d.	21%	n.d.	43%	n.d.
<b>1f</b>	H		38.1%	n.d.	16%	n.d.	61%	n.d.
<b>1g</b>	H		72.7%	38.88 (4.41 ± 0.06)	16%	n.d.	16%	n.d.
<b>1h</b>	H		41.2%	n.d.	38%	n.d.	53%	n.d.
<b>1i</b>	H		32.8%	n.d.	13%	n.d.	24%	n.d.
<b>1j</b>	H		46.2%	n.d.	27%	n.d.	n.a.	n.d.
<b>1k</b>	H		55.3%	n.d.	33%	n.d.	71%	51.07 (4.29 ± 0.06)
		CHDI-00390576	100%	30.4 (4.52 ± 0.04)	42%	n.d.	100%	0.02 (7.69 ± 0.10)
		TMP269	70%	58.54 (4.23 ± 0.039)	13%	n.d.	39%	n.d.

Presented data are calculated from at least two experiments each performed in duplicates. IC<sub>50</sub> values were calculated for compounds with an inhibition of more than 50 %. Standard deviation of percent inhibition values is less than 14 %. Vehicle control was defined as 0 % inhibition. n.d. = not determined.

Table 2: Cell viability (MTT assay) and whole-cell HDAC inhibition assay in the human monocytic cell line THP-1.



Cpd.	R <sub>1</sub>	R <sub>2</sub>	cell viability (MTT)		HDAC inhibition			
			% inhibition of 100 μM	IC <sub>50</sub> [μM] (pIC <sub>50</sub> ± SEM)	Boc-Lys(Ac)-AMC		Boc-Lys(TFAc)-AMC	
					% inhibition of 100 μM	IC <sub>50</sub> [μM] (pIC <sub>50</sub> ± SEM)	% inhibition of 100 μM	IC <sub>50</sub> [μM] (pIC <sub>50</sub> ± SEM)
<b>1l</b>	H		80.2%	9.24 (5.04 ± 0.04)	93%	0.7 (6.16 ± 0.18)	100%	0.08 (7.11 ± 0.03)
<b>1m</b>	Me		33.9%	n.d.	78%	n.d.	100%	0.51 (6.29 ± 0.02)
<b>1n</b>	H		47.0%	n.d.	73%	1.91 (5.72 ± 0.17)	100%	13.71 (4.86 ± 0.05)
<b>1o</b>	Me		31.4%	n.d.	65%	36.25 (4.44 ± 0.068)	98%	1.27 (5.9 ± 0.06)
<b>1p</b>	H		48.6%	n.d.	64%	n.d.	97%	14.51 (4.84 ± 0.07)
<b>1q</b>	Me		33.4%	n.d.	31%	n.d.	100%	6.39 (5.19 ± 0.082)
<b>1r</b>	H		49.0%	n.d.	25%	n.d.	100%	5.51 (5.26 ± 0.078)
<b>1s</b>	-		38.6%	n.d.	23%	n.d.	100%	5.51 (5.26 ± 0.077)
<b>1t</b>	H		63.3%	47.34 (4.33 ± 0.07)	n.a.	n.d.	18%	n.d.
		CHDI-00390576	100%	30.4 (4.52 ± 0.04)	42%	n.d.	100%	0.02 (7.69 ± 0.10)
		TMP269	70%	58.54 (4.23 ± 0.039)	13%	n.d.	39%	n.d.

Presented data are calculated from at least two experiments each performed in duplicates. IC<sub>50</sub> values were calculated for compounds with an inhibition of more than 50 %. Standard deviation of percent inhibition values is less than 14 %. Vehicle control was defined as 0 % inhibition. n.d. = not determined. n.a. = not active.

### 2.3. Inhibitory activity on HDAC2, HDAC4, HDAC6 and HDAC8

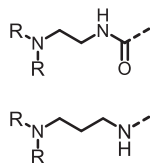
For further evaluation, the synthesized compounds **1a-t** were screened against recombinant human HDAC2, HDAC4, HDAC6 and HDAC8 isozymes (Table 3 and Table 4) CHDI-00390576 and TMP269 were included as class IIa selective HDACi reference compounds. Due to the poor water-solubility of TMP269, the literature IC<sub>50</sub> values are displayed as references. Among the screened *meta*-substituted TFMO-derivatives **1a-k**, compounds **1a** and **1h** displayed an inhibitory activity towards HDAC4 in the micromolar range. In case of the inhibitor **1a**, no direct discrimination between HDAC4 (IC<sub>50</sub>(HDAC4) = 18.0 μM) and HDAC6 (IC<sub>50</sub>(HDAC6) = 19.53 μM) was observed, whereas the bulkier naphthalene derivative **1h** (IC<sub>50</sub>(HDAC4) = 24.1 μM) exhibited a >4-fold preference over the other HDACs. However, the employment of various cap groups in case of the *meta*-derivatives **1c**, **1e-g** and **1j** led to a complete loss of HDAC inhibition. Among the tested *para*-substituted TFMO-derivatives **1l-t**, we have successfully identified seven compounds **1l-r** that displayed a HDAC4 inhibitory activity in the nanomolar range. Compound **1l** was the most active and selective HDAC4 inhibitor (IC<sub>50</sub>(HDAC4) = 12 nM) with a 511/482/355 higher selectivity for HDAC4 than HDAC2/6/8 in the tested series. It demonstrated an approximately 13/8-fold stronger HDAC4 inhibition than TMP269 and the class IIa selective hydroxamate-based compound CHDI-00390576. The elongation of the alkyl chain of compound **1l**, in case of compound **1n**, led to a 12-fold diminished HDAC4 inhibitory activity (IC<sub>50</sub>(HDAC4) = 0.14 μM) with a 181-fold higher HDAC4 selectivity compared to HDAC2 and a 40/48-fold HDAC4-preference over HDAC6/8. Furthermore, the *N*-methylated amide derivative of **1l** (**1o**) showed an approximately 17-fold reduced inhibition of HDAC4 (IC<sub>50</sub>(HDAC4) = 0.198 μM) with a 175/85/55-fold preference over HDAC2/6/8. Surprisingly, the employment of the bulky indole moiety **1p** maintained the HDAC4 inhibitory activity in the nanomolar range (IC<sub>50</sub>(HDAC4) = 0.722 μM) with a ≥ 139-fold preference over the other HDACs. However, the inhibitor **1p** was 60-fold less potent against HDAC4 than compound **1l**. Interestingly, the compound **1m**, led to a HDAC4 inhibition in the low nanomolar range (IC<sub>50</sub>(HDAC4) = 24.5 nM) with decreased selectivity indices for HDAC2 and HDAC6 (SI(HDAC2/4) = 331, SI(HDAC6/4) = 83) compared to **1l**, but a significant increased selectivity over HDAC8 (SI(HDAC8/4) > 4081).

The phenyl substituted compound **1q** resulted in a 26-fold reduced HDAC4 inhibition and selectivity ( $IC_{50}(\text{HDAC4}) = 0.631 \mu\text{M}$ ) compared to compound **1m**. The employment of a dimethyl-aminoaniline moiety in the CAP region (**1r**) led to a 77-fold diminished HDAC4 inhibitory activity ( $IC_{50}(\text{HDAC4}) = 0.928 \mu\text{M}$ ) in comparison to compound **1l**. The piperidine derivative **1s** showed a similar HDAC4 inhibition as compound **1r** ( $IC_{50}(\text{HDAC4}) = 1.18 \mu\text{M}$ ), but with a decreased preference towards the other HDACs. The introduction of a quinoline cap group (**1t**) was not well tolerated and demonstrated a significant shift of the HDAC4 inhibitory activity to the micromolar range ( $IC_{50}(\text{HDAC4}) = 64.7 \mu\text{M}$ ) compared to compound **1l**.

In summary, we have discovered a new series of *para*-substituted TFMO-derivatives as potent and selective HDAC4 inhibitors. Among the tested substances **1a-t**, the compound **1l** was identified as a highly potent HDAC4 inhibitor ( $IC_{50}(\text{HDAC4}) = 12 \text{ nM}$ ) in the nanomolar range with a 511/482/355-fold selectivity over HDAC2/6/8. Initial SAR studies revealed that an elongation of the alkyl chain length of **1l** led to a reduced HDAC4 inhibitory activity. However, the HDAC inhibition of selected isozymes of compound **1u**, a propyl-derivative of compound **1l**, is currently under investigation.

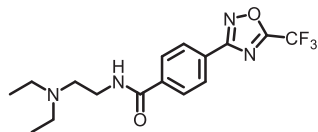
Furthermore, the HDAC class IIa selective inhibitor **1l** displayed a more pronounced HDAC4 inhibition than the lead structure TMP269. **1l** demonstrated an approximately 13/8-fold stronger HDAC4 inhibition than TMP269 and the class IIa selective hydroxamate-based compound CHDI-00390576. Subject of future work will be the lead structure optimization of compound **1l** in its linker, cap and ZBG region to improve its potency, water solubility and metabolic stability (Figure 1). Furthermore, the elucidation of the binding mode of compound **1l** within the catalytic site of HDAC4, via crystallisation studies, is subject of future studies.

**CAP modifictaion:**  
prolongation, truncation  
and cyclisation



R = Me, Et, Propyl,  
heterocyclic aliphatic  
amines: morpholine,  
piperidine

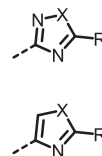
**Linker modifictaion:**  
substituted benzene, 6-membered  
heterocycles (e.g. pyridines)



**CAP CU Linker ZBG**

**Compound 11:** selective HDAC4i  
IC<sub>50</sub>(HDAC4) = 12 nM  
SI (HDAC2/4) = 511  
SI (HDAC6/4) = 482  
SI (HDAC8/4) = 355

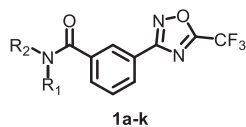
**ZBG modifictaion:**



X = O, S, NH  
R = CF<sub>3</sub>, CHF<sub>2</sub>, CH<sub>2</sub>F, CH<sub>2</sub>OH

Figure 1: Lead structure optimization of compound **11**.

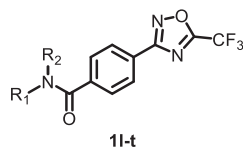
Table 3: Inhibitory activity of **1a-k**, CHDI-00390576 and TMP269 on recombinant human HDAC2, HDAC4, HDAC6 and HDAC8.



Cpd.	R <sub>1</sub>	R <sub>2</sub>	IC <sub>50</sub> [μM] (pIC <sub>50</sub> ± SEM)			
			HDAC2	HDAC4	HDAC6	HDAC8
<b>1a</b>	Me		n.d.	18.0 (4.75 ± 0.04)	19.53 (4.71 ± 0.03)	26.4 (4.58 ± 0.05)
<b>1b</b>	H		>100	n.d.	>100	>100
<b>1c</b>	H		>100	>100	>100	>100
<b>1d</b>	H		>100	n.d.	>100	>100
<b>1e</b>	Benzyl		>100	>100	>100	>100
<b>1f</b>	H		>100	>100	>100	>100
<b>1g</b>	H		>100	>100	>100	>100
<b>1h</b>	H		>100	24.1 (4.62 ± 0.09)	>100	>100
<b>1i</b>	H		>100	n.d.	>100	>100
<b>1j</b>	H		>100	>100	>100	>100
<b>1k</b>	H		>100	n.d.	>100	>100
		CHDI-00390576	>100	0.097 (7.01 ± 0.03)	5.98 (5.22 ± 0.04)	24.77 (4.61 ± 0.02)
		TMP269*	>100	0.157	8.2	4.2

Data shown is at least from two experiments each performed at least as duplicates and the IC<sub>50</sub> value of pooled data is reported when IC<sub>50</sub> < 100 μM. \*Data taken from Lobera et al.<sup>[29]</sup>

Table 4: Inhibitory activity of **1l-t**, CHDI-00390576 and TMP269 on recombinant human HDAC2, HDAC4, HDAC6 and HDAC8.



Cpd.	R <sub>1</sub>	R <sub>2</sub>	IC <sub>50</sub> [μM] (pIC <sub>50</sub> ± SEM)			
			HDAC2	HDAC4	HDAC6	HDAC8
<b>1l</b>	H		6.13 (5.21 ± 0.08)	0.012 (7.93 ± 0.03)	5.79 (5.24 ± 0.09)	4.26 (5.37 ± 0.04)
<b>1m</b>	Me		8.12 (5.09 ± 0.03)	0.0245 (7.61 ± 0.04)	2.03 (5.69 ± 0.04)	>100
<b>1n</b>	H		25.4 (4.60 ± 0.03)	0.139 (6.86 ± 0.03)	5.61 (5.25 ± 0.07)	6.72 (5.17 ± 0.042)
<b>1o</b>	Me		34.79 (4.50 ± 0.04)	0.198 (6.70 ± 0.04)	16.89 (4.77 ± 0.09)	10.8 (4.97 ± 0.04)
<b>1p</b>	H		>100	0.722 (6.14 ± 0.04)	>100	>100
<b>1q</b>	Me		>100	0.631 (6.20 ± 0.639)	19.57 (4.71 ± 0.06)	71.79 (4.14 ± 0.086)
<b>1r</b>	H		>100	0.928 (6.03 ± 0.04)	>100	>100
<b>1s</b>	-		80.03 (4.1 ± 0.027)	1.18 (5.93 ± 0.012)	55.41 (4.26 ± 0.11)	16.1 (4.79 ± 0.031)
<b>1t</b>	H		>100	64.7 (4.19 ± 0.51)	>100	>100
		CHDI-00390576	>100	0.097 (7.01 ± 0.03)	5.98 (5.22 ± 0.04)	24.77 (4.61 ± 0.02)
		TMP269*	>100	0.157	8.2	4.2

Data shown is at least from two experiments each performed at least as duplicates and the IC<sub>50</sub> value of pooled data is reported when IC<sub>50</sub> < 100 μM. \*Data taken from Lobera et al.<sup>[29]</sup>

### 3. Conclusions

Lysine acetylation has emerged as a major target for the regulation of posttranslational modifications of histones and numerous other proteins such as transcription factors and cellular proteins. Acetylation, mediated by histone acetyltransferases (HATs), is a dynamic equilibrium reversed by a class of enzymes known as histone deacetylases (HDACs). HDACs have a crucial role in various physiological and pathological processes e.g. in cell differentiation, proliferation and apoptosis. HDAC4, 5, 7 and 9 constitute the class IIa HDAC subtype within the HDAC family. Class IIa HDACs possess distinctive features that distinguish them from the other HDAC classes as they do not “erase” acetylated lysines and are rarely associated to histone tails. Selective HDAC class IIa are of relevance for the treatment of e.g. cancer and neurodegenerative diseases like Huntington’s disease. Due to the conserved active site of HDACs, only a few class IIa-selective HDAC inhibitors have been identified. Here, we report the synthesis and biological evaluation of *meta*- and *para*-substituted TFMO-derivatives **1a-t** exhibiting an amide as connecting unit. We have successfully identified seven potent and selective HDAC inhibitors in the nanomolar range. The most potent and selective HDAC class IIa inhibitor was compound **1l** ( $IC_{50}(\text{HDAC4}) = 12 \text{ nM}$ ) with a 511/482/355-fold selectivity over HDAC2/6/8. **1l** demonstrated an approximately 13/8-fold stronger HDAC4 inhibition than TMP269 and the class IIa selective hydroxamate-based compound CHDI-00390576. Further biological evaluation will focus on the combination studies of our class IIa selective HDACi with proteasome inhibitors in the leukemia cell lines HL-60 and RPM-8226 as well as in the human tongue squamous carcinoma cell line Cal27 and the human ovarian cancer cell line A2780.

### Acknowledgements

YA, AJS, MUK, and TK gratefully acknowledge support from the Deutsche Forschungsgemeinschaft (DFG) for grant number KA 1942/1-1 to MUK and grant number KU 1577/2-1 to TK, and the support from the DFG research training group GRK2158 (270650915/GRK2158). We further acknowledge the CHDI Foundation Inc. for providing the compound CHDI-00390576.

## Supplementary information

Experimental procedures and analytical data for compounds **1a-t** and **4-7** are provided as supplementary information.

## References

- [1] A. J. Guise, R. A. Mathias, E. A. Rowland, F. Yu, I. M. Cristea, *Proteomics* **2014**, *14*, 2156–2166.
- [2] M. Haberland, R. L. Montgomery, E. N. Olson, *Nat. Rev. Genet.* **2011**, *10*, 32–42.
- [3] A. D. Goldberg, C. D. Allis, E. Bernstein, *Cell* **2007**, *128*, 635–638.
- [4] X.-J. Yang, E. Seto, *Nat. Rev. Mol. Cell Biol.* **2008**, *9*, 206–218.
- [5] I. Berger, C. Bieniossek, C. Schaffitzel, M. Hassler, E. Santelli, T. J. Richmond, *J. Biol. Chem.* **2003**, *278*, 17625–17635.
- [6] B. M. Sefton, *Curr. Protoc. Cell Biol.* **1998**, *00*, 14.1.1-14.1.3.
- [7] M. N. Melo-Braga, M. Schulz, Q. Liu, A. Swistowski, G. Palmisano, K. Engholm-Keller, L. Jakobsen, X. Zeng, M. R. Larsen, *Mol. Cell. Proteomics* **2014**, *13*, 311–328.
- [8] C. M. Grozinger, C. A. Hassig, S. L. Schreiber, *Proc. Natl. Acad. Sci. U. S. A.* **1999**, *96*, 4868–4873.
- [9] H. Y. Kao, M. Downes, P. Ordentlich, R. M. Evans, *Genes Dev.* **2000**, *14*, 55–66.
- [10] T. A. McKinsey, in *Handb. Exp. Pharmacol.*, **2011**, pp. 57–78.
- [11] B. C. Harrison, K. Huynh, G. L. Lundgaard, S. M. Helmke, M. B. Perryman, T. A. McKinsey, *FEBS Lett.* **2010**, *584*, 1103–1110.
- [12] J. S. Martini, P. Raake, L. E. Vinge, B. R. DeGeorge, J. K. Chuprun, D. M. Harris, E. Gao, A. D. Eckhart, J. A. Pitcher, W. J. Koch, *Proc. Natl. Acad. Sci. U. S. A.* **2008**, *105*, 17206.
- [13] T. A. McKinsey, *Cardiovasc. Res.* **2007**, *73*, 667–677.
- [14] A. Lahm, C. Paolini, M. Pallaoro, M. C. Nardi, P. Jones, P. Neddermann, S. Sambucini, M. J. Bottomley, P. Lo Surdo, A. Carfí, et al., *Proc. Natl. Acad. Sci. U. S. A.* **2007**, *104*, 17335–17340.
- [15] W. Fischle, F. Dequiedt, M. J. Hendzel, M. G. Guenther, M. A. Lazar, W. Voelter, E. Verdin, *Mol. Cell* **2002**, *9*, 45–57.
- [16] M. Parra, *FEBS J.* **2015**, *282*, 1736–1744.
- [17] H. L. Fitzsimons, *Neurobiol. Learn. Mem.* **2015**, *123*, 149–158.
- [18] E. Di Giorgio, C. Brancolini, *Epigenomics* **2016**, *8*, 251–269.
- [19] L. G. Harris, S. H. Wang, S. K. Mani, H. Kasiganesan, C. J. Chou, D. R. Menick,

*Nucleic Acids Res.* **2016**, *44*, 3610–3617.

- [20] J. E. Bradner, N. West, M. L. Grachan, E. F. Greenberg, S. J. Haggarty, T. Warnow, R. Mazitschek, *Nat. Chem. Biol.* **2010**, *6*, 238–243.
- [21] W. Fischle, V. Kiermer, F. Dequiedt, E. Verdin, *Biochem. Cell Biol.* **2001**, *79*, 337–348.
- [22] M. Martin, R. Kettmann, F. Dequiedt, *Int. J. Dev. Biol.* **2009**, *53*, 291–301.
- [23] A. S. Carvalho, H. Ribeiro, P. Voabil, D. Penque, O. N. Jensen, H. Molina, R. Matthiesen, *Mol. Cell. Proteomics* **2014**, *13*, 3294–3307.
- [24] C. L. Zhang, T. A. McKinsey, S. Chang, C. L. Antos, J. A. Hill, E. N. Olson, *Cell* **2002**, *110*, 479–488.
- [25] A. Clocchiatti, E. Di Giorgio, S. Ingraio, F.-J. Meyer-Almes, C. Tripodo, C. Brancolini, *FASEB J.* **2013**, *27*, 942–954.
- [26] M. M. Mihaylova, D. S. Vasquez, K. Ravnskjaer, P. D. Denechaud, R. T. Yu, J. G. Alvarez, M. Downes, R. M. Evans, M. Montminy, R. J. Shaw, *Cell* **2011**, *145*, 607–621.
- [27] M. Mielcarek, C. Landles, A. Weiss, A. Bradaia, T. Seredenina, L. Inuabasi, G. F. Osborne, K. Wadel, C. Touller, R. Butler, et al., *PLoS Biol.* **2013**, *11*, e1001717.
- [28] C. A. Luckhurst, O. Aziz, V. Beaumont, R. W. Bürli, P. Breccia, M. C. Maillard, A. F. Haughan, M. Lamers, P. Leonard, K. L. Matthews, et al., *Bioorg. Med. Chem. Lett.* **2019**, *29*, 83–88.
- [29] M. Lobera, K. P. Madauss, D. T. Pohlhaus, Q. G. Wright, M. Trocha, D. R. Schmidt, E. Baloglu, R. P. Trump, M. S. Head, G. A. Hofmann, et al., *Nat. Chem. Biol.* **2013**, *9*, 319–325.

Supporting Information

**The Second Generation of  
Potent and Selective  
Class IIa Histone Deacetylase Inhibitors**

*Yodita Asfaha<sup>\*#</sup>, Alexander Jan Skerhut<sup>\*#</sup>, Leandro A. Alves-Avelar<sup>\*</sup>, Nadine Horstick-Muche<sup>\*</sup>,  
Matthias U. Kassack<sup>\*#</sup>, Thomas Kurz<sup>\*#</sup>*

\*Institut für Pharmazeutische und Medizinische Chemie, Heinrich-Heine-Universität  
Düsseldorf, Universitätsstr. 1, 40225 Düsseldorf, Germany. #YA and AJS share first authorship,  
MUK and TK share senior and corresponding authorship.

## Experimental section

### General methods

All chemicals and solvents were purchased from commercial suppliers (Sigma Aldrich, Alfa Aesar, Fluorochem, TCI, abcr and Acros Organics) and used without further purification. All anhydrous reactions were carried out in flame-dried Schlenk-flasks and under argon atmosphere. Dry solvents were used directly from Seal<sup>®</sup> bottles from Acros Organics. Analytic Thin Layer Chromatography (TLC) was carried out with Macherey Nagel precoated silica gel plates (ALUGRAM<sup>®</sup> Xtra SIL G/UV<sub>254</sub>). Detection was achieved with ultraviolet irradiation (254 nm) and/or staining with potassium permanganate solution (9 g KMnO<sub>4</sub>, 60 g K<sub>2</sub>CO<sub>3</sub>, 15 mL of a 5% aqueous NaOH-solution, and 900 mL demineralised water). Flash column chromatography was performed with CombiFlashRf200 (TeleDyneIsco) with the solvent mixtures specified in the corresponding procedure.

### Physical data

Proton (<sup>1</sup>H) and carbon (<sup>13</sup>C) NMR spectra were recorded on Bruker Avance III – 300, Bruker Avance DRX – 500 or Bruker Avance III – 600. Spectra were referenced to the residual non-deuterated solvent signal (<sup>1</sup>H-NMR: DMSO-*d*<sub>6</sub> (2.50 ppm), <sup>13</sup>C-NMR: DMSO-*d*<sub>6</sub> (39.52 ppm); <sup>1</sup>H-NMR: CDCl<sub>3</sub> (7.26 ppm), <sup>13</sup>C-NMR: CDCl<sub>3</sub> (77.16 ppm)). Chemical shifts are quoted in parts per million (ppm). Signal patterns are indicated as: singlet (s), doublet (d), triplet (t), quartet (q), or multiplet (m). Coupling constants, *J*, are measured in Hz. Proton (<sup>1</sup>H) and carbon (<sup>13</sup>C) NMR spectra were recorded by the NMR-Divisions of the Department of Chemistry (Heinrich Heine University Duesseldorf). Electrospray Ionisation (ESI) mass spectra were carried out by the Mass spectrometry-Division of the Heinrich Heine University Duesseldorf, using Bruker Daltonics UHR-QTOF maXis 4G (Bruker Daltonics). Melting points (mp.) were determined using a Büchi M-565 melting point apparatus and are uncorrected.

Analytical HPLC analysis were carried out on a Knauer HPLC system comprising an Azura P 6.1L pump, an Optimas 800 autosampler, a Fast Scanning Spectro-Photometer K-2600 and a Knauer Reversed Phase column (SN: FK36). UV absorption was detected at 254 nm. The solvent gradient table is shown below. The purity of all final compounds was 95% or higher.

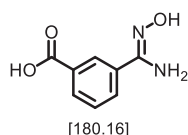
Table 1: The solvent gradient table for analytic HPLC analysis.

Time / min	Water + 0.1% TFA	ACN + 0.1% TFA
Initial	90	10
0.50	90	10
20.0	0	100
30.0	0	100
31.0	90	10
40.0	90	10

### General procedure 1: Formation of amidoximes

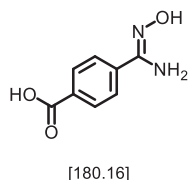
Following the procedure of Lobera et al.,<sup>[1]</sup> 1.00 eq of the respective nitrile **2**, **3** and 0.4 mol% of 8-hydroxyquinoline were dissolved in EtOH (10 mL/mmol). To this reaction mixture, 2.00 eq hydroxylamine hydrochloride in water (2.0 mL/mmol) and 1.60 eq potassium carbonate in water (1 mL/mmol) were added. The mixture was stirred at reflux for 6 h. The solvent was then removed under reduced pressure. The residue was diluted with water and the aqueous phase acidified to pH = 3. The formed precipitate was then filtered, washed with water and acetone to furnish the corresponding amidoxime **4** and **5**.

### Synthesis of 3-(*N'*-hydroxycarbamimidoyl)benzoic acid (**4**)



3-Cyanobenzoic acid **2** (2.94 g, 20.0 mmol, 1.00 eq) was subjected to General procedure 1. The amidoxime **4** (3.10 g, 17.2 mmol, 86%) was obtained as a white solid. All spectroscopic data were in agreement with the literature.<sup>[1]</sup>

### Synthesis of 4-(*N'*-hydroxycarbamimidoyl)benzoic acid (**5**)



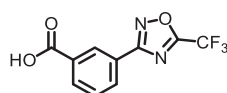
4-Cyanobenzoic acid **3** (4.50 g, 30.0 mmol, 1.00 eq) was subjected to General procedure 1 to provide the amidoxime **5** (4.68 g, 26.0 mmol, 87%) as a yellow solid. All spectroscopic data were in agreement with the literature.<sup>[2]</sup>

### General procedure 2: Formation of the TFMO-moiety

A solution of the respective amidoxime **4** and **5** (1.00 eq) in anhydrous toluene (1 mmol/mL) was cooled to 0 °C and 3.00 eq trifluoroacetic anhydride was added dropwise. The reaction mixture was slowly allowed to warm to rt and then refluxed for further 8 h. The solvent was removed under reduced pressure, and the crude solid diluted with ethyl acetate. The organic

layer was washed with brine (3x25 mL), dried over Na<sub>2</sub>SO<sub>4</sub>, filtered and the solvent removed under reduced pressure. The crude product was purified by recrystallisation (ethyl acetate/*n*-hexane) yielding the products **6** and **7**.

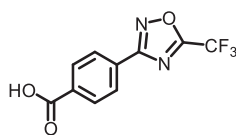
### Synthesis of 3-(5-(trifluoromethyl)-1,2,4-oxadiazol-3-yl)benzoic acid (**6**)



[258.16]

3-(*N*'-Hydroxycarbamimidoyl)benzoic acid (**4**) (979 mg, 5.43 mmol, 1.00 eq) was subjected to General procedure 2 to furnish the product **6** (624 mg, 2.42 mmol, 45%) as a white solid. All spectroscopic data were in agreement with the literature. <sup>[1]</sup>

### Synthesis of 4-(5-(trifluoromethyl)-1,2,4-oxadiazol-3-yl)benzoic acid (**7**)



[258.16]

4-(*N*'-Hydroxycarbamimidoyl)benzoic acid (**5**) (1.80 g, 10.0 mmol, 1.00 eq) was subjected to General procedure 2 to afford 3-(5-(trifluoromethyl)-1,2,4-oxadiazol-3-yl)benzoic acid (**7**) (1.55 g, 6.00 mmol, 60%) as a white solid.

<sup>1</sup>H NMR (300 MHz, DMSO-*d*<sub>6</sub>) δ = 8.08 – 8.24 (m, 4H), 13.38 (s, 1H) ppm.

<sup>13</sup>C NMR (75 MHz, DMSO) δ = 115.65 (q), 127.56, 128.04, 130.20, 134.20, 165.47, 165.24 (q), 167.86 ppm.

HPLC analysis: *R*<sub>t</sub> = 12.483 min, 95.8%.

HRMS (ESI+) = calcd. for C<sub>12</sub>H<sub>8</sub>F<sub>3</sub>N<sub>3</sub>O<sub>3</sub> [M+ACN]<sup>+</sup> = 299.0518, found: 299.2219.

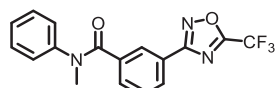
mp.: 251°C.

### General procedure 3: HATU-coupling

For the synthesis of the amides **1a-t**, 1.00 eq of the respective carboxylic acid **6** and **7** was dissolved in dry DMF (0.1 mmol/mL) and 1.00 eq HATU as well as 2.00 eq DIPEA were added. After stirring for 15 min at rt, the corresponding amine (1.00 eq) was added and the resulting mixture stirred for further 16 h at rt. The solvent was removed under reduced pressure and

the residue diluted with EtOAc. The organic layer was washed with saturated NaHCO<sub>3</sub> (3x 50 mL), brine (1x 50 mL), dried over Na<sub>2</sub>SO<sub>4</sub> and filtered. After removing the solvent, the crude product was purified as stated.

### Synthesis of *N*-methyl-*N*-phenyl-3-(5-(trifluoromethyl)-1,2,4-oxadiazol-3-yl)benzamide (**1a**)



[347.30]

3-(5-(Trifluoromethyl)-1,2,4-oxadiazol-3-yl)benzoic acid (**6**) (387 mg, 1.50 mmol, 1.00 eq) was converted with *N*-methylaniline (161 mg, 1.50 mmol, 1.00 eq) according to General procedure 3. The crude product was purified by flash chromatography (*n*-hexane/EtOAc) to afford **1a** (250 mg, 0.72 mmol, 48%) as a beige solid.

<sup>1</sup>H NMR (600 MHz, DMSO-*d*<sub>6</sub>) δ = 3.41 (s, 3H), 7.16 (tt, *J* = 6.8, 1.6 Hz, 1H), 7.21 – 7.29 (m, 4H), 7.46 (dt, *J* = 15.3, 7.7 Hz, 2H), 7.95 (dt, *J* = 7.6, 1.6 Hz, 1H), 7.98 (d, *J* = 1.8 Hz, 1H) ppm.

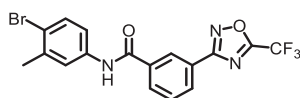
<sup>13</sup>C NMR (151 MHz, DMSO-*d*<sub>6</sub>) δ = 37.86, 115.69 (q, *J* = 273.2 Hz), 124.11, 126.77, 127.01, 127.17, 128.09, 129.08, 129.18, 131.99, 137.61, 144.10, 115.69 (q, *J* = 273.2 Hz), 167.82, 168.20 ppm.

HPLC analysis: *R*<sub>t</sub> = 14.650 min, >99%.

HRMS (ESI+) = calcd. for C<sub>17</sub>H<sub>13</sub>F<sub>3</sub>N<sub>3</sub>O<sub>2</sub> [M+H]<sup>+</sup> = 348.0954, found: 348.0957.

mp.: 60.6 °C.

### Synthesis of *N*-(4-bromo-3-methylphenyl)-3-(5-(trifluoromethyl)-1,2,4-oxadiazol-3-yl)benzamide (**1b**)



[426.19]

3-(5-(Trifluoromethyl)-1,2,4-oxadiazol-3-yl)benzoic acid (**6**) (774 mg, 3.00 mmol, 1.00 eq) was coupled with 4-bromo-3-methylaniline (558 mg, 3.00 mmol, 1.00 eq) according to General procedure 3. The crude product was purified by flash chromatography (*n*-hexane/EtOAc) and then further purified by recrystallisation (*n*-hexane/ EtOAc) to afford **1b** (344 mg, 0.81 mmol, 27%) as a white solid.

$^1\text{H}$  NMR (600 MHz,  $\text{DMSO-}d_6$ )  $\delta$  = 2.36 (s, 3H), 7.56 (d,  $J$  = 8.6 Hz, 1H), 7.61 (dd,  $J$  = 8.7, 2.6 Hz, 1H), 7.77 – 7.82 (m, 2H), 8.26 (ddt,  $J$  = 17.3, 7.9, 1.4 Hz, 2H), 8.62 (t,  $J$  = 1.8 Hz, 1H), 10.56 (s, 1H) ppm.

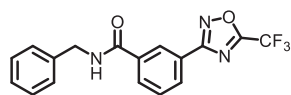
$^{13}\text{C}$  NMR (151 MHz,  $\text{DMSO-}d_6$ )  $\delta$  = 22.67, 115.76 (q,  $J$  = 273.0 Hz), 118.23, 119.97, 122.85, 124.73, 126.51, 129.86, 130.33, 131.67, 132.15, 135.77, 137.34, 138.39, 164.31, 165.22 (q,  $J$  = 43.8 Hz), 168.05 ppm.

HPLC analysis:  $R_t$  = 17.500 min, >99%.

HRMS (ESI+) = calcd. for  $\text{C}_{17}\text{H}_{12}\text{BrF}_3\text{N}_3\text{O}_2$  [M] = 426.0059, found: 426.0063.

mp.: 179.2 °C.

### Synthesis of *N*-benzyl-3-(5-(trifluoromethyl)-1,2,4-oxadiazol-3-yl)benzamide (**1c**)



[347.30]

3-(5-(Trifluoromethyl)-1,2,4-oxadiazol-3-yl)benzoic acid (**6**) (387 mg, 1.50 mmol, 1.00 eq) was treated with benzylamine (161 mg, 1.50 mmol, 1.00 eq) according to General procedure 3. The crude product was purified by flash chromatography (*n*-hexane/EtOAc) to provide **1c** (350 mg, 1.01 mmol, 67%) as a white solid.

$^1\text{H}$  NMR (600 MHz,  $\text{DMSO-}d_6$ )  $\delta$  = 4.52 (d,  $J$  = 5.9 Hz, 2H), 7.25 (tp,  $J$  = 5.6, 2.8 Hz, 1H), 7.32 – 7.37 (m, 4H), 7.74 (t,  $J$  = 7.8 Hz, 1H), 8.21 (ddt,  $J$  = 19.5, 7.9, 1.4 Hz, 2H), 8.59 (t,  $J$  = 1.8 Hz, 1H), 9.36 (t,  $J$  = 5.9 Hz, 1H) ppm.

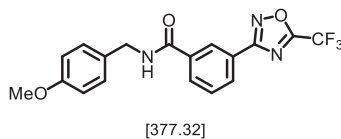
$^{13}\text{C}$  NMR (151 MHz,  $\text{DMSO-}d_6$ )  $\delta$  = 42.79, 115.76 (q,  $J$  = 273.2 Hz), 124.68, 126.18, 126.81, 127.31, 128.31, 129.79, 129.94, 131.25, 135.41, 164.99, 165.17 (q,  $J$  = 43.6 Hz), 168.12 ppm.

HPLC analysis:  $R_t$  = 14.850 min, >99%.

HRMS (ESI+) = calcd. for  $\text{C}_{16}\text{H}_{18}\text{F}_3\text{N}_4\text{O}_4$  [M+H]<sup>+</sup> = 387.1275, found: 387.1279.

mp.: 113.0 °C.

### Synthesis of *N*-(4-methoxybenzyl)-3-(5-(trifluoromethyl)-1,2,4-oxadiazol-3-yl)benzamide (**1d**)



3-(5-(Trifluoromethyl)-1,2,4-oxadiazol-3-yl)benzoic acid (**6**) (258 mg, 1.00 mmol, 1.00 eq) was converted with 4-methoxybenzylamine (137 mg, 1.00 mmol, 1.00 eq) according to General procedure 3. The crude product was purified by flash chromatography (*n*-hexane/EtOAc) to provide **1d** (205 mg, 0.54 mmol, 54%) as a white solid.

$^1\text{H}$  NMR (600 MHz,  $\text{DMSO-}d_6$ )  $\delta$  = 3.73 (s, 3H), 4.44 (d,  $J$  = 5.9 Hz, 2H), 6.87 – 6.92 (m, 2H), 7.25 – 7.30 (m, 2H), 7.73 (t,  $J$  = 7.8 Hz, 1H), 8.14 – 8.18 (m, 1H), 8.19 – 8.23 (m, 1H), 8.57 (t,  $J$  = 1.7 Hz, 1H), 9.29 (t,  $J$  = 5.9 Hz, 1H) ppm.

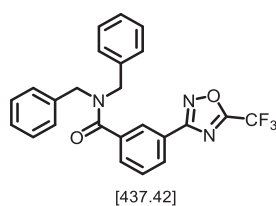
$^{13}\text{C}$  NMR (151 MHz,  $\text{DMSO-}d_6$ )  $\delta$  = 42.27, 55.05, 113.72, 114.86 (q,  $J$  = 271.5 Hz), 124.66, 126.17, 128.72, 129.77, 129.89, 131.24, 131.38, 135.51, 158.26, 164.88, 165.04, 165.32, 165.62, 168.13 ppm.

HPLC analysis:  $R_t$  = 14.333 min, >99%.

HRMS (ESI+) = calcd. for  $\text{C}_{18}\text{H}_{15}\text{F}_3\text{N}_3\text{O}_3$   $[\text{M}+\text{H}]^+$  = 378.1060, found: 378.1058.

mp.: 129.6 °C.

### Synthesis of *N,N*-dibenzyl-3-(5-(trifluoromethyl)-1,2,4-oxadiazol-3-yl)-benzamide (**1e**)



3-(5-(Trifluoromethyl)-1,2,4-oxadiazol-3-yl)benzoic acid (**6**) (258 mg, 1.00 mmol, 1.00 eq) was coupled with dibenzylamine (203 mg, 1.00 mmol, 1.00 eq) according to General procedure 3. The crude product was purified by flash chromatography (*n*-hexane/EtOAc) to furnish **1e** (249 mg, 0.57 mmol, 57%) as a white solid.

$^1\text{H}$  NMR (600 MHz,  $\text{DMSO-}d_6$ )  $\delta$  = 4.44 (s, 2H), 4.64 (s, 2H), 7.16 (s, 2H), 7.36 (d,  $J$  = 32.7 Hz, 9H), 7.68 (td,  $J$  = 7.7, 0.6 Hz, 1H), 7.74 – 7.80 (m, 1H), 8.06 (td,  $J$  = 1.8, 0.6 Hz, 1H), 8.12 (ddd,  $J$  = 7.8, 1.8, 1.2 Hz, 1H) ppm.

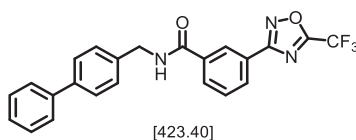
$^{13}\text{C}$  NMR (75 MHz,  $\text{DMSO-}d_6$ )  $\delta$  = 47.38, 51.60, 115.71 (q,  $J$  = 273.1 Hz), 124.81, 125.27, 126.79, 127.35, 127.74, 128.38, 128.70, 130.00, 130.38, 136.34, 136.88, 137.33, 165.13 (q,  $J$  = 43.9 Hz), 167.88, 169.99 ppm.

HPLC analysis:  $R_t$  = 17.967 min, >99%.

HRMS (ESI+) = calcd. for  $\text{C}_{24}\text{H}_{19}\text{F}_3\text{N}_3\text{O}_2$   $[\text{M}+\text{H}]^+$  = 438.1424, found: 483.1427.

mp.: 82.0 °C.

### Synthesis of *N*-([1,1'-biphenyl]-4-ylmethyl)-3-(5-(trifluoromethyl)-1,2,4-oxadiazol-3-yl)benzamide (**1f**)



3-(5-(Trifluoromethyl)-1,2,4-oxadiazol-3-yl)benzoic acid (**6**) (258 mg, 1.00 mmol, 1.00 eq) was treated with 4-phenylbenzylamine (187 mg, 1.00 mmol, 1.00 eq) according to General procedure 3. The crude product was purified by flash chromatography (*n*-hexane/EtOAc) to afford **1f** (247 mg, 0.65 mmol, 65%) as a white solid.

$^1\text{H}$  NMR (600 MHz,  $\text{DMSO-}d_6$ )  $\delta$  = 4.57 (d,  $J$  = 5.9 Hz, 2H), 7.33 – 7.37 (m, 1H), 7.45 (td,  $J$  = 8.4, 7.9, 2.0 Hz, 4H), 7.61 – 7.67 (m, 4H), 7.75 (t,  $J$  = 7.8 Hz, 1H), 8.22 (ddt,  $J$  = 13.6, 7.9, 1.4 Hz, 2H), 8.61 (t,  $J$  = 1.8 Hz, 1H), 9.40 (t,  $J$  = 5.9 Hz, 1H) ppm.

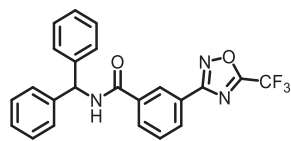
$^{13}\text{C}$  NMR (151 MHz,  $\text{DMSO-}d_6$ )  $\delta$  = 42.55, 115.76 (q,  $J$  = 273.2 Hz), 124.70, 126.18, 126.57, 126.66, 127.31, 127.97, 128.90, 129.82, 129.97, 131.28, 135.40, 138.66, 138.81, 139.97, 165.02, 165.18 (q,  $J$  = 43.8 Hz), 168.12 ppm.

HPLC analysis:  $R_t$  = 16.733 min, 97.9%.

HRMS (ESI+) = calcd. for  $\text{C}_{23}\text{H}_{17}\text{F}_3\text{N}_3\text{O}_2$   $[\text{M}+\text{H}]^+$  = 424.1267, found: 424.1266.

mp.: 188.1 °C.

### Synthesis of *N*-benzhydryl-3-(5-(trifluoromethyl)-1,2,4-oxadiazol-3-yl)benzamide (**1g**)



[423.40]

3-(5-(Trifluoromethyl)-1,2,4-oxadiazol-3-yl)benzoic acid (**6**) (258 mg, 1.00 mmol, 1.00 eq) was converted with benzhydrylamine hydrochloride (220 mg, 1.00 mmol, 1.00 eq) according to General procedure 3. The crude product was purified by flash chromatography (*n*-hexane/EtOAc) to provide **1g** (256 mg, 0.61 mmol, 61%) as a white solid.

<sup>1</sup>H NMR (600 MHz, DMSO-*d*<sub>6</sub>) δ = 9.63 (d, *J* = 8.6 Hz, 1H), 8.61 (t, *J* = 1.8 Hz, 1H), 8.23 (ddt, *J* = 7.9, 3.1, 1.5 Hz, 2H), 7.74 (t, *J* = 7.8 Hz, 1H), 7.40 – 7.35 (m, 8H), 7.30 – 7.26 (m, 2H), 6.46 (d, *J* = 8.6 Hz, 1H) ppm.

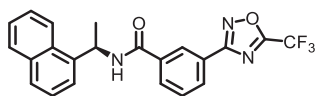
<sup>13</sup>C NMR (151 MHz, DMSO-*d*<sub>6</sub>) δ = 56.55, 115.75 (q, *J* = 273.2 Hz), 124.58, 126.51, 127.07, 127.68, 128.36, 129.67, 130.05, 131.72, 135.40, 142.03, 164.79, 165.17 (q, *J* = 43.7 Hz), 168.13 ppm.

HPLC analysis: *R*<sub>t</sub> = 16.433 min, >99%.

HRMS (ESI+) = calcd. for C<sub>23</sub>H<sub>17</sub>F<sub>3</sub>N<sub>3</sub>O<sub>2</sub> [M+H]<sup>+</sup> = 424.1267, found: 424.1267.

mp.: 162.1 °C.

### Synthesis of (*R*)-*N*-(1-(naphthalen-1-yl)ethyl)-3-(5-(trifluoromethyl)-1,2,4-oxadiazol-3-yl)benzamide (**1h**)



[411.38]

3-(5-(Trifluoromethyl)-1,2,4-oxadiazol-3-yl)benzoic acid (**6**) (258 mg, 1.00 mmol, 1.00 eq) was coupled with (*R*)-(+)-1-(1-naphthyl)ethylamine (171 mg, 1.00 mmol, 1.00 eq) according to General procedure 3. The crude product was purified by flash chromatography (*n*-hexane/EtOAc) to obtain **1h** (316 mg, 0.77 mmol, 77%) as a white solid.

<sup>1</sup>H NMR (600 MHz, DMSO-*d*<sub>6</sub>) δ = 1.66 (d, *J* = 6.9 Hz, 3H), 6.00 (p, *J* = 7.1 Hz, 1H), 7.49 – 7.55 (m, 2H), 7.58 (ddd, *J* = 8.3, 6.6, 1.3 Hz, 1H), 7.64 – 7.69 (m, 1H), 7.73 (t, *J* = 7.8 Hz, 1H), 7.84 (d,

$J = 8.1$  Hz, 1H), 7.95 (dd,  $J = 7.9, 1.4$  Hz, 1H), 8.18 – 8.24 (m, 3H), 8.59 (d,  $J = 1.8$  Hz, 1H), 9.30 (d,  $J = 7.7$  Hz, 1H) ppm.

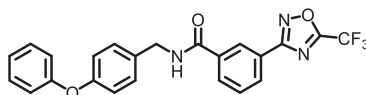
$^{13}\text{C}$  NMR (151 MHz, DMSO- $d_6$ )  $\delta = 21.31, 44.96, 115.76$  (q,  $J = 273.3$  Hz), 122.64, 123.09, 124.60, 125.48, 125.60, 126.23, 126.29, 127.34, 128.68, 129.68, 129.94, 130.46, 131.49, 133.38, 135.51, 140.06, 164.27, 165.17 (q,  $J = 43.7$  Hz), 168.14 ppm.

HPLC analysis:  $R_t = 16.383$  min, >99%.

HRMS (ESI+) = calcd. for  $\text{C}_{22}\text{H}_{17}\text{F}_3\text{N}_3\text{O}_2$   $[\text{M}+\text{H}]^+ = 412.1267$ , found: 412.1269.

mp.: 163.8 °C.

### Synthesis of *N*-(4-phenoxybenzyl)-3-(5-(trifluoromethyl)-1,2,4-oxadiazol-3-yl)benzamide (1i)



[439.39]

3-(5-(Trifluoromethyl)-1,2,4-oxadiazol-3-yl)benzoic acid (**6**) (258 mg, 1.00 mmol, 1.00 eq) was treated with 2-phenoxyaniline (191 mg, 1.00 mmol, 1.00 eq) according to General procedure 3. The crude product was purified by flash chromatography (*n*-hexane/EtOAc) and by recrystallisation (*n*-hexane/EtOAc) to furnish **1i** (229 mg, 0.54 mmol, 54%) as white crystals.

$^1\text{H}$  NMR (600 MHz, DMSO- $d_6$ )  $\delta = 6.99 - 7.02$  (m, 2H), 7.04 – 7.08 (m, 2H), 7.10 – 7.14 (m, 1H), 7.35 – 7.42 (m, 2H), 7.77 – 7.84 (m, 3H), 8.27 (ddd,  $J = 9.4, 6.9, 1.6$  Hz, 2H), 8.63 (t,  $J = 1.8$  Hz, 1H), 10.56 (s, 1H) ppm.

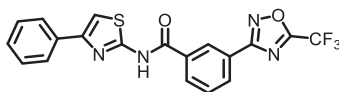
$^{13}\text{C}$  NMR (151 MHz, DMSO- $d_6$ )  $\delta = 115.76$  (q,  $J = 273.3$  Hz), 118.04, 119.22, 122.29, 123.09, 124.72, 126.52, 129.83, 129.98, 130.19, 131.61, 134.67, 135.99, 152.41, 157.21, 164.13, 165.22 (q,  $J = 43.8$  Hz), 168.08 ppm.

HPLC analysis:  $R_t = 17.300$  min, >99%.

HRMS (ESI+) = calcd. for  $\text{C}_{22}\text{H}_{15}\text{F}_3\text{N}_3\text{O}_3$   $[\text{M}+\text{H}]^+ = 426.1060$ , found: 426.1058.

mp.: 171 °C.

### Synthesis of *N*-(4-phenylthiazol-2-yl)-3-(5-(trifluoromethyl)-1,2,4-oxadiazol-3-yl)benzamide (1j)



[416.38]

3-(5-(Trifluoromethyl)-1,2,4-oxadiazol-3-yl)benzoic acid (**6**) (258 mg, 1.00 mmol, 1.00 eq) was coupled with 2-amino-4-phenylthiazole (180 mg, 1.00 mmol, 1.00 eq) according to General procedure 3. The crude product was purified by flash chromatography (*n*-hexane/EtOAc) to furnish **1j** (140 mg, 0.34 mmol, 34%) as a beige solid.

<sup>1</sup>H NMR (600 MHz, DMSO-*d*<sub>6</sub>) δ = 7.31 – 7.37 (m, 1H), 7.45 (t, *J* = 7.7 Hz, 2H), 7.72 (s, 1H), 7.81 (t, *J* = 7.8 Hz, 1H), 7.94 – 7.99 (m, 2H), 8.31 (dt, *J* = 7.8, 1.4 Hz, 1H), 8.38 – 8.42 (m, 1H), 8.82 (t, *J* = 1.8 Hz, 1H), 13.12 (s, 1H) ppm.

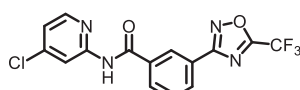
<sup>13</sup>C NMR (151 MHz, DMSO-*d*<sub>6</sub>) δ = 108.82, 114.89 (q), 124.92, 125.81, 127.24, 127.89, 128.78, 130.06, 131.11, 132.14, 133.26, 134.32, 149.29, 158.37, 165.27 (q, *J* = 43.8 Hz), 165.71, 168.01 ppm.

HPLC analysis: *R*<sub>t</sub> = 17.283 min, >99%.

HRMS (ESI+) = calcd. for C<sub>19</sub>H<sub>12</sub>F<sub>3</sub>N<sub>4</sub>O<sub>2</sub>S[M+H]<sup>+</sup> = 417.0628, found: 417.0629.

mp.: 208 °C.

### Synthesis of *N*-(4-chloropyridin-2-yl)-3-(5-(trifluoromethyl)-1,2,4-oxadiazol-3-yl)benzamide (1k)



[368.70]

3-(5-(Trifluoromethyl)-1,2,4-oxadiazol-3-yl)benzoic acid (**6**) (1.03 g, 4.00 mmol, 1.00 eq) was treated with 4-chloropyridin-2-amine (514 mg, 4.00 mmol, 1.00 eq) according to General procedure 3. The crude product was purified by flash chromatography (*n*-hexane/EtOAc/0.1% NEt<sub>3</sub>) and then further purified by recrystallisation (*n*-hexane/diethylether) yielding **1k** (348 mg, 0.94 mmol, 24%) as a white solid.

<sup>1</sup>H NMR (300 MHz, DMSO-*d*<sub>6</sub>) δ = 7.33 (dd, *J* = 5.4, 1.9 Hz, 1H), 7.70 – 7.85 (m, 1H), 8.23 – 8.36 (m, 2H), 8.40 (dd, *J* = 5.4, 0.6 Hz, 1H), 8.61 – 8.74 (m, 1H), 11.43 (s, 1H) ppm.

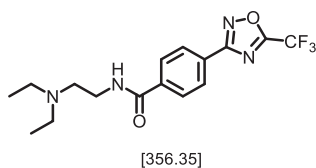
$^{13}\text{C}$  NMR (151 MHz,  $\text{DMSO-}d_6$ )  $\delta$  = 114.26, 116.69 (q), 120.06, 124.66, 127.21, 129.82, 130.70, 132.06, 134.94, 144.00, 149.46, 153.25, 165.24 (q,  $J$  = 43.9 Hz), 165.43, 168.04 ppm.

HPLC analysis:  $R_t$  = 15.517 min, 95.3%.

HRMS (ESI+) = calcd. for  $\text{C}_{15}\text{H}_9\text{ClF}_3\text{N}_4\text{O}_2$   $[\text{M}+\text{H}]^+$  = 369.0361, found: 369.0366.

mp.: 108.5 °C.

### Synthesis of *N*-(2-(diethylamino)ethyl)-4-(5-(trifluoromethyl)-1,2,4-oxadiazol-3-yl)benzamide (**1l**)



4-(5-(Trifluoromethyl)-1,2,4-oxadiazol-3-yl)benzoic acid (**7**) (258 mg, 1.00 mmol, 1.00 eq) was converted with *N,N*-diethylethylenediamine (140  $\mu\text{L}$ , 1.00 mmol, 1.00 eq) according to General procedure 3. The crude product was purified by flash chromatography (*n*-hexane/EtOAc) to afford **1l** (215 mg, 0.60 mmol, 60%) as a white solid.

$^1\text{H}$  NMR (300 MHz,  $\text{CDCl}_3$ )  $\delta$  = 1.06 (t,  $J$  = 7.1 Hz, 7H), 2.60 (q,  $J$  = 7.1 Hz, 4H), 2.70 (t,  $J$  = 5.9 Hz, 2H), 3.41 – 3.60 (m, 2H), 7.10 (s, 1H), 7.87 – 7.97 (m, 2H), 8.15 – 8.24 (m, 2H) ppm.

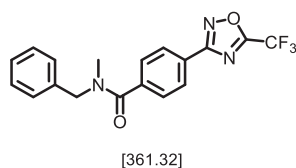
$^{13}\text{C}$  NMR (75 MHz,  $\text{DMSO-}d_6$ )  $\delta$  = 11.85, 37.68, 46.74, 51.36, 110.22, 115.65 (q,  $J$  = 273.3 Hz), 121.08, 126.46, 127.29, 128.10, 138.05, 164.78, 165.02, 165.36, 167.93 ppm.

HPLC analysis:  $R_t$  = 9.683 min, 99%.

HRMS (ESI+) = calcd. for  $\text{C}_{16}\text{H}_{20}\text{F}_3\text{N}_4\text{O}_2$   $[\text{M}+\text{H}]^+$  = 357.1533, found: 357.1535.

mp.: 68.6 °C.

### Synthesis of *N*-benzyl-*N*-methyl-4-(5-(trifluoromethyl)-1,2,4-oxadiazol-3-yl)benzamide (**1m**)



4-(5-(Trifluoromethyl)-1,2,4-oxadiazol-3-yl)benzoic acid (**7**) (258 mg, 1.00 mmol, 1.00 eq) was treated with *N*-benzylmethylamine (140  $\mu\text{L}$ , 1.00 mmol, 1.00 eq) according to General

procedure 3. The crude product was purified by flash chromatography (*n*-hexane/EtOAc) to obtain **1m** (260 mg, 0.72 mmol, 72%) as a white solid.

<sup>1</sup>H NMR (600 MHz, DMSO-*d*<sub>6</sub>) δ = 2.89 (d, *J* = 53.4 Hz, 3H), 4.48 (s, 1H), 4.71 (s, 1H), 7.10 – 7.46 (m, 4H), 7.68 (dd, *J* = 26.6, 7.9 Hz, 2H), 8.12 (dd, *J* = 27.3, 7.9 Hz, 2H) ppm.

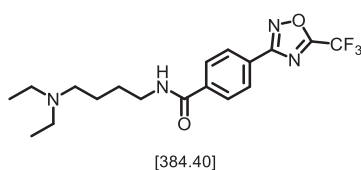
<sup>13</sup>C NMR (151 MHz, DMSO-*d*<sub>6</sub>) δ = 34.73 (d, *J* = 608.2 Hz), 51.94 (d, *J* = 630.0 Hz), 115.74 (q, *J* = 273.0 Hz), 125.20, 126.76, 127.27, 127.46, 127.56, 127.60, 127.67, 127.99, 128.64, 128.77, 136.63, 137.12, 140.09, 140.19, 165.16 (q, *J* = 43.9 Hz), 167.97, 169.29, 169.87 ppm.

HPLC analysis: *R*<sub>t</sub> = 15.150 min, 99%.

HRMS (ESI+) = calcd. for C<sub>18</sub>H<sub>15</sub>F<sub>3</sub>N<sub>3</sub>O<sub>2</sub> [M+H]<sup>+</sup> = 362.1111, found: 362.113.

mp.: 89.8 °C.

### Synthesis of *N*-(4-(diethylamino)butyl)-4-(5-(trifluoromethyl)-1,2,4-oxadiazol-3-yl)benzamide (**1n**)



4-(5-(Trifluoromethyl)-1,2,4-oxadiazol-3-yl)benzoic acid (**7**) (258 mg, 1.00 mmol, 1.00 eq) was converted with *N,N*-diethylbutane-1,4-diamine (182 μL, 1.00 mmol, 1.00 eq) according to General procedure 3. The crude product was purified by flash chromatography (CH<sub>2</sub>Cl<sub>2</sub>/ 30% MeOH in CH<sub>2</sub>Cl<sub>2</sub>/ 0.1% NEt<sub>3</sub>) to obtain **1n** (320 mg, 0.83 mmol, 83%) as a white solid.

<sup>1</sup>H NMR (300 MHz, DMSO-*d*<sub>6</sub>) δ = 0.97 (t, *J* = 7.1 Hz, 6H), 1.39 – 1.62 (m, 4H), 2.40 – 2.60 (m, 6H), 3.29 (q, *J* = 6.5 Hz, 2H), 8.01 – 8.08 (m, 2H), 8.12 – 8.18 (m, 2H), 8.70 (t, *J* = 5.6 Hz, 1H) ppm.

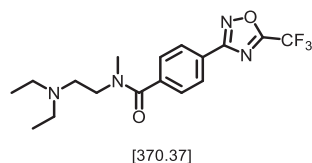
<sup>13</sup>C NMR (75 MHz, DMSO-*d*<sub>6</sub>) δ = 11.22, 23.75, 26.92, 46.30, 51.79, 115.75 (d, *J* = 273.2 Hz), 126.55, 127.38, 128.28, 138.17, 164.91, 165.18, 165.49, 167.99 ppm.

HPLC analysis: *R*<sub>t</sub> = 9.919 min, >99%.

HRMS (ESI+) = calcd. for C<sub>18</sub>H<sub>24</sub>F<sub>3</sub>N<sub>4</sub>O<sub>2</sub> [M+H]<sup>+</sup> = 385.1846, found: 385.1848.

mp.: 84.4 °C.

### Synthesis of *N*-(2-(diethylamino)ethyl)-*N*-methyl-4-(5-(trifluoromethyl)-1,2,4-oxadiazol-3-yl)benzamide (**1o**)



4-(5-(Trifluoromethyl)-1,2,4-oxadiazol-3-yl)benzoic acid (**7**) (258 mg, 1.00 mmol, 1.00 eq) was coupled with *N,N*-diethyl-*N'*-methylethylenediamine (133 mg, 1.00 mmol, 1.00 eq) according to General procedure 3. The crude product was purified by flash chromatography (CH<sub>2</sub>Cl<sub>2</sub>/30% MeOH in CH<sub>2</sub>Cl<sub>2</sub>/ 0.1% NEt<sub>3</sub>) to afford **1o** (268 mg, 0.72 mmol, 72%) as a yellowish oil.

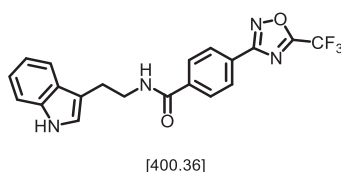
<sup>1</sup>H NMR (600 MHz, DMSO-*d*<sub>6</sub>) δ = 0.79 (t, *J* = 7.1 Hz, 3H), 0.99 (t, *J* = 7.1 Hz, 3H), 2.26 (q, *J* = 7.1 Hz, 2H), 2.46 (t, *J* = 6.8 Hz, 1H), 2.51 – 2.56 (m, 2H), 2.63 (t, *J* = 6.9 Hz, 1H), 2.96 (d, *J* = 46.7 Hz, 3H), 3.24 (t, *J* = 6.8 Hz, 1H), 3.52 (t, *J* = 6.8 Hz, 1H), 7.61 (dd, *J* = 16.6, 7.8 Hz, 2H), 8.12 (t, *J* = 6.2 Hz, 2H) ppm.

<sup>13</sup>C NMR (151 MHz, DMSO-*d*<sub>6</sub>) δ = 11.59, 12.10, 32.81, 37.76, 40.06, 45.10, 46.59, 46.74, 49.05, 49.54, 50.16, 115.75 (q, *J* = 273.0 Hz), 124.81, 124.95, 127.32, 127.52, 127.78, 127.93, 140.77, 165.15 (q, *J* = 43.6 Hz), 167.98, 168.81, 169.75 ppm.

HPLC analysis: *R*<sub>t</sub> = 9.719 min, 99.8%.

HRMS (ESI+) = calcd. for C<sub>17</sub>H<sub>22</sub>F<sub>3</sub>N<sub>4</sub>O<sub>2</sub> [M+H]<sup>+</sup> = 371.1689, found: 371.1686.

### Synthesis of *N*-(2-(1*H*-indol-3-yl)ethyl)-4-(5-(trifluoromethyl)-1,2,4-oxadiazol-3-yl)benzamide (**1p**)



4-(5-(Trifluoromethyl)-1,2,4-oxadiazol-3-yl)benzoic acid (**7**) (258 mg, 1.00 mmol, 1.00 eq) was converted with tryptamine (160 mg, 1.00 mmol, 1.00 eq) according to General procedure 3. The crude product was purified by flash chromatography (*n*-hexane/EtOAc) and then further

purified by recrystallisation (*n*-hexane/ EtOAc) to obtain **1p** (180 mg, 0.45 mmol, 45%) as a beige solid.

<sup>1</sup>H NMR (300 MHz, DMSO-*d*<sub>6</sub>) δ = 2.98 (t, *J* = 7.5 Hz, 2H), 3.58 (td, *J* = 7.4, 5.6 Hz, 2H), 7.03 (dddd, *J* = 25.8, 8.0, 7.0, 1.2 Hz, 2H), 7.20 (d, *J* = 2.3 Hz, 1H), 7.35 (dt, *J* = 8.1, 0.9 Hz, 1H), 7.59 (dd, *J* = 7.6, 1.1 Hz, 1H), 8.02 – 8.21 (m, 4H), 8.85 (t, *J* = 5.6 Hz, 1H), 10.82 (s, 1H) ppm.

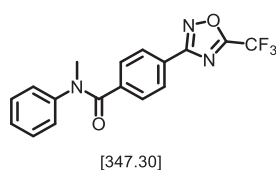
<sup>13</sup>C NMR (151 MHz, DMSO-*d*<sub>6</sub>) δ = 25.08, 40.35, 111.38, 111.80, 115.75 (q, *J* = 273.1 Hz), 118.23, 118.26, 120.92, 122.63, 126.58, 127.27, 127.39, 128.30, 136.25, 138.14, 165.13, 165.18 (q, *J* = 43.7 Hz), 167.97 ppm.

HPLC analysis: *R*<sub>t</sub> = 14.467 min, >99%.

HRMS (ESI+) = calcd. for C<sub>19</sub>H<sub>18</sub>F<sub>3</sub>N<sub>4</sub>O<sub>2</sub> [M+H]<sup>+</sup> = 391.1376, found: 391.1378.

mp.: 167.0 °C.

#### Synthesis of *N*-methyl-*N*-phenyl-4-(5-(trifluoromethyl)-1,2,4-oxadiazol-3-yl)benzamide (**1q**)



4-(5-(Trifluoromethyl)-1,2,4-oxadiazol-3-yl)benzoic acid (**7**) (258 mg, 1.00 mmol, 1.00 eq) was coupled with *N*-methylaniline (120 μL, 1.00 mmol, 1.00 eq) according to General procedure 3. The crude product was purified by flash chromatography (*n*-hexane/EtOAc) to yield **1q** (258 mg, 0.74 mmol, 74%) as a white solid.

<sup>1</sup>H NMR (300 MHz, DMSO-*d*<sub>6</sub>) δ = 3.40 (s, 3H), 7.06 – 7.35 (m, 5H), 7.47 (d, *J* = 8.0 Hz, 2H), 7.89 (d, *J* = 8.2 Hz, 2H) ppm.

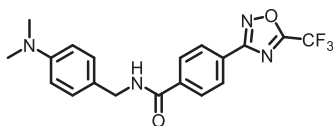
<sup>13</sup>C NMR (151 MHz, DMSO-*d*<sub>6</sub>) δ = 37.69, 115.70 (q, *J* = 273.2 Hz), 124.88, 126.77, 126.84, 127.18, 129.12, 129.17, 140.26, 143.97, 165.04 (q, *J* = 43.6 Hz), 167.80, 168.48 ppm.

HPLC analysis: *R*<sub>t</sub> = 14.717 min, 98.7%.

HRMS (ESI+) = calcd. for C<sub>17</sub>H<sub>13</sub>F<sub>3</sub>N<sub>3</sub>O<sub>2</sub> [M+H]<sup>+</sup> = 348.0954, found: 348.0954.

mp.: 89.7 °C.

## Synthesis of *N*-(4-(dimethylamino)benzyl)-4-(5-(trifluoromethyl)-1,2,4-oxadiazol-3-yl)benzamide (**1r**)



[390.36]

4-(5-(Trifluoromethyl)-1,2,4-oxadiazol-3-yl)benzoic acid (**7**) (258 mg, 1.00 mmol, 1.00 eq) was treated with 4-dimethylaminobenzylamine dihydrochloride (228 mg, 1.00 mmol, 1.00 eq) according to General procedure 3. The crude product was purified by flash chromatography (CH<sub>2</sub>Cl<sub>2</sub>/30% MeOH in CH<sub>2</sub>Cl<sub>2</sub>/ 0.1% NEt<sub>3</sub>) and recrystallized (*n*-hexane/EtOAc) to furnish **1r** (141 mg, 0.36 mmol, 36%) as a green solid.

<sup>1</sup>H NMR (300 MHz, DMSO-*d*<sub>6</sub>) δ = 2.85 (s, 6H), 4.38 (d, *J* = 5.9 Hz, 2H), 6.66 – 6.74 (m, 2H), 7.12 – 7.22 (m, 2H), 8.06 – 8.12 (m, 2H), 8.13 – 8.21 (m, 2H), 9.13 (t, *J* = 5.9 Hz, 1H) ppm.

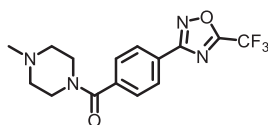
<sup>13</sup>C NMR (75 MHz, DMSO-*d*<sub>6</sub>) δ = 40.29, 42.36, 112.38, 115.75 (d, *J* = 273.1 Hz), 126.63, 126.89, 127.40, 128.39, 138.03, 149.64, 164.90, 164.99, 165.48, 167.96 ppm.

HPLC analysis: *R*<sub>t</sub> = 10.103 min, 99%.

HRMS (ESI+) = calcd. for C<sub>19</sub>H<sub>18</sub>F<sub>3</sub>N<sub>4</sub>O<sub>2</sub> [M+H]<sup>+</sup> = 391.1376, found: 391.1376.

mp.: 182.6 °C.

## Synthesis of (4-methylpiperazin-1-yl)(4-(5-(trifluoromethyl)-1,2,4-oxadiazol-3-yl)phenyl)methanone (**1s**)



[340.31]

4-(5-(Trifluoromethyl)-1,2,4-oxadiazol-3-yl)benzoic acid (**7**) (258 mg, 1.00 mmol, 1.00 eq) was treated with 1-methylpiperazine (111 μL, 1.00 mmol, 1.00 eq) according to General procedure 3. The crude product was purified by flash chromatography (CH<sub>2</sub>Cl<sub>2</sub>/30% MeOH in CH<sub>2</sub>Cl<sub>2</sub>/ 0.1% NEt<sub>3</sub>) to furnish **1s** (255 mg, 0.75 mmol, 75%) as a yellow solid.

<sup>1</sup>H NMR (300 MHz, DMSO-*d*<sub>6</sub>) δ = 2.23 (s, 3H), 2.37 (d, *J* = 19.8 Hz, 5H), 3.64 (s, 2H), 7.53 – 7.70 (m, 2H), 8.04 – 8.26 (m, 2H) ppm.

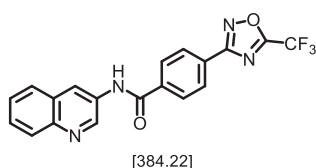
$^{13}\text{C}$  NMR (75 MHz,  $\text{DMSO-}d_6$ )  $\delta$  = 45.29, 54.21, 115.64 (d,  $J$  = 273.1 Hz), 125.12, 127.48, 127.86, 139.66, 164.76, 165.34, 167.74, 167.93 ppm.

HPLC analysis:  $R_t$  = 8.552 min, 96.8%.

HRMS (ESI+) = calcd. for  $\text{C}_{15}\text{H}_{16}\text{F}_3\text{N}_4\text{O}_2$   $[\text{M}+\text{H}]^+$  = 341.1220, found: 341.1221

mp.: 77.8 °C.

### Synthesis of *N*-(quinolin-3-yl)-4-(5-(trifluoromethyl)-1,2,4-oxadiazol-3-yl)benzamide (**1t**)



4-(5-(Trifluoromethyl)-1,2,4-oxadiazol-3-yl)benzoic acid (**7**) (258 mg, 1.00 mmol, 1.00 eq) was converted with 3-aminoquinoline (144 mg, 1.00 mmol, 1.00 eq) according to General procedure 3. The crude product was purified by flash chromatography ( $\text{CH}_2\text{Cl}_2$ / 30% MeOH in  $\text{CH}_2\text{Cl}_2$ / 0.1%  $\text{NEt}_3$ ) to yield **1t** (112 mg, 0.29 mmol, 29%) as a white solid.

$^1\text{H}$  NMR (600 MHz,  $\text{DMSO-}d_6$ )  $\delta$  = 7.60 (ddd,  $J$  = 8.1, 6.9, 1.1 Hz, 1H), 7.68 (tq,  $J$  = 7.9, 1.1 Hz, 1H), 7.95 – 8.02 (m, 2H), 8.26 (t,  $J$  = 1.0 Hz, 4H), 8.84 – 8.89 (m, 1H), 9.16 (dd,  $J$  = 2.4, 1.2 Hz, 1H), 10.92 (s, 1H) ppm.

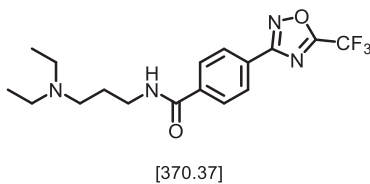
$^{13}\text{C}$  NMR (151 MHz,  $\text{DMSO-}d_6$ )  $\delta$  = 115.76 (d,  $J$  = 273.1 Hz), 123.64, 127.10, 127.34, 127.57, 127.70, 127.86, 128.19, 128.58, 128.96, 132.66, 137.68, 144.50, 145.43, 165.15, 165.27 (d,  $J$  = 43.9 Hz), 167.90 ppm.

HPLC analysis:  $R_t$  = 11.786 min, 98.4%.

HRMS (ESI+) = calcd. for  $\text{C}_{19}\text{H}_{12}\text{F}_3\text{N}_4\text{O}_2$   $[\text{M}+\text{H}]^+$  = 385.0907, found: 385.0904.

mp.: 240.1 °C.

Synthesis of *N*-(3-(diethylamino)propyl)-4-(5-(trifluoromethyl)-1,2,4-oxadiazol-3-yl)benzamide (**1u**)



4-(5-(Trifluoromethyl)-1,2,4-oxadiazol-3-yl)benzoic acid (**7**) (258 mg, 1.00 mmol, 1.00 eq) was treated with 3-(diethylamino)propylamine (132 mg, 1.00 mmol, 1.00 eq) according to General procedure 3. The crude product was purified by flash chromatography (CH<sub>2</sub>Cl<sub>2</sub>/30% MeOH in CH<sub>2</sub>Cl<sub>2</sub>/ 0.1% NEt<sub>3</sub>) to provide **1u** (281 mg, 0.76 mmol, 76%) as a white solid.

<sup>1</sup>H NMR (300 MHz, DMSO-*d*<sub>6</sub>) δ = 1.09 (t, *J* = 7.2 Hz, 6H), 1.74 – 1.90 (m, 2H), 2.83 (t, *J* = 7.1 Hz, 6H), 3.35 (q, *J* = 6.6 Hz, 2H), 8.01 – 8.10 (m, 2H), 8.14 – 8.22 (m, 2H), 8.83 (t, *J* = 5.6 Hz, 1H) ppm.

<sup>13</sup>C NMR (75 MHz, DMSO-*d*<sub>6</sub>) δ = 9.93, 24.85, 37.37, 46.38, 49.40, 115.83 (d, *J* = 273.3 Hz), 126.78, 127.53, 128.39, 137.97, 165.29 (d, *J* = 43.8 Hz), 165.48, 168.03 ppm.

HPLC analysis: *R*<sub>t</sub> = 9.786 min, 98.4%.

HRMS (ESI+) = calcd. for C<sub>17</sub>H<sub>22</sub>F<sub>3</sub>N<sub>4</sub>O<sub>2</sub> [M+H]<sup>+</sup> = 371.1689, found: 371.1694

mp.: 77.3 °C.

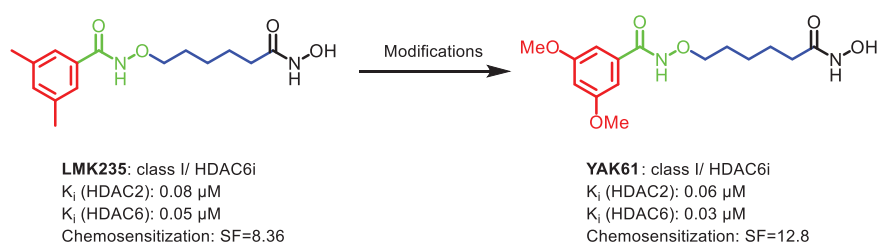
## References

- [1] M. Lobera, K. P. Madauss, D. T. Pohlhaus, Q. G. Wright, M. Trocha, D. R. Schmidt, E. Baloglu, R. P. Trump, M. S. Head, G. A. Hofmann, et al., *Nat. Chem. Biol.* **2013**, *9*, 319–325.
- [2] K. Liu, H. Lu, L. Hou, Z. Qi, C. Teixeira, F. Barbault, B.-T. Fan, S. Liu, S. Jiang, L. Xie, *J. Med. Chem.* **2008**, *51*, 7843–7854.

## Summary and Outlook

Studies over the past decades have demonstrated that histone deacetylases (HDACs) participate in the regulation of the expression and activity of numerous proteins involved in cancer development and progression. By catalyzing the removal of acetyl groups of histones, HDACs generate a condensed chromatin structure and therefore alter transcription of oncogenes and tumor suppressor genes. HDACs can also act on a variety of non-histone proteins including signaling molecules and transcription factors implicated in the control of cell growth, differentiation and apoptosis. As crucial epigenetic regulators, HDACs are clinically validated cancer targets. Besides the natural product romidepsin, four trichostatin A derived HDAC inhibitors (HDACi) (vorinostat, belinostat, panobinostat, chidamide) are approved for the treatment of lymphoma and myeloma. Because of their chemosensitizing properties in various types of cancer, HDACi are useful combination partners for established anticancer drugs such as cisplatin.

The first project focused on the structural optimization of LMK235. Due to the promising anticancer properties of LMK235, modifications of the cap group were performed to increase the antiproliferative and synergistic activity with cisplatin in cisplatin-resistant cancer cells. Among the synthesized compounds, **YAK61** displayed a similar inhibition of HDAC2 and HDAC6 compared to LMK235, but was slightly more effective in reversing the cisplatin resistance of Cal27CisR (Scheme 1).

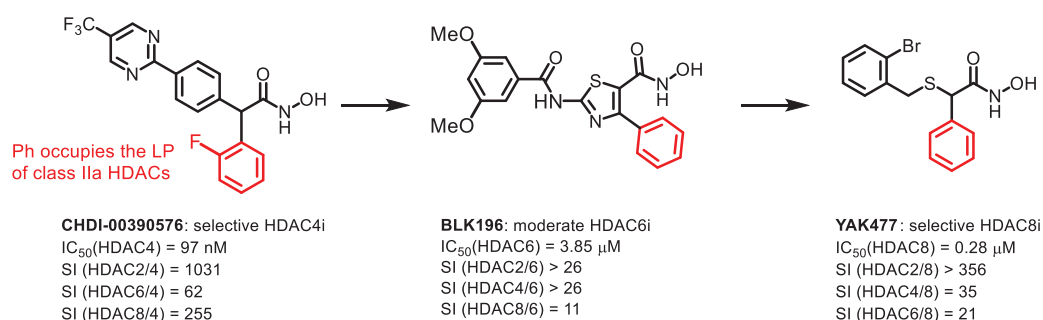


Scheme 1: Modification of LMK235 in its cap region (highlighted in red).

So far, the most common HDACi under preclinical and clinical evaluation are nonselective HDACi (pan-inhibitor). This unselectivity is thought to cause the pan-HDACi associated severe adverse effects and their limited therapeutic efficacy in solid tumors as single agents. Therefore, the design and development of isozyme-selective HDACi provide a promising approach to widen the therapeutic window and to reduce the side effects that have been

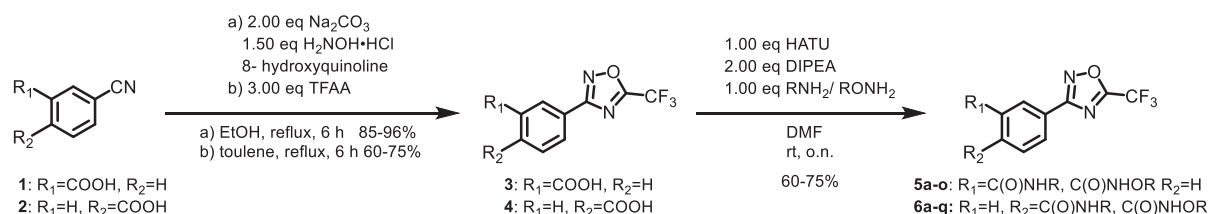
observed for pan HDACi. Furthermore, selective HDACi present important pharmacological tool molecules to elucidate the biological role of individual HDACs in health and disease. In contrast to the established role of class I HDACs in cancer, the significance of class IIa HDACs for cancer treatment is controversially discussed.

The second research project focused on the design and development of class IIa selective HDAC inhibitors. The first strategy aimed to generate class IIa selective HDAC inhibitors by addressing the lower pocket which is only present in class IIa HDACs. Starting from the lead structure CHDI-00390576, 4-phenyl substituted thiazolyl-based hydroxamates exhibiting various cap groups and  $\alpha$ -phenyl substituted derivatives demonstrating a hydroxamic acid as ZBG were proposed to address the lower pocket of class IIa HDACs (Scheme 2). Preliminary docking results indicated an isozyme selectivity by addressing the lower pocket of class IIa HDACs with the respective phenyl-substituent (colored in red). Based on the preliminary *in-silico* studies, the evaluated thioether-based hydroxamates were expected to display a potential HDAC4 and/or HDAC8 inhibitory activity. Surprisingly, this new series of thiazolyl based hydroxamates revealed a moderate HDAC6 inhibitory activity in the low micromolar range. The hydroxamic acids **BLK196** and **YAK320** did not show a HDAC4 inhibition up to 100  $\mu$ M, whilst **YAK312**, exhibiting a 4-pyridinyl CAP moiety displayed a moderate HDAC4 inhibitory activity in the micromolar range. The thioether-based hydroxamic acid **YAK477** was identified as a highly active and selective HDAC8 inhibitor in the nanomolar range ( $IC_{50}(\text{HDAC8}) = 0.28 \mu\text{M}$ ) with a  $\geq 356$ -fold selectivity over HDAC2 and a 35/21-fold preference over HDAC4/6. Further approaches to target the lower pocket with various  $\alpha$ -phenyl substituted scaffolds e.g.  $\alpha$ - and  $\beta$ -amino acid derivatives did not lead to potent and selective class IIa HDACs inhibitors.



Scheme 2: The first strategy to address the lower pocket of class IIa HDACs.

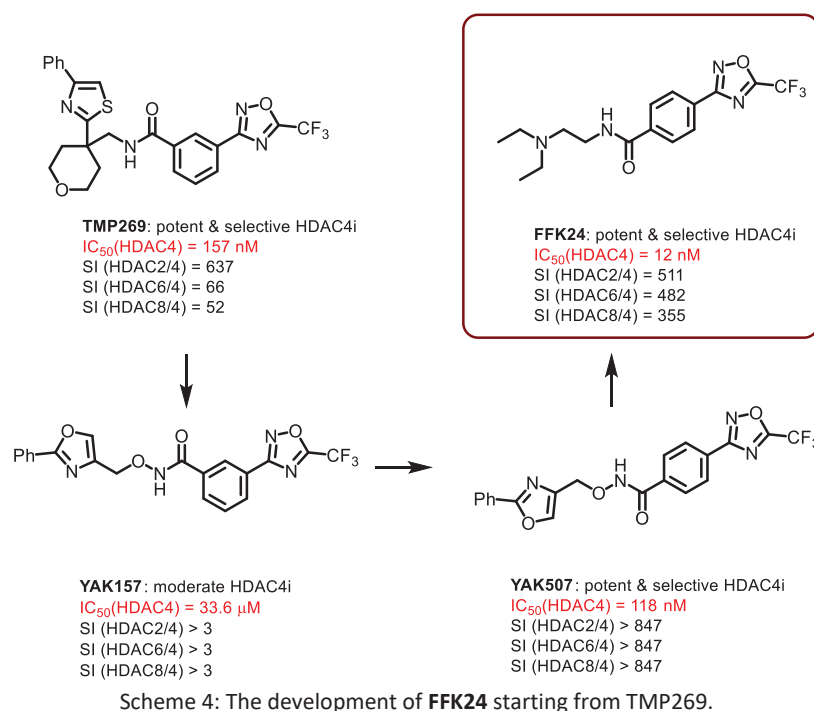
The second strategy to design HDAC class IIa selective inhibitors was the introduction of the 5-(trifluoromethyl)-1,2,4-oxadiazole (TFMO) moiety as a selectivity directing ZBG. Starting from the lead structure TMP269, *meta*- and *para*-substituted TFMO-derivatives **5a-o** and **6a-q** were synthesized with a variable alkoxyamide/amide connecting unit according to Scheme 3.



Scheme 3: The synthesis of *meta*- and *para*-substituted TFMO-derivatives **5a-o** & **6a-q**.

The *para*-substituted TFMO-derivative **YAK507** displayed an approximately 1.3-fold increased HDAC4 inhibition ( $IC_{50}(\text{HDAC4}) = 118 \text{ nM}$ ) compared to the lead structure TMP269 with a more than 800-fold selectivity over HDAC2/6/8. Moreover, **YAK507** displayed a 285-fold stronger inhibitory activity towards HDAC4 in comparison to its corresponding *meta*-substituted TFMO-derivative **YAK157** ( $IC_{50}(\text{HDAC4}) = 33.6 \mu\text{M}$ ). SAR studies revealed that the *para*-substituted TFMO derivatives showed a stronger inhibitory activity towards HDAC4 than the corresponding *meta*-substituted TFMO derivatives. Therefore, the *para*-substituted TFMO derivatives were optimized within the connecting unit and the cap region which resulted in the highly potent and selective class IIa HDAC inhibitor **FFK24** ( $IC_{50}(\text{HDAC4}) = 12 \text{ nM}$ ) with a 511/482/355-fold selectivity over HDAC2/6/8 (Scheme 4). **FFK24** demonstrated an approximately 13/8-fold stronger HDAC4 inhibition than TMP269 and the class IIa selective hydroxamate-based compound CHDI-00390576. Regarding the HDAC isozyme inhibition profile, **FFK24** is among the most promising class IIa HDAC inhibitors.

## Summary and Outlook



In summary, 90 final compounds were synthesized successfully. The two *para*-substituted TFMO-based compounds **FFK29** ( $IC_{50}(\text{HDAC4}) = 24.5 \text{ nM}$ ) and **FFK24** ( $IC_{50}(\text{HDAC4}) = 12 \text{ nM}$ ) were identified as highly potent and selective class IIa HDAC inhibitors in the low nanomolar range (Figure 1).

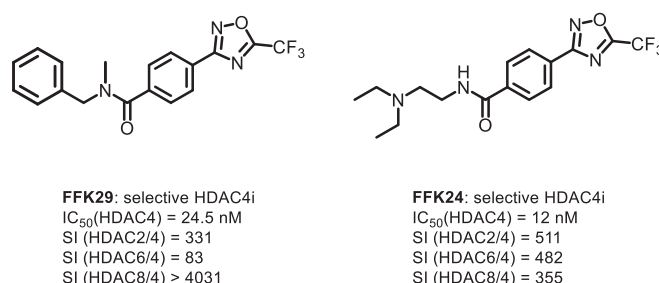
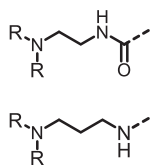


Figure 1: The two potent and selective HDAC4 inhibitors **FFK24** and **FFK29**.

Subject of future work will be the lead structure optimization of **FFK24** in its linker, cap and ZBG region to improve its potency, water solubility and metabolic stability (Figure 2). Furthermore, the elucidation of the binding mode of **FFK24** within the catalytic site of HDAC4, via crystallisation studies, is subject of future studies. Further biological evaluation will focus on the combination studies of our class IIa selective HDACi with proteasome inhibitors in the leukemia cell lines HL-60 and RPM-8226 as well as in the human tongue squamous carcinoma cell line Cal27 and the human ovarian cancer cell line A2780.

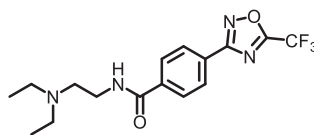
## Summary and Outlook

**CAP modifictaion:**  
prolongation, truncation  
and cyclisation



R = Me, Et, Propyl,  
heterocyclic aliphatic  
amines: morpholine,  
piperidine

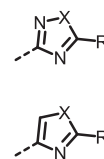
**Linker modifictaion:**  
substituted benzene, 6-membered  
heterocycles (e.g. pyridines)



**CAP CU Linker ZBG**

**Compound 11:** selective HDAC4i  
IC<sub>50</sub>(HDAC4) = 12 nM  
SI (HDAC2/4) = 511  
SI (HDAC6/4) = 482  
SI (HDAC8/4) = 355

**ZBG modifictaion:**



X = O, S, NH  
R = CF<sub>3</sub>, CHF<sub>2</sub>, CH<sub>2</sub>F, CH<sub>2</sub>OH

Figure 2: Lead structure optimization of **FFK24**.

Interestingly, the thioether-based hydroxamate **YAK477** (IC<sub>50</sub>(HDAC8) = 0.28 μM) has been identified as a highly potent and selective HDAC8 inhibitor in the nanomolar range. Further studies will focus on the structural optimization of **YAK477** to improve HDAC8 selectivity and e.g. water solubility as well as pharmacokinetic properties. The elucidation of the binding mode of **YAK477** within the catalytic pocket of HDAC8 via crystallization studies is subject of future research.